


ADVERTIMENT. L'accés als continguts d'aquesta tesi queda condicionat a l'acceptació de les condicions d'ús establertes per la següent llicència Creative Commons:  <https://creativecommons.org/licenses/?lang=ca>

ADVERTENCIA. El acceso a los contenidos de esta tesis queda condicionado a la aceptación de las condiciones de uso establecidas por la siguiente licencia Creative Commons:  <https://creativecommons.org/licenses/?lang=es>

WARNING. The access to the contents of this doctoral thesis it is limited to the acceptance of the use conditions set by the following Creative Commons license:  <https://creativecommons.org/licenses/?lang=en>



Departament de Bioquímica i Biologia Molecular
Unitat de Bioquímica de Biociències

Connecting microbiota and neurodegenerative diseases

Thesis presented by Jofre Seira Curto to obtain the degree of Doctor in Biochemistry,
Molecular Biology and Biomedicine under the supervision of Dr. Natalia Sánchez de Groot

Unitat de Biociències del Departament de Bioquímica i Biologia Molecular
Universitat Autònoma de Barcelona

Dra. Natalia Sanchez de Groot

Jofre Seira Curto

Cerdanyola del Vallès, Juny 2025

Index

Acknowledgments.....	6
Summary	9
Articles included in the thesis.....	11
List of abbreviations.....	12
Introduction.....	13
1. Alzheimer's disease.....	13
1.1 Pathological hallmarks of the disease.....	14
1.2 Tau protein.....	17
2. Aβ peptides.....	18
2.1 The A β peptide sequence	19
2.2 A β peptide aggregation.....	19
2.3 The A β peptide structure	22
2.4 A β prion properties.....	25
2.5 Intrinsic aggregation modifiers	26
2.6 Extrinsic aggregation modifiers.....	28
Endogenous proteins.....	28
Lipids.....	28
Metals.....	29
Nucleic acids	29
Exogenous aggregation proteins	30
3. The human microbiome	30
3.1 Amyloids in the microbiome	31
3.2 Microbiome amyloids and neurodegenerative disease.....	32
Aims.....	36
CHAPTER I: Aβ40 Aggregation under Changeable Conditions.....	37
CHAPTER II: Exogenous Prion-Like Proteins and Their Potential to Trigger Cognitive Dysfunction	51
Chapter III: Exogenous Amyloid Sequences: Their Role in Amyloid-Beta Heterotypic Aggregation	77
General Discussion and Future perspectives.....	98
1. CHAPTER I: Aβ40 Aggregation under Changeable Conditions.....	98
2. CHAPTER II: Exogenous Prion-Like Proteins and Their Potential to Trigger Cognitive Dysfunction	100
3. CHAPTER III: Exogenous Amyloid Sequences: Their Role in Amyloid-Beta Heterotypic Aggregation ...	102
Concluding remarks	104
References	105
Appendix 1- Supplementary information of chapter 1	118

Appendix 2- Supplementary information of chapter 2	125
---	------------

Acknowledgments

Voldria començar aquesta tesi agraïnt a totes aquelles persones que han fet possible que aquesta tesi tirés endavant. Moltes gràcies a tots aquells amb qui he compartit algun moment durant aquests anys.

Agrair a la Natàlia que va decidir confiar en mi des del primer moment i ho ha seguit fent al llarg de tota la tesi. Construir aquest tesi i anar veient com s'ha construït el grup ha estat molt enriquidor. Ha estat molt important el seu suport en els moments que els experiments no anaven com voldria, que els agregats no anaven o les plaques no arribaven. M'has ensenyat moltes coses durant aquests anys i estic molt agraït de que hagi dirigit la meua tesi. També agrair als companys de laboratori, des dels que hi ha ara fins els que han anat passant. Però sobretot els que hi ha ara, segons el que em diu el Genís des del final del despatx mentre escric aquests agraïments. Agrair a la Rosario, l'Estrella, el Genís (sense coaccions), l'Adàn i la Marina entre tots els altres que han format part del laboratori. Gràcies a ells han fet que aquests quatre anys estiguessin plens de moments divertits i plens d'aprenentatge.

Agrair també als companys de la torre, a la Carmen, el Roberto, el Jordi Sysbio, l'Alba, el Jordi Màster, el Raul, la Zoe i el Marc. Pels moments en que ens hem donat suport mútuament i han fet que tot fes més amè. Especial menció a la Carmen, els Jordis, l'Alba, la Zoe i l'Amalia pels moments de rol que hem anat compartint durant la tesi, no tants com voldríem però ha quedat clar que nosaltres si que fem pocions. Agrair també a tots els membres de la unitat de Biofísica, en especial al Josep i la Núria pel seu suport durant els 4 anys i per sempre estar disposats a que els hi anés a fer preguntes.

Agrair als tècnics, a l'Helena per preparar les nostres coses i per mantenir tota la torre en funcionament i al Santi i la Magda per la seva ajuda amb les pràctiques. Agrair al servei de microscòpia, especialment al Martí que tot i ser de l'espanyol m'ha ajudat molt durant aquests anys a aclarir que passava amb el Jeol i a que aprenguéssim a no fer saltar el buit.

Mencionar també al Tartaglia lab que em van acollir durant 3 mesos i em van ensenyar molt, especialment el Jakob que em va ensenyar el seu amor per l'RNA i em va guiar per Gènova quan acabava d'arribar. Els agraeixo molt a tots la seva acollida ja fos a Gènova com a Calosso i fer-me sentir un més del grup. També vull agrair a tots a la gent que he anat coneixent a través de la ciència, ja sigui en congressos, cursos o estades.

Fora de la ciència agrair als meus amics, als que menciono, però també als que no, que sinó s'allargaven molt els agraïments i s'em queixaven. A l'Arnau, al Garci i a l'Ignasi pels moments

divertits durant aquests anys. També agrair als Pats, ja desconfinats, estar sempre al costat i com hem anat compartint les nostres experiències en l'investigació i també per jugar a jocs de taula òbviament. Menció especial pel Pau quan venia els divendres a jugar a cartes al laboratori, i encara que l'Europa hagi pujat de categoria el Sant Andreu seguirà sent millor.

Agrair especialment a la Clàudia per haver pogut compartir aquests dos últims anys de la tesi. M'ha ajudat molt en aquest procés i que m'ha acompanyat sempre que calia inclòs venint a Gènova per assegurar-te que podia sobreviure sol. Gràcies per fer-me feliç durant la tesi i gràcies per avançar per seguir-me fent feliç després!

Per últim agrair a tota la meua família, ja estiguessin a Terrassa o a Peramola. Especialment agrair als meus pares, per ajudar-me sempre que ha calgut i a fer-me de taxi sempre que ha estat necessari ja fos per anar a la UAB, com per al ALBA, a l'aeroport o a treure'm a passejar a l'exterior quan necessitava desconnectar. Gràcies per haver-me animat i per haver-me cuidat durant però sobretot també abans de la tesi. També agrair al Franc, per sempre fer-me costat i sempre tenir curiositat pel que estava fent. Per venir a veurem a Anglaterra i a Itàlia espero que em segueixis venint a visitar quan estigui fora i portis jocs de taula!

Summary

[Català]

La malaltia d'Alzheimer és un trastorn neurològic molt prevalent i la principal causa de demència a nivell mundial. Els seus principals trets patològics són les plaques amiloides i els garbuixos neurofibril·lars, que corresponen a acumulacions de pèptids β -amiloide i proteïnes tau agregades. Una de les principals qüestions sobre el desenvolupament de la malaltia és entendre com aquestes proteïnes, habitualment no patogèniques, acaben seguint una via d'agregació aberrant que condueix a la malaltia. Tot i que s'han estudiat molts factors, encara no es coneixen del tot els mecanismes implicats.

Aquesta tesi investiga el comportament agregatiu del pèptid β -amiloide i els elements que interfereixen en la seva agregació. Primer, hem estudiat les seves propietats electrostàtiques analitzant com les alteracions del pH i de la força iònica modifiquen la seva agregació. Hem mostrat que canvis localitzats en el pH o la força iònica, similars als que es poden donar en compartiments petits com els endosomes, poden generar espècies agregatives que es propaguen més ràpidament que aquelles formades en condicions fisiològiques.

En segon lloc, hem analitzat com les proteïnes exògenes de tipus prionoide derivades de la microbiota intestinal poden interferir en l'agregació dels pèptids β -amiloide. Això és important perquè la microbiota intestinal és una comunitat bacteriana present en el nostre organisme al llarg de tota la vida, la qual cosa incrementa la probabilitat d'interaccions entre proteïnes bacterianes i humanes, amb possibles conseqüències negatives per a la salut. En aquest estudi, hem observat que el microbioma conté proteïnes de tipus prionoide capaces d'agregar-se, actuant com els prions dels llevats, i de provocar la sembra creuada (cross-seeding) dels pèptids β -amiloide. També hem vist que aquestes proteïnes són tòxiques per a cèl·lules neuroblastoma humanes i poden provocar deteriorament cognitiu en models de *Caenorhabditis elegans*.

En conclusió, aquest estudi posa en relleu diversos factors que poden alterar l'agregació dels pèptids β -amiloide, posant especial èmfasi en les proteïnes exògenes de tipus prionoide pel seu potencial efecte perjudicial. A causa de l'exposició continuada a la microbiota intestinal al llarg de la vida, aquestes proteïnes poden representar un factor de risc potencial en la patogènesi de la malaltia d'Alzheimer, tal com demostra la seva capacitat per afavorir l'agregació i el deteriorament cognitiu en sistemes model.

Summary

[English]

Alzheimer's disease is a prevalent neurological disorder and the leading cause of dementia worldwide. Its main pathological hallmarks are amyloid plaques and neurofibrillary tangles, which are accumulations of aggregated A β peptides and tau proteins, respectively. Both proteins are present under non-pathological conditions. One of the main questions about the development of the disease is how these usually non-pathogenic proteins shift to an aberrant aggregation pathway leading to the disease. Although many factors have been studied, they are still not fully elucidated.

This thesis investigates A β aggregation behavior and the elements that interfere with its aggregation. Firstly, we have studied its electrostatic properties by analyzing how pH and ionic strength alterations modify aggregation. In this way, we have shown how localized changes in pH or ionic strength, such as those occurring in small compartments like endosomes, can produce aggregative species that are able to propagate faster than others formed under physiological conditions.

Secondly, we have studied how exogenous prion-like proteins derived from the gut microbiota can interfere with A β peptides aggregation. This is important because the gut microbiota is a bacterial community present in our organism all along our lives. This increases the probability of interactions between bacterial and human proteins, which could negatively affect our health. In this study, we have seen that the microbiome contains prion-like proteins capable of aggregating, acting like yeast prions, and cross-seeding amyloid β peptides. Furthermore, those proteins were found to be toxic in human neuroblastoma cells and to cause cognitive impairment in *Caenorhabditis elegans* models.

In conclusion, this study highlights several factors that can alter A β aggregation, with exogenous prion-like proteins emerging as particularly concerning. Due to lifelong exposure to the gut microbiota, these proteins represent a potential risk factor in AD pathogenesis, as demonstrated by their capacity to drive aggregation and cognitive decline in model systems.

.

Articles included in the thesis

1. Seira Curto, J., Fernandez, M. R., Cladera, J., Benseny-Cases, N., & Sanchez de Groot, N. (2023). A β 40 Aggregation under Changeable Conditions. International Journal of Molecular Sciences, 24(9). <https://doi.org/10.3390/ijms24098408>
2. Seira Curto, J., Dominguez Martinez, A., Perez Collell, G., Barniol Simon, E., Romero Ruiz, M., Franco Bordés, B., Sotillo Sotillo, P., Villegas Hernandez, S., Fernandez, M. R., & Sanchez de Groot, N. (2025). Exogenous prion-like proteins and their potential to trigger cognitive dysfunction. Molecular Systems Biology. <https://doi.org/10.1038/S44320-025-00114-4>
3. Seira Curto, J., Hernandez, S. V., Fernandez, M. R., & Groot, N. S. de. (2025). Exogenous Amyloid Sequences: Their Role in Amyloid-Beta Heterotypic Aggregation. BioRxiv, 2025.01.24.634659. <https://doi.org/10.1101/2025.01.24.634659>

The following review article was made during the thesis and used as a reference for the final thesis although not fully included in it.

4. Seira Curto, J., Surroca Lopez, A., Casals Sanchez, M., Tic, I., Fernandez Gallegos, M. R., & Sanchez de Groot, N. (2022). Microbiome Impact on Amyloidogenesis. In Frontiers in Molecular Biosciences (Vol. 9, p. 926702). Frontiers Media S.A.

List of abbreviations

Aβ	Amyloid β peptide
Aβ40	Amyloid β peptide 40
Aβ42	Amyloid β peptide 42
Apolipoprotein E	ApoE
APP	Amyloid precursor protein
cryoEM	Cryo Electron Microscopy
CryoET	Cryo Electron Tomography
Cyclin-dependent kinase 5	CDk5
Glycogen synthase kinase 3	GSK3
Ile	Isoleucine
Leu	Leucine
Phe	Phenylalanine
Protein Phosphatase 1	PP1
Protein Phosphatase 2	PP2
SR-FTIR	Syncrotron Radiation Fourier Transform Infra-red spectroscopy
Tyr	Tyrosine
Trp	Tryptophan
Val	Valine

Introduction

1. Alzheimer's disease

Alzheimer's disease is a multifactorial and progressive neurodegenerative disorder and is the most common form of dementia. The disease is characterized by cognitive impairment and a decline in visuospatial perception (Binetti et al., 1998). The symptoms, which are normally manifested at an advanced age (>65 years), vary depending on the state of the disease's progression. The primary symptoms are alterations in locomotion, loss of memory, and a decline in the immune system that affects daily life actions (Knopman et al., 2021). Alzheimer's disease has a global distribution (Figure 1) with a higher prevalence in countries with an older population. The current prevalence of Alzheimer's disease is around 57 million cases, with studies estimating an increase to around 150 million cases globally by 2050 (Nichols et al., 2022). The increased prevalence of the disease at advanced ages explains this rise in the number of cases, as there has been a global increase in the population's average age. The people affected need a series of treatments and care that carry a high economic cost. A significant portion of the direct cost for patient care is that the disease has a profound impact on the patient's relatives, as in the advanced stages, patients are often unable to care for themselves (Grabher, 2018). This cost and the widespread prevalence pose a threat to healthcare systems, resulting in less access to treatment for low-income households (Alzheimer's Impact Movement, 2016). Alzheimer's disease's first symptoms appear long after the disease has started from a molecular point of view. This increases the difficulty of diagnosis and treatment (Alzheimer's association, 2023). This is because Alzheimer's disease diagnosis has long been based only on clinical symptoms that appear at the later stages of the disease. In recent years, diagnosis has been improved, and it can now be detected at earlier stages. However, it is important to detect the disease as early as possible (Clark & Karlawish, 2003; Self & Holtzman, 2023). Treating Alzheimer's disease before cognitive symptoms become noticeable could slow disease progression and make it possible to avoid associated cognitive decline. However, when diagnosed at later stages, it is much more difficult to prevent disease progression. Current treatments, such as brexpiprazole or donepezil, address the symptoms of the disease and are unable to target the underlying causes; thus, they can alleviate the symptoms but not cure the disease. In recent years, some treatments targeting the causes of the disease have been approved by the FDA (Jaqua et al., 2024). This is the case of lecanemab and donanemab, drugs that can reduce cognitive decline and improving quality

of life. However, these drugs are not capable of stopping the disease (Jaqua et al., 2024; Self & Holtzman, 2023). This highlights the importance of enhancing current treatments and gaining a deeper understanding of how the disease is triggered and how it progresses.

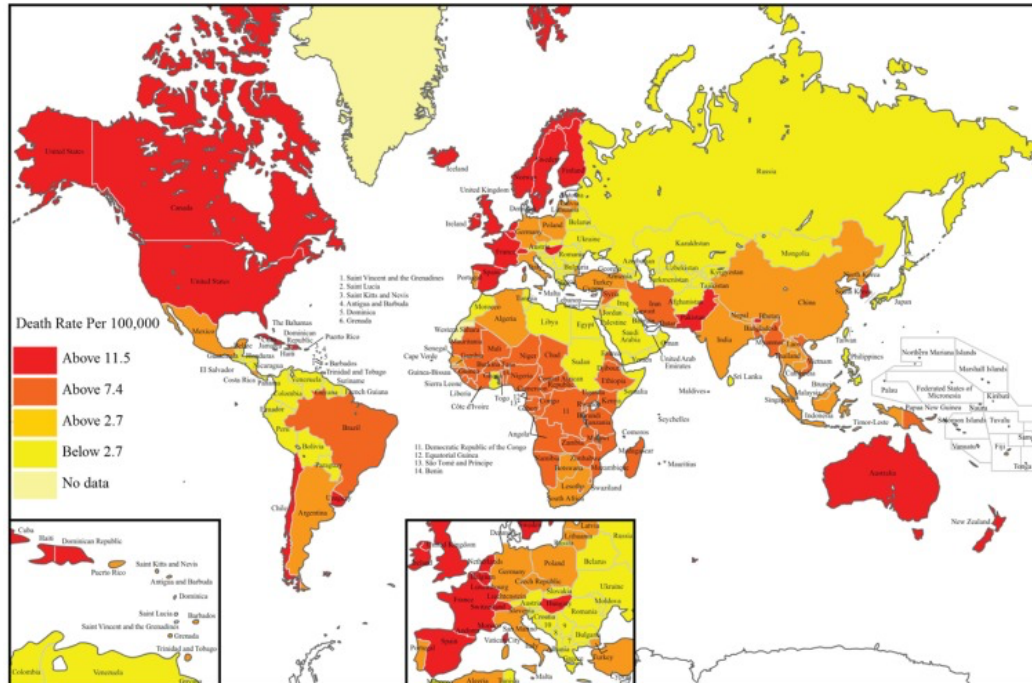


Figure 1 Global death distribution caused due to Alzheimer's disease and dementia according to WHO in 2011 (Manivannan et al., 2015)

1.1 Pathological hallmarks of the disease

Regarding the causes of Alzheimer's disease, several hallmarks have been detected. However, no clear path leading to the disease has been determined. Only in around 10% of the cases are the factors causing the disease known, and these are primarily familial variants in which the disease develops at a much younger age than usual (Dorszewska et al., 2016; Piaceri et al., 2013). The causes of sporadic forms of the disease, which account for 90% of cases, are mostly unknown (Dorszewska et al., 2016; Piaceri et al., 2013). The first and most studied factors have been the presence of neurofibrillary tangles and amyloid plaques, characterized by intramolecular beta sheet structure. These hallmarks were first seen by Alois Alzheimer and were studied more thoroughly in the second half of the 20th century, leading to the current state of knowledge (Shemesh & Spira, 2010).

Amyloid plaques are extracellular accumulations of aggregated A β peptides, primarily located in the hippocampus and the frontal cortex, and are present from the earliest stages

of the disease (Furcila et al., 2019; Hoesen & Hyman, 1990; Shemesh & Spira, 2010). The hippocampus is a brain region associated with the formation of new memories, while the frontal cortex is involved in planning and executing activities. These areas, in addition to exhibiting amyloid plaques, often show high levels of neuronal death. In contrast, neurofibrillary tangles are intracellular aggregates of Tau protein that appear in later stages of the disease (Duyckaerts et al., 2009; Furcila et al., 2019; Shemesh & Spira, 2010). Tau is typically a soluble protein, but in Alzheimer's disease, tau becomes hyperphosphorylated and misfolds, leading to the formation of insoluble aggregates.

The amyloid plaques can be classified according to their density. For example, dense plaques are formed by fibrils, while diffuse plaques are formed by amorphous aggregates (Figure 2). It has been hypothesized that the diffuse plaques could be a previous step in the formation of the dense plaques and could have the first toxic effects (Duyckaerts et al., 2009). This has raised concerns about the potential differences in toxicity between various forms of the amyloid peptide.

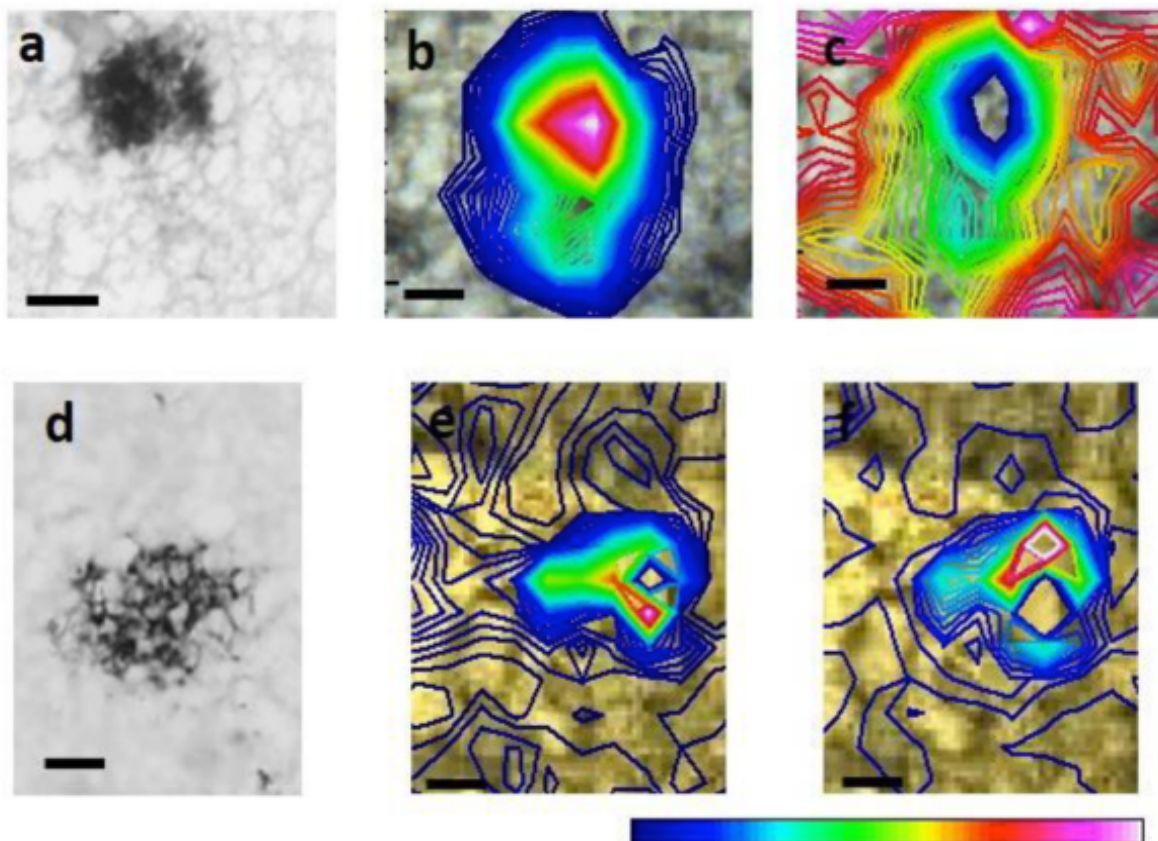


Figure 2 SR- μ FTIR and anti-A β antibody imaging of different types of plaques (Álvarez-Marimon et al., 2021) a) Fibrillary plaque stained with anti-A β antibody staining. b) Absorbance ratios corresponding to fibrillary amyloid aggregation ($1630\text{ cm}^{-1}/1657\text{ cm}^{-1}$) c) Absorbance ratios corresponding to unordered ($1645\text{ cm}^{-1}/1657\text{ cm}^{-1}$). d) Unordered plaque stained with anti-A β antibody staining. b) Absorbance ratios corresponding to fibrillary amyloid aggregation ($1630\text{ cm}^{-1}/1657\text{ cm}^{-1}$) c) Absorbance ratios corresponding to unordered ($1645\text{ cm}^{-1}/1657\text{ cm}^{-1}$).

Both the tau and the A β peptides are conserved functional endogenous proteins, thus research has focused on how their aggregation is initiated. Other factors apart from forming part of the neurofibrillary tangles and amyloid plaques are that most familial Alzheimer's disease cases have mutations to genes related to the amyloid precursor protein (APP) or its processing (Hatami et al., 2017). Also, Alzheimer's disease is more prevalent in individuals presenting Down syndrome, a pattern that has been related to the presence of APP gene on chromosome 21, the chromosome triplicated in this syndrome (Wiseman et al., 2015). This has led to the development of the amyloid-cascade hypothesis and the amyloid hypothesis. Both hypotheses posit to the formation of an initial aberrant and toxic amyloid aggregate, that causes a cascade of events and leads to the development of the disease (Karran et al., 2011; Selkoe & Hardy, 2016). This is further reinforced by the clear association between disease progression and the presence of amyloid plaques. However, other hypotheses such as the vascular hypothesis, have been proposed. The vascular hypothesis is based on the number of amyloid plaques that are associated with blood vessels, as hypoperfusion can cause cognitive decline and memory loss (De La Torre, 2010; Scheffer et al., 2021). Hypoperfusion leads to ischemia, causing oxidative stress in the neurons surrounding blood vessels. According to this theory, amyloid plaques may originate from microhemorrhages that cause ischemia, leading to an overproduction of the A β peptide (Kalaria, 2000; Scheffer et al., 2021). Another theory involves oxidative stress, as the stress level is increased in Alzheimer's patients. This oxidative stress has been linked to the accumulation of metal ions observed in amyloid plaques (Álvarez-Marimon et al., 2021; Huang et al., 2016).

Recently, the microbiome has gained increasing attention, as the relationship between pathogens and neurodegeneration has been established (Seira Curto et al., 2022). Amyloid structures from microorganisms could possibly interfere with host proteins, leading to the formation of aggregates. This is the case in Parkinson's disease, where it has been suggested that the protein misfolding process could begin in the gut (Kwon et al., 2024). In addition, patients with chronic infections are more susceptible to neurodegenerative diseases. Based on these observations, our goal is to study how these microbial proteins could affect the aggregation of A β peptides (Butler & Walker, 2021). A β peptides, and to a lesser extent Tau, circulate throughout the body under non-pathogenic conditions and may therefore be exposed to proteins from the microbiome (Avila et al., 2004).

1.2 Tau protein

The Tau protein occurs at increased concentrations in the axons of neurons. The function of Tau is associated with microtubule stabilization and vesicle transport (Avila et al., 2004; Guo et al., 2017). However, in pathological conditions the protein is hyperphosphorylated and aggregated forming insoluble fibrils (Figure 3) (Mishan et al., 2019). The hyperphosphorylated tau protein has been correlated with cytotoxicity, being able to promote apoptotic cell death (Avila et al., 2004; Guo et al., 2017). Although there is a correlation between extracellular neurofibrillary tangles and neuronal death (Sebastián-Serrano et al., 2018), it has been suggested, as for A β peptides, that the fibrillar forms are more inert and less toxic than the intermediate conformations (Ghag et al., 2018). Intracellular tangles have been also observed and are suggested to cause cell death (Fukutani et al., 1995). The pathological hyperphosphorylation seems to be due to a dysregulation of control pathways. In those cases, the phosphatases PP1 and PP2 malfunction, while the kinases GSK3 and CDK5 are active, leading to hyperphosphorylation of the tau protein due to an imbalance between the activities of the phosphatases and kinases (Bennecib et al., 2000; Rios et al., 2023; Rissman et al., 2004). Tau hyperphosphorylation also causes a disassembly of the cytoskeleton, one of the causes of neuronal dysfunction (B. Li et al., 2007). Apart from Alzheimer's disease, tau accumulation has been linked with another group of disorders which is known as tauopathies. (Mishan et al., 2019)

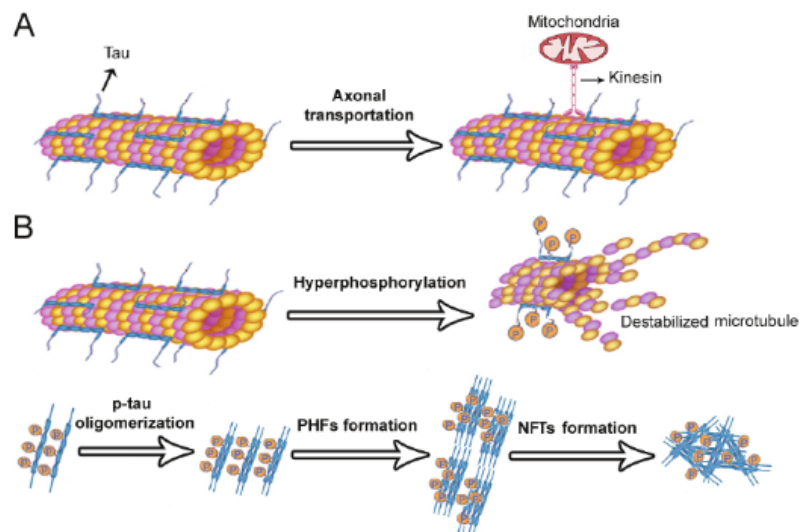


Figure 3 Tau protein in physiological and pathological conditions (Mishan et al., 2019). a) Physiologically tau binds to microtubules, stabilizing them. b) In pathological conditions, tau is hyperphosphorylated, leading to microtubule destabilization and leading to the formation of oligomers and ultimately, the development of neurofibrillary tangles.

2. A β peptides

A β peptides originate from the processing of the transmembrane protein APP and are usually found extracellularly, hence being exposed to microbial proteins. Normally, APP is processed by α -secretases, leading to a non-amyloidogenic pathway, while in Alzheimer's disease, there is an increase in the processing by β -secretases and γ -secretases (Figure 4) that leads to the formation of different amyloid peptides, from a length of 39 to 43 amino acids, with A β 40 and A β 42 being the most prevalent species (O'Brien & Wong, 2011; Rahman et al., 2020). In non-pathogenic conditions, both peptides are found in the organism, A β 40 being more prevalent (O'Brien & Wong, 2011; Rahman et al., 2020). However, in the case of the amyloid plaques, their concentrations are reversed A β 42 being the most prevalent. This is mainly due to their physicochemical qualities, A β 42 being much more hydrophobic than A β 40 (Murphy & Levine, 2010). The A β peptides occur in the cerebrospinal fluid and plasma. The functions of APP and the amyloid peptides have not been fully elucidated. APP possibly functions in vesicle traffic and neuronal survival; the A β peptide has been reported to be a signaling molecule, involved in bone healing, bone regeneration and antimicrobial defenses (Coronel et al., 2018). Since A β 42 levels may increase under pathological conditions, the A β 42/A β 40 ratio in the plasma is used as a diagnostic marker for the disease (Pérez-Grijalba et al., 2019).

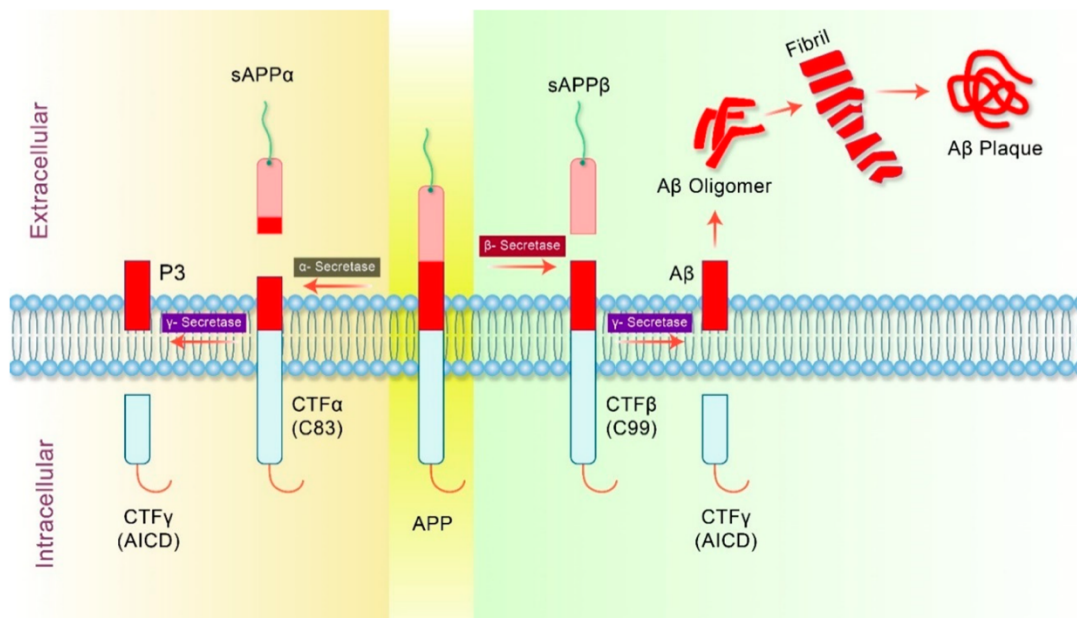


Figure 4 APP processing pathways in Alzheimer's disease (Rahman et al., 2020). In the non-amyloidogenic pathway APP is cleaved by α -secretase giving an intracellular fragment CTF α and an extracellular fragment sAPP α . CTF α can be further cleaved by γ -secretases giving P3 and CTF γ . In the amyloidogenic pathway APP is first processed by β -secretases giving extracellular sAPP β and CTF β which is further cleaved by γ -secretases giving CTF γ and the A β peptides.

2.1 The A β peptide sequence

The amyloid peptides range from a length of 39 to 43 amino acids, with A β 40 and A β 42 being the most prevalent forms. In healthy individuals, A β 40 accounts for about 90% of the total amount, while A β 42 accounts for around 10%. However, in the case of the amyloid plaques, these concentrations are reversed, with A β 42 being the most abundant form. This is due to their physicochemical properties, as A β 42 is much more hydrophobic than A β 40 (Murphy & Levine, 2010).

The hydrophobicity and aggregation propensity of A β peptides are determined by their amino acid sequences (Figure 5).



Figure 5. Sequence comparison of A β 40 and A β 42. Hydrophobic amino acids are shown in red. The two common aggregation prone regions (“hot spots”) are highlighted with blue lines.

The primary difference lies in two additional hydrophobic amino acids at the C-terminus, which increase the aggregation propensity of A β 42. This enhanced propensity to aggregate has been linked to the higher toxicity of A β 42 and may explain its accumulation in the amyloid plaques (Sgourakis et al., 2007).

2.2 A β peptide aggregation

A β peptides aggregate forming amyloid fibrils characterized by an intramolecular β -sheet structure. Its formation starts with the association of monomeric peptides, generating oligomers that subsequently lead to the growth of amyloid fibrils. This has been described as a low-energy folding process distinct from the protein globular landscape, where the oligomers represent local minima of the folding energy, and the amyloid fibrils are a global minimum (Dill et al., 2008; Raskatov & Teplow, 2017). Normally, protein folding should yield a stable structure without forming aggregates; however, changes in the environment or

external factors cause a switch to this conformational pathway, leading to aggregation (Figure 6). In familial Alzheimer's, mutations alter the peptide sequence, making the protein more prone to aggregation. In other cases, environmental factors such as changes in pH or interference with already aggregated proteins can lead to changes in the aggregation pathway. In this work, we have focused on studying these environmental effects and how they alter the aggregative behavior.

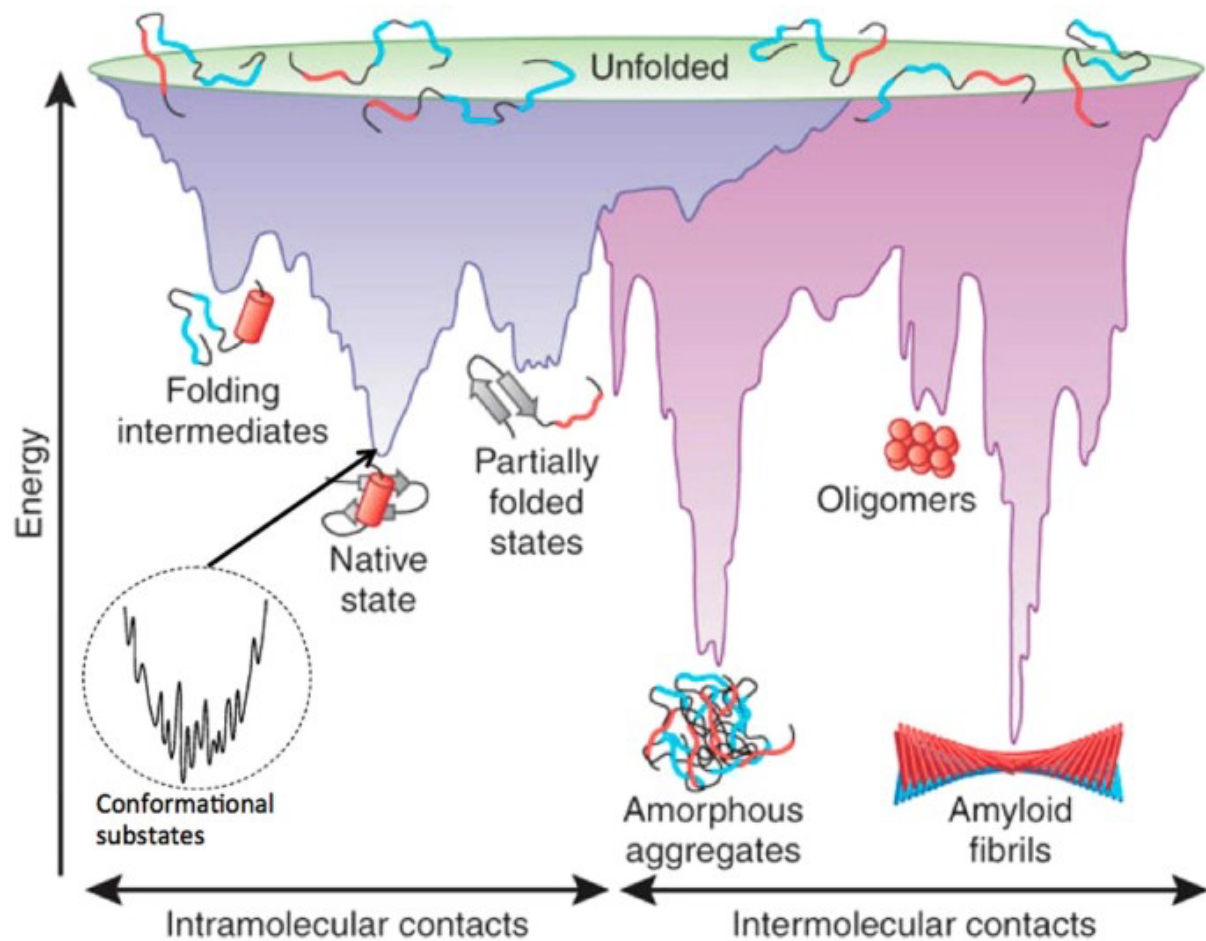


Figure 6 Energy landscape for protein folding and aggregation (Raskatov & Teplow, 2017). It is shown how unfolded proteins have the maximum free energy levels and folding them can lead to the native state which is the more stable point that can be reached through intramolecular contact. On the other hand, aggregating proteins can move to the part of the funnel driven by intermolecular contacts, being oligomers one of the less stable forms, being local minima and the amyloid fibrils being the total minima.

The aggregation of A β peptides can result in different conformations (amorphous, fibrillar or oligomeric), depending on the state and local conditions under which the aggregation occurs. The oligomeric conformations are an intermediate formed during fibrilization (Sengupta et al., 2016), whereas amorphous aggregates are energy minima states that, unlike fibrils, lack a defined structure. Amorphous aggregates are usually formed due to environmental factors

that promote rapid aggregation, preventing them from organizing into fibrils. These aggregates, together with the oligomeric species, exhibit higher toxicity than the fibrils alone.

The kinetics of the A β peptides aggregating into amyloid fibrils, has been highly monitored through several methods, one of the most used ones is the thioflavin-T fluorescent dye. Thioflavin T intercalates between the beta-sheets of the amyloid fiber, which reduces its vibrational mobility. As a result, when excited at the appropriate wavelength, it emits energy in the form of fluorescence (Xue et al., 2017). The increase in fluorescence enables monitoring of the formation of new amyloid fibrils from monomers. Although it has been highly studied, no direct correlation between kinetics and disease has been established. Also, high variability in the kinetics has been observed. Hence, it is very important to study the conditions that alter the aggregation kinetics and ensure the stability of the compounds used for it. Thioflavin T kinetics of A β peptides obtained *in vitro* follow a sigmoidal curve characterized by three phases: (i) lag, (ii) exponential and (iii) plateau (Figure 7). This has been defined as a nucleation process that proceeds in a stepwise manner (Meisl et al., 2016; Seira Curto et al., 2025).

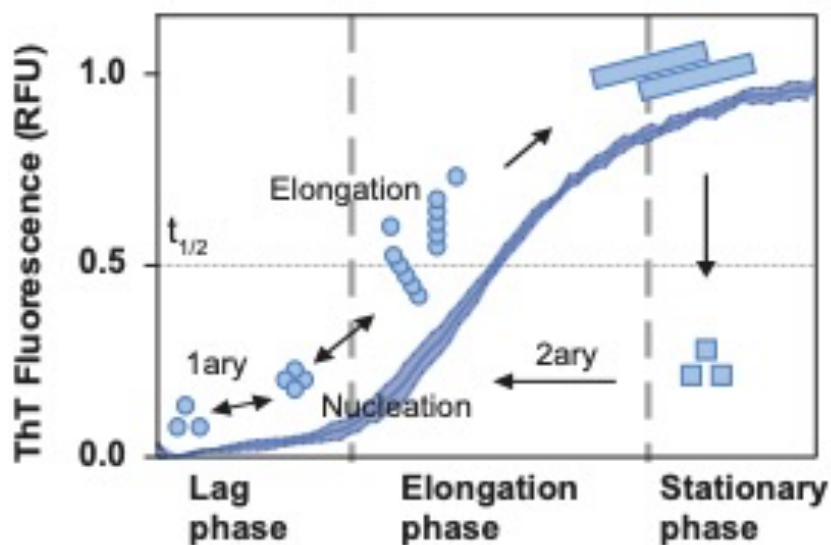


Figure 7 Schematic representation of a Thioflavin T amyloid kinetics (Seira Curto et al., 2025). The first step of the process is the lag phase, characterized by primary nucleation processes. The second step is the Elongation phase, characterized by secondary nucleation, elongation and fragmentation process. The third step is the plateau or stationary phase, which is characterized by an equilibrium between aggregation and disaggregation processes.

The lag phase is characterized by primary nucleation, where monomers bind together to form nucleation cores. The nucleation cores comprise several monomeric molecules that act as points of initial fibril formation. The formation of the nucleation cores is the slowest part of

the process and depends on the aggregative propensity of the molecules and their interaction with the environment. Between the end of the lag phase and the beginning of the exponential phase, there is a critical number of nucleation cores that can be used to grow amyloid fibrils through elongation processes. New fibrils can grow from monomers binding the already existing fibrils, through a secondary nucleation process. In addition, the formed fibrils can break apart, forming new nucleation cores, which is accompanied by a rapid increase in the fluorescence. In the case of elongation and secondary nucleation processes, we can have one-step mechanisms, where monomers directly bind to the existing fibril, either becoming part of the fibril or initiating a new fibril core. Additionally, two-step processes may occur, in which monomers first bind to fibrils, forming intermediate fibril-monomer complexes that subsequently convert into mature fibrils or new nucleation cores. Although these processes can take place, they don't usually act together which is why several types of models have been established for the different types of aggregation kinetics (Meisl et al., 2016; Wei et al., 2025). Characterizing the kinetics can enhance our understanding of how the fibrils form. The final part of the kinetics is the plateau phase. The plateau phase is reached when most of the monomers have aggregated. At this point, an equilibrium is established between the aggregation and disaggregation processes.

From a biomedical perspective, identifying which A β peptide conformations exhibit toxicity is essential. The oligomers appear to be more toxic than fibrils and may therefore be linked to the disease. Fibrils, protofibrils, and oligomers have been reported to bind to microglia, promoting the release of pro-inflammatory cytokines that lead to neuroinflammation and neurodegeneration (Sondag et al., 2009). Oligomers also seem to be involved in this inflammatory reaction by interacting with membrane receptors. Apart from this, oligomers can also increase membrane permeabilization (Ghag et al., 2018; Sengupta et al., 2016).

2.3 The A β peptide structure

Amyloid fibrils, independently of their polypeptide sequence, exhibit a characteristic amyloid fold consisting of stacked β -strands arranged in a cross- β architecture. The fibrils usually have a diameter of between 10 and 20 nm and are composed of a varying number of protofilaments that can assemble in different arrangements (Fitzpatrick et al., 2013). Inside the aggregate the β -strands are arranged perpendicularly, forming a cross- β -sheet motif. This motif was one of the first characterized through its X-ray pattern, where reflections at 4.7Å

and at 10 Å indicate the distances between the β -strands and between adjacent β -sheets respectively as shown in Figure 8 (Fitzpatrick et al., 2013; Nelson et al., 2005; Vahdat Shariatpanahi, 2019). Initially, this cross- β -sheet arrangement was thought to form structurally uniform fibrils. These early structures were obtained from fibrils assembled *in vitro* and from synthetic peptide.

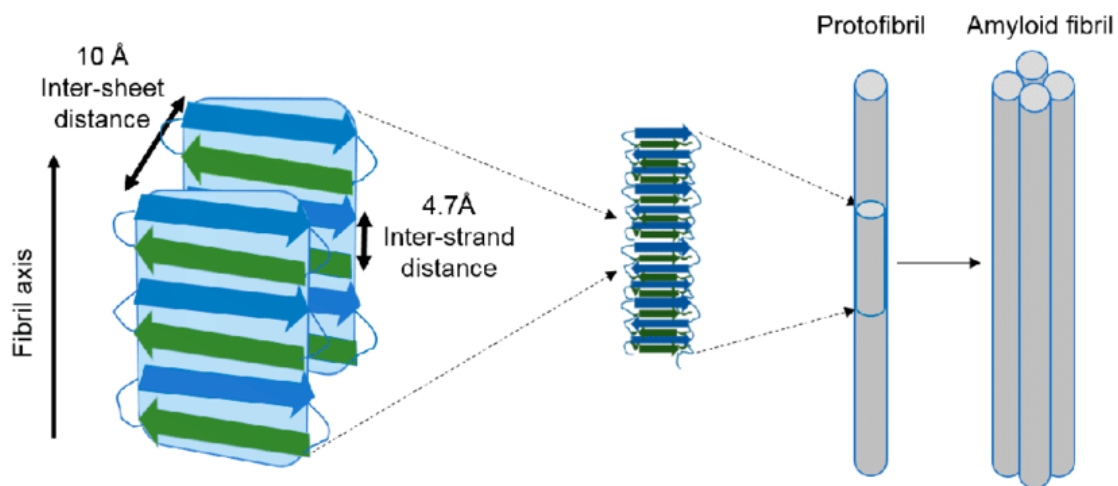


Figure 8 Schematic representation of the cross- β sheet structure showing the inter-sheet and inter-strand distances and their distribution in protofibrils that conform the amyloid fibrils (Vahdat Shariatpanahi, 2019).

However, due to the development of cryo-electron microscopy (cryoEM) a large number of structures have been obtained. These samples have shown numerous different structures arising from a single polypeptide sequence (Aubrey & Radford, 2025; Wilkinson et al., 2023). Although all amyloid fibrils contain β -strands, the arrangement of both the strand and the protofibrils can vary among fibrils formed from the same peptide as shown in Figure 9, where how the structure can vary even in the same fibril can be seen. Interestingly, fibrils obtained from *in vivo* samples are significantly more homogeneous than those prepared *in vitro* (Aubrey & Radford, 2025). The polymorphism of amyloid fibrils occurs at various levels, from the amino acid sequence to the composition and number of monomers within the fibril core, leading to variations in fibrils characteristics. It is important to note that fibril structures influence both the protein's functional role and also its toxicity, as only certain amyloid fibril structures are associated with pathogenesis (Marshall et al., 2014). Hence, it would be valuable to determine the factors that determine these conformations, as blocking their formation could potentially halt disease progression. The current challenge in amyloid research is that, although many structures have been solved, there is no clear connection

between the structure and toxicity or functionality. In this field, possible improvements in cryo-electron tomography (cryoET) could provide insight into the structures of the fibrils in *in vivo* settings (Gilbert et al., 2024). Regarding oligomers, these are not as well characterized due to their transient nature, small size, and heterogeneity, which are key problems for techniques such as cryoEM. It is essential to note that when referring to oligomers, we are not dealing with a single, stable group of molecules with a shared structure, but rather a heterogeneous population of molecules with different conformations (Shea & Daggett, 2022).

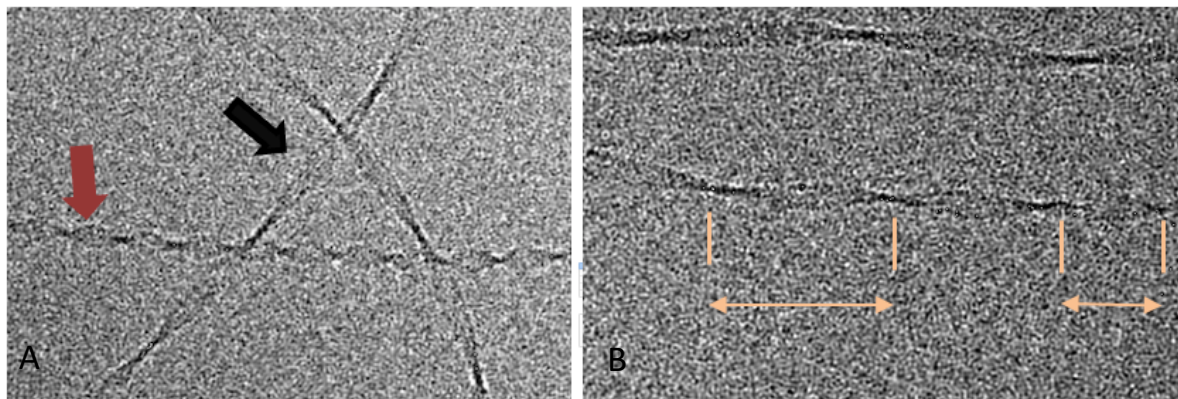


Figure 9 The same sequence can have different folds. Preliminary data obtained by our group in the CryoEM facilities at ALBA synchrotron in collaboration with Damià Garriga. a) From the same preparation of Aβ peptides in presence of exogenous prion-like proteins two clear conformations are spotted. Pointed by the black arrow the one with a bigger helical rise while the one with the red arrow points at a fiber with a much smaller helical rise making a much bigger number of twists per the same length. b) The helical rise changes in the same fibril as shown by the orange arrow showing the variability even inside a same fibril.

This polymorphism and abundance of structures highlight the importance of studying the factors that can alter the aggregate structures and determine their final conformational pattern. Amyloid plaques are exposed to a wide range of elements, including proteins, nucleic acids, and metals (Álvarez-Marimon et al., 2021; Suzuki & Nakaya, 2008). Moreover, amyloid peptides respond differently to changes in ionic strength and pH. While exogenous factors can further alter protein aggregation (Seira Curto et al., 2023). It is essential to investigate the interplay among these factors to better understand their implications for fibril formation and disease progression.

2.4 A β prion properties

Another important factor concerning the pathogenic role of A β is its prion-like properties. A β peptides are considered prion-like due to their ability to aggregate and transmit the pathological conformations from cell to cell, promoting the spread of neurodegenerative processes in a manner similar to prion proteins. Prions are a group of amyloids that are also capable of propagating between cells and organisms and, by doing so, are infectious (Sabate et al., 2015). For this reason, they share many common properties with non-prion amyloids. Amyloids are characterized by having a common fold pattern, the cross- β -sheet. This pattern allows for interplay between molecules, as they have similar structures (Chiti & Dobson, 2006; Jain, 2024). In the case of A β , although it is not transmissible under normal conditions, some rare cases of transmission have been reported (Banerjee et al., 2024). In those cases, the patients were directly treated with elements isolated from humans such as human growth hormone (Banerjee et al., 2024). This transmissibility of conformation makes it even more crucial to detect the disease at the early stages and to eliminate the aberrant A β peptide, as its conformation can be transmitted. A common feature of amyloids is their hydrophobicity and the ability to form hydrophobic interactions (Monsellier et al., 2008; Rousseau et al., 2006; Stefani, 2012). This hydrophobicity is necessary at least in short specific regions, known as hot spots, that act as facilitators and lead the aggregation of the full protein or peptide (De Groot et al., 2005; Espargaró et al., 2015; Esteras-Chopo et al., 2005; López De La Paz & Serrano, 2004). They are characterized by a significant presence of hydrophobic residues, including both aliphatic (Val, Leu, and Ile) and aromatic residues (Phe, Tyr, and Trp) (Espargaró et al., 2015; Monsellier et al., 2008). Thus, the removal of these hot spots can eliminate the protein's aggregation ability, while the addition of hydrophobic sequences can restore it (De Groot et al., 2005; Espargaró et al., 2015; Esteras-Chopo et al., 2005). They also generally have opposite charges, as this favors the attraction between separate molecules. These hot spots are usually flanked by gatekeeper regions, which are responsible for maintaining tight control over aggregation. These regions are rich in proline, which is incompatible with the cross- β -sheet structure and charged residues that increase repulsion (E Rousseau et al.; Monsellier et al., 2008). Such hot spot regions, which have clearly defined parameters, can be predicted using molecular models. Several computational tools are available to predict proteins capable of aggregating into amyloid fibrils. For example, AGGRESCAN and Zyggregator analyze the properties of each amino acid and its neighboring residues to identify aggregation-prone

regions (Conchillo-Solé et al., 2007; Planas-Iglesias et al., 2024; Tartaglia & Vendruscolo, 2008).

2.5 Intrinsic aggregation modifiers

It is important to determine the factors that alter A β peptide aggregation by changing properties such as concentration, pH or salt levels. Among these, concentration is one of the main factors distinguishing *in vitro* from *in vivo*. The *in vitro* methods can reach higher concentrations of the isolated peptide than those typically present *in vivo*. An increase in peptide concentration promotes both the aggregation rate and the type of aggregates formed. Thus, concentration can determine not only whether the peptides aggregate but also whether the resulting aggregates are amorphous or fibrillar (Novo et al., 2018).

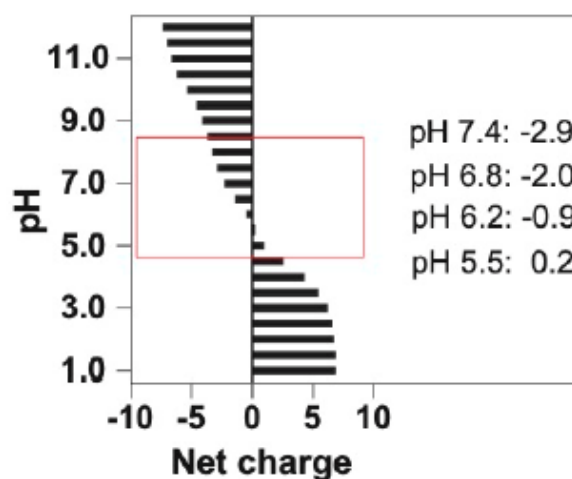


Figure 10 A β peptide charge at different pH values (Seira Curto et al., 2023). A β 40 at physiological pH has a negative charge while at acidic pH two histidine protonate leading to a more positive charge.

The pH and ionic strength of the media are important, as the aggregation of the peptide is correlated with its electrochemical properties. Alzheimer's patients have a lower pH in the brain and cerebrospinal fluid (Decker et al., 2021). In addition, alterations of endosomal and lysosomal pH have been associated with malfunctions in A β peptide clearance and the formation of extracellular plaques (Lee et al., 2022; Prasad & Rao, 2018). This malfunctioning of peptide clearance can cause an accumulation of A β peptides, leading to an acceleration of the aggregation process. The ionic strength can modulate A β peptide aggregation, as at a neutral pH the peptide has a negative charge (Figure 10); salts can shield the peptide's charge, leading to a more ordered aggregation process compared to conditions without salt (Meisl et al., 2017). The amyloids formed under a highly acidic pH differ in toxicity compared to those

formed at a neutral pH (Benseny-Cases et al., 2007, 2012). In this context, the first part of the present study aimed to investigate how aggregates form across a pH range (pH 5.5 to 7.4) similar to those observed in altered endosomes and lysosomes *in vivo* and how salts can play an important role under these conditions.

Another important factor that alters peptide aggregation is its interaction with previously aggregated A β peptides in a process called seeding, where pre-aggregated molecules act as additional nucleation sites that recruit monomers, altering the aggregation process. As explained above, the formation of nucleation cores is the limiting factor that determines the length of the lag phase; hence, the presence of pre-aggregated structures can significantly accelerate the aggregation process (Olsson et al., 2018). Importantly, *in vivo* the seeding can occur between different species of the A β peptides, increasing the aggregation complexity (X. Li et al., 2022; Ren et al., 2019). Seeding and cross-seeding processes are also capable of transmitting folding patterns. Since amyloid fibers can have multiple structures, specific seeds can transmit their structure as strains of A β fibrils (Cohen et al., 2016; D. Li & Liu, 2022; Makowski, 2020). This property permits the extraction of structures from tissues by isolating the fibrils and then amplifying their concentration in the presence of new monomers, increasing their availability for subsequent analysis (Yang et al., 2022). From a biological perspective, this property suggests that a pathological amyloid conformation could form at a specific location, under particular conditions or due to an external cause, and then propagate throughout the organism much like an infectious disease (D. Li & Liu, 2022).

The last intrinsic factor that we consider is time, a factor that is often overlooked. Amyloid fibrils are generally considered stable and unchanging over time. However, recent experiments have shown that this assumption is not untenable. Amyloid fibrils at the plateau phase do not remain stable; rather, the fibrils can change their structure, forming new folds with different properties (Wilkinson et al., 2023; Willis et al., 2025). In this way, the fibrils kinetics do not stop at the plateau phase. Although the concept of fibril maturation is not new, it was previously unknown how the folding pattern could change after fibril formation. This factor, together with the strain-transmissible effects, could explain, in part, the apparent homogeneity observed in amyloid fibrils obtained from *in vivo* samples. The amyloid samples from patients have undergone a long maturation process that could have led to a prominent species that would be transmitted to newly synthesized monomers. This could make it even

more difficult to identify the toxic species that caused the disease, this amyloid fibril may become erased from the patient at the end stages of the disease.

2.6 Extrinsic aggregation modifiers

After analyzing the intrinsic factors that affect A β peptide aggregation, it is also crucial to consider extrinsic elements, those not related to the polypeptide sequence itself, including both endogenous factors from the organism and exogenous molecules that may enter the system.

Endogenous proteins

Several proteins have been demonstrated to interact with the A β peptides or play a role in their clearance and oligomerization. One of the most well-studied examples is apolipoprotein E (ApoE), whose primary role is lipid transportation as a component of lipoproteins (Hatters et al., 2006). However, mutations of this protein are correlated with a higher prevalence of Alzheimer's disease and an earlier onset of the disease (Muñoz et al., 2019; Prasad & Rao, 2018; Wisniewski & Drummond, 2020). It is essential to investigate the effects of protein interaction with the A β peptides, as they can enhance the aggregative propensity or lead to specific pathological conformations. A β peptides are evolutionarily conserved; they have important functions and are bound to interact with other proteins. Additionally, there may be potential inhibitors of this pathological conformation that could inspire new therapeutic approaches.

Lipids

Lipids have significant interactions with A β peptides. Firstly, the peptides originate near the cell membrane, where they are cleaved from APP, and there is an association between cell membranes and amyloid plaques (Cecchi & Stefani, 2013; Mrdenovic et al., 2022). The toxicity of A β peptides has also been associated with their interaction with membranes, as they can insert into the membrane, forming pore-like structures and increasing membrane permeability (Viles, 2023). Another notable observation is that lipidic membranes can accelerate the formation of oligomeric species of A β peptides. This makes lipids a sensitive element, as they are exposed to an increased concentration of A β peptides. Additionally, the

lipidic layer, particularly the negatively charged microenvironment, can influence the behavior of the peptide and expose it to aberrant aggregative amyloids (Sun et al., 2017).

Metals

There is a direct relationship between metals and A β peptides. Amyloids contain metal-binding sites, and accumulations of metals surrounding the amyloid plaques have been observed in human and mouse brains (Figure 11) (Álvarez-Marimon et al., 2021). Also, metals can alter A β aggregation kinetics (Abelein, 2023; Ha et al., 2007). The fact that metals are associated with oxidative processes has sparked research into the oxidative toxicity of A β peptides. As mentioned previously, metals colocalize with amyloid plaques in tissues associated with lipid peroxidation (Álvarez-Marimon et al., 2021; Sultana et al., 2009). For this reason, it has been suggested that metals may accumulate due to the fibrils and thereby cause oxidative damage. In line with this, amyloid plaques without oxidative damage have lower amounts of metals.

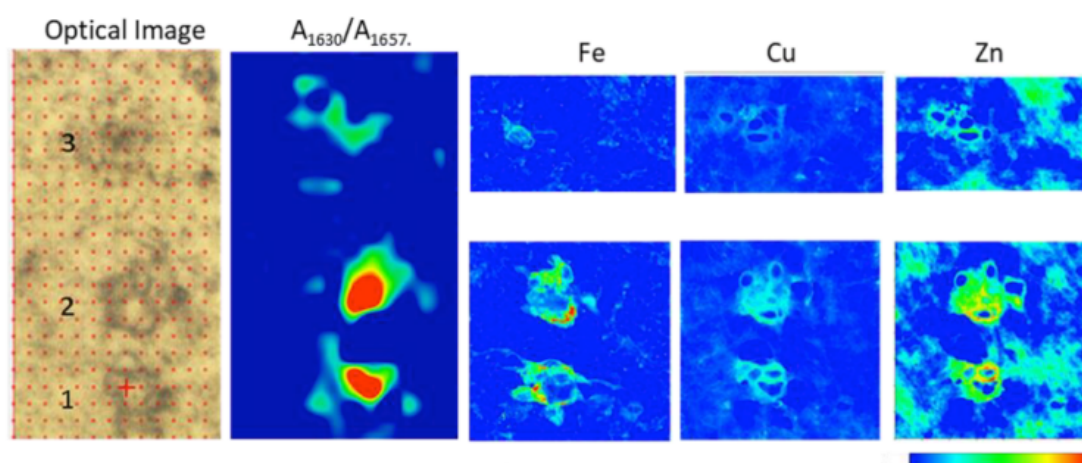


Figure 11 SR- μ FTIR and ST-nXRF showing the colocalization of amyloid plaques and metals (Álvarez-Marimon et al., 2021). Optical image with the three amyloid plaques numbered. μ FTIR distribution of β -sheet aggregation ($1630\text{ cm}^{-1}/1657\text{ cm}^{-1}$) and metal distribution of the same area for iron, copper and zinc.

Nucleic acids

Nucleic acids are usually not associated with A β peptides, as they are located in different areas, although in some cases, contact between them may occur, and it is important to consider these possible scenarios. A β peptides in early stages of the disease can aggregate intracellularly, where they may come in contact with nucleic acids (Chung et al., 2022; Villarejo et al., 2022). Also, contact could occur in cases of cell death and apoptosis. It has also

been reported that amyloid fibrils containing nucleic acids can cause systemic autoimmunity, illustrating the dangers of this association (Di Domizio et al., 2012).

Exogenous aggregation proteins

Another type of exogenous factor that can alter the aggregation of A β peptides arises from external influences. A β peptides can be cross-seeded by various aggregating proteins (Ren et al., 2019; Zhou et al., 2012). In this study, we focus on exogenous prion-like proteins of bacterial origin, which are capable of forming amyloid fibrils (An et al., 2016; Giraldo, 2024). These proteins are of particular interest because the organism is exposed to a large number of such molecules during its lifetime. Interactions with exogenous prion-like proteins may shift A β peptides from their typical non-pathological pathway toward aggregation, thereby contributing to disease.

3. The human microbiome

The term microbiome refers to the microorganisms living in the human body. The human microbiome comprises more than 1000 bacterial species harboring more than 150 times the number of human genes (NIH, 2009; Qin et al., 2010). The majority of the microbiome is located in the gut, where the number of human cells is 10 times smaller than the number of microbial cells (Qin et al., 2010). The metabolic activity of the microbiome surpasses that of the liver and plays a role in various vital processes, including carbohydrate fermentation and absorption (Bhattacharjee & Lukiw, 2013; Hill & Lukiw, 2015). The microbiome also acts as a defense against pathogens through a competitive effect and by supporting infection and disease resistance (Bhattacharjee & Lukiw, 2013). For these reasons, the microbiota has been referred to as the largest diffuse organ system found in the human body. However, the microbiome should not be seen as something fixed. Its composition can be altered by age, diet, environment, and other factors. It is important to consider this variability, as no two individuals share the same microbiome. Additionally, changes in its composition can lead to dysbiosis, which negatively impacts human health. An imbalance in the microbiota is associated with inflammatory and autoimmune disorders and can contribute to diseases such as obesity, diabetes and cancer (Dua P, 2015; Hill et al., 2014; Liu et al., 2022; Miller et al., 2021). In this study, we will focus on the emerging relationship between neurodegenerative diseases and the human microbiome. First, there is a bidirectional communication system

between the gut and the brain, the so-called gut-brain axis. Individuals with neurodegenerative diseases have an altered gut microbiome, which frequently precedes the appearance of cognitive symptoms (Friedland & Chapman, 2017; Hill-Burns et al., 2017; Peterson, 2020). A clear example is *Helicobacter pylori*, a recognized risk factor for developing Alzheimer's disease. Alzheimer's disease patients have a higher presence of antibodies against these bacterial species in the cerebrospinal fluid and infection has been reported to increase the risk of developing Alzheimer's disease by at least 11% (Albaret et al., 2020; Kountouras et al., 2006). Another important factor concerning *Helicobacter pylori* is that the proteins that this bacterium produces are capable of crossing the blood-brain barrier, leading to neuroinflammation (Noori et al., 2023).

3.1 Amyloids in the microbiome

Amyloids are widespread in the bacterial world and serve different functional roles. In different habitats, such as seawater or sludge, the proportion of amyloid-positive bacteria has been reported to range from 5% to 40% (Larsen et al., 2007). These findings indicate that amyloids are not a rare feature limited to a few bacterial species, but rather a common and widespread phenomenon within the bacterial domain. This has been supported by computational approaches that have shown that 0.3% of all bacterial genes contain prion-like domains (Harrison, 2019). Although this percentage may seem low, it represents an average across all known bacterial genes and in some species, such as *Staphylococcus aureus*, this can reach up to 18% (Iglesias et al., 2015; Yuan & Hochschild, 2017).

Microbiome amyloids are generally extracellular proteins (Blanco et al., 2012) interacting with the environment as sensors and contributing to bacterial adaptation (Barnhart & Chapman, 2006; Gebbink et al., 2005). Their extracellular location could be associated with a reduction in bacterial intracellular toxicity and the associated energetic costs. Their functionalities are usually associated with adhesion, biofilm formation and invasion (Barnhart & Chapman, 2006; Gebbink et al., 2005). Other functionalities are illustrated by Microcin E492, a bacteriocin that, when exported in monomeric and oligomeric forms, creates pores that induce bacterial lysis. However, when it is in an amyloid fibrillar form, it acts as a reservoir and only when specific environmental changes occur are the monomers released, producing the toxicity (Shahnawaz & Soto, 2012). In the case of adhesins, these fibrillar amyloids form biofilms that are involved

in host colonization (Dueholm et al., 2010; Larsen et al., 2008). It is interesting to observe how bacteria are prepared for the toxicity that could be caused by these functional amyloids. The amyloids' function is safeguarded by chaperones that protect against intracellular aggregation, by spatial compartmentalization for precise localization of the aggregation and by temporal control, preventing aggregation until necessary. These tight regulations indicate that, although functional, bacterial amyloids require careful control similar to human amyloids.

One of the best-studied examples is Curli, a bacterial amyloid involved in extracellular matrix formation. Curli proteins are encoded by seven genes organized into two operons (Bhoite et al., 2019), allowing a tight regulation of their production. Additionally, two specific chaperones prevent amyloid formation until the proteins are transported outside the cell (Evans et al., 2015). All this highlights that while amyloids are functional and beneficial for the bacteria, they can also pose a risk to the cell. This is particularly relevant since these bacteria can reside within the human body.

3.2 Microbiome amyloids and neurodegenerative disease

Due to the large number of amyloids produced by the microbiome, it is important to understand their interplay with neurodegenerative diseases. Proteins produced by the microbiome can remain in contact with the host for years or even decades later if the bacteria responsible for their production persist within the microbiota. Consequently, the probability of interactions between microbial and human amyloids is high and should not be overlooked. Studying the gut-brain axis is particularly important, as imbalances in the microbiota can contribute to disease development, as illustrated in Figure 12.

Patients with Alzheimer's disease or Parkinson's disease have altered gut microbiota populations (Hill-Burns et al., 2017; Peterson, 2020). In the case of Parkinson's disease, this relationship between the gut and brain has been clearly established. In a key study, rats were colonized by two *E. coli* strains, one encoding no aggregation-prone Curli proteins and the other an aggregation-prone variant. Those colonized with the aggregation-prone strain showed increased cerebral inflammation and accumulation of alpha-synuclein (Chen et al., 2016). A similar experiment was carried out by implanting human microbiota into mice; those

with more locomotor problems were those from which the microbiota came from Parkinson's disease patients (Sampson et al., 2016). These experiments have shown a clear correlation between Parkinson's disease and the microbiota. In Alzheimer's disease, alterations in the microbiome of mouse models can either protect or exacerbate the disease, depending on the bacterial composition (Harach et al., 2017; Loh et al., 2024). Beyond amyloid interactions, other microbiota-derived factors also contribute to the disease development. For example, sodium butyrate produced by *Clostridium butyricum* has a neuroprotective effect by inhibiting microglial activation. In Alzheimer's disease mouse models, elevating butyrate levels by expanding *Clostridium butyricum* populations reduced proinflammatory cytokines levels (Loh et al., 2024).

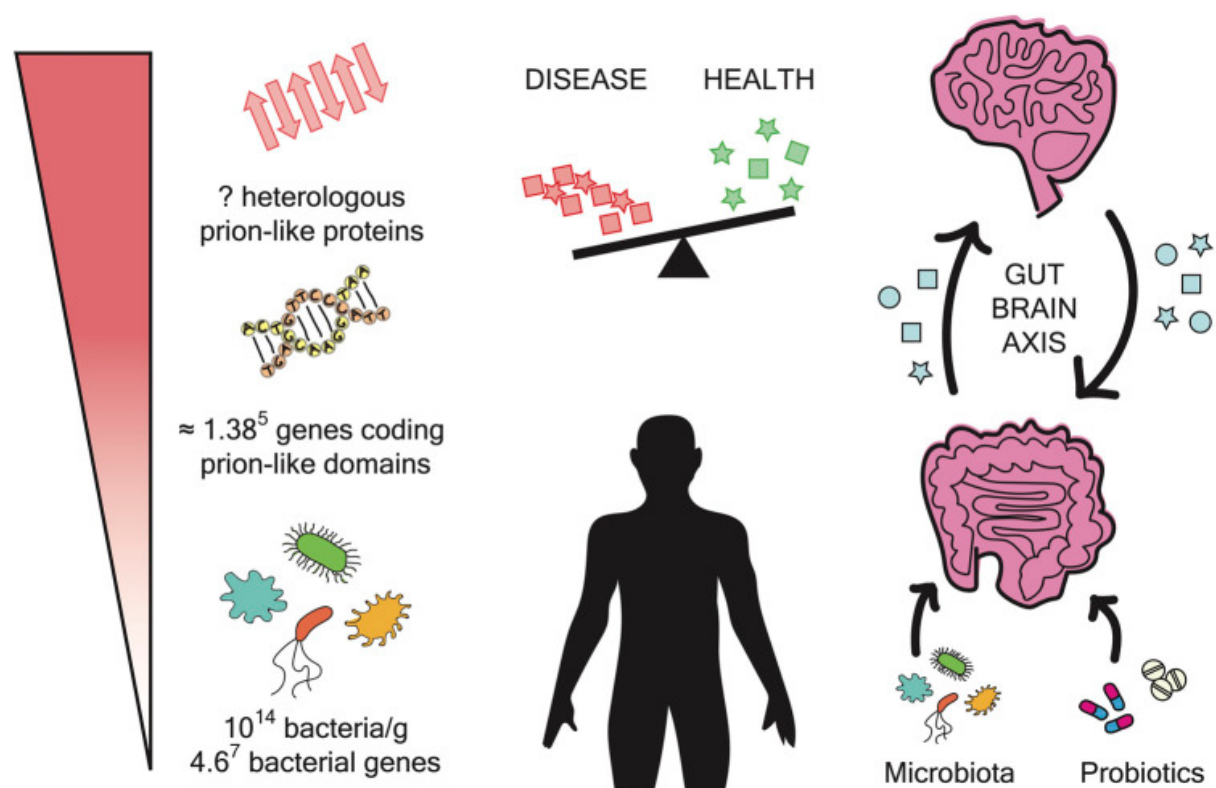


Figure 12 Microbiome impact on amyloidogenesis (Seira Curto et al., 2022). The gut microbiome has a high number of bacteria and possible prion-like proteins. These prion-like proteins can interfere with the human host and cross-seed amyloidogenic proteins. Maintaining a balanced microbiota is important, as imbalances may contribute to disease development. Probiotics could be a therapeutic strategy capable of restoring microbiota balance and positively influence neurodegenerative disease progression.

An important question concern how these bacterial amyloids cross the blood-brain barrier. This appears to be through the vagus nerve and systemic circulation (S. Kim et al., 2019). The vagus nerve connects the brain and the gut, serving as a possible avenue for pathological proteins to enter the brain. In addition, it functions at a sensory level by transmitting signals to the brain that can trigger neuroinflammatory reactions (Han et al., 2022; Kasarello et al.,

2023; Peterson, 2020). Regarding alpha-synuclein aggregates, they have been demonstrated to reach the brain via the vagus nerve (S. Kim et al., 2019). Increases in bacterial RNA and bacterial populations have been observed in the brains of Alzheimer's disease patients (Emery et al., 2017; Pisa et al., 2017). This ability to enter the brain has also been demonstrated for bacterial amyloids such as Curli and FapC and for bacteria such as *Escherichia coli* and *Neisseria Meningitidis* (Coureuil et al., 2017; K. S. Kim, 2001). This demonstrates that the ability to cross the blood-brain barrier is not an isolated phenomenon and must be considered, given the prolonged exposure time of the host to these bacteria and their metabolites.

Another question of interest concerns whether bacterial amyloid proteins are capable of doing this cross-seeding. Bacterial amyloids have been reported to be able to mimic the host amyloids and cross-seed, thereby propagating their conformations. One clear example is that of biofilm-associated amyloids (BAPs), which, when injected into mouse brains, promote alpha-synuclein aggregation (Fernández-Calvet et al., 2024). Nasal infection with *Saccharomyces cerevisiae* in mouse models of Parkinson's disease worsens the disease, as the Sup35 prion accelerates alpha-synuclein aggregation (Meng et al., 2023). Also, Curli and FapC are able to seed alpha-synuclein and A β peptides both in worms and mice (Javed et al., 2020; Lundmark et al., 2005; Zhou et al., 2012). This evidence supports the hypothesis that these bacterial amyloids are capable of promoting the aggregation of human amyloids by a cross-seeding mechanism. This fact underscores the importance of identifying bacterial amyloids and assessing their toxicity and ability to trigger A β peptides aggregation. The cross-seeding must be studied thoroughly to determine if it is merely an accelerative effect or if it has more significant implications, such as transmitting their folding patterns. Human amyloids with conformations derived from bacterial amyloids could be the ones having increased toxicity. Additionally, bacterial proteins may alter the aggregation pathways in other ways, increasing the presence of toxic non-fibrillary aggregates such as oligomers and amorphous aggregates.

It would be interesting to see if the bacterial amyloids could also interfere with the A β aggregation, generating new polymorphs with properties different from those of the fibrils formed by the A β unexposed to the microbiome amyloids and different from the fibrils formed by the microbiome amyloids.

Studying the interaction between microbiome peptides and A β peptides is currently challenging due to the large number of prion-like proteins present in the microbiome. One possible simplification approach would be to focus on the amyloid cores. Removing these regions abolishes the amyloid properties, while their addition can induce aggregation (De Groot et al., 2005; Espargaró et al., 2015; Esteras-Chopo et al., 2005). This property has been successfully exploited in the yeast Sup35 functional prion model, since its translation termination factor function depends on its ability to aggregate. This functionality, combined with an adenine intermediate gene truncated by a stop codon, enables the nonsense suppression assay, which allows rapid screening for [PSI⁺] prion activity (Balbirnie et al., 2001; Krishnan & Lindquist, 2005; Kushnirov et al., 2000). Focusing on the amyloid cores also facilitates the implementation of large-scale studies, as working with small peptides is much more feasible than with full-length proteins. This approach allows researchers to evaluate whether these amyloid cores can aggregate *in vitro* and interact with A β peptides, thereby altering their aggregation process.

Although our research focuses on the amyloid microbiome peptides and how they can alter the A β peptides aggregation, it is essential to consider that the microbiome can influence neurodegenerative disease through multiple pathways. This highlights the broader significance of microbiome-host interactions and the necessity of understanding their role in disease progression.

Aims

The main aim of this thesis is to contribute to the understanding of how the interplay between the microbiome and the human organism influences the development of neurodegenerative diseases, such as Alzheimer's. To this end, the work is primarily focused on identifying the factors that affect the aggregation of A β peptides.

The research conducted throughout this thesis began with efforts to improve our understanding of A β aggregation, particularly its dynamics *in vivo*, and to enhance the reproducibility of aggregation kinetics *in vitro*. Subsequently, the presence of amyloids in the microbiome was investigated, along with their potential threat to the nervous system and their ability to modulate A β aggregation at multiple levels.

The results obtained are presented in three different chapters, and the specific aims addressed in each are listed below:

Chapter I

- Determine the effects of physiological pH changes on A β 40 aggregation.
- Assess the role of ionic strength in stabilizing the aggregation process.

Chapter II

- Use computational tools to analyze the presence of prion-like proteins in the gut microbiome.
- Characterize the amyloidogenic and propagation capabilities of the identified prion-like proteins, both *in vitro* and in microbial models.
- Determine the ability of prion-like protein candidates to interfere with A β 40 aggregation.
- Assess the toxicity of prion-like protein candidates in human neuroblastoma cells and *C. elegans* models.

Chapter III

- Characterize the influence of microbiome-derived prion-like proteins on A β 40 and A β 42 co-aggregation and on subsequent propagation events.

CHAPTER I: A β 40 Aggregation under Changeable Conditions

This chapter contains the article published in International Journal of Molecular Sciences “Seira Curto, J., Fernandez, M. R., Cladera, J., Benseny-Cases, N., & Sanchez de Groot, N. (2023). A β 40 Aggregation under Changeable Conditions. International Journal of Molecular Sciences, 24(9). <https://doi.org/10.3390/ijms24098408>”

The supplementary data associated with this work is available in Section “Appendix 1” of this thesis.



Article

A β 40 Aggregation under Changeable Conditions

Jofre Seira Curto ¹, Maria Rosario Fernandez ¹ , Josep Cladera ², Núria Benseny-Cases ^{2,*}
and Natalia Sanchez de Groot ^{1,*}

¹ Unitat de Bioquímica, Departament de Bioquímica i Biologia Molecular, Universitat Autònoma de Barcelona, 08193 Barcelona, Spain; jofre.seira@uab.cat (J.S.C.); rosario.fernandez@uab.cat (M.R.F.)

² Unitat de Biofísica, Departament de Bioquímica i Biologia Molecular, Centre d'Estudis en Biofísica, Universitat Autònoma de Barcelona, 08193 Barcelona, Spain; josep.cladera@uab.cat

* Correspondence: nuria.benseny@uab.cat (N.B.-C.); natalia.sanchez@uab.cat (N.S.d.G.)

Abstract: Homeostasis is crucial for cell function, and disturbances in homeostasis can lead to health disorders. Under normal conditions, intracellular pH is maintained between 7.35 and 7.45. Altered endosomal and lysosomal pH together with a general drop in brain pH are associated with the aggregation of amyloid- β -peptide (A β) and the development of Alzheimer's disease. Under acidic conditions, close to the A β isoelectric point, the absence of charges favors the formation of intermolecular contacts and promotes aggregation. Here, we analyzed how pH levels affect the aggregation of A β 40 considering the variations in brain pH and the coexistence of different aggregated conformations. Our results suggest that different macromolecular conformations can interact with each other and influence the aggregation process. In addition, we showed that neutral pH and physiological salt concentrations favor a slow aggregation, resulting in ordered, stable fibrils, with low cytotoxic effects. Overall, we highlight the complexity of the aggregation processes occurring in different physiological and pathological environments.

Keywords: amyloid- β -peptide; charge repulsion; aggregation



Citation: Seira Curto, J.; Fernandez, M.R.; Cladera, J.; Benseny-Cases, N.; Sanchez de Groot, N. A β 40 Aggregation under Changeable Conditions. *Int. J. Mol. Sci.* **2023**, *24*, 8408. <https://doi.org/10.3390/ijms24098408>

Academic Editors: Konstantin K. Turoverov and Irina M. Kuznetsova

Received: 4 April 2023

Revised: 28 April 2023

Accepted: 4 May 2023

Published: 7 May 2023



Copyright: © 2023 by the authors. Licensee MDPI, Basel, Switzerland. This article is an open access article distributed under the terms and conditions of the Creative Commons Attribution (CC BY) license (<https://creativecommons.org/licenses/by/4.0/>).

1. Introduction

The intracellular space is complex and dynamic. Cellular homeostasis depends on the maintenance and regulation of internal conditions in time and space. Impaired homeostasis is an age-related problem that has been observed in many neurodegenerative diseases. In these disorders, impaired removal of misfolded and aggregated proteins can trigger a cascade of events that ultimately leads to cell death [1–3].

Similarly, the maintenance of an appropriate acid–base balance is essential for the correct functioning of human body processes [4]. Under normal physiological conditions, the intracellular and interstitial pH is between 7.35 and 7.45. Changes in pH can inhibit enzymatic activity, interrupt metabolic pathways, and disturb the membrane transport of proteins. Significantly lower pH has been measured in the brain and cerebrospinal fluid (CSF) of patients with Alzheimer's disease (AD) [5] (Figure 1A). In addition, alteration of endosomal and lysosomal pH has been related with problems in amyloid- β -peptide (A β) clearance and the formation of extracellular A β plaques [2,6].

A β is generated through the proteolytic cleavage of α -, β -, and γ -secretases on amyloid precursor protein (APP), a single-pass transmembrane protein [7–9]. This cleavage can produce different extracellular A β peptides with lengths ranging from 37 to 49; however, the most abundant forms are A β 40 (~90%) and A β 42 (~10%) [10–12]. In a disease context, A β 42 is the main major constituent of the amyloid plaques in the brains of patients with Alzheimer's disease, whereas A β 40 aggregates accumulate at the arteriolar walls in cerebral amyloid angiopathy [12–14]. The two extra residues at the C-terminus A β 42 result in faster aggregation kinetics compared to A β 40. Interestingly, under mixed conditions, both peptides can interact and influence each other's aggregation [15–18]. A β can enter

the cell via endocytosis for subsequent degradation by lysosomes [2,6,19]. When cell homeostasis is affected, this degradation pathway can fail, causing A β accumulation and aggregation. Additionally, the acidity of these organelles can accelerate the aggregation process (Figure 1A) [2,6,20].

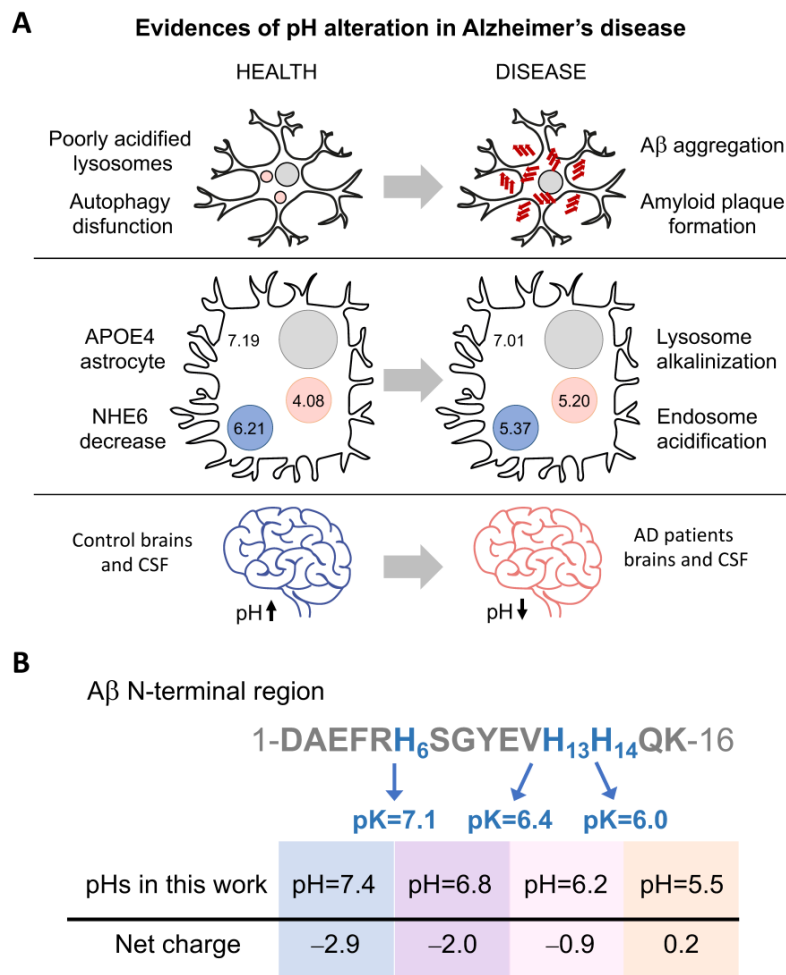


Figure 1. pH influences the net charge of A β and Alzheimer's disease development. **(A)** Three pieces of evidence of pH alterations in Alzheimer's disease. (i) Poor acidification of autolysosomes results in autophagy dysfunction and precedes A β deposition and amyloid plaque formation [2]. (ii) In ApoE4 astrocytes (with the E4 allele of apolipoprotein E), downregulation of the Na⁺/H⁺ exchanger NHE6 results in over-acidification of the endosomes and pH increase in lysosomes [6]. (iii) Lower pH has been measured in the brains and cerebrospinal fluid (CSF) of patients with Alzheimer's disease (AD) [5]. **(B)** Scheme of the A β N-terminal sequence, comprising histidines whose protonation is affected in the pH range analyzed in this study. The scheme shows the amino acid position and pK of the histidines and the net charge at each pH.

Protein aggregation is highly influenced by hydrophobicity and net charge [4,21–24]. When the pH approaches the isoelectric point (pI), the absence of charges removes the repulsion forces and favors the formation of intermolecular contacts involved in the aggregation process. The presence of salt ions can have a similar effect by shielding repulsive ionic interactions [25]. Our previous studies with A β 40 showed that the aggregates formed at neutral or acidic pH have different structures and cell toxicities [23,24]. However, the processes inside the cell are dynamic, and pH can change regularly in organelles [4,6]. Based on this, we aim to go forward here and shed light on the different toxic protein species that can arise under moderate pH and salt concentration changes. For this purpose, we analyzed how pH levels affect the aggregation of A β 40 considering the changeable

conditions of the intracellular space and the pH alterations that can occur locally in the extracellular space. Based on the pH reported for the altered endosomes and lysosomes in AD (Figure 1B), we focused on a range of pH from 5.5 to 7.4 and salt from 0 to 150 mM of NaCl (the most abundant salt found in multicellular organisms [25–27] widely used in aggregation assays [25,26,28,29]). We characterized the biophysical differences between the aggregates that form under these conditions considering the possible coexistence of different aggregated conformations and their ability to interact and interconvert. We found that salt and pH modulate the structure, stability, and cellular toxicity of the aggregates. Overall, we propose that even small cellular changes in pH and salt concentration could result in a complex and variable mixture of multimeric forms, which are able to interfere with each other to different degrees.

2. Results

2.1. pH and Salt Effect on A β 40 Aggregation

Taking into consideration the different intracellular environments where the presence of A β 40 has been detected [6], and with the aim of understanding how pH and NaCl concentration may influence the kinetics and conformation of A β 40 aggregates, we measured amyloid aggregation at different pH and NaCl conditions. Here, we specifically tested four different pH values (7.4, 6.8, 6.2, and 5.5) (Figure 1B), similar to those previously measured in endosomes and lysosomes (Figure 1A), and seven concentrations of NaCl ranging from 0 to physiological conditions (150 mM), to understand the extent to which the presence of this salt influences the aggregation of A β 40 at different pH values.

A β 40 aggregation was monitored every 10 min under quiescent conditions at 37 °C (Figures 2A–D and S1). In general, lag time and half-life ($t_{1/2}$) decrease when the pH becomes more acidic, consistent with the charge reduction (from -3 to nearly 0) when approaching the isoelectric point (pI , 5.3) (Figures 2E,F and S2). The increase in salt has a similar effect, which can be explained by the reduction of repulsive forces exerted by the peptide's negative charges (Figure 2E,F). However, at a pH close to the pI , the repulsion effect was lower, we did not observe any effect of NaCl on the aggregation process, and the half-lives were similar for all conditions (Figure 2D). In contrast, when the net charge was -3 (pH 7.4) and the salt concentration was low (from 0 to 25 mM), the aggregation kinetics were too slow to be measured over the time scale reported here (16 h) (Figure 2A). Kinetic analysis for longer times showed that they achieved a plateau and remained stable (Figure S3). Meisl and coworkers obtained similar results when analyzing the effect of ionic strength on A β 42 aggregation [25]. They found that the reduction in electrostatic repulsion surrounding the peptide can accelerate the incorporation of new monomers into the fibrils, which in turn reduces the impact that the fragmentation can have on the elongation speed [25].

To study the aggregates' conformation, we chose a 100 mM NaCl concentration, which is close to the physiological values, and two extreme pHs (7.4 vs. 5.5). We analyzed the morphology of the aggregates using transmission electron microscopy (TEM) (Figure 2F,G) and the secondary conformation using infrared spectroscopy (IR) (Figures 2H and S4). Under these experimental conditions, the aggregates at pH 7.4 are arranged into long and straight fibrillar structures that tend to group into clumps. However, at pH 5.5 the aggregates are shorter, less ordered, and more dispersed. This agrees with the IR absorbance spectra, which show the presence of oligomeric/amorphous aggregates at pH 5.5 and, in a lower amount, at pH 6.2. The IR spectra at these pH values show a characteristic band at 1690 cm^{-1} together with a clear beta-sheet band at 1623 cm^{-1} , which is associated with the presence of an antiparallel β -sheet, which is typical of oligomers and amorphous aggregates. Several studies have associated the presence of bands at 1623 cm^{-1} and 1690 cm^{-1} to antiparallel beta, whereas the sole presence of the band around 1620 cm^{-1} is associated with parallel (fibrillar) beta-sheet structures [30,31]. Consistently, at pH 7.4, we detected only the 1623 cm^{-1} absorption peak characteristic of the beta-sheet structure, suggesting the presence of fibrils (Figure 2H and Figure S4). Conversely, at a net charge

above -5 (pH 11), no signal of β -sheet structure (1623 cm^{-1}) or amorphous aggregates (1690 cm^{-1}) was detected, just a wide peak at 1645 cm^{-1} typical of an unfolded monomeric form [32]. In agreement with this, the initial stock sample at pH 11 only showed monomeric particles under dynamic light scattering (DLS) [33,34], and no aggregated structures were observed at the TEM grid (Figure S5).

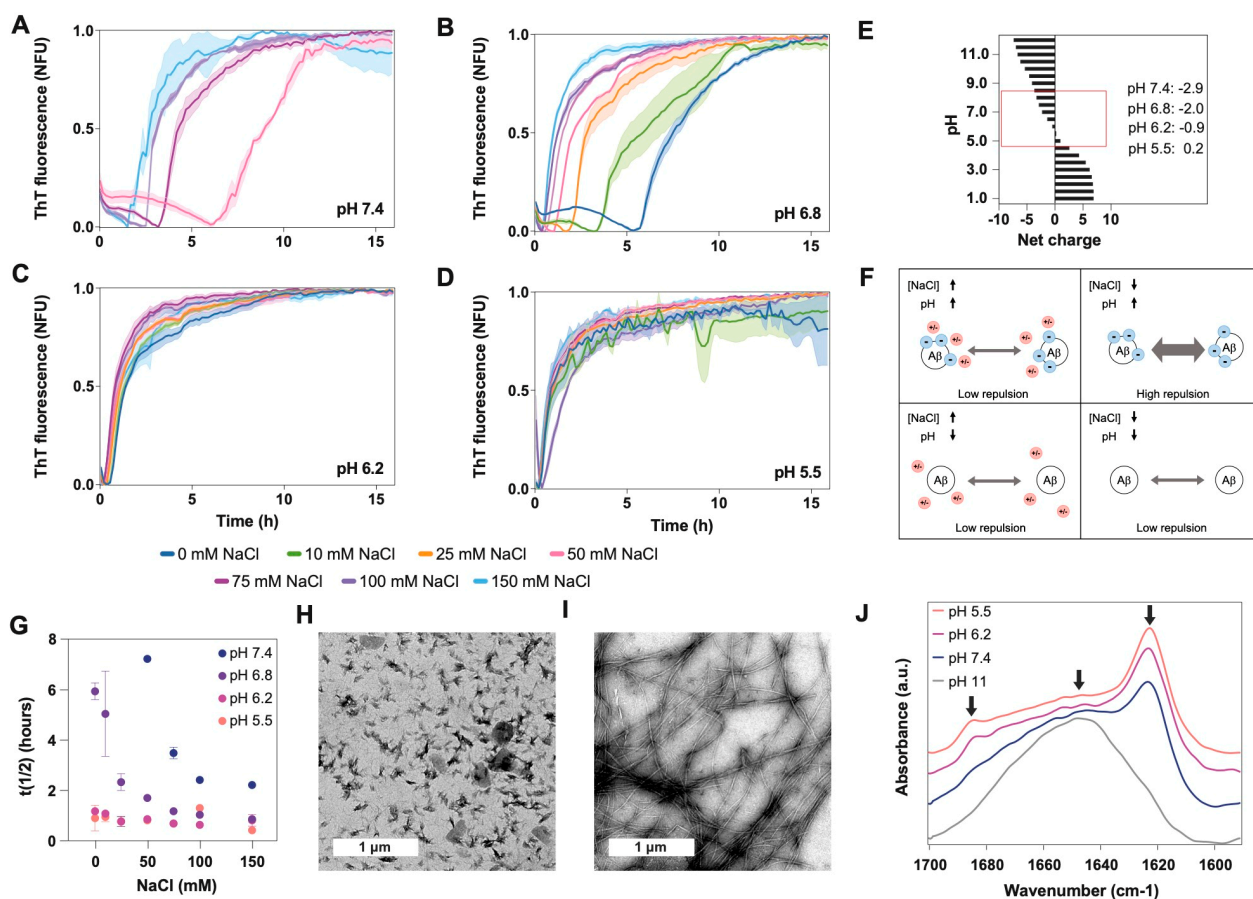


Figure 2. Effect of pH on Aβ40 aggregation and conformation. We measured aggregation kinetics at four different pH values: (A) 7.4, (B) 6.8, (C) 6.2, and (D) 5.5. For each pH, we also analyzed seven NaCl concentrations ranging from 0 to 150 mM. (E) Plot showing the Aβ40 net charge at different pH values, calculated with Protein Calculator v3.3 (Chris Putnam, Scripps Research Institute). (F) Scheme showing the repulsive forces between Aβ molecules at high and low pH and high and low NaCl concentrations. (G) Plot showing the relationship between the half-life ($t(1/2)$) of the kinetics presented in panels (A–D) and the NaCl concentration. TEM images of aggregates formed at (H) pH 5.5 and (I) pH 7.4. (J) FTIR spectra of Aβ40 aggregates incubated at four different pH values (5, 6, 7.4, and 10) and for 24 h. Arrows indicate the position of the following wavelengths: 1690 cm^{-1} , 1645 cm^{-1} and 1623 cm^{-1} . The spectrum at pH 10 demonstrates that the initial stock solution does not contain beta-sheet structure. It just shows a wide band at 1645 cm^{-1} corresponding to random structures, indicating that the peptide is monomeric at the beginning of the experiments. The peaks at 1690 cm^{-1} and 1623 cm^{-1} indicate the presence of antiparallel beta-sheet structures.

2.2. pH Exchange and Cross-Seeding

To understand how pH changes can affect the structure of preformed aggregates and the interaction between them, we analyzed (i) the effect of pH change (Figure 3A) and (ii) the cross-seeding between aggregates formed at different pH values (Figure 3B). The TEM images show that the aggregates grown in acidic conditions are pH sensitive, and after 24 h of increasing the pH to neutral, the aggregates progressed to straight fibrils, which were shorter than those grown at pH 7.4. These fibrils were also more abundant, to a

similar extent as the amorphous aggregates at acidic pH (Figure 3C). Meanwhile, when the pH of the aggregates grown at 7.4 was decreased, no significant structural changes were observed (Figure 3D).

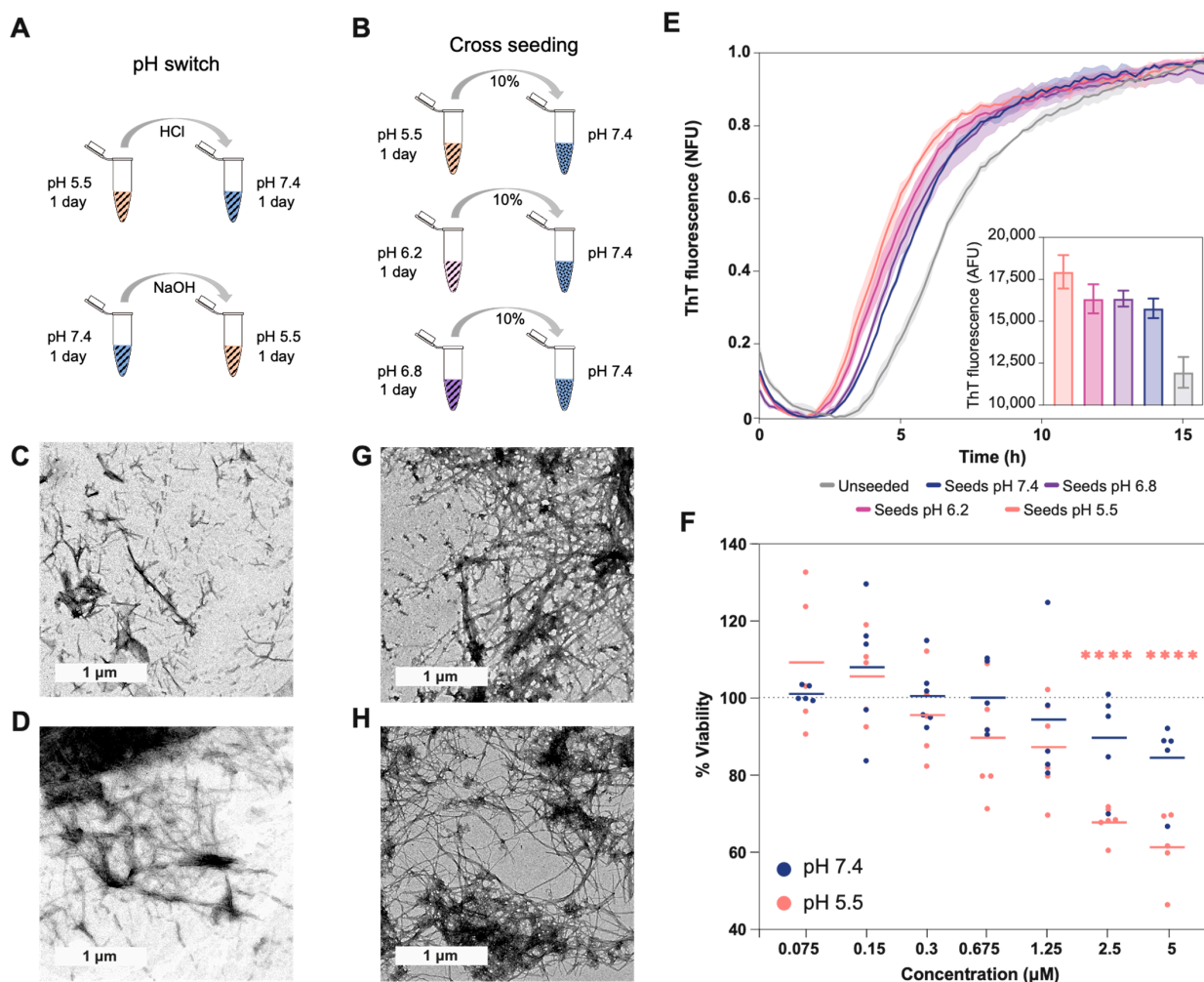


Figure 3. Effect of cross-seeding and pH switch on A β 40 aggregation and conformation. (A) Scheme showing the different steps of the pH switch assay (related to images (C,D)). (B) Scheme showing the different steps of the cross-seeding assay (related to images (E,G,H)). The striped pattern indicates that A β 40 is aggregated, and the dotted pattern that A β 40 is soluble. TEM images for the aggregates formed: (C) with the first 24 h at pH 5.5 and the second ones at 7.4, (D) with the first 24 h at pH 7.4 and the second ones at 5.5, (G) at pH 7.4 with seeds formed at pH 5.5, and (H) at pH 5.5 with seeds formed at pH 7.4. (E) Aggregation kinetics at pH 7.4 with and without different seed types. The fluorescence measured with seeds formed at pH 5.5 is significantly larger than with the seeds formed at pH 7.4 (p -value < 0.01). The inside plot shows no normalized fluorescence after 16 h of aggregation. The $t_{1/2}$ in hours for the different samples are as follows: unseeded (6.61 ± 0.10), seeds pH 7.4 (5.38 ± 0.01), seeds pH 6.8 (5.1 ± 0.259), seeds pH 6.2 (4.83 ± 0.17), and seeds pH 5.5 (4.44 ± 0.19). (F) The percentage of cell viability after incubation with different concentrations of A β 40 aggregated at different pH values (measured using the MTT assay). The plot shows triplicates of the two independent assays. The lines represent the mean corresponding to each concentration of the added aggregates. The significance against the control of 100% viability was measured using the Bonferroni test (****, <0.0001). At concentrations of 2.5 μ M and 5 μ M of aggregates, the fluorescence difference between seeds formed at pH 5.5 and seeds formed at pH 7.4 is also significant ($p = 0.001$ and $p = 0.0003$, respectively). The measurements of the different controls are shown in Figure S6.

Based on the observed morphological changes and the labile character of the aggregates formed at acidic pH, we analyzed their ability to seed the aggregation at pH 7.4 (Figure 3E). This is important because fibril fragility is associated with the presence of shorter aggregates, the release of a larger number of growing ends, and the acceleration of the aggregation process [22,35]. Accordingly, we measured shorter half-life times ($t_{1/2}$) when A β 40 was seeded with aggregates formed at a low pH, indicating a higher seeding ability. Interestingly, the TEM images from the different seeding assays showed aggregates with similar morphology: mature fibrils that, in some cases, formed clumps (Figure 3G,H).

2.3. A β 40 Aggregates Toxicity

Less stable aggregates are associated with the formation of more endpoints and higher cellular damage [22,35]. Along these lines, we measured cell viability, using the MTT assay, after 24 h of incubation with A β 40 aggregated at pH 5.5 and 7.4 (Figures 3F and S6). The colorimetric measures showed a significant decrease in viability at concentrations above 1.25 μ M, but only in cells incubated with aggregates formed at pH 5.5 when the viability decreased to close to 40%. Importantly, we previously demonstrated, using μ FTIR, that cell culture conditions do not affect the presence of A β 40 amyloid fibrils formed at pH 7.4 or pH 5.5 [36]. In addition, this assay showed an increased level of oxidation in cells incubated with aggregates formed at pH 5.5 [36], in agreement with the present results.

3. Discussion

3.1. pH Effect on A β 40 Aggregation

Recent studies have recapitulated the intracellular origin of the A β aggregates [1–3,6,19,37], which are related to autophagy impairment and pH imbalances. Lee and co-workers observed, in AD mouse models, that the poor acidification of autolysosomes results in autophagy dysfunction and precedes A β deposition and amyloid plaque formation [2]. In the case of the E4 allele of apolipoprotein E (ApoE4, the strongest genetic factor in sporadic AD), downregulation of the Na⁺/H⁺ exchanger NHE6 results in overacidification of endosomes and inhibition of A β clearance [6]. In this context, in ApoE4 astrocytes, the pH of the endosome was reduced from 6.21 to 5.37, and the pH of the lysosome increased from 4.08 to 5.20.

However, pH alterations were not only detected in these intracellular organelles [11,19,29,38–42]. The postmortem brains and cerebrospinal fluid of AD patients also show a significantly lower, although moderate, pH compared to the controls. Infusion of low-pH cerebrospinal fluid, in APP-PS1 mice, increases A β plaque load [4]. Moreover, a pH reduction can also be found under inflammatory and apoptotic processes and at the surface of anionic phospholipid membranes [5,43]. Overall, these events could place A β close to pI, reducing its solubility and favoring its self-association and aggregation [4,21,22].

As the pH changes from physiological (7.4) to the pI (5.3) [44], His6, His13, and His14 are protonated successively, generating new interactions and favoring the transition from soluble to aggregated [20,26]. Acidity affects the morphology and toxicity of A β aggregates (Figures 2 and 3). Protein aggregation is a very sensitive process, and the interaction and rearrangement of the molecules during the aggregate assembly could be influenced by multiple factors (temperature, charges, hydrophobicity, ionic strength), resulting in different macromolecular conformations or strains [21–24,36,38,41,45]. Amorphous and less organized structures are also associated with lower stability, large reactivity, and cellular toxicity [21–24,36,39,41,45]. Thus, small changes in the A β uptake and degradation could affect the self-assembly process [1–3,6,37,46,47]. Moreover, under changeable conditions, different conformational assemblies can coexist, interact, and influence each other's aggregation.

3.2. Effect of pH Exchange and Cross-Seeding on A β 40 Aggregation

Here, we evaluated the effect of changes in the electrostatic repulsion on A β 40 aggregation, taking into consideration the different environments that this peptide can encounter

in the cell [1,6,22,37–39,48,49]. We also presumed that the conditions in the cell can change and that different A β 40 assemblies can rise and interact. Based on this assumption, we performed a series of experiments, ranging from neutral (7.4) to acidic pH (5.5) and from physiological concentrations to 0 μ M of NaCl. We also analyzed the effect of pH alteration, decreasing the pH from neutral or increasing it from an acidic solution. Following these alterations, we analyzed the coexistence of assemblies grown under different conditions.

In agreement with previous publications, our experiments support electrostatic repulsion as a driving force in aggregation, modulated by the change of pH and salt concentration [23–26,38,41,50,51]. The pH decrease from 7.4 to 5.5 results in a net charge variation from -3 to 0.2, and by getting closer to A β 40's pI, the aggregation kinetics become faster (Figure 4). Similarly, the increase in NaCl reduces the repulsion between the negative charges, accelerating aggregation, except under acidic pH, when the charges are already nearly neutralized. The aggregates formed at different pH values have different morphologies and structural content. As previously reported, under neutral conditions, the aggregates are more fibrillar and contain fewer oligomeric and protofibril structures than under acidic pH conditions [23,24,51]. A faster aggregation process may hinder the correct assembly of the different molecules, resulting in less ordered aggregates than fibrils presenting antiparallel β -sheet structures, similar to those detected in vitro in the early stages of the amyloid fibril formation process [30,31]. Here, we altered the aggregation conditions by incubating the preformed aggregates at a second different pH or by seeding the process with different assemblies (Figure 3A,B). Overall, different aggregates were observed at different pH values. Aggregates grown under acidic conditions are pH sensitive and can seed aggregation stronger than those formed at neutral pH, resulting in a larger amount of aggregates (Figure 3E). This could be a consequence of the different arrangements of these assemblies. In general, less ordered forms, such as oligomers or protofibrils, are associated with lower stability and higher toxicity (such as the generation of reactive oxygen species or the disruption of membranes) [1,23,24,39,51–53]. In line with this, we have previously reported that, in leakage experiments, the aggregates formed at pH 5.5 have a higher capacity to disrupt phosphatidylcholine model membranes than fibrils formed at pH 7.4 [23].

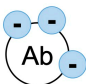











	Assembly	Conformation	Properties
<p>pH = 7.4</p>  <p>Ab</p> <p>Net charge -3</p>	<p>High repulsion</p>  <p>Slow nucleation</p> 	<p>Highly ordered aggregates</p> 	<p>pH-resistant</p>  <p>Low toxicity</p> 
<p>pH = 5.5</p>  <p>Ab</p> <p>Net charge 0</p>	<p>Low repulsion</p>  <p>Fast nucleation</p> 	<p>Less ordered aggregates</p> 	<p>pH-sensitive</p>  <p>High toxicity</p> 

Figure 4. Effect of pH on A β 40 aggregation, conformation, and toxicity. This table summarizes the differences between the aggregates formed at pH 7.4 and pH 5.5. At these pH values, A β 40 has a different net charge (−3 vs. 0), resulting in different repulsion forces and aggregation speeds. Meanwhile, at pH 7.4 the aggregates are ordered and pH resistant and exhibit low toxicity. At pH 5.5, the aggregates presented abundant oligomers and protofibrils, which are pH sensitive and toxic.

In relation to the stability of the different aggregates, we observed that the aggregates formed at pH 7.4 barely changed their morphology at acidic pH, while those formed at pH 5.5 evolved to a more ordered form when placed at neutral pH (Figure 4). This suggests that aggregates formed at pH 7.4 may be more stable (less pH sensitive) than those grown at pH 5.5. In addition, the smaller size and higher abundance of aggregates formed at pH 5.5 may also provide more end-points for amyloid fibril growth [22].

3.3. A β 40 Aggregation under Complex Conditions

Low pH can be found in intracellular organelles as well as in the presence of oxidized or pre-apoptotic membranes. These membranes present negative charges on their surfaces, which increase the concentration of protons and cause a local pH decrease [23]. In addition, pathological vascular events, such as ischemia and microhemorrhages related to AD, can cause a lack of oxygen, leading to a local decrease in pH in the extracellular space [54]. In patients with Alzheimer's disease, there are changes in the concentrations of several ions. For example, Vitvitsky and co-workers found an increased concentration of positive ions, Na⁺ and K⁺, in comparison with control brains, pointing to a possible accelerated aggregation process [55].

A β 's pH dependence may also be associated with the formation of different conformational strains and with disease heterogeneity [21,39,56]. Accordingly, seeding experiments with A β aggregates obtained from the brains of patients with AD affected by different phenotypes resulted in structurally distinct fibrils [21,22,57]. In this way, oligomers have been reported to be less stable and more toxic than amyloid fibrils [1,23,24,39,51–53]. Phenotypic severity has been also associated with fibril fragility, because its fragmentation releases new growing ends that can seed new fibrils and accelerate the aggregation process [22,35]. Our results showed that the aggregates formed under acidic conditions present higher cytotoxicity and seeding. This agrees with our previous work where larger amounts of oligomers were present at lower pHs [23,24], but also suggests the presence of a larger number of endpoints. These results also point to an amplifying effect (Figure 3E); although aggregation is slow at neutral pH, the presence, at some point, of seeds formed at lower pHs could rapidly saturate the cell with highly stable aggregates and trigger the formation of extracellular plaques [2]. In fact, the study of AD mouse model APP/PS1 brains using FTIR microscopy has demonstrated the presence of non-fibrillar aggregates in situ, which is compatible with the FTIR spectra of oligomers and aggregates formed at low pH in the early stages of the disease (3–6 months). At later stages of the disease, a decrease in this type of aggregate was observed, and a higher number of fibrillary plaques were found [58]. The present work agrees with the co-existence of different macromolecular conformations and their possible cooperation triggering a harmful aggregation process [21]. In addition, it supports neutral pH and physiological salt concentrations being conditions that favor a slow aggregation process, resulting in ordered, stable, and less cytotoxic fibrils. This agrees with previous works showing that fibrils are safer aggregates than oligomers or protofibrils [22,35]. Based on these results, blocking or slowing down the aggregation process by favoring electrostatic repulsion could be an effective strategy to reduce toxic effects [2,6]. Moreover, owing to the sensitivity of aggregates to these variable conditions, it is possible to control the conformation of aggregates and their properties, a strategy already exploited by the cell to form functional amyloid structures [59]. In the case of A β , this could be a positive and evolutionarily selected property to activate its antimicrobial activity, since on the bacterial membranes the negative charges could favor A β 's aggregation and the consequent cell disruption [60]. Overall, the data presented here highlight the complexity of the aggregation processes occurring inside the cell and in the extracellular space and support the idea that the physio-pathological processes able to modify pH can play a significant role in triggering the onset of A β 40 aggregation.

4. Material and Methods

4.1. A β 40 Peptide Preparation

Synthetic A β 40 (DAEFRHDSGYEVHHQKLVFFAEDVGSNKGAIIGLMVGGVV-NH₂) was purchased from Proteogenix (Schiltigheim, France). Stock solutions were prepared by dissolving 1 mg of the peptide to a final concentration of 250 μ M and adding 20 mM sodium phosphate buffer, 0.04% NH₃, and NaOH to a final pH of 11. Then, the peptide was sonicated for ten minutes (Fisherbrand Pittsburgh, PA, USA, FB15051) without sweep mode and stored at -80°C until needed [23].

All samples were prepared in low protein-binding microcentrifuge tubes (ThermoFisher Scientific, Waltham, MA, USA). The pH was measured at the start and end of all the aggregation reactions to confirm that it remained stable. For the pH change assays, 100 μ L of sample after 24 h of aggregation at pH 7.4 was used, and 20 mM HCl was added to reach a pH of 5.5. For aggregates formed at pH 5.5, 20 mM NaOH was added to reach a pH of 7.4. For the seeding assays, 300 μ L of preformed aggregates was obtained after 24 h of aggregation and 5 min of sonication. Preformed seeds were added to the corresponding aggregation reactions to a final seed concentration of 2.5 mM. The monomeric concentration of A β 40 used was 25 μ M. The control of unseeded reaction has the buffers at pH 7.4 and 25 μ M of monomeric A β 40 (everything but the seeds).

4.2. ThT Aggregation Kinetics

Thioflavin T was dissolved in Milli-Q water at 5 mM stock, filtered with a 0.2 μ m filter, diluted to 0.5 mM, and stored at -20°C prior to use. ThT fluorescence was measured every 10 min using a 440 nm excitation filter and a 480 nm emission filter using bottom-optics in a plate reader (TECAN Infinite+ NANO). Samples were placed in a flat-bottom, black, non-binding 96-well plate (Greiner bio-one). A total of 100 μ L of sample was added per well. Each condition was measured in triplicate. The A β 40 peptide stock, initially at pH 11, was diluted to 25 μ M in sodium phosphate buffer under the corresponding pH and salt conditions. HCl was added at a concentration of 15 mM to reach a pH of 5.5. The pH in the wells was measured both at the start and end of the experiment to ensure the pH stability throughout the aggregation process. ThT was added to 20 mM final concentration. The aggregation reaction was performed at 37°C , under quiescent conditions. The $t_{1/2}$ is the time necessary, at a given condition, to reach 50% of the final fluorescence signal. The lag phase was calculated by considering its ending as the point at which it reached 10% of the final fluorescence.

4.3. Dynamic Light Scattering

The monomeric state of A β 40 at the stock solution (250 μ M, pH 11) was analyzed using a NANOTRAC FLEX in situ particle size analyzer (Microtrac TM). A total of 50 μ L of the sample was added to the tip of the laser of the DLS equipment, and a 90 s analysis was performed.

4.4. Transmission Electron Microscopy

After 16 h of aggregation in low protein-binding microcentrifuge tubes, under the corresponding conditions, a 10 μ L sample was placed onto carbon-coated copper grids, incubated for 5 min, and dried with Whatman paper. The grids were washed with distilled water, negatively stained with 2% (*w/v*) uranyl acetate for 2 min, and then dried. Micrographs were obtained using a JEM-1400 (JEOL, Tokyo, Japan) transmission electron microscope (TEM) operated at an accelerating voltage of 80 keV.

4.5. Infrared Spectroscopy

Infrared spectroscopy was performed as described by Benseny-Cases, 2007 [24]. Briefly, 100 μ M peptide was incubated for 11, 15, and 24 h in sodium phosphate buffer in D₂O at the corresponding pH at 37°C under quiescent conditions. Then, 30 mL of peptide was deposited between two CaF₂ windows separated by a 50 mm Teflon separator. All

measurements were carried out on an FTIR Mattson Polaris spectrometer equipped with a liquid-nitrogen-cooled mercury–cadmium–telluride (MCT) detector at 37 °C. The spectrometer was purged continuously with dry air. For each spectrum, an average of one thousand scans were averaged at an instrumental resolution of 2 cm^{−1}. The spectra were recorded in the range of 400 to 4000 cm^{−1}. To obtain the infrared spectrum of the peptide, the spectrum of the solvent was subtracted from the sample, and all spectra were corrected for the atmospheric water vapor contribution. Each experiment was repeated three times.

4.6. Cell Cytotoxicity Assay

Neuroblastoma SH-SY5Y cells were cultured in Dulbecco's modified Eagle's medium (DMEM) supplemented with 10% (*v/v*) heat-inactivated fetal bovine serum, 1% glutamine, and 1% (*v/v*) penicillin/streptomycin. The cells were maintained at 37 °C and 5% CO₂ in a 75 cm² cell culture flask. Differentiation to neuronal cells started 24 h after plating by replacement of the maintenance medium with differentiation culture medium for 7 days and refreshment every 72 h. The differentiation culture medium consisted of DMEM supplemented with 2.5% inactivated FBS, 1% penicillin/streptomycin, 1% glutamine, and 10 μM retinoic acid. Differentiation was monitored microscopically by morphological assessment.

For the cytotoxicity assay, the cells were seeded in 96-well plates and treated at a density of 2×10^4 cells/well. Aβ40 at pH 5.5 and pH 7.4 was added at different concentrations, and after 24 h of incubation, cell viability was detected by MTT assay. After removing the medium, 10 μL of 3-(4,5-dimethylthiazol-2-yl)-2,5-diphenyltetrazolium bromide (MTT) solution (5 mg/mL) and 100 μL of the medium were added to each well and incubated at 37 °C for 4 h. Then, 150 μL of dimethyl sulfoxide was added to each well to dissolve the formazan after discarding the supernatant. Absorbance values were quantified using a plate reader (TECAN Spark) at a wavelength of 490 nm. For each pH, the data are expressed as a percentage of viability with respect to non-treated cells. The non-treated cells were grown in a medium containing the same amount of buffer, at the corresponding pH, but without Aβ40. Figure S6 compares these two controls (pH 7.4 and pH 5.5) and a culture of cells non-treated and without the addition of any extra buffer (neither pH 7.4 nor pH 5.5).

Supplementary Materials: The following supporting information can be downloaded at: <https://www.mdpi.com/article/10.3390/ijms24098408/s1>.

Author Contributions: N.B.-C. and N.S.d.G. conceived the manuscript structure. J.S.C., M.R.F., N.B.-C. and N.S.d.G. wrote the main manuscript text. J.S.C., N.B.-C. and N.S.d.G. prepared the figures and revised the manuscript. Conceptualization, N.B.-C. and N.S.d.G.; methodology, N.B.-C., N.S.d.G. and J.S.C.; validation, J.S.C.; formal analysis, J.S.C.; investigation, J.S.C., N.B.-C. and N.S.d.G.; resources, J.C., N.B.-C. and N.S.d.G.; writing—original draft preparation, J.C., J.S.C., M.R.F., N.B.-C. and N.S.d.G.; supervision, J.C., M.R.F., N.B.-C. and N.S.d.G. All authors have read and agreed to the published version of the manuscript.

Funding: This research was funded by grants 2022-FISDUR-0072 (AGAUR), FPU21/03897, RYC2019-026752-I, and PID2020-117454RA-I00 which is funded by MCIN/AEI/10.13039/501100011033. It was also funded by a national award from L'Oréal-UNESCO For Women in Science Programme.

Institutional Review Board Statement: Not applicable.

Informed Consent Statement: Not applicable.

Data Availability Statement: Not applicable.

Acknowledgments: The authors would like to thank Marc Torrent Burgas (Autonomous University of Barcelona, Spain) for his critical comments on the manuscript.

Conflicts of Interest: The authors declare no conflict of interest.

References

- Cataldo, A.M.; Peterhoff, C.M.; Troncoso, J.C.; Gomez-Isla, T.; Hyman, B.T.; Nixon, R.A. Endocytic Pathway Abnormalities Precede Amyloid β Deposition in Sporadic Alzheimer's Disease and Down Syndrome: Differential Effects of APOE Genotype and Presenilin Mutations. *Am. J. Pathol.* **2000**, *157*, 277–286. [\[CrossRef\]](#) [\[PubMed\]](#)
- Lee, J.H.; Yang, D.S.; Goulbourne, C.N.; Im, E.; Stavrides, P.; Pensalfini, A.; Chan, H.; Bouchet-Marquis, C.; Bleiwas, C.; Berg, M.J.; et al. Faulty Autolysosome Acidification in Alzheimer's Disease Mouse Models Induces Autophagic Build-up of A β in Neurons, Yielding Senile Plaques. *Nat. Neurosci.* **2022**, *25*, 688–701. [\[CrossRef\]](#)
- Friedrich, R.P.; Tepper, K.; Röncke, R.; Soom, M.; Westermann, M.; Reymann, K.; Kaether, C.; Fändrich, M. Mechanism of Amyloid Plaque Formation Suggests an Intracellular Basis of Abeta Pathogenicity. *Proc. Natl. Acad. Sci. USA* **2010**, *107*, 1942–1947. [\[CrossRef\]](#) [\[PubMed\]](#)
- Quade, B.N.; Parker, M.D.; Occhipinti, R. The Therapeutic Importance of Acid-Base Balance. *Biochem. Pharmacol.* **2021**, *183*, 114278. [\[CrossRef\]](#)
- Decker, Y.; Németh, E.; Schomburg, R.; Chemla, A.; Fülöp, L.; Menger, M.D.; Liu, Y.; Fassbender, K. Decreased PH in the Aging Brain and Alzheimer's Disease. *Neurobiol. Aging* **2021**, *101*, 40–49. [\[CrossRef\]](#)
- Prasad, H.; Rao, R. Amyloid Clearance Defect in ApoE4 Astrocytes Is Reversed by Epigenetic Correction of Endosomal PH. *Proc. Natl. Acad. Sci. USA* **2018**, *115*, E6640–E6649. [\[CrossRef\]](#) [\[PubMed\]](#)
- De Strooper, B.; Vassar, R.; Golde, T. The Secretases: Enzymes with Therapeutic Potential in Alzheimer Disease. *Nat. Rev. Neurol.* **2010**, *6*, 99–107. [\[CrossRef\]](#)
- De Groot, N.S.; Burgas, M.T. Is Membrane Homeostasis the Missing Link between Inflammation and Neurodegenerative Diseases? *Cell. Mol. Life Sci.* **2015**, *72*, 4795–4805. [\[CrossRef\]](#)
- Kim, M.; Bezprozvanny, I. Analysis of Non-Amyloidogenic Mutations in APP Supports Loss of Function Hypothesis of Alzheimer's Disease. *Int. J. Mol. Sci.* **2023**, *24*, 2092. [\[CrossRef\]](#)
- Maler, J.M.; Klafki, H.W.; Paul, S.; Spitzer, P.; Groemer, T.W.; Henkel, A.W.; Esselmann, H.; Lewczuk, P.; Kornhuber, J.; Wiltfang, J. Urea-Based Two-Dimensional Electrophoresis of Beta-Amyloid Peptides in Human Plasma: Evidence for Novel Abeta Species. *Proteomics* **2007**, *7*, 3815–3820. [\[CrossRef\]](#)
- Cereghetti, G.; Kissling, V.M.; Koch, L.M.; Arm, A.; Afanasyev, P.; Linsenmeier, M.; Eichmann, C.; Zhou, J.; Cao, Y.; Pfizenmaier, D.M.; et al. A Conserved Mechanism Regulates Reversible Amyloids via PH-Sensing Regions. *SSRN Electron. J.* **2022**, *2022*, 484600. [\[CrossRef\]](#)
- Jan, A.; Gokce, O.; Luthi-Carter, R.; Lashuel, H.A. The Ratio of Monomeric to Aggregated Forms of Abeta40 and Abeta42 Is an Important Determinant of Amyloid-Beta Aggregation, Fibrillogenesis, and Toxicity. *J. Biol. Chem.* **2008**, *283*, 28176–28189. [\[CrossRef\]](#)
- Biffi, A.; Greenberg, S.M. Cerebral Amyloid Angiopathy: A Systematic Review. *J. Clin. Neurol.* **2011**, *7*, 1–9. [\[CrossRef\]](#)
- Gatti, L.; Tinelli, F.; Scelzo, E.; Arioli, F.; Di Fede, G.; Obici, L.; Pantoni, L.; Giaccone, G.; Caroppo, P.; Parati, E.A.; et al. Understanding the Pathophysiology of Cerebral Amyloid Angiopathy. *Int. J. Mol. Sci.* **2020**, *21*, 3435. [\[CrossRef\]](#) [\[PubMed\]](#)
- Braun, G.A.; Dear, A.J.; Sanagavarapu, K.; Zetterberg, H.; Linse, S. Amyloid- β Peptide 37, 38 and 40 Individually and Cooperatively Inhibit Amyloid- β 42 Aggregation. *Chem. Sci.* **2022**, *13*, 2423–2439. [\[CrossRef\]](#)
- Morel, B.; Carrasco-Jiménez, M.P.; Jurado, S.; Conejero-Lara, F. Rapid Conversion of Amyloid-Beta 1-40 Oligomers to Mature Fibrils through a Self-Catalytic Bimolecular Process. *Int. J. Mol. Sci.* **2021**, *22*, 6370. [\[CrossRef\]](#)
- Chang, H.W.; Ma, H.I.; Wu, Y.S.; Lee, M.C.; Chung-Yueh Yuan, E.; Huang, S.J.; Cheng, Y.S.; Wu, M.H.; Tu, L.H.; Chan, J.C.C. Site Specific NMR Characterization of Abeta-40 Oligomers Cross Seeded by Abeta-42 Oligomers. *Chem. Sci.* **2022**, *13*, 8526–8535. [\[CrossRef\]](#)
- Gu, L.; Guo, Z. Alzheimer's A β 42 and A β 40 Form Mixed Oligomers with Direct Molecular Interactions. *Biochem. Biophys. Res. Commun.* **2021**, *534*, 292–296. [\[CrossRef\]](#)
- Le Bras, A. New Insights into the Origin of Amyloid Plaques. *Lab Anim. (NY)* **2022**, *51*, 187. [\[CrossRef\]](#)
- Zhao, W.; Ai, H. Effect of PH on A β 42 Monomer and Fibril-like Oligomers-Decoding in Silico of the Roles of PK Values of Charged Residues. *Chemphyschem* **2018**, *19*, 1103–1116. [\[CrossRef\]](#) [\[PubMed\]](#)
- Soto, C.; Pritzkow, S. Protein Misfolding, Aggregation, and Conformational Strains in Neurodegenerative Diseases. *Nat. Neurosci.* **2018**, *21*, 1332–1340. [\[CrossRef\]](#)
- Chuang, E.; Hori, A.M.; Hesketh, C.D.; Shorter, J. Amyloid Assembly and Disassembly. *J. Cell Sci.* **2018**, *131*, jcs189928. [\[CrossRef\]](#) [\[PubMed\]](#)
- Benseny-Cases, N.; Klementieva, O.; Maly, J.; Cladera, J. Granular Non-Fibrillar Aggregates and Toxicity in Alzheimer's Disease. *Curr. Alzheimer Res.* **2012**, *9*, 962–971. [\[CrossRef\]](#)
- Benseny-Cases, N.; Cócera, M.; Cladera, J. Conversion of Non-Fibrillar β -Sheet Oligomers into Amyloid Fibrils in Alzheimer's Disease Amyloid Peptide Aggregation. *Biochem. Biophys. Res. Commun.* **2007**, *361*, 916–921. [\[CrossRef\]](#) [\[PubMed\]](#)
- Meisl, G.; Yang, X.; Dobson, C.M.; Linse, S.; Knowles, T.P.J. Modulation of Electrostatic Interactions to Reveal a Reaction Network Unifying the Aggregation Behaviour of the A β 42 Peptide and Its Variants. *Chem. Sci.* **2017**, *8*, 4352–4362. [\[CrossRef\]](#)
- Abelein, A.; Jarvet, J.; Barth, A.; Gräslund, A.; Danielsson, J. Ionic Strength Modulation of the Free Energy Landscape of A β 40 Peptide Fibril Formation. *J. Am. Chem. Soc.* **2016**, *138*, 6893–6902. [\[CrossRef\]](#) [\[PubMed\]](#)

27. Klement, K.; Wieligmann, K.; Meinhardt, J.; Hortschansky, P.; Richter, W.; Fändrich, M. Effect of Different Salt Ions on the Propensity of Aggregation and on the Structure of Alzheimer's A β (1–40) Amyloid Fibrils. *J. Mol. Biol.* **2007**, *373*, 1321–1333. [\[CrossRef\]](#)
28. Wood, S.J.; Maleeff, B.; Hart, T.; Wetzel, R. Physical, Morphological and Functional Differences between PH 5.8 and 7.4 Aggregates of the Alzheimer's Amyloid Peptide A β . *J. Mol. Biol.* **1996**, *256*, 870–877. [\[CrossRef\]](#)
29. Xing, X.; Liu, C.; Yang, H.; Nouman, M.F.; Ai, H. Folding Dynamics of A β 42 Monomer at PH 4.0–7.5 with and without Physiological Salt Conditions—Does the B1 or B2 Region Fold First? *New J. Chem.* **2020**, *44*, 18000–18013. [\[CrossRef\]](#)
30. Cerf, E.; Sarroukh, R.; Tamamizu-Kato, S.; Breydo, L.; Derclayes, S.; Dufr enes, Y.F.; Narayanaswami, V.; Goormaghtigh, E.; Ruyschaert, J.M.; Raussens, V. Antiparallel Beta-Sheet: A Signature Structure of the Oligomeric Amyloid Beta-Peptide. *Biochem. J.* **2009**, *421*, 415–423. [\[CrossRef\]](#)
31. Sarroukh, R.; Goormaghtigh, E.; Ruyschaert, J.M.; Raussens, V. ATR-FTIR: A “Rejuvenated” Tool to Investigate Amyloid Proteins. *Biochim. Biophys. Acta* **2013**, *1828*, 2328–2338. [\[CrossRef\]](#)
32. Fraser, P.E.; Nguyen, J.T.; Surewicz, W.K.; Kirschner, D.A. PH-Dependent Structural Transitions of Alzheimer Amyloid Peptides. *Biophys. J.* **1991**, *60*, 1190–1201. [\[CrossRef\]](#)
33. Maiti, P.; Lomakin, A.; Benedek, G.B.; Bitan, G. Despite Its Role in Assembly, Methionine 35 Is Not Necessary for Amyloid Beta-Protein Toxicity. *J. Neurochem.* **2010**, *113*, 1252–1262. [\[CrossRef\]](#) [\[PubMed\]](#)
34. Bitan, G.; Kirkitadze, M.D.; Lomakin, A.; Vollers, S.S.; Benedek, G.B.; Teplow, D.B. Amyloid-Protein (A) Assembly: A40 and A42 Oligomerize through Distinct Pathways. *Proc. Nat. Acad. Sci. USA* **2003**, *100*, 330–335. [\[CrossRef\]](#) [\[PubMed\]](#)
35. Cushman, M.; Johnson, B.S.; King, O.D.; Gitler, A.D.; Shorter, J. Prion-like Disorders: Blurring the Divide between Transmissibility and Infectivity. *J. Cell Sci.* **2010**, *123*, 1191–1201. [\[CrossRef\]](#) [\[PubMed\]](#)
36. Benseny-Cases, N.;  lvarez-Marimon, E.; Castillo-Michel, H.; Cotte, M.; Falcon, C.; Cladera, J. Synchrotron-Based Fourier Transform Infrared Microspectroscopy (MFTIR) Study on the Effect of Alzheimer's A β Amorphous and Fibrillar Aggregates on PC12 Cells. *Anal. Chem.* **2018**, *90*, 2772–2779. [\[CrossRef\]](#)
37. Hu, X.; Crick, S.L.; Bu, G.; Frieden, C.; Pappu, R.V.; Lee, J.M. Amyloid Seeds Formed by Cellular Uptake, Concentration, and Aggregation of the Amyloid-Beta Peptide. *Proc. Natl. Acad. Sci. USA* **2009**, *106*, 20324–20329. [\[CrossRef\]](#)
38. Tian, Y.; Viles, J.H. PH Dependence of Amyloid- β Fibril Assembly Kinetics: Unravelling the Microscopic Molecular Processes. *Angew. Chemie Int. Ed.* **2022**, *61*, e202210675. [\[CrossRef\]](#)
39. Su, Y.; Chang, P.T. Acidic PH Promotes the Formation of Toxic Fibrils from β -Amyloid Peptide. *Brain Res.* **2001**, *893*, 287–291. [\[CrossRef\]](#)
40. Edwin, N.J.; Hammer, R.P.; McCarley, R.L.; Russo, P.S. Reversibility of Beta-Amyloid Self-Assembly: Effects of PH and Added Salts Assessed by Fluorescence Photobleaching Recovery. *Biomacromolecules* **2010**, *11*, 341–347. [\[CrossRef\]](#)
41. Shammass, S.L.; Knowles, T.P.J.; Baldwin, A.J.; MacPhee, C.E.; Welland, M.E.; Dobson, C.M.; Devlin, G.L. Perturbation of the Stability of Amyloid Fibrils through Alteration of Electrostatic Interactions. *Biophys. J.* **2011**, *100*, 2783–2791. [\[CrossRef\]](#) [\[PubMed\]](#)
42. Lambeth, T.R.; Julian, R.R. Proteolysis of Amyloid β by Lysosomal Enzymes as a Function of Fibril Morphology. *ACS Omega* **2021**, *6*, 31520–31527. [\[CrossRef\]](#) [\[PubMed\]](#)
43. Kinney, J.W.; Bemiller, S.M.; Murtishaw, A.S.; Leisgang, A.M.; Salazar, A.M.; Lamb, B.T. Inflammation as a Central Mechanism in Alzheimer's Disease. *Alzheimer's Dement* **2018**, *4*, 575–590. [\[CrossRef\]](#) [\[PubMed\]](#)
44. Hortschansky, P.; Schroeckh, V.; Christopeit, T.; Zandomenoghi, G.; F ndrich, M. The Aggregation Kinetics of Alzheimer's β -Amyloid Peptide Is Controlled by Stochastic Nucleation. *Protein Sci.* **2005**, *14*, 1753–1759. [\[CrossRef\]](#)
45. Wu, J.;  sterlund, N.; Wang, H.; Sterneke-Hoffmann, R.; Pupart, H.; Ilag, L.L.; Gr slund, A.; Luo, J. Identifying the Role of Co-Aggregation of Alzheimer's Amyloid- β with Amorphous Protein Aggregates of Non-Amyloid Proteins. *Cell Reports Phys. Sci.* **2022**, *3*, 101028. [\[CrossRef\]](#)
46. Chafekar, S.M.; Baas, F.; Scheper, W. Oligomer-Specific A β Toxicity in Cell Models Is Mediated by Selective Uptake. *Biochim. Biophys. Acta-Mol. Basis Dis.* **2008**, *1782*, 523–531. [\[CrossRef\]](#)
47. Campioni, S.; Mannini, B.; Zampagni, M.; Pensalfini, A.; Parrini, C.; Evangelisti, E.; Relini, A.; Stefani, M.; Dobson, C.M.; Cecchi, C.; et al. A Causative Link between the Structure of Aberrant Protein Oligomers and Their Toxicity. *Nat. Chem. Biol.* **2010**, *6*, 140–147. [\[CrossRef\]](#) [\[PubMed\]](#)
48. Rennick, J.J.; Nowell, C.J.; Pouton, C.W.; Johnston, A.P.R. Resolving Subcellular PH with a Quantitative Fluorescent Lifetime Biosensor. *Nat. Commun.* **2022**, *13*, 6023. [\[CrossRef\]](#)
49. Valappil, D.K.; Mini, N.J.; Dilna, A.; Nath, S. Membrane Interaction to Intercellular Spread of Pathology in Alzheimer's Disease. *Front. Neurosci.* **2022**, *16*, 1572. [\[CrossRef\]](#)
50. Diaz-Espinoza, R.; Nova, E.; Monasterio, O. Overcoming Electrostatic Repulsions during Amyloid Assembly: Effect of PH and Interaction with Divalent Metals Using Model Peptides. *Arch. Biochem. Biophys.* **2017**, *621*, 46–53. [\[CrossRef\]](#) [\[PubMed\]](#)
51. Benseny-Cases, N.; Klementieva, O.; Cladera, J. In Vitro Oligomerization and Fibrillogenesis of Amyloid-Beta Peptides. *Subcell. Biochem.* **2012**, *65*, 53–74. [\[CrossRef\]](#) [\[PubMed\]](#)
52. Walsh, D.M.; Selkoe, D.J. A Beta Oligomers—A Decade of Discovery. *J. Neurochem.* **2007**, *101*, 1172–1184. [\[CrossRef\]](#) [\[PubMed\]](#)
53. Benilova, I.; Karran, E.; De Strooper, B. The Toxic A β Oligomer and Alzheimer's Disease: An Emperor in Need of Clothes. *Nat. Neurosci.* **2012**, *15*, 349–357. [\[CrossRef\]](#)

54. De La Torre, J.C. Is Alzheimer's Disease a Neurodegenerative or a Vascular Disorder? Data, Dogma, and Dialectics. *Lancet Neurol.* **2004**, *3*, 184–190. [[CrossRef](#)]
55. Vitvitsky, V.M.; Garg, S.K.; Keep, R.F.; Albin, R.L.; Banerjee, R. Na⁺ and K⁺ Ion Imbalances in Alzheimer's Disease. *Biochim. Biophys. Acta-Mol. Basis Dis.* **2012**, *1822*, 1671–1681. [[CrossRef](#)] [[PubMed](#)]
56. Qiang, W.; Yau, W.M.; Lu, J.X.; Collinge, J.; Tycko, R. Structural Variation in Amyloid- β Fibrils from Alzheimer's Disease Clinical Subtypes. *Nature* **2017**, *541*, 217–221. [[CrossRef](#)] [[PubMed](#)]
57. Petkova, A.T.; Leapman, R.D.; Guo, Z.; Yau, W.M.; Mattson, M.P.; Tycko, R. Self-Propagating, Molecular-Level Polymorphism in Alzheimer's Beta-Amyloid Fibrils. *Science* **2005**, *307*, 262–265. [[CrossRef](#)] [[PubMed](#)]
58. Benseny-Cases, N.; Álvarez-Marimon, E.; Aso, E.; Carmona, M.; Klementieva, O.; Appelhans, D.; Ferrer, I.; Cladera, J. In Situ Identification and G 4-P PI-His-Ma l-d End Rim Er-Induced Reduction of Early-Stage Amyloid Aggregates in Alzheimer's Disease Transgenic Mice Using Synchrotron-Based Infrared Imaging. *Sci. Rep.* **2021**, *11*, 18368. [[CrossRef](#)] [[PubMed](#)]
59. Otzen, D.; Riek, R. Functional Amyloids. *Cold Spring Harb. Perspect. Biol.* **2019**, *11*. [[CrossRef](#)]
60. Soscia, S.J.; Kirby, J.E.; Washicosky, K.J.; Tucker, S.M.; Ingelsson, M.; Hyman, B.; Burton, M.A.; Goldstein, L.E.; Duong, S.; Tanzi, R.E.; et al. The Alzheimer's Disease-Associated Amyloid β -Protein Is an Antimicrobial Peptide. *PLoS ONE* **2010**, *5*, e9505. [[CrossRef](#)]








Disclaimer/Publisher's Note: The statements, opinions and data contained in all publications are solely those of the individual author(s) and contributor(s) and not of MDPI and/or the editor(s). MDPI and/or the editor(s) disclaim responsibility for any injury to people or property resulting from any ideas, methods, instructions or products referred to in the content.

CHAPTER II: Exogenous Prion-Like Proteins and Their Potential to Trigger Cognitive Dysfunction

This chapter contains the article published in Molecular Systems Biology “Seira Curto, J., Dominguez Martinez, A., Perez Collell, G., Barniol Simon, E., Romero Ruiz, M., Franco Bordés, B., Sotillo Sotillo, P., Villegas Hernandez, S., Fernandez, M. R., & Sanchez de Groot, N. (2025). Exogenous prion-like proteins and their potential to trigger cognitive dysfunction. Molecular Systems Biology. <https://doi.org/10.1038/S44320-025-00114-4> ”

The supplementary data associated with this work is available in Section “Appendix 2” of this thesis.

Exogenous prion-like proteins and their potential to trigger cognitive dysfunction

Jofre Seira Curto ¹, Adan Dominguez Martinez ^{1,2}, Genis Perez Collell¹, Estrella Barniol Simon ¹, Marina Romero Ruiz ¹, Berta Franco Bordés ¹, Paula Sotillo Sotillo¹, Sandra Villegas Hernandez¹, Maria Rosario Fernandez ^{1✉} & Natalia Sanchez de Groot ^{1✉}

Abstract

The gut is exposed to a wide range of proteins, including ingested proteins and those produced by the resident microbiota. While ingested prion-like proteins can propagate across species, their implications for disease development remain largely unknown. Here, we apply a multidisciplinary approach to examine the relationship between the biophysical properties of exogenous prion-like proteins and the phenotypic consequences of ingesting them. Through computational analysis of gut bacterial proteins, we identified an enrichment of prion-like sequences in *Helicobacter pylori*. Based on these findings, we rationally designed a set of synthetic prion-like sequences that form amyloid fibrils, interfere with amyloid-beta-peptide aggregation, and trigger prion propagation when introduced in the yeast Sup35 model. When *C. elegans* were fed bacteria expressing these prion-like proteins, they lost associative memory and exhibited increased lipid oxidation. These data suggest a link between memory impairment, the conformational state of aggregates, and oxidative stress. Overall, this work supports gut microbiota as a reservoir of exogenous prion-like sequences, especially *H. pylori*, and the gut as an entry point for molecules capable of triggering cognitive dysfunction.

Keywords Microbiome; Neurodegeneration; Prion Protein; Aggregation; Amyloid

Subject Categories Digestive System; Microbiology, Virology & Host Pathogen Interaction; Neuroscience

<https://doi.org/10.1038/s44320-025-00114-4>

Received 3 May 2024; Revised 16 April 2025;

Accepted 2 May 2025

Published online: 27 May 2025

Introduction

Amyloid-forming proteins can exhibit prion-like properties, facilitating the transmission of their aggregated form between cells. A phenomenon observed in Alzheimer's disease (AD) and Parkinson's disease (PD), where amyloid-associated proteins propagate within the neuronal system of patients (amyloid- β -peptide (A β) and tau for AD, and alpha-synuclein for PD)

(Banerjee et al, 2024; Duyckaerts et al, 2019). Moreover, this is a global event that can occur between species (Ritchie and Barria, 2021). Hence, it is of great interest to explore the structural and sequential properties that define how amyloid proteins trigger aggregation or cross-seed non-orthologous polypeptides (Ritchie and Barria, 2021; Sampson, 2025).

Prion-like proteins are polypeptides that can adopt different conformations thanks to possessing large, disordered regions. It has also been reported that these regions can contain a segment capable of driving the aggregation of the entire protein, which is the basis for the amyloid stretch hypothesis (Sabate et al, 2015; Pallarès et al, 2016; Esteras-Chopo et al, 2005). When isolated, this segment, known as the amyloid core, can not only self-assemble but also trigger the aggregation of other prion-like sequences (Krishnan and Lindquist, 2005; Osherovich et al, 2004). These core sequences are rich in amino acids that despite being associated with disordered conformations also keep amyloid propensity such as asparagine (N), glutamine (Q), and tyrosine (Y). This enhanced propensity to aggregate within a disordered segment acts as a nucleation point that favors an ordered self-assembly without the requirement of conformational unfolding (Sabate et al, 2015). Moreover, the presence and strength of these amyloid cores influence the prionogenic potential of the protein that carries them (Osherovich et al, 2004).

The origin of many neurodegenerative diseases such as AD is sporadic, and thus associated with environment and lifestyle. Recent insights have implicated both diet (Grant and Blake, 2023; Jansens et al, 2019; Lambrecht et al, 2019) and gut microbiota as potentially pivotal factors in the onset and progression of these diseases (Walker and Czyz, 2023; Walker et al, 2021; Fang et al, 2020; Hashim and Makpol, 2022). In this line, antibiotic treatments and microbiota transplantation have been raised as plausible strategies to modulate pathology (Sampson et al, 2016).

The brain-gut microbiota axis is believed to act as a bidirectional link between the gastrointestinal (GI) tract and the central nervous system. In the gut, extracellular proteins are accessible for interactions with host molecules and are also susceptible to degradation (Holmqvist et al, 2014; Kim et al, 2019b), especially in the small intestine, thus facilitating the exposure of aggregation-prone segments. Gut microorganisms and their products can be found in the brain and the vagus nerve serves to transport bacteria

¹Unitat de Bioquímica, Departament de Bioquímica i Biologia Molecular, Universitat Autònoma de Barcelona, Barcelona, Spain. ²Institut de Neurociències, Universitat Autònoma de Barcelona, Bellaterra, Barcelona 08193, Spain. ✉E-mail: rosario.fernandez@uab.cat; natalia.sanchez@uab.cat

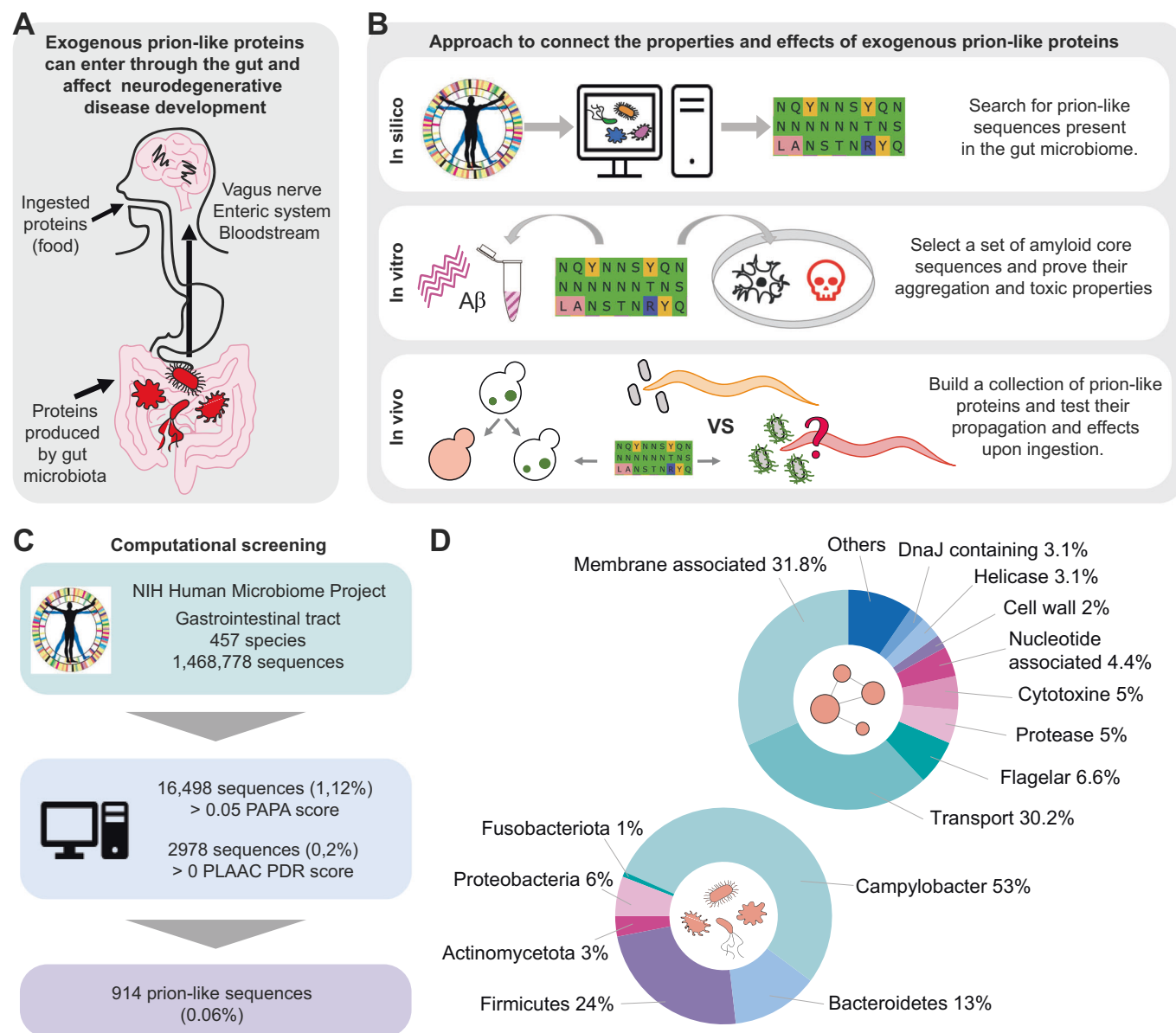


Figure 1. Studying exogenous prion-like proteins.

(A) The gastrointestinal tract is exposed to a diverse array of prion-like proteins, some of which are ingested while others may be produced by the resident microbiota. These proteins and their fragments can traverse the enteric system, the vagus nerve, or the bloodstream to reach the brain. (B) Diagram illustrating the approach employed in this study to investigate the properties and impacts of exogenous prion-like proteins. Top: Initial identification of prion-like sequences within the gut microbiome. Middle: Validation of computational predictions through the selection of amyloid core sequences for assessment of aggregation and toxicity. Bottom: Utilization of validated amyloid cores to construct exogenous prion-like proteins for testing their propagation and effects following ingestion in *C. elegans*. (C) Flowchart illustrating the procedure for screening of prion-like sequences in the gut microbiome and selecting amyloid-forming core candidates. (D) Top: Pie chart depicting the distribution of annotated descriptions within the 914 prion-like sequences identified in the gut microbiome. It just shows those annotations found with at least 2% of frequency. Bottom: Pie chart illustrating the distribution of phyla associated with the 914 prion-like sequences detected in the gut microbiome. It just shows those phyla found with at least 1% of frequency. Information about the genera within each phylum and its enrichment/depletion with respect to the original list is presented in Dataset EV2.

and their metabolites from the GI tract to the brain (Fig. 1A), thereby supporting their potential impact on the development and progression of neurodegenerative diseases (Bauer et al, 2016; Bonaz et al, 2018; Kim et al, 2021; Vidal-Veuthy et al, 2022; Kim et al, 2019a; Holmqvist et al, 2014; Walker and Czyz, 2023; Ritchie and Barria, 2021; Friedland and Chapman, 2017; Thapa et al, 2023).

One possible explanation of this connection is the ability of microbiota amyloid proteins to cross-seed the aggregation of host proteins. Supporting this idea, curli extracellular amyloid aggregates formed by *Escherichia coli* have been shown to accelerate alpha-synuclein aggregation in PD animal models (Walker et al, 2022; Wang et al, 2021; Sampson et al, 2020). Worryingly,

numerous homologs of the curli amyloid protein (CsgA) are found across the prokaryotic kingdom, each exhibiting different effects on alpha-synuclein aggregation (Bhoite et al, 2022; Fernández-Calvet et al, 2024). Despite this, the link between the pathologic phenotype, toxic mechanism, and molecular properties of amyloid proteins remains elusive.

To shed light on this question, our strategy integrates multi-disciplinary experiments from in silico sequence studies to phenotypical analyses in animal models. This approach facilitates the understanding of the connection between biophysical properties and the ability to trigger neurodegenerative diseases (Fig. 1B). Our computational work detected sequences with prion-like properties in 63% of the species classified as from the GI tract in an NIH Human Microbiome Project (NIH-HMP) (Peterson et al, 2009; Park et al, 2019) dataset, with a special enrichment of prion-like sequences in *Helicobacter pylori*. The amyloid cores of these sequences were rationally applied in a series of interconnected in vitro, and in vivo analyses. We designed a set of synthetic prion-like proteins to be introduced into the *C. elegans* digestive tract, which led to sensory memory impairment and lipid oxidation. The formation of immature and more reactive protein aggregates (He et al, 2012; Nimmrich et al, 2008; Lesné et al, 2013) appears to be associated with this. Overall, our findings offer insights into the relationship between the ingestion of exogenous prion-like sequences and neurodegenerative diseases, providing knowledge that may be valuable for the prevention and treatment of these diseases.

Results

Screening for prion-like sequences in the gut microbiome

Previous publications have reported an average of 0.3% prion-like sequences per genome in the bacterial domain (Seira Curto et al, 2022; Iglesias et al, 2015; Espinosa Angarica et al, 2013; Harrison, 2019; Lancaster et al, 2014; Toombs et al, 2012; Sabate et al, 2015; Gil-Garcia et al, 2021). To investigate their prevalence within the gut microbiome, we screened the protein sequences collected in the NIH Human Microbiome Project (NIH-HMP) (Peterson et al, 2009; Park et al, 2019) using three different algorithms: PAPA (prion aggregation prediction algorithm, <https://combi.cs.colostate.edu/supplements/papa/>) (Toombs et al, 2012), PLAAC (prion-like amino acid composition, <http://plaac.wi.mit.edu>) (Lancaster et al, 2014), and pWALTZ (Fig. 1C, <https://bioinf.uab.es/pWALTZ>) (Sabate et al, 2015). These approaches identify disordered sequences with a prion-like composition and provide a score that reflects the probability of a sequence behaving as a prion.

The original list derived from the NIH-HMP (http://downloads.hmpdacc.org/data/reference_genomes/body_sites/Gastrointestinal_tract.pep.fsa) (Peterson et al, 2009; Park et al, 2019) contained 457 species and 2,540,637 sequences, from which 1,468,784 are unique entries (Fig. 1C; Appendix Fig. S1). Using PAPA, we obtained 16,498 sequences (1.12%) with a positive prion aggregation propensity and when using a more stringent PLAAC score, we obtained 2978 sequences (0.20%) that had a prion-like domain. Merging these two sets of data, we identified 914 sequences (0.06%) that met both criteria, which we refer to as the positive

prion-like set (Dataset EV1). The proportion of prion-like sequences obtained with our approach (0.06%) aligns with previous reports of prion-like sequences in the bacterial domain (Seira Curto et al, 2022; Iglesias et al, 2015; Espinosa Angarica et al, 2013; Harrison, 2019; Lancaster et al, 2014; Toombs et al, 2012; Sabate et al, 2015; Gil-Garcia et al, 2021). These 914 sequences are found in 284 species, corresponding to 63% of the species collected in the GI NIH-HMP dataset. Given the ability of prion-like proteins to spread across species, this finding supports the hypothesis of gut microbiota being a reservoir of proteins with infectious potential (Seira Curto et al, 2022).

Functional and taxonomic analysis of the prion-like sequences

One striking feature of the 914 positive prion-like sequences is the high proportion of hypothetical or uncharacterized proteins, which constitute 40% of the set (Peterson et al, 2009; Park et al, 2019) (Dataset EV1). Most of the sequences collected in the NIH-HMP have been identified via genome shotgun sequencing, and those identified as hypothetical are open reading frames without a characterized homolog in the protein databases. By examination of the disordered regions predicted by MobiDB-lite (UniProt) (Peterson et al, 2009; Park et al, 2019), it is possible to detect repeated patterns (Appendix Fig. S1 and Dataset EV1), which suggests that these proteins may have conserved yet unidentified cellular roles that require a prion-like composition (Visconti et al, 2019; Ijaq et al, 2015; Desler et al, 2012).

The remaining 60% of positive prion-like sequences, with estimated homology, can be grouped into 10 categories according to their annotated descriptions (Fig. 1D and Dataset EV1). The two main categories are membrane-associated (31.8%) and transporter (30.2%) proteins, which play direct roles in facilitating interactions between bacterial cells and the extracellular milieu.

The sequences collected in the NIH-HMP GI set are associated with 457 bacteria species. A preliminary analysis of the 914 positive prion-like sequences revealed that most belong to species whose phyla have been previously related to neurodegenerative pathologies, particularly AD (Khaled et al, 2023; Panza et al, 2019; Vogt et al, 2017). However, for a global vision of their presence, we analyzed how the positive prion-like sequences are distributed within the different phyla and compared them to the original GI NIH-HMP set (Fig. 1D and Dataset EV2).

Half of the prion-like sequences correspond to *Campylobacter* (53%; Fig. 1D). In our list, this phylum is predominantly represented by *Helicobacter pylori* species, and the *Helicobacter* genus presents a seven-fold enrichment compared to the sequences collected in the GI NIH-HMP set (Dataset EV2). The second most abundant phylum in terms of prion-like sequences was Firmicutes, which accounts for 24% of the identified sequences. However, it is important to note that these high quantities may be due to their abundance in the former list (48%; Dataset EV2). This phylum includes genera such as *Coprobacillus* (6%), *Eubacterium* (6.5%), *Ruminococcus* (6.5%), *Lachnospiraceae* (6.5%), *Lactobacillus* (19%), and *Clostridium* (22%), collectively representing the predominant members. 13% of the prion-like sequences come from the Bacteroidetes phylum, which is one of the most prevalent phyla in the human gut microbiome (Khiabani et al, 2023). The last phylum with more than 5% of prion-like sequences in the positive

list is Proteobacteria (Pseudomonadota), which includes several pathogenic bacteria (such as *Acinetobacter* or *Neisseria*) and the widely studied *E. coli*. However, in proportion, there are three times fewer sequences from this phylum in the prion-like positive list than in the GI NIH-HMP set.

Computationally selected amyloid cores self-nucleate into amyloid-like fibrils

To validate the screening and to design a collection of exogenous prion-like sequences, we selected the amyloid cores of 10 prion-like positive sequences (Methods, Figs. 1B and EV1–2 and Dataset EV3). For this aim, we used pWALTZ, an algorithm that identifies the 21-amino-acid segment, within a Q/N-rich disordered region, with the highest amyloidogenic potential (Sabate et al, 2015). This length is sufficient for the formation of transmissible β -folds of the HET-s yeast prion domain (Wan and Stubbs, 2014; Wasmer et al, 2010) and is the minimal size that maximizes the discrimination between prionic and non-prionic sequences (Sabate et al, 2015).

To ensure sufficient amyloid propensity for the experimental assays, the amyloid cores were selected based on defined criteria, including pWALTZ scores above 73.55, Q/N-rich content, and host-interaction implications (see Methods). These sequences represent a diverse set of protein functions enriched in prion-like characteristics (Table EV1). The selected amyloid cores (see Methods) were named using a prefix corresponding to their species of origin, followed by a number from 1 to 10, reflecting their pWALTZ score and grouping by protein description (Table EV1, Dataset EV3). Their polypeptide sequences were chemically synthesized, and their ability to self-assemble into fibrillar aggregates was tested. The synthetic peptides were diluted in the aggregation buffer and then incubated at 37 °C without agitation. The presence of amyloid aggregates was assessed using transmission electron microscopy (TEM), Fourier-transform infrared spectroscopy (FT-IR), and binding to the amyloid dyes thioflavin-T (ThT) and Congo red (CR). All peptides exhibited the ability to form fibrillar structures (Fig. 2A) that were rich in beta-sheet conformations (Fig. 2B). Additionally, all peptides exhibited positive binding for at least one of the amyloid-specific dyes (Fig. 2C,D; Appendix Fig. S2). Together, these findings demonstrate the capacity of the predicted amyloid cores to catalyze self-nucleation into amyloid fibrils.

A set of eight control sequences with low aggregation propensity was designed to demonstrate that the observed amyloid properties are intrinsic to the selected prion-like sequences rather than artifacts (Methods). Five of these negative control sequences were derived from amyloid cores with low pWALTZ scores, while the remaining three were generated with a random amino acid composition based on the Swiss-Prot database. Using TEM, Thioflavin-T, and Congo Red we confirmed that these sequences did not self-assemble into amyloid-like aggregates (Appendix Figs. S3–5).

Interference with host protein aggregation

We next investigated the cytotoxic properties of candidate sequences to understand how exogenous prion-like proteins might interfere with host protein aggregation. Considering their possible alteration in AD patients (Vogt et al, 2017), we examined their capacity to interfere with the aggregation of the amyloid- β peptide (A β).

Pre-aggregated peptides were incubated with soluble A β 40 (Seira Curto et al, 2023) and the aggregation kinetics were monitored following the ThT fluorescence intensity (Fig. 3A; Appendix Fig. S6). The half-life (Fig. 3B) and lag times (Fig. 3C) exhibited a significant influence in 9 out of 10 peptides tested. Most peptides accelerated the aggregation kinetics, except for HA10, which slowed it down (Fig. 3A–C; Appendix Fig. S6).

In the analysis of the relationship between the peptide's composition and its effect on A β 40 aggregation, there was a robust correlation between the peptide net charge and lag-time kinetics, except for RI6 (Fig. 3D). A more positive net charge results in faster A β 40 aggregation, whereas a more negative charge results in slower aggregation. This effect may be attributed to electrostatic repulsion forces. Under the experimental conditions used (pH 7.4 and 100 mM NaCl), A β 40 carries a negative charge (−2.9) (Seira Curto et al, 2023; Wood et al, 1996). As a result, positively charged peptides may neutralize the net charge favoring A β 40 assembly, while negatively charged peptides may enhance the repulsive forces present in the mixture. This has also been observed in screening for A β aggregation inhibitors (Liao et al, 2012; Chan et al, 2012; Liu et al, 2016). Moreover, these works also report that these electrostatic forces work similarly for A β 42 (the main isoform located in the amyloid plaques), which despite having two extra amino acids have the same net charge at physiological conditions.

To test whether the full protein, and not just the amyloid-forming core, can form fibrillar aggregates and influence A β 40 aggregation kinetics, the parental protein that contains the BH4 amyloid core (C9L6N5, a protein with a DNAJ domain) was also tested. This protein, composed of 212 amino acids, was expressed in *E. coli* and purified (Appendix Fig. S7). The purified protein was able to aggregate into fibrillar structures (Appendix Fig. S7). Subsequent incubation of A β 40 with pre-aggregated C9L6N5 accelerated the aggregation kinetics similarly to the amyloid-forming core (Appendix Fig. S7). This result supports that not only the amyloid-forming cores but also the proteins from which these sequences originate can form fibrillar aggregates (Battie et al, 2017; Osherovich et al, 2004; Pallarès et al, 2018) and seed host molecules.

Toxicity and oxidative stress in neuron-differentiated cells

We next assessed whether the amyloid core peptides derived from bacteria residing in the gut could induce phenotypic hallmarks associated with neurodegenerative diseases in neuronal differentiated (SH-SY5Y) cells. We first analyzed whether the aggregates maintain their β -sheet conformation under cell culture conditions using an FTIR microscope (μ FTIR), a technique employed to measure the presence of amyloid aggregates in cells (Benseny-Cases et al, 2018) (Methods, Appendix Figs. S8–9). Then, we evaluated their potential to induce cell death using the MTT assay and oxidative stress using the DCFDA/H2DCFDA assay (Royall and Ischiropoulos, 1993) (Fig. 3E,F; Appendix Fig. S9).

The MTT assays showed that peptides with a net charge close to 0 exhibited greater toxicity compared to those with a higher charge (Fig. 3G). This suggests that electrostatic interactions might play a protective role against cytotoxicity. While differing from the A β results, where positively charged peptides accelerated the aggregation kinetics (Fig. 3D), this also indicates the existence of additional mechanisms contributing to toxicity.

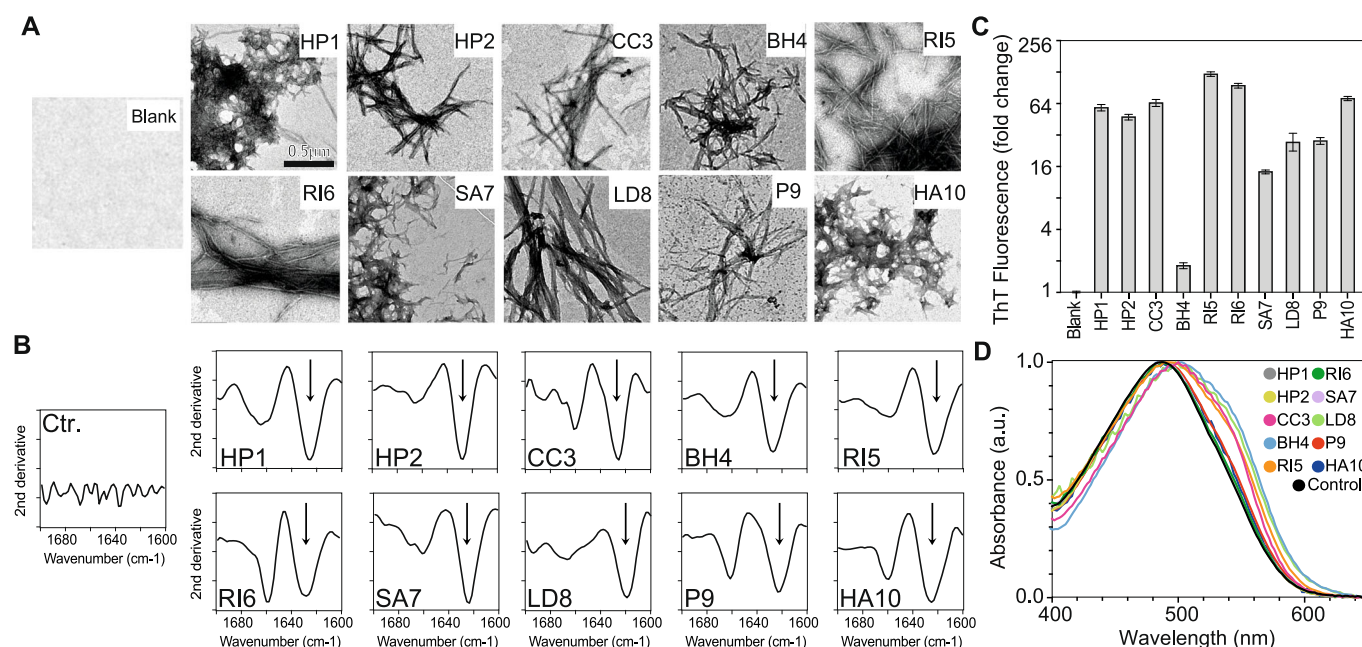


Figure 2. Amyloid aggregation of sequences from bacteria residing in the gut.

(A) TEM images showing fibrillar aggregates formed by the selected amyloid cores. (B) FTIR spectrum of the aggregated peptides. The arrows indicate the b-sheet intermolecular signal. (C) Thioflavin-T fluorescence increase (fold change) upon binding the aggregated peptides. All samples with aggregated peptides are significantly more fluorescent than Th-T alone. Statistical analysis was performed using multiple unpaired two-tailed t-tests, corrected for multiple comparisons using the Benjamini-Hochberg method (FDR set at 5%). The exact statistical values are provided in Dataset EV4. (D) Congo Red absorbance in the presence of the aggregate's peptides (Appendix Fig. S2 for individual scans). Control is buffer with CR, without aggregates. All experiments (from (A) to (D)) were performed with three biological replicates ($N = 3$), each consisting of three technical replicates. Source data are available online for this figure.

Polar, uncharged polypeptides tend to exhibit amphipathic characteristics that facilitate their interaction with membranes. Similar to antimicrobial peptides, these interactions can lead to membrane disruption and subsequent cell toxicity (Elliott et al, 2020). The observed general drop in cell viability to below 70% (Fig. 3E) suggests that the selected amyloid cores from the gut microbiome can induce cellular damage upon aggregation.

The production of cellular reactive oxygen species (ROS), significantly increased in six out of ten peptides compared to the control without aggregates (Fig. 3F). These data suggest that the reduced cell viability (Fig. 3E) can, in part, be attributed to oxidative stress. Overall, our results suggest that prion-like aggregates can cause cellular damage through membrane interactions and ROS production (De Groot and Burgas, 2015; Auten and Davis, 2009), supporting their potential contribution to disease (Fig. 3H).

Among all the peptides tested, the aggregates of HP1 and HP2 exhibited especially high toxicity (Fig. 3E; Appendix Fig. S10) and reduced cell viability to nearly 30% at 10 μ M. These two amyloid cores may be important sequences for the oligomerization and toxic potential of their parental proteins, two putative vacuolating cytotoxins (Dataset EV3).

Bacterial amyloid cores from the gut are functional in yeast

Although all the core sequences formed amyloid fibrils and exhibited cytotoxicity, each sequence has distinct properties, which

were reflected in their different ways of displaying these traits (Figs. 2 and 3). This combined with the amyloid stretch hypothesis, which states that the amyloidogenicity of a protein is comprised in short protein stretches (Esteras-Chopo et al, 2005), leads us to hypothesize that incorporating these amyloid cores into the same prion-like framework would result in a series of chimeras with different prion properties (Zambrano et al, 2015; Sabate et al, 2015; Osheroch et al, 2004; Von Der Haar et al, 2007).

The exchange of prion-like domains is commonly studied in the yeast prion Sup35 since it allows monitoring protein aggregation and propagation easily through an in vivo nonsense suppression assay. Additionally, Sup35 has been shown to accelerate the aggregation of tau and alpha-synuclein proteins in AD and PD models, respectively (Meng et al, 2023; Flach et al, 2022). These effects were demonstrated through intrahippocampal inoculation of Sup35NM fibrils in P301S tau transgenic mice, and through nasal infection with *Saccharomyces cerevisiae* in α -syn A53T transgenic mice.

The residues 7–13 recapitulate the amyloid properties of the full-length Sup35 (Burra et al, 2021), and the deletion of the first 40 residues, known as the nucleation domain, destroys the prion phenotype [PSI⁺] (Balbirnie et al, 2001; Krishnan and Lindquist, 2005). Based on this, we removed the first 40 amino acids of the yeast prion Sup35 and replaced them with our collection of amyloid cores (Fig. 4A; Appendix Supplementary Data) (Parham et al, 2001; Wickner et al, 2015). The sequential analysis of the resultant chimeras shows similar aggregation and prion-like propensities as the original Sup35 (Appendix Supplementary Data). This indicates

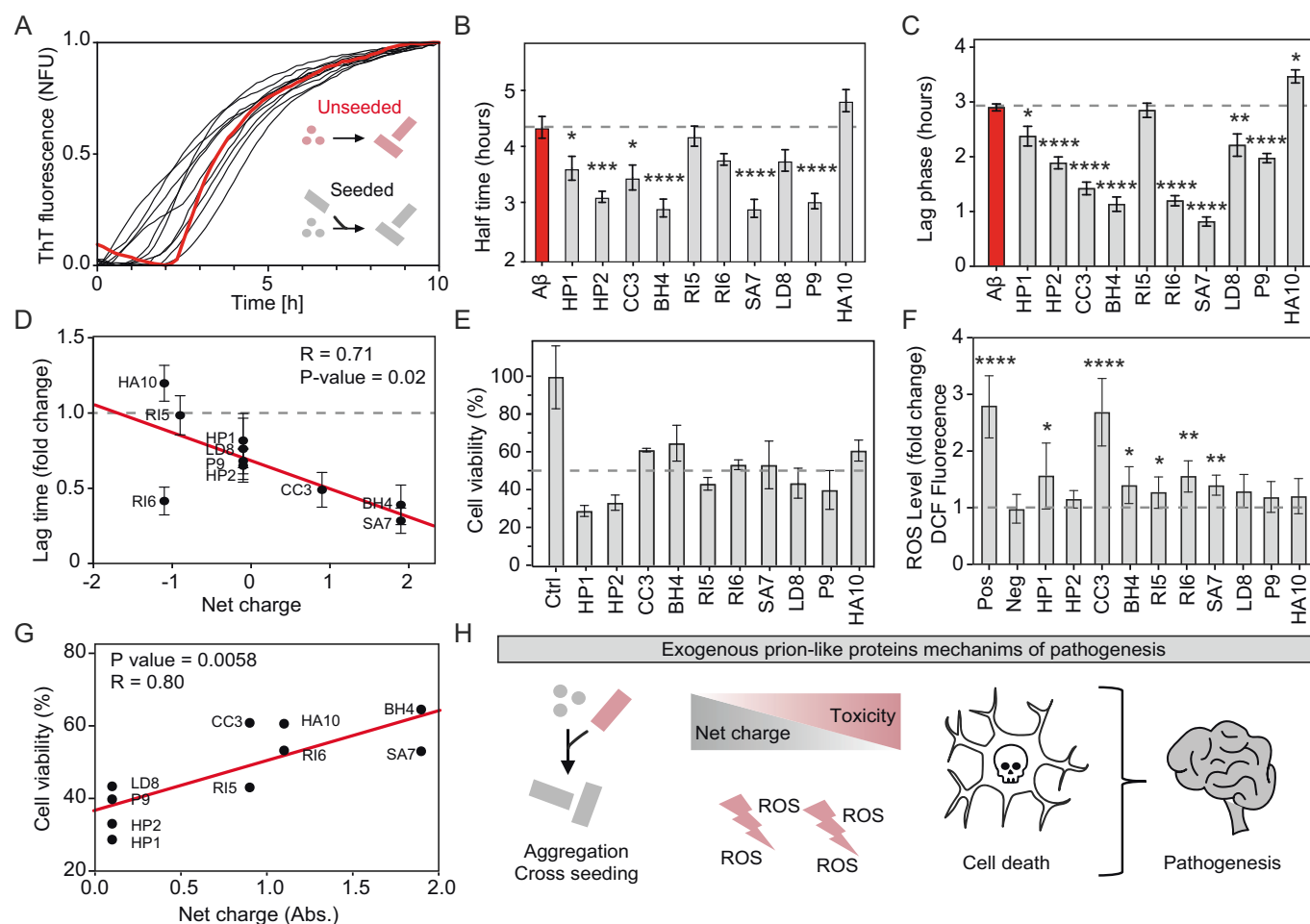


Figure 3. Seeding and toxicity potential of sequences from the gut microbiome.

(A) Aggregation kinetics of A β 40 peptide seeded by amyloid-forming cores from the gut microbiome (for individual kinetics, see Appendix Fig. S6). The kinetic assays were conducted with four biological replicates, each with three technical replicates. (B) Half-times of seeded aggregation kinetics (four biological replicates, each with three technical replicates). Error bars indicate SEM. In all panels (B, C, E, F), significance relative to the appropriate control (A β , Ctrl, or Neg) was assessed using multiple unpaired two-tailed t-tests, corrected for multiple comparisons using the Benjamini-Hochberg method (FDR set at 5%; * $q < 0.05$, ** $q < 0.01$, *** $q < 0.001$, **** $q < 0.0001$). The exact statistical values are provided in Dataset EV4. (C) Lag phases of seeded aggregation kinetics (four biological replicates, each with three technical replicates). Error bars indicate SEM. (D) Linear correlation between lag time and the net charge of the amyloid-forming cores used for seeding. The plot also shows the Pearson correlation coefficient (R) and the p -value calculated from an F-test. Without RI6, R increases to 0.95. (E) Viability of neuron-differentiated SH-SY5Y cells assessed by MTT assay after incubation with 10 μ M peptide aggregates. All cells incubated with aggregated peptides showed significantly lower viability (FDR 5%) than control cells (Ctrl) without peptides. Error bars indicate SD, centered on the mean. Three biological replicates ($N = 3$) were conducted, each consisting of three technical replicates. For results at lower concentrations, see Appendix Fig. S10. (F) DCFDA/H2DCFDA cellular ROS assay. The first column (Pos) shows the signal from the positive control (TBHP). Fluorescence was measured after 4 h of exposure to the peptides. Bars show the fluorescence fold change relative to the negative control (Neg). Error bars indicate SD, centered on the mean. Three biological replicates ($N = 3$) were conducted, each consisting of three technical replicates. (G) Linear correlation between peptide net charge and cell viability after treatment with 10 μ M peptide aggregates. The plot also shows the Pearson correlation coefficient (R) and the p -value calculated from an F-test. (H) Schematic representation of the proposed role of aggregation in pathogenesis. Source data are available online for this figure.

that the bacterial-derived amyloid cores can functionally substitute the Sup35 nucleation domain, as the new proteins retain the ability to aggregate and propagate, supporting their role as exogenous prion-like proteins.

We used the nonsense suppression assay to evaluate the formation and propagation of the Sup35 aggregates ([PSI⁺]) (Parham et al, 2001), including those variants incorporating bacterial-derived amyloid cores (see Methods). As positive and negative controls, we employed cells expressing unmodified Sup35 prion sequence (Sup35NM) and Sup35 lacking the first forty amino acids (Δ Sup35), respectively. Microscopy analysis revealed that

Sup35NM concentrates the fluorescence in bright foci, while Δ Sup35 exhibits a homogeneous distribution throughout the cytosol, indicating aggregation and solubility, respectively (Fig. 4B and Dataset EV5). In agreement with the computational prediction (Appendix Supplementary Data), all the cells expressing a Sup35 variant carrying an amyloid core (from HP1 to HA10) exhibited fluorescent foci (Fig. 4B).

Consistently, the [PSI⁺] prion propagation assay displayed 100% white colonies in Sup35NM, dropping to 30% in Δ Sup35 (Fig. 4C,D). In the case of cells expressing a Sup35 variant, despite presenting a high [PSI⁺] diversity, all showed a significant increase

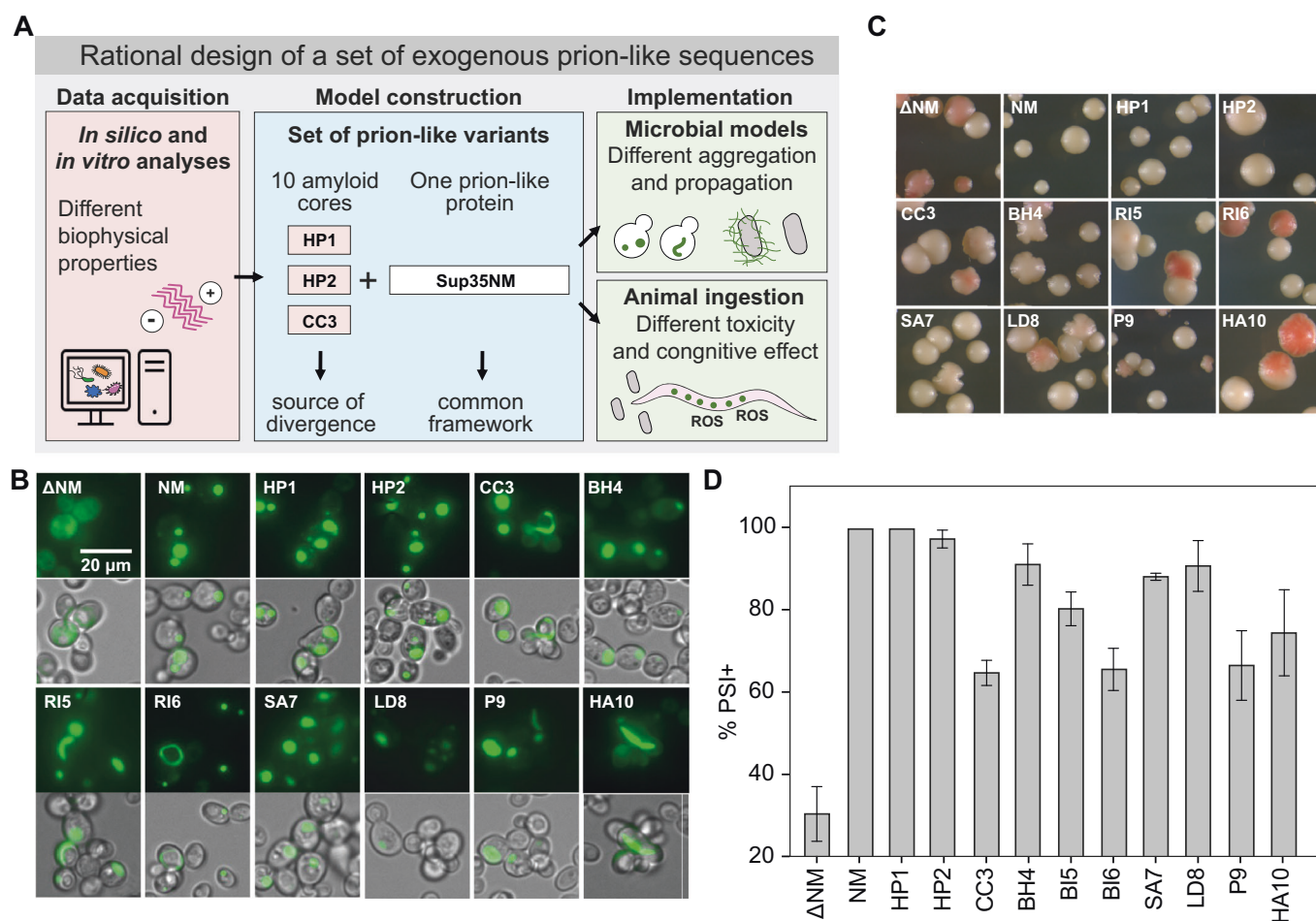


Figure 4. Aggregation and propagation analysis in yeast.

(A) Diagram illustrating how we designed the set of exogenous prion-like sequences studied in this work. Left panel: We first looked for 10 different amyloid-cores within the gut microbiome and analyzed their potential to trigger amyloid aggregation. Medium panel: The amyloid cores were introduced into the same protein (Sup35) to create 10 chimeras with different prionic properties. Right panel: Their aggregation and propagation were tested in vivo in yeast and bacteria models. Finally, the chimeras, expressed by bacteria, were studied as exogenous prion-like proteins that are ingested by *C. elegans*. (B) Fluorescent images showing intracellular aggregates of the Sup35-GFP variants. (C) Representative images of white/red colonies from the non-sense suppression assay. (D) Percentage of [PSI⁺] (prionic behavior) for each yeast strain analyzed. All assays were performed in three biological triplicates ($N=3$). Error bars indicate SD. Yeast strains expressing Sup35 chimeras with the predicted amyloid cores exhibited significantly higher [PSI⁺] levels (indicating better prion propagation) compared to the strain without a prion core (Δ NM). Statistical significance was assessed using multiple unpaired two-tailed t-tests, corrected for multiple comparisons using the Benjamini-Hochberg method (FDR set at 5%; all samples resulted in $q < 0.05$). The exact statistical values are provided in Dataset EV4. Source data are available online for this figure.

in the number of white colonies ([PSI⁺]) compared to Δ Sup35 (Fig. 4D).

Overall, both assays underscore the significance of the nucleation domain in driving Sup35 aggregation and propagation. The data also show that all the bacterial protein fragments selected can trigger Sup35 nucleation and can replicate its prion transmission in vivo in yeast. It is worth noting that this result is not obvious, since only prion-like and amyloidogenic sequences can restore the Sup35 aggregation and propagation abilities (Alberti et al, 2009; Zambrano et al, 2015; Sabate et al, 2015; Osherovich et al, 2004; Cascarina et al, 2017).

A deeper analysis of the microscopy images shows differences in the colonies and the aggregated forms between Sup35 variants. Importantly, the color stability of the [PSI⁺] colonies is indicative of

the prion-like protein capacity to keep the aggregated conformation through different generations. We observed that some Sup35 chimeras form long ring intracellular structures (Fig. 4B, Dataset EV5), and that the presence of more than 10% of cells with ring forms is associated with the formation of color-revertant colonies (indicative of a low-stability aggregated conformation). These ring forms are large, early aggregated stages that can progress to a mature single punctate conformation through the fragmentation activity of the HSP104 chaperone (Tyedmers et al, 2010; Sharma et al, 2017). In line with our results, the presence of long intracellular fibers has also been associated with less stable [PSI⁺], possibly due to lower amounts of prion seeds (propagons) small enough to propagate between cells; meanwhile, the punctate focus is associated with the formation of efficiently transmissible [PSI⁺]

(Chernova et al, 2017; Liebman and Chernoff, 2012; Derkatch and Liebman, 2013). Among all the prion-like variants, BH4 was the only one not presenting rings or multiple foci, indicating the formation of especially mature and stable aggregates (De Groot et al, 2015; Carija et al, 2017).

The Sup35 variants HP1, HP2, BH4, SA7, and LD8 demonstrated the highest percentage of $[PSI^+]$ conversion and, like Sup35NM, are robustly stable, as is evident by the absence of revertant colonies. Of these, HP1, HP2, and LD8, also displayed multiple fluorescent punctate foci, mirroring the pattern observed in Sup35NM (Fig. 4B, Dataset EV5). Interestingly, in vitro, upon incubation with SH-SY5Y, these three sequences also led to some of the lowest cell viabilities. Similarly, recent studies on variants of TDP-43 in yeast show that the presence of multiple punctate foci corresponds to more dynamic, liquid-like deposits with enhanced toxicity (Bolognesi et al, 2019). As observed in the in vitro assay, this toxicity may be associated with the original roles that these sequences may have in the parental protein (Dataset EV2–3).

The low aggregation-prone control sequences (Appendix Fig. S11) were introduced at the N-terminal of Sup35-GFP to demonstrate that not all sequences can trigger foci assembly, as this requires a prion- or amyloid-like composition. As expected, the resultant chimeras failed to form intracellular aggregates in yeast, except for L2, where 13% of the cells exhibited foci (substantially lower than the 61% to 100% observed in strains expressing aggregation-prone bacterial sequences). Overall, the nonsense suppression assay was consistent with the sequence analyses (Appendix Supplementary Data) demonstrating that the Sup35 variants carrying the bacteria amyloid cores can aggregate and propagate in a prion-like manner. Hence, this assay went further by showing different aggregation and propagation patterns.

Aggregation in a bacteria-based C-DAG system

With the aim of (i) simulating protein aggregation within a bacterial context and (ii) building a comestible gut-colonizing vehicle for our collection of exogenous prion-like proteins, we introduced the same set of Sup35NM chimeras expressed in yeast into the bacteria-based C-DAG system (Fig. 5A). In this system, the proteins are fused to the CsgAss exportation signal of the curli fibers (Appendix Supplementary Data), and the protein aggregation propensity can be monitored by measuring the formation of extracellular aggregates (Sivanathan and Hochschild, 2013).

To detect the formation of extracellular aggregates, we grew *E. coli* C-DAG cells on CR plates. The presence of extracellular aggregates is revealed by the development of reddish colonies. All strains, except for BH4 and RI5, displayed a robust signal, notably surpassing that exhibited by the soluble M domain of Sup35 (Sup35M) (Fig. 5B; Appendix Fig. S12). We also observed by TEM that all strains except Sup35M and Δ Sup35 displayed abundant large and fibrillar aggregated structures surrounding the cells (Fig. 5C).

When the Sup35 variants containing the rationally designed low aggregation-prone sequences were expressed by the *E. coli* C-DAG cells, no extracellular aggregates were observed (Appendix Fig. S13). Similar to the results in yeast, these findings emphasize the critical role of the nucleation core in driving Sup35 aggregation and demonstrate that sequence variations lead to distinct aggregation behaviors.

Bacterial extracellular fibrils induce loss of associative memory

Once analyzed their aggregation and propagation capabilities, we used the C-DAG system as a vehicle to introduce the exogenous prion-like proteins into the *C. elegans* gut to analyze their effects on the host, in particular, a neurodegenerative disease phenotype (Figs. 5A and 6A). By studying the same protein sequences across different assays, from biophysics to phenotypic analyses, we aim to combine these results to achieve a mechanistic understanding (Fig. 1B).

We start by monitoring alterations in the sensory memory of two different strains of *C. elegans*: the laboratory wild-type N2 (Fig. 6) and the AD model CL2355, which has a pan-neuronal expression of A β 42 (Appendix Fig. S14). The animals were fed the *E. coli* C-DAG collection expressing the Sup35NM chimeras (Fig. 5A). Subsequently, we performed a short-term associative memory assay (STAM) (see Methods) that links the presence of food with the chemoattractant butanone, a volatile odorant (Fig. 6A), to assess the cognitive status of the worms (Stein and Murphy, 2014). Both *C. elegans* models were fed *E. coli* expressing either the Δ NM or NM variants of Sup35. Compared to N2, CL2355 presented lower values in both indices, learning and memory. Interestingly, N2 worms that were fed bacteria that form aggregates (Sup35NM), exhibited a memory index similar to that of CL2355 worms, which were fed bacteria unable to form extracellular aggregates (Δ Sup35). Since both bacteria strains share the same genotype, these results suggest that the ingestion of the extracellular aggregates produced by Sup35NM causes cognitive impairment in the wild-type animal (N2) similar to those associated with the model of AD (CL2355). Furthermore, this assay also showed that the disease phenotype in CL2355 could be exacerbated when Sup35NM bacteria were included in its diet.

After validating the STAM assay to measure the neurodegenerative phenotype in N2, we fed the nematodes with *E. coli* expressing the Sup35NM variants containing the bacteria-derived amyloid cores. As a control, we first compared the non-conditioned worms (naive) and, as expected, no significant differences were observed between the animals fed with Δ Sup35 and those fed with the strains capable of forming extracellular aggregates (Fig. 6B, N data points). This indicates that without prior conditioning, all the animals respond similarly to the chemoattractant. However, during the learning assay (Fig. 6B, L data points), N2 worms fed with bacteria expressing HP1, HP2, RI5, RI6, or HA10 exhibited an index value less than half of that measured for those worms fed with bacteria expressing Δ Sup35 or Sup35NM. This suggests that the consumption of these bacterial strains and their extracellular aggregates has a stronger physiological impact on learning ability. Notably, the only variable among these conditions is the *E. coli* strain consumed and, consequently, the specific chimera it expresses.

When added to the nematodes' diet, 8 out of 10 bacteria strains triggered a significant memory decline (Fig. 6B, M data points), measured as a reduced chemotaxis index compared to Δ Sup35. This indicates that most of the prion-like chimeras can form aggregates that, upon ingestion, lead to a decline in the cognitive abilities of the worm. However, some proteins had a more pronounced effect on learning (HP1, HP2, RI5, RI6, and HA10), while others predominantly influenced memory (SA7, LD8, and P9) (Stein and

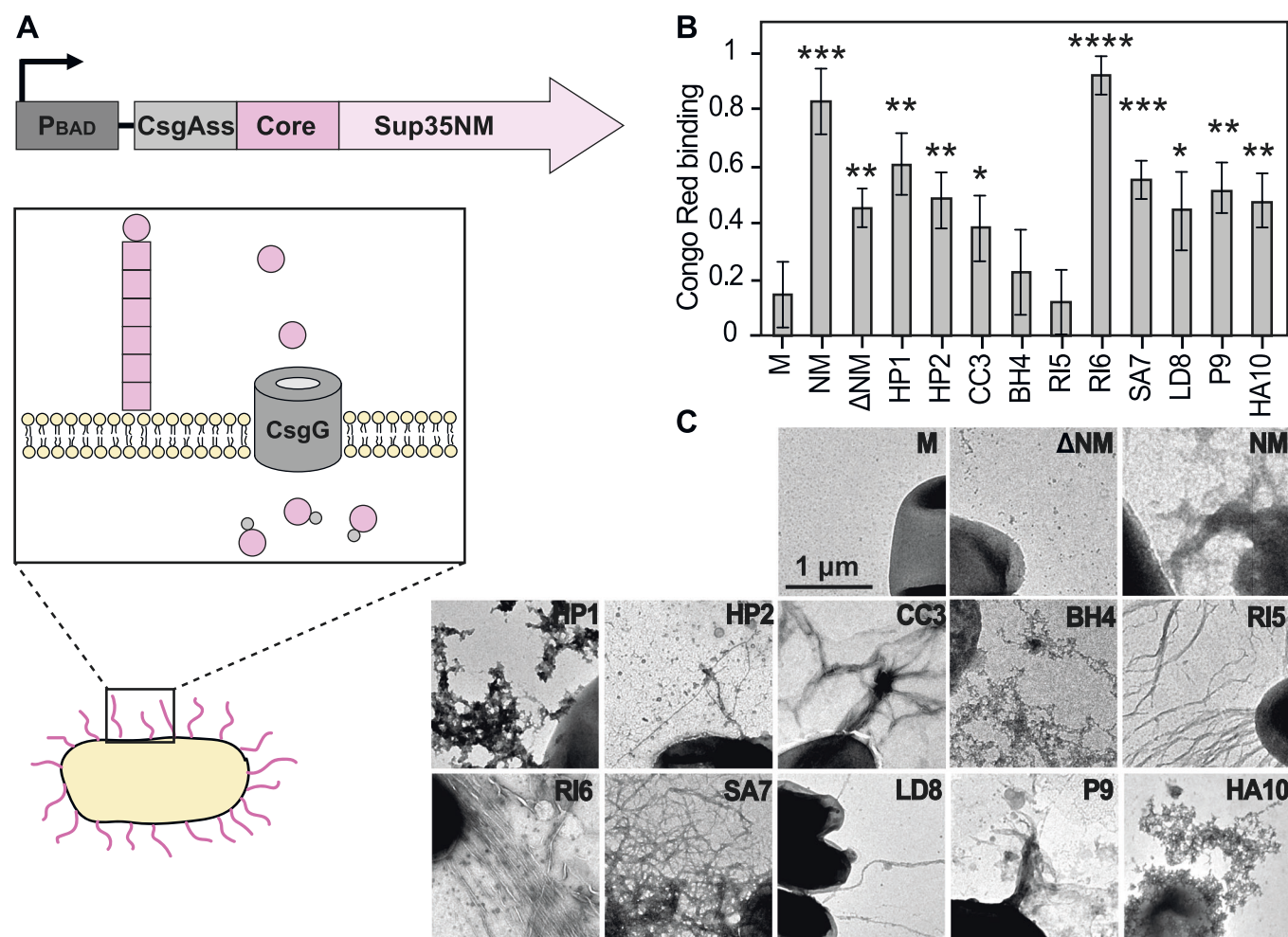


Figure 5. Aggregation in bacteria C-DAG system.

(A) Diagram showing the C-DAG construct integrated into *E. coli* cells and how the expression of Sup35p chimeras can form extracellular protein aggregates. (B) Measurement of the colony red intensity using ImageJ, normalized between maximum and minimum values. Asterisks indicate the significance in red color increase compared to Sup35M, the variant encoding the soluble Sup35 medium region. Error bars indicate SD, centered on the mean ($N = 4$ technical replicates). Statistical analysis was performed using multiple unpaired two-tailed t-tests, corrected for multiple comparisons using the Benjamini-Hochberg method (FDR set at 5%; * $q < 0.05$, ** $q < 0.01$, *** $q < 0.001$, **** $q < 0.0001$). The exact statistical values are provided in Dataset EV4. (C) TEM images showing fibrillar aggregated structures around *E. coli* cells. Source data are available online for this figure.

Murphy, 2014). In contrast, the ingestion of bacteria expressing three of the low aggregation-prone Sup35 controls (L1, L2, and R1) did not result in significant learning or memory deficits (Appendix Fig. S15). These analyses of cognitive abilities highlight the roles of aggregation and prion-like behavior as key factors in toxicity, underscoring the far-reaching influence of the microbiota's amyloidogenic sequences on cognitive function (Fig. 1A). Moreover, the results also point out that different prion-like aggregates can impact cognitive abilities in distinct ways (Fig. 6B).

Ingestion of exogenous prion-like proteins increases lipid oxidation

To explore the factors underlying the worms' cognitive decline, we analyzed them using synchrotron radiation μ FTIR (SR- μ FTIR). This technique measures the absorption spectra of the molecular bonds without the need for labeling. It is a non-invasive method

that captures the distinct chemical signatures of cells (Baker et al, 2014) and also *C. elegans* specimens (Gonzalez-Moragas et al, 2017; Muñoz-Juan et al, 2024). Here, we utilized SR- μ FTIR to analyze the lipid oxidation and the protein/lipid proportion (Fig. 6C,D; Appendix Figs. S16–18). These analyses show that, in general, the worms with better memory indices tended to present lower lipid oxidation levels together with lower protein/lipid signals (Fig. 6E). Hence, these results suggest a possible protein accumulation and an increase in ROS in the nematodes showing a cognitive decline. This agrees with the cellular analysis of the amyloid cores (Fig. 3F), which also suggested that oxidative stress could have a significant contribution to their toxicity.

To further investigate how the entry of exogenous amyloid proteins results in the accumulation and subsequent generation of ROS, we examined a nematode intestinal lysosome-related organelle known as the gut granule (Hermann et al, 2005; Dell'Angelica et al, 2000) (Fig. 7; Appendix Fig. S19). These

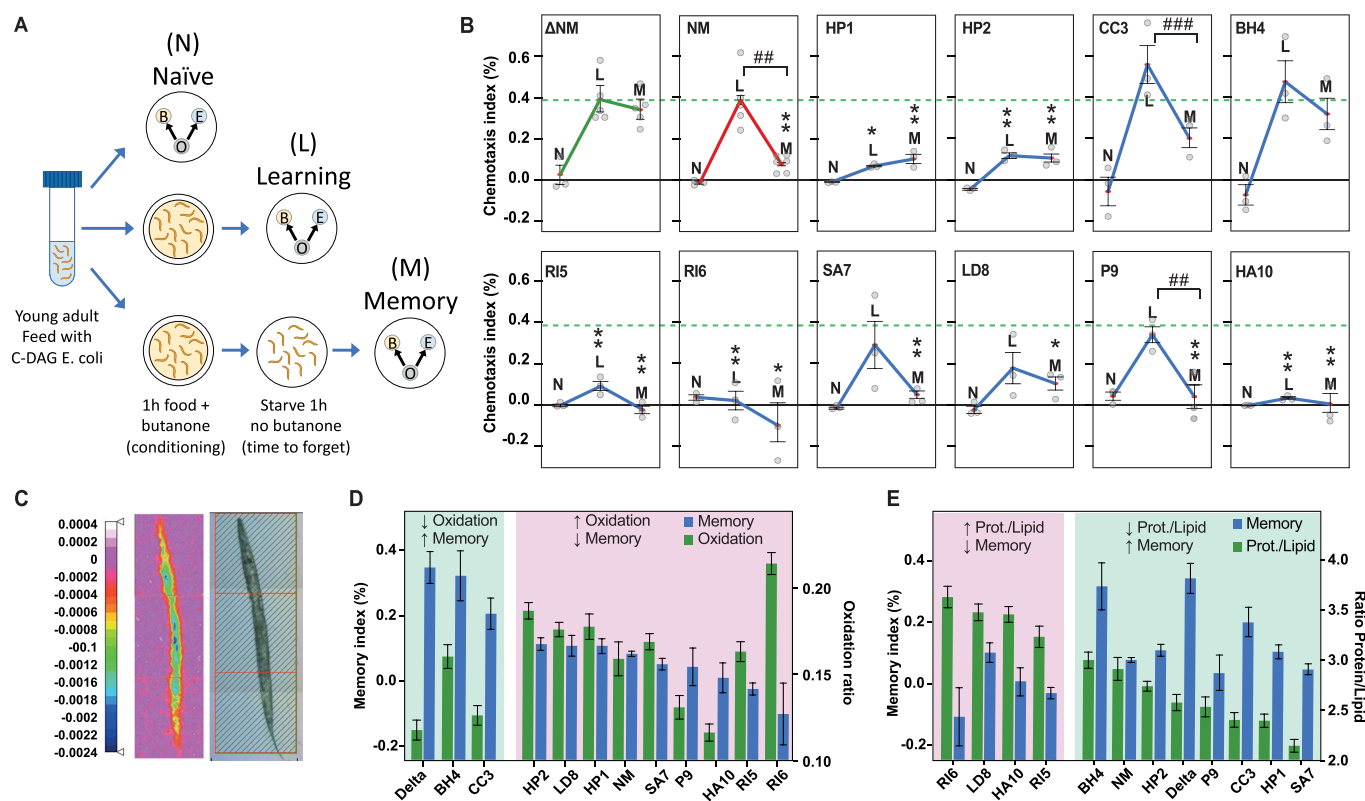


Figure 6. Cognitive effects on *C. elegans*.

(A) Diagram showing the three different conditions of the STAM assay. (B) Plots showing the three chemotaxis indices measured: naive (N), learning (L), and memory (M). Each data point represents 300–500 worms. The green dashed line indicates the learning index measured with ingestion of Δ Sup35 (Δ NM). Error bars represent the SEM. Asterisks (*) indicate significance relative to the corresponding Δ NM condition (Naive, Learning, or Memory), based on multiple unpaired two-tailed t-tests corrected using the FDR with the Benjamini–Hochberg method (FDR set at 5%; $N = 3$ biological replicates of 300–500 worms each; * $q < 0.05$, ** $q < 0.01$, *** $q < 0.001$, **** $q < 0.0001$). The exact statistical values are provided in Dataset EV4. (#) Hash symbols indicate significance between indices of worms fed the same bacterial strain but exposed to different conditions (Learning vs. Memory). Significance was assessed using an ordinary two-way ANOVA followed by Bonferroni's multiple comparisons test ($N = 3$ biological replicates of 300–500 worms each; # $p < 0.05$, ## $p < 0.01$, ### $p < 0.001$). The exact statistical values are provided in Dataset EV4. (C) mFTIR of a *N2* nematode feed with CC3 strain. Shows the distribution along the nematode body of the amyloid signal (1629/1654). For this parameter, we observed no significant increase between the worms ingesting Δ Sup35 (Δ NM) and those fed with the other Sup35 variants. (D) Comparison between memory indices and whole-body oxidation ratio measured with mFTIR (error bars are SEM; for oxidation ratio $N \geq 42$, the measures were taken uniformly along the body of 10 different worms). A linear regression analysis is presented in Appendix Fig. S16. The samples are arranged from highest to lowest memory index values. The green zone indicates worms with higher memory index values, while the red zone represents those with lower memory index values. (E) Comparison between memory indices and whole-body protein/lipid ratio measured with mFTIR (error bars are SEM; for protein/lipid ratio $N \geq 42$, the measures were taken uniformly along the body of 10 different worms). A linear regression analysis is presented in Fig. S16. The samples are arranged from highest to lowest Protein/Lipid IR signal ratio. The red zone indicates worms with a higher Protein/Lipid IR signal ratio, while the green zone represents those with a lower one. Source data are available online for this figure.

organelles are one of the nematode's first defenses against the entrance of exogenous menaces through the intestine (Hajdú et al, 2023). They are involved in digestion and nutrient storage and are able to sequester and neutralize ingested toxins and pathogens to prevent damage (Roh et al, 2012; Chun et al, 2017; Ardelli and Prichard, 2013). Recently, they have also been associated with the stress response and with a reduction in protein aggregation in a Huntington's disease model (Brunquell et al, 2018).

The gut granules contain several autofluorescent compounds (Fig. 7A) whose intensity increases with oxidative stress and cellular damage (Navarro-Hortal et al, 2024; Ayuda-Durán et al, 2020). The ingestion of the *E. coli* C-DAG collection increased the number of gut granules (Appendix Fig. S19) and their fluorescence intensity (Appendix Fig. S20) compared to the consumption of the *E. coli* OP50 strain, the standard nematode food and a biofilm-defective

mutant (Arata et al, 2020). This observation suggests an increase in gut granule activity and that the products expressed by the *E. coli* C-DAG bacteria may interfere with these organelles more than those produced by the OP50 strain. In agreement with previous studies on oxidative stress (Navarro-Hortal et al, 2024; Ayuda-Durán et al, 2020), our analyses with SR- μ FTIR indicate that the lipid oxidation signal in the nematode intestine is linked with the number of fluorescent foci (Fig. 7B). Overall, this result connects the aggregates produced by the ingested bacteria with the oxidative levels of the nematode and the number of gut granule organelles.

The aggregates' properties define the cognitive deficit

We next compared the number of gut granules with the memory index, revealing that the worms with lower indices tend to have

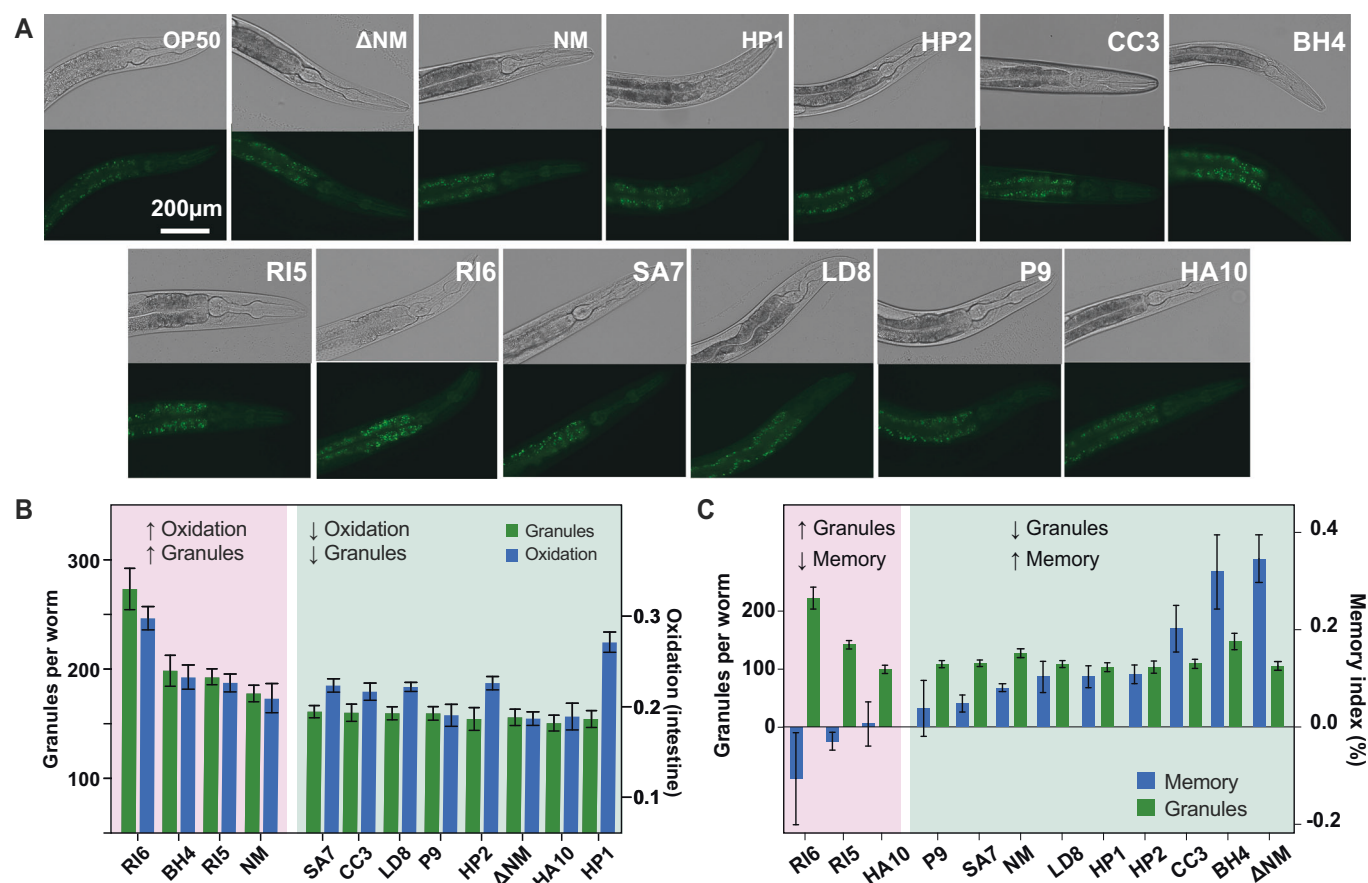


Figure 7. Oxidative stress and gut granules fluorescence.

(A) Fluorescent images showing the presence of gut granules in the analyzed worms. At the top transmitted light, and at the bottom fluorescence. (B) Comparison of lipid oxidation within the intestinal section and the number of gut granules ($N = 10$ different worms). Lipid oxidation and granule number were significantly different between the red group (RI6, BH4, RI5, NM) and the green group (SA7, CC3, LD8, P9, HP2, ΔNM, HA10, HP1), as determined by unpaired two-tailed t-tests ($p = 8.72 \times 10^{-7}$ for lipid oxidation and $p = 1.76 \times 10^{-6}$ for granule number). Each group's values were pooled and analyzed independently. Error bars represent the standard error of the mean (SEM). (C) Comparison of memory index ($N = 3$ biological replicates of 300–500 worms each) and the number of gut granules ($N = 10$ different worms). Memory index and granule number were significantly different between the red group (RI6, RI5, HA10) and the green group (P9, SA7, NM, LD8, HP1, HP2, CC3, BH4, ΔNM), as determined by unpaired two-tailed t-tests ($p = 0.0106$ for memory and $p = 2.45 \times 10^{-7}$ for number of granules). Each group's values were pooled and analyzed independently. Error bars represent the standard error of the mean (SEM). Source data are available online for this figure.

more gut granules (Fig. 7C; Appendix Fig. S16). This result suggests that the accumulation of components in the gut granules and the oxidation associated with the intake of *E. coli* C-DAG strains may be related to the severity of memory loss.

Similarly, the worms ingesting *E. coli* strains that formed intensely red colonies in the presence of CR tend to have a lower memory index (Appendix Fig. S21), except for RI5, which produced an especially faint red color. In addition, the proteins that result in the formation of abundant ring structures in yeast are associated with worms with lower memory indexes (Appendix Fig. S22).

Taking all the assays together, there appears to be a parallel progression in the number of gut granules, the intensity of red colonies, and the formation of ring aggregates in yeast, which seems to be linked with memory loss (Fig. 7C; Appendix Fig. S22). The intensity of red in the *E. coli* colonies is associated with the ability of the extracellular aggregates to bind CR. In yeast, the ring structures are precursors of the foci, with poorer propagation and enhanced toxicity (Chernova et al, 2017; Derkach and Lieberman,

2013; Barbitoff et al, 2022). On the contrary, the formation of large stable foci has been associated with a protective strategy against oxidative damage (Carija et al, 2017). In this line, an increase in gut granule fluorescence has been associated with an increase in lipid oxidation (Navarro-Hortal et al, 2024; Ayuda-Durán et al, 2020). Considering all factors together, we hypothesize that the inability to progress to mature and inert aggregates (He et al, 2012; Nimmrich et al, 2008; Lesné et al, 2013) may lead to the formation of promiscuous conformations (Nimmrich et al, 2008; Lesné et al, 2013) that generate more ROS and ultimately promote stronger cognitive decline.

Discussion

The gut serves as a potential entry point for various exogenous molecules, including prions. There, the microbiota can act as a source of amyloid-promoting proteins with proven effects on host

health(Walker et al, 2022; Wang et al, 2021; Sampson et al, 2020; Bhoite et al, 2022; Fernández-Calvet et al, 2024; Seira Curto et al, 2022). To explore the impact of exogenous prion-like proteins on the host, we assembled a collection of potential amyloidogenic sequences. These sequences were computationally designed based on gut microbiome analysis, providing a synthetic and simplified approach that does not intend to represent any specific natural protein but instead aims to offer a broad overview of prion-like sequences. The resulting peptides were capable of self-assembling into amyloid-like fibrillar structures, with the ability to interfere with Aβ aggregation and induce ROS production in neuron-differentiated cells.

The identified prion-like sequences are associated with diverse functional categories, including membrane receptors, transporters, and adhesins, indicating their involvement in critical interactions with host cells and the environment (Visconti et al, 2019; Ijaq et al, 2015; Desler et al, 2012). Notably, certain bacterial proteins, like curli fibers found in *E. coli*, may enhance bacterial colonization and pathogenesis, potentially influencing neurodegenerative processes(Chen et al, 2016; Friedland et al, 2020; Van Gerven et al, 2018; Kuwajima et al, 2022; Kosolapova et al, 2020; Wang et al, 2021).

Among the bacteria species detected, *Helicobacter pylori* stood out due to the high number of sequences coding for prion-like proteins (Dataset EV2). Additionally, many AD patients have experienced active and/or latent *Helicobacter* infections, pointing to a potential role in the development of the pathology (Go, 2002; Panza et al, 2019; Khaled et al, 2023). Notably, HP1 and HP2 are fragments of two putative vacuolating cytotoxins, proteins known to assemble into disrupting pores upon interaction with host cell membranes (Connolly et al, 2024). Despite their short lengths, HP1 and HP2 exhibited significant toxicity, highlighting their potential involvement in host-pathogen interactions and their contribution to disease processes.

Importantly, species encoding prion-like sequences also share phyla with others known for health benefits, such as Firmicutes (Huttenhower et al, 2012), highlighting the gut microbiota's complexity in disease development. Hence, further studies are necessary to better understand the relationship between bacterial species and neurodegenerative diseases and to explore potential therapeutic interventions targeting the gut microbiome.

The systematic platform presented here facilitated the analysis of exogenous prion-like proteins across multidisciplinary experiments, enabling the connection between structural and prionogenic properties with toxic and phenotypic effects. Our sequential engineering work corroborates the amyloid stretch hypothesis, demonstrating that the exchange of an amyloid core keeps the capacity to aggregate and propagate while modulating the prionic behavior.

Overall, while numerous protein sequences remain unidentified despite their potential health implications (Appendix Fig. S1), our findings indicate that many different sequences can influence the host and induce various effects on cognitive abilities (Fig. 6). This sequential diversity is also reflected in the increasing number of bacteria amyloid-promoting proteins with reported effects on host health(Walker et al, 2022; Wang et al, 2021; Sampson et al, 2020; Bhoite et al, 2022; Fernández-Calvet et al, 2024; Seira Curto et al, 2022). We hypothesize that, in our case, oxidative stress generation contributes to this deleterious outcome, highlighting the complex interplay between the molecules transiting the gut and neurodegenerative diseases. Our research provides valuable insights into the

role of exogenous prion-like proteins and underscores the importance of elucidating their mechanisms for identifying potential therapeutic targets and further investigating the gut-brain axis in disease pathogenesis.

Methods

Reagents and tools table

Reagent/Resource	Reference or Source	Identifier or Catalog Number
Experimental models		
The 74D-694 derivative yeast strain: MATa, ade1-14 ^{UGA} , trp1-289, his3-Δ200, ura3-52, leu2-3,112 sup35::loxP [pYK810] [PIN ⁺]	Gasset-Rosa and Giraldo (2015)	NA
SH-SY5Y	ATCC	CRL-2266
<i>C. elegans</i> N2	Caenorhabditis Genetics Center	N2
<i>C. elegans</i> CL2355 Alzheimer's model	Caenorhabditis Genetics Center	CL2355
VS39 <i>E. coli</i> strain from C-DAG system	Sivanathan and Hochschild (2013)	NA
Recombinant DNA		
pUKC1620	Parham et al (2001), Gasset-Rosa and Giraldo (2015)	NA
pESC-URA	Agilent Technologies	217454
pVS72	Sivanathan and Hochschild (2013)	NA
pVS105	Sivanathan and Hochschild (2013)	NA
pet11-BH4-6HIS	GenScript	NA
Oligonucleotides and sequence-based reagents		
PCR primers	This study	Table EV5
Antibodies		
Anti-GFP, rabbit serum	Invitrogen™, ThermoFischer Scientific	A6455
Anti-His rabbit	Thermo	RM 146
Anti-rabbit horseradish peroxidase conjugate	BioRad	1662408EDU
ECL KIT	Thermo	32106
Chemicals, Enzymes and other reagents		
KOD Hot start polymerase	Novagen, Toyobo	71086
FastDigest DpnI	ThermoScientific	FD1704
DMEM-F12 Glutamax	Gibco	10565018
Pen-strep	Gibco	15140148
FBS	Gibco	A5256701
SH-SY5Y	ATCC	CRL-266
Trypsin	Gibco	25300-120
AB40	Genscript	RP10004
Non-binding 96-well Plate	Greiner	655906

Reagent/Resource	Reference or Source	Identifier or Catalog Number
Thioflavin T	Sigma	596200
MTT	Fisher	10133722
DCFDA/H2DCFDA	Thermo	D399
DMSO	Fisher	BP231-1
Congo Red	Thermo	B24310.14
pET21b	Novagen	69741
HFIP	Thermo	A12747.22
His Trap FF	Cytiva	17524802
Software		
Graphpad Prism	www.graphpad.com	NA
Opus 7.5	Bruker	NA
PSORTb v3.0	www.psort.org	NA
pWALTZ	https://bioinf.uab.es/pWALTZ	NA
PAPA	https://combi.cs.colostate.edu/supplements/papa/	NA
PLAAC	http://plaac.wi.mit.edu/	NA
Other		
EVOS M5000 Imagen System	Leica Microsystems GmbH, Mannheim, Germany	NA
TECAN Infinite+ NANO	TECAN Trading AG, Switzerland	NA
JEM-1400	JEOL, Tokyo, Japan	NA
Hyperion 3000 Microscope	Bruker, Germany	NA
Thermo Omnic 7.1	Thermo Scientific, Inc.	NA
Leica MZFLIII stereomicroscope	Leica Microsystems GmbH, Mannheim, Germany	NA
Vertex 70 spectrometer	Bruker, Germany	NA

List of positive prion-like proteins

The proteins encoded in the gut microbiome's genome were sourced from the NIH Human Microbiome Project (University of Maryland, 2009; Park et al, 2019). The original list is available at: http://downloads.hmpdacc.org/data/reference_genomes/body_sites/Gastrointestinal_tract.pep.fsa. After refining the list to remove duplicate entries, we identified 457 distinct organism names and 1,468,778 protein sequences. This shorter list is available at the figshare repository (<https://doi.org/10.6084/m9.figshare.25710048.v1>). This compilation of proteins underwent screening to identify prion-like proteins using two distinct algorithms: PAPA (Toombs et al, 2012) and PLAAC (Lancaster et al, 2014). These approaches seek proteins featuring prion-like domains and assign a score to each, indicating the probability of behaving as a prion.

Based on prior studies and our expertise (Iglesias et al, 2015), we identified potential prion-like proteins by employing a combination of criteria from the three different algorithms. Specifically, we

employed a PAPA score threshold of 0.05 to denote a positive prion aggregation propensity. Additionally, we considered a PLAAC PRD score above 0 as indicative of sequential domains capable of initiating the aggregation process.

Selection of amyloid core sequences

We selected 10 amyloid core segments for experimental validation. We first arranged all the sequences by their pWALTZ score to prioritize candidates with a higher propensity to self-assemble. The pWALTZ algorithm was applied to the 80-amino-acid regions previously predicted by PAPA (Iglesias et al, 2015), providing the 21-amino-acid segment with the highest aggregation propensity within it (Gil-Garcia et al, 2021; Iglesias et al, 2015; Sabate et al, 2015) (Table EV1). The candidates were chosen from those with a Q/N proportion of at least 20% and a score above 73.55, the default cut-off, to guarantee amyloid-forming sequences, both in vitro and in vivo (Sabate et al, 2015).

We excluded sequences labeled as hypothetical, those containing cysteine residues, and those with multiple transmembrane domains. We chose sequences from bacterial strains associated with genera previously reported to be altered in AD patients (Vogt et al, 2017; Panza et al, 2019; Khaled et al, 2023) and with a high likelihood of being extracellular (PSORTb tool (Tenaillon et al, 2010)).

From this shorter list of sequences that fulfill these criteria, we prioritized sequences covering the protein functions that are more enriched in prion-like proteins such as protease (RI5 and RI6 are trypsin-like), cytotoxin (HP1 and HP2 are putative vacuolating cytotoxins), DnaJ-containing domain (such as CC3 and BH4), and nucleotide-associated proteins (P9).

From the list of other functions, we chose sequences with descriptions with host interacting implications such as “penicillin-binding protein” (SA7) or that indicate aggregation such as “aggregation promoting” (LD8) or “curli associated” (HA10). When several options were left, we chose those with higher pWALTZ scores or two candidates with sequential differences (e.g., composition or length).

Overall, we constructed a diverse collection of sequences from both Gram groups, different genera, and annotated descriptions (Fig. 1D, Table EV1, Figs. EV1–2, Dataset EV3).

Protein alignment and consensus sequence

The alignments between the 10 different amyloid-forming core candidates and the consensus sequence were obtained using the Unipro UGENE software v43.0 (Okonechnikov et al, 2012) for sequence visualization.

Protein location prediction using PSORTb

For protein location prediction, we employed PSORTb v3.0 (Yu et al, 2010). This allowed us to anticipate the potential locations of the protein candidates. The algorithm was executed with ‘bacteria’ selected as the organism type, and the appropriate Gram stain was chosen for each organism. The best localization scores were used to generate Dataset EV3.

Control peptides design

We designed eight control sequences to rule out the possibility of artificial effects during the experiments performed.

We designed the control sequences using two distinct strategies. The first strategy utilized amyloid cores with lower pWALTZ scores, while the second used the amino acid composition of proteins curated in Swiss-Prot.

For the first approach, we start by randomizing sequences with lower pWALTZ scores within the positive set. To ensure low amyloidogenic and prion-forming propensity, we implemented the following modifications:

- Substituting hydrophobic residues with glycine, an amino acid with very low prion propensity (Sabate et al, 2015).
- Maintaining a Q/N content between 9.5% and 38% while ensuring a net charge below 3, to avoid repulsive forces that might artificially inhibit aggregation and to preserve some sequence similarity with the prion-positive set.

The resulting sequences were as follows:

```
>L1
GYHEGQGGYHDDGGQHGGYHGG

>L2
SGHGSHESSGGSQQSRGSGGTS

>L3
NSMERNSSNSSGHGNNQDSNN

>L4
KSDQQGSHEQGMQSGMGDGMT

>L5
NNGESGGNNSGGSNNDNTSSQ
```

We developed a second set of control sequences using a Python script (see below) to generate random sequences of 21 residues with an amino acid composition similar to natural proteins based on Swiss-Prot database (<https://web.expasy.org/docs/relnotes/relstat.html>).

The sequences generated were:

```
>R1
GELAMARRGNPTLGGITRKRS

>R2
IDWRANVTDEPQVAAGAHTVE

>R3
KAEHTDTLMQEGARRTTDNQG
```

Python script used:

```
import random
# Define the amino acids and their frequencies
amino_acids = [
```

```
('A', 8.25), ('C', 1.38), ('D', 5.46), ('E', 6.71),
('F', 3.86), ('G', 7.07), ('H', 2.27), ('I', 5.91),
('K', 5.80), ('L', 9.64), ('M', 2.41), ('N', 4.06),
('P', 4.74), ('Q', 3.93), ('R', 5.52), ('S', 6.65),
('T', 5.36), ('V', 6.85), ('W', 1.10), ('Y', 2.92)
]
# Create a list of amino acids according to their
frequency aa_list = []
for aa, freq in amino_acids:
    aa_list.extend([aa] * int(freq * 100)) # Scale up for
    better distribution
# Function to generate a random protein sequence of a
    given length
def generate_protein_sequence(length):
    return ''.join(random.choice(aa_list) for _ in
        range(length))
# Generate a random sequence of 21 residues
sequence = generate_protein_sequence(21)
print(sequence)
```

Using these approaches, we obtained eight different sequences of 21 amino acids. These sequences showed negative results for aggregation and prion propensity when tested with various algorithms used in this study (PAPA score below 0.05, PLAAC PRD 0, pWALTZ score below 50) as well as Aggrescan (Conchillo-Solé et al, 2007). The pWALTZ values for these control peptides are not provided because they are below 50.0, which is the established threshold for distinguishing prion-like sequences (Zambrano et al, 2015). For this reason, the pWALTZ algorithm does not generate scores below this cutoff.

Peptide preparation

All samples were prepared in low protein-binding microcentrifuge tubes (ThermoFisher Scientific, Waltham, MA, USA).

The amyloid-forming cores were acquired lyophilized from the Peptide Synthesis Facility, Department of Experimental and Health Sciences, Universitat Pompeu Fabra (UPF). Peptides were then solubilized in 1,1,1,3,3,3-hexafluoroisopropanol (HFIP) and separated into different aliquots and were dried overnight in a fume hood at room temperature. Different buffers and concentrations were tested to find the best conditions for amyloid aggregate formation. The best results were obtained by redissolving the peptides with DMSO to maintain them as monomers and diluting them in 50 mM phosphate buffer (PB) pH 7.4 at a final concentration ranging from 50 to 400 μ M and left overnight for aggregation (see Dataset EV2).

Synthetic A β 40 (DAEFRHDSGYEVHHQKLVFFAEDVGSNKGAIIGLMVGGVV-NH₂) was purchased from GenScript (Rijswijk, Netherlands). Stock solutions were prepared by dissolving 1 mg of the peptide to a final concentration of 250 μ M and adding 20 mM sodium phosphate buffer, 0.04% NH₃, and NaOH to a final pH of 11. Then, the peptide was sonicated for 10 min (Fisherbrand Pittsburgh, PA, USA, FB15051) without sweep mode and stored at -80°C . For toxicity and seeding experiments, the peptide was left to aggregate at room temperature for 24 h.

Congo Red binding to protein aggregates

Congo Red (CR) binding to aggregated peptides was analyzed by acquiring the absorbance spectra in the 400–650 nm range using a

Cary 300 spectrophotometer (Varian). The assay was performed in a total volume of 150 μL (15 μL of aggregated peptide samples, 15 μL of CR 200 μM , and 120 μL of 50 mM PB pH 7.4). Before dye addition, all samples were sonicated for 5 min in the ultrasonic bath. Once the dye was added, samples were incubated at room temperature for 5 min before the measurement. Each spectrum was compared with that of CR alone (without peptide, as shown in Fig. 2). To avoid buffer interference, the absorbance spectrum of the buffer was subtracted from all measurements prior to their analysis. A result is considered positive if the maximum absorbance peak of CR shifts towards higher wavelengths.

Thioflavin-T binding and aggregation kinetics

Thioflavin-T (ThT) was dissolved in Milli-Q water to 5 mM, filtered with a 0.2- μm filter, diluted to 0.5 mM, and stored at -20°C . ThT fluorescence for aggregation kinetics was measured every 10 min and at the endpoint for ThT binding of the peptides using a 440-nm excitation filter and a 480-nm emission filter using bottom-optics in a plate reader (TECAN Infinite+ NANO). Samples were placed in a flat-bottom, black, non-binding 96-well plate (Greiner Bio-One). A total of 100 μL of sample was added per well. Each condition was measured in triplicate.

For the ThT binding experiments, the fluorescence of the peptides was measured after 72 h of aggregation of the peptides at a final concentration of 10 μM . Measurements were then compared to the negative control to determine the fold change in ThT fluorescence intensity.

For the seeding experiments, the A β 40 peptide stock, initially at pH 11, was diluted to 25 μM in 20 mM sodium phosphate buffer and 100 mM NaCl, and the corresponding pre-aggregated peptide was added to 2.5 μM after 5 min of sonication. Control experiments were conducted under the same conditions, including controls without A β 40 but with peptide and with just buffer and Th-T. All samples and controls were prepared in triplicate. The pH in the wells was measured both at the start and end of the experiment to ensure pH stability throughout the aggregation process and to confirm that there were no differences in the pH of the different conditions. ThT was added to a final concentration of 20 mM. The aggregation reaction was performed at 37°C without agitation with four independent replicates. The $t_{1/2}$ is the time necessary under a given condition to reach 50% of the final fluorescence signal. The lag phase was calculated by considering its end as the point at which it reached 10% of the final fluorescence. For each condition, we measured four experimental replicates with three technical replicates each.

Transmission electron microscopy

A 10 μL sample of aggregated peptide or *E. coli* was placed onto carbon-coated copper grids, incubated for 1 min, and dried with Whatman paper (Seira Curto et al, 2023). The grids were washed with distilled water, negatively stained with 2% (w/v) uranyl acetate for 1 min, and then dried. Micrographs were obtained using a JEM-1400 (JEOL, Tokyo, Japan) transmission electron microscope at an accelerating voltage of 80 keV.

Infrared spectroscopy

SR- μFTIR of *C. elegans*, cell cultures, and the aggregated peptides alone was performed at the MIRAS beamline at ALBA synchrotron

(Catalonia, Spain) using a Hyperion 3000 Microscope that was equipped with a 36 \times magnification objective coupled to a Vertex 70 spectrometer (Bruker). The measuring range was 650–4000 cm^{-1} and the spectra collection was carried out in transmission mode at 4 cm^{-1} resolution, 10 $\mu\text{m} \times 10 \mu\text{m}$ aperture dimensions, and from 128–256 co-added scans. Zero filling was performed with fast Fourier transform (FFT), so that in the final spectra, there was one point every 2 cm^{-1} . Background spectra were collected from a clean area of the CaF_2 window every 15 min. A mercury–cadmium–telluride (MCT) detector was used, and the microscope and spectrometer were continuously purged with nitrogen gas.

C. elegans at the L3 stage were chosen because of the high absorbance at later stages. After 24 h of exposure to the different strains of *E. coli*, L3-worms were washed with MQ water, transferred to a CaF_2 window, and dried under a vacuum for 24 h. For data acquisition, a Hyperion 3000 microscope equipped with 36 \times magnification coupled to a Vertex 70 spectrometer (Bruker, Billerica, MA) purged with dry air with an MCT detector was used. The spectra were collected in transmission mode at 4 cm^{-1} spectral resolution, 8 \times 8 μm aperture dimensions. A total of 128 scans were co-added for each spectrum with a spectral range from 900 to 4000 cm^{-1} . SR- μFTIR data was analyzed using OPUS 7.5 (Bruker) and Unscrambler X 10.5 software (CAMO Software, Oslo, Norway). The spectra were acquired in 10 different worms per condition at different locations of the worm. Background spectra were collected from a clean area of each CaF_2 window.

Fourier transform infrared (FTIR) spectral analysis

Spectra were acquired in two different ways: (a) at least 50 spectra on single cells were acquired for each sample in a given sample region; (b) maps with a dimension of minimum 50 \times 50 μm with a step size of 6 \times 6 μm . Fourier transform infrared (FTIR) spectra of single independent cells, the spectra from the different cell maps, and the independent spectra of amyloid aggregates without cells were analyzed using Thermo Omnic 7.1 (Thermo Scientific, Inc.) and Opus 7.5 (Bruker) software. Spectra exhibiting a low signal-to-noise ratio were eliminated.

For data processing, the second derivative of the spectra was calculated using a Savitsky–Golay algorithm with a nine-point filter and a polynomial order of 2 to eliminate the baseline contribution. Unscrambler X was used to perform PCA of the dataset. PCA was applied for the second derivative of the spectra. Unit vector normalization was applied after secondary derivation for PCA. Principal components (PCs) were calculated using the nonlinear iterative partial least squares (NIPALS) algorithm on mean-centered data. Since the PCA procedure allows weighting of the individual variables relative to each other, a constant value (1.00, equal weight) was assigned to all variables (the different wavenumbers in the 650–4000 cm^{-1} region) as the recommended value. Ratios were calculated over the following peaks of interest: 1629 cm^{-1} for amide I β -sheet structures (denoted A_{1629}), 1654 cm^{-1} , at which both the amyloid peptide and the cells have (in the derivative spectrum) a signal distinct from zero (A_{1665}), 1740 cm^{-1} for $\nu(\text{C}=\text{O})$ (carbonyl) (A_{1740}), 2925 cm^{-1} for CH_2 asymmetric stretching vibrations (A_{2925}), and 2960 cm^{-1} for CH_3 asymmetric stretching vibrations (A_{2960}). To calculate the amyloid peptide aggregation rate the ratio A_{1629}/A_{1654} was calculated.

Origin 9.1 software was used for the ratio calculation, t-test analysis, and graphical representation.

For the *C. elegans* analysis, the spectra with a low signal-to-noise ratio or with a high presence of Mie scattering were eliminated. The spectra were then corrected using a concave rubberband baseline in the range 3100–1400 cm⁻¹. Ratios were then collected for the following peaks: 1630 cm⁻¹ for amide I β -sheet structures, 1654 cm⁻¹ for α -helices structures, 1740 cm⁻¹ for ν (C=O) (carbonyl), 2919 cm⁻¹ and 2960 cm⁻¹ for CH₂ and CH₃ asymmetric stretching vibrations, and 3012 cm⁻¹ for unsaturated bonds in the carbonate chain. To measure the amount of lipid oxidation, we calculated:

$$\frac{1741 \text{ cm}^{-1}(\text{lipid oxidation})}{(2960 \text{ cm}^{-1} + 2919 \text{ cm}^{-1})(\text{total lipid})}$$

and to measure the proportion of protein/lipid we calculated:

$$\frac{1654 \text{ cm}^{-1}}{(2960 \text{ cm}^{-1} + 2919 \text{ cm}^{-1})}$$

Cell cytotoxicity assay

The SH-SY5Y cell line was authenticated by STR profiling and tested for mycoplasma contamination by ATCC prior to the start of the experiments. Following thawing, cells were cultured in Dulbecco's modified Eagle's medium/F-12 supplemented with Glutamax (DMEM/F12 Glutamax), 10% (v/v) heat-inactivated fetal bovine serum, and 1% (v/v) penicillin/streptomycin. The cells were maintained at 37 °C and 5% CO₂ in a 75-cm² cell culture flask. Differentiation to neuronal cells was started 24 h after plating by replacement of the maintenance medium with differentiation culture medium for 7 days and refreshment every 72 h. The differentiation culture medium consisted of DMEM/F-12 Glutamax supplemented with 2.5% inactivated FBS and 10 μ M retinoic acid. Differentiation was monitored microscopically by morphological assessment.

For the cytotoxicity assay, the cells were seeded in 96-well plates and treated at a density of 10⁴ cells/well. The different peptides were added at 0.25–10 μ M and, after 24 h of incubation, cell viability was detected by MTT assay. After removing the medium, 10 μ L of 3-(4,5-dimethylthiazol-2-yl)-2,5-diphenyltetrazolium bromide (MTT) solution (5 mg/mL) and 100 μ L of the medium were added to each well and incubated at 37 °C for 4 h. Then, 150 μ L of dimethyl sulfoxide was added to each well to dissolve the formazan after discarding the supernatant. Absorbance values were quantified using a plate reader (TECAN Spark) at 580 nm. For each pH, the data are expressed as the percentage viability with respect to untreated cells. The untreated cells were grown in medium containing the same amount of buffer at the corresponding pH but without A β 40 or the corresponding peptide.

For the ROS assay, the cells were seeded in 96-well plates and treated at a density of 10⁴ cells/well. The different peptides were added at 10 μ M and after 4 h of incubation, ROS were detected by DCFDA/H2DCFDA assay (Royall and Ischiropoulos, 1993).

Expression and purification

A pET11 vector (Novagen) containing the full sequence of C9L6N5 (BH4) (GenScript) with a C-terminal His-tag was introduced into *E. coli* BL21. The bacteria were grown in LB at 37 °C. At an OD₆₀₀

of 0.5, 1 mM IPTG was added and then the culture was left overnight at 22 °C. Afterward, the cells were centrifuged, and the pellet was resuspended in PBS with 5 mM imidazole, RNase A, and DNase I and sonicated. Then the lysate was ultracentrifuged and the supernatant was added to a His-Trap FF (Cytiva, Barcelona, Spain) column, which was washed with a gradient of PBS with imidazole buffer, reaching a maximum concentration of 200 mM imidazole. The protein purity was assessed with an SDS-PAGE gel and a Western blot to ensure it was the protein of interest.

The purified samples were separated by SDS-PAGE gels in duplicate. One was stained with Coomassie blue and the other was transferred to nitrocellulose membranes. After the transfer, the membranes were blocked with 4% bovine serum albumin. The membrane was incubated with an anti-His rabbit primary antibody (Thermo Scientific; 1:1000). The secondary antibody was an anti-rabbit horseradish peroxidase conjugate (Bio-Rad; 1:3000). The reaction was developed with an ECL kit (Thermo Scientific).

Yeast strain and nonsense suppression system

The yeast strain used in this project was derived from 74D-694 *MATa*, *ade1-14^{UGA}*, *trp1-289*, *his3 Δ -200*, *ura3-52*, *leu2-3,112 sup35::loxP* [pYK810] [*PIN⁺*] (Von Der Haar et al, 2007). The N-terminal Sup35p modified chimeras (where the residues 2-40 are replaced with 21-residue peptides) were encoded in a centromeric pUCK1620 plasmid bearing a *HIS3* selection marker (Dataset EV6 and Reagents and Tools table). The strain and the original SUP35-pUCK1620 vector was kindly provided by Dr R. Giraldo (Gasset-Rosa and Giraldo, 2015).

In our assay, the full-length Sup35 version and their peptide-containing chimeras (Fig. 4A) are expressed constitutively at physiological levels to maintain essential terminator factor activity. The original full-length Sup35 was exchanged with the new peptide-containing chimeras by plasmid shuffling with 5-FOA (Fan and Xiao, 2021). To prompt aggregation, an additional copy of only the N and M domains fused to GFP was transiently overproduced under a galactose-inducible promoter in the vector pESC-URA (Agilent Technologies). This strategy allowed us to induce prion conversion when necessary and simultaneously monitor protein aggregation using fluorescent microscopy. The initial 40 residues of Sup35p and the NM domain fused to GFP were replaced with the selected amyloid cores (Fig. 3A).

In the nonsense suppression assay, the *ADE1* gene (*ade1-14*), causes the accumulation of a red pigment (an adenine precursor) that colors colonies red when Sup35 is soluble (non-prion colonies [*psi⁻*]), and white or pink when it becomes insoluble (prion colonies [*PSI⁺*]). Since the conversion to [*PSI⁺*] is a rare event, we induced it by over-expressing the NM segment of Sup35 fused to GFP (Appendix Supplementary Data); this increases the rate of prion conversion and facilitates monitoring of the aggregation inside the cell.

Fluorescent foci detection in yeast

Yeast cells grown for 3–5 days on SD medium plates were inoculated into synthetic medium with raffinose (instead of glucose) and without histidine or uracil (SRaf -His, -Ura), and subsequently grown at 30 °C under vigorous agitation for 3 days. To induce expression of NM-GFP chimeras, yeast was inoculated

into synthetic medium with 2% galactose and 2% raffinose 1 day before the GFP assay as they are under the *GAL10* promoter. On the day of the experiment, the cells were examined and recorded using fluorescence microscopy (EVOS M5000) on a 96-well plate.

Nonsense suppression assay

In this assay, a preculture was initiated in SD -His -Ura medium, using 2% glucose as the carbon source, for 3 days at 30 °C. This 3-day interval serves to repress expression prior to the onset of the assay. Subsequently, yeast cells were washed with PBS buffer and induced to express the NM-GFP fusions by inoculating with fresh media containing 2% galactose and 2% raffinose and incubated two days at 30 °C. All cultures were adjusted to an OD₆₀₀ of 1 and plated at a 1/1000 dilution on ¼ YPD plates (1% bacto-yeast extract, 2% bacto-peptone, 2% glucose, 2% bacto-agar), then incubated for 4–5 days at 30 °C. After incubation, plates were transferred to 4 °C for an additional 5–7 days and subsequently examined for red and white colony phenotypes. Images were captured for each plate using a Leica MZFLIII stereomicroscope (Leica Microsystems GmbH, Mannheim, Germany) at 8× magnification. All assays were conducted in at least triplicate with colony counts exceeding 200 per plate. Colony counting was carried out for each assay, followed by t-student analysis for comparison against the negative control. Red colonies were indicative of the [*psi*⁻] phenotype, while white colonies indicated a stable [*PSI*⁺] phenotype characterized by efficient transmission between cells. Pink colonies were observed as indicative of an unstable [*PSI*⁺] phenotype, attributed to factors including low transmission between cells and/or high reversion between the aggregated and soluble forms of Sup35p.

Colony-color phenotype assay to detect extracellular aggregates

For the expression and extracellular aggregation of the Sup35p chimeras, we utilized the *E. coli* strain VS39 (kindly provided by Ann Hochschild). This strain is deficient in curli genes (*csgA*, *csgB*, and *csgC*), resistant to kanamycin, and contains a pACYC-derived plasmid named pVS76. This plasmid orchestrates the synthesis of the outer-membrane curli protein, CsgG, regulated by an IPTG-inducible promoter. Additionally, VS39 carries a cat gene that is constitutively transcribed and provides resistance to chloramphenicol.

The *Sup35NM* genes were obtained by modifying the pEXPORT plasmid pVS72, which harbors an intact *Sup35NM*. The final plasmids were subsequently transformed into the VS39 strain. The detailed sequence information of the final constructs is provided in the Dataset EV6 and Reagents and Tools table. In this study, we also incorporated the pEXPORT plasmid pVS105 encoding the Sup35 medium (Sup35M) region of the gene.

To measure the capacity to form extracellular aggregates among the various Sup35p variants, bacterial cells were spotted on CR-inducing plates. These plates consist of LB agar supplemented with 100 µg/ml carbenicillin, 25 µg/ml chloramphenicol, 0.2% w/v L-arabinose, 1 mM IPTG, and 10 µg/ml CR. Following a 5-day incubation period at 22 °C, the plates were subjected to imaging to assess the extent of CR binding. To obtain quantitative data, red

color intensity values were derived from quadruplicate samples using ImageJ (Nguyen et al, 2014).

C. elegans strains and maintenance

We utilized the wild-type N2 strain (dvIs50 [pCL45 (snb-1::Abeta 1-42::3' UTR(long) + mtl-2::GFP)] and the strain CL2355 expressing Aβ42 pan-neuronal (dvIs50 [pCL45 (snb-1::Abeta 1-42::3' UTR(long) + mtl-2::GFP)] both obtained from the Caenorhabditis Genetics Center (CGC). During the experiments, the nematodes were incubated at 20 °C. For control conditions, the worms were grown on standard nematode growth medium (NGM) plates that had been seeded with *E. coli* OP50 as a food source. When the C-DAG *E. coli* strains were used, NGM plates were prepared with antibiotics (Carbenicillin and Chloramphenicol), and inducers (Arabinose and IPTG). These plates were seeded with bacteria cultures expressing the C-DAG system to enhance the presence of extracellular aggregates.

To synchronize the nematode population, we subjected them to 5% hypochlorite treatment, followed by a 24-h rotation at 80 rpm in M9 buffer without any food source. Following this procedure and until they reached the young adult stage, each group of worms was incubated with the respective bacterial strain.

C. elegans butanone associative short-term learning assay (STAM)

The STAM employed three replicates of a starting population of starved worms that were subsequently divided and subjected to three distinct conditions, with 300–500 worms each, prior to the chemotaxis assay (Fig. 6A). These conditions were (i) a naive population that had not been conditioned with the odorant, (ii) a population tested immediately after conditioning (learning index), and (iii) a population tested an hour after conditioning (memory index). The chemotaxis assay was conducted on plates on which each differently treated population was positioned equidistantly from a spot containing NaN₃ and butanone (the chemoattractant) and another spot containing NaN₃ and ethanol, a compound to which the worms had not been previously exposed (Stein and Murphy, 2014; Kauffman et al, 2011).

The butanone associative learning assay was performed following established methods (Kauffman et al, 2011). Young adults were washed in M9 and collected by gravity sedimentation in a 15-mL conical tube to remove bacteria. Some animals were immediately transferred to the chemotaxis plate to assay the naive condition (CI (naive)). The rest were starved in M9 for 1 h. After the starvation, animals were conditioned for 1 h on NGM plates seeded with the corresponding *E. coli* strain and containing a 2-µL drop of 10% butanone, diluted in absolute ethanol, on the lid.

The conditioned worms (immediately after conditioning, learning index (LI), or after 1 h of starvation, memory index (MI)) were washed with M9 and transferred to the chemotaxis plate. For the chemotaxis assay, 10 cm unseeded NGM plates were used, and three circles (each 1 cm in diameter) on the bottom and both sides of the plate were marked. Then, 1 µL of 1 M sodium azide and 1 µL of 10% of butanone were added to the left spot, and the same amount of sodium azide and pure ethanol control were added to the right spot. The animals were placed on the bottom

spot. After 1 h, the numbers of worms located in the butanone and ethanol spots as well as at the original bottom spots were counted. Each chemotaxis assay was performed with 300–500 worms and in triplicate.

Our standard formula to calculate the chemotaxis index is as follows:

$$CI = [(Number\ of\ worms\ in\ the\ butanone\ zone) - (Number\ of\ worms\ in\ the\ ethanol\ zone)] / (Total\ number\ of\ worms)$$

With unconditioned worms, we calculated the CI (naive):

$$CI\ (naive) = [(Number\ of\ worms\ in\ the\ butanone\ zone) - (Number\ of\ worms\ in\ the\ ethanol\ zone)] / (Total\ number\ of\ worms)$$

Immediately after conditioning, we calculated the learning index as:

$$LI = CI\ (right\ after\ conditioning) - CI\ (naive)$$

After conditioning followed by 1 h of starvation, we calculated the memory index as:

$$MI = CI\ (after\ conditioning\ and\ starvation) - CI\ (naive).$$

C. elegans gut granule autofluorescence detection

The EVOS microscope (EVOSTM M5000 Imaging System) was employed to capture autofluorescence images of *C. elegans* using a green fluorescent protein (GFP) filter and a transmission filter. The images were acquired from animals treated identically to those used in the chemotaxis assays. To visualize gut granules, we centered the images on the first two intestine rings, which correspond to the region with the highest fluorescence intensity. Subsequently, ImageJ software was used for image analysis. The selected region for analysis was carefully chosen to avoid the presence of the gonads, thus mitigating potential interference.

Statistics

GraphPad PRISM 8 software was used for statistical analysis of the obtained data.

Blinding statement

Blinding procedures were partially implemented in this study. While the experimental design and peptide selection were based on computational aggregation propensity predictions (pWALTZ), the researchers conducting the experimental assays (including ThT fluorescence, TEM imaging, toxicity assays, and behavioral assays in *C. elegans*) were provided only with sample identifiers (peptide or strain names) without prior knowledge of their predicted aggregation propensities. This ensured that data collection and analysis were conducted without bias regarding the expected amyloid-forming potential of each sequence. Full double-blinding was not possible due to the necessity of experimental design oversight.

Data availability

The datasets used and generated in this study are available in the following databases: Gut microbiome sequences (filtered single-domain list): Figshare (<https://doi.org/10.6084/m9.figshare.25710048.v1>).

The source data of this paper are collected in the following database record: [biostudies:S-SCDT-10_1038-S44320-025-00114-4](https://www.ebi.ac.uk/biostudies/studies/S-SCDT-10_1038-S44320-025-00114-4).

Expanded view data, supplementary information, appendices are available for this paper at <https://doi.org/10.1038/s44320-025-00114-4>.

Peer review information

A peer review file is available at <https://doi.org/10.1038/s44320-025-00114-4>

References

- Alberti S, Halfmann R, King O, Kapila A, Lindquist S (2009) A systematic survey identifies prions and illuminates sequence features of prionogenic proteins. *Cell* 137:146–158
- Arata Y, Oshima T, Ikeda Y, Kimura H, Sako Y (2020) OP50, a bacterial strain conventionally used as food for laboratory maintenance of *C. elegans*, is a biofilm formation defective mutant. *microPublication Biol* <https://doi.org/10.17912/micropub.biology.000216>
- Ardevli BF, Prichard RK (2013) Inhibition of P-glycoprotein enhances sensitivity of *Caenorhabditis elegans* to ivermectin. *Vet Parasitol* 191:264–275
- Auten RL, Davis JM (2009) Oxygen toxicity and reactive oxygen species: the devil is in the details. *Pediatr Res* 66:121–127
- Ayuda-Durán B, González-Manzano S, González-Paramás AM, Santos-Buelga C (2020) *Caenorhabditis elegans* as a model organism to evaluate the antioxidant effects of phytochemicals. *Molecules* 25:3194
- Baker MJ, Trevisan J, Bassan P, Bhargava R, Butler HJ, Dorling KM, Fielden PR, Fogarty SW, Fullwood NJ, Heys KA et al (2014) Using Fourier transform IR spectroscopy to analyze biological materials. *Nat Protoc* 9:1771–1791
- Balbirnie M, Grothe R, Eisenberg DS (2001) An amyloid-forming peptide from the yeast prion Sup35 reveals a dehydrated beta-sheet structure for amyloid. *Proc Natl Acad Sci USA* 98:2375–2380
- Banerjee G, Farmer SF, Hyare H, Jaunmuktane Z, Mead S, Ryan NS, Schott JM, Werring DJ, Rudge P, Collinge J (2024) Iatrogenic Alzheimer's disease in recipients of cadaveric pituitary-derived growth hormone. *Nat Med* 30:394–402
- Barbitoff YA, Matveenko AG, Zhouravleva GA (2022) Differential interactions of molecular chaperones and yeast prions. *J Fungi* 8:122
- Battle C, De Groot NS, Iglesias V, Navarro S, Ventura S (2017) Characterization of soft amyloid cores in human prion-like proteins. *Sci Rep* 7:12134
- Bauer KC, Huus KE, Finlay BB (2016) Microbes and the mind: emerging hallmarks of the gut microbiota-brain axis. *Cell Microbiol* 18:632–644
- Benseny-Cases N, Álvarez-Marimón E, Castillo-Michel H, Cotte M, Falcon C, Cladera J (2018) Synchrotron-based fourier transform infrared microspectroscopy (μFTIR) study on the effect of Alzheimer's Aβ amorphous and fibrillar aggregates on PC12 cells. *Anal Chem* 90:2772–2779
- Bhoite SS, Han Y, Ruotolo BT, Chapman MR (2022) Mechanistic insights into accelerated α-synuclein aggregation mediated by human microbiome-associated functional amyloids. *J Biol Chem* 298:102088
- Bolognesi B, Faure AJ, Seuma M, Schmiedel JM, Tartaglia GG, Lehner B (2019) The mutational landscape of a prion-like domain. *Nat Commun* 10:4162
- Bonaz B, Bazin T, Pellissier S (2018) The Vagus Nerve at the Interface of the Microbiota-Gut-Brain Axis. *Front Neurosci* 12:49
- Brunquell J, Morris S, Snyder A, Westerheide SD (2018) Coffee extract and caffeine enhance the heat shock response and promote proteostasis in an HSF-1-dependent manner in *Caenorhabditis elegans*. *Cell Stress Chaperones* 23:65–75
- Burra G, Maina MB, Serpell LC, Thakur AK (2021) Nucleation-dependent aggregation kinetics of yeast Sup35 fragment GNNQQNY. *J Mol Biol* 433:166732

- Carija A, Navarro S, de Groot NS, Ventura S (2017) Protein aggregation into insoluble deposits protects from oxidative stress. *Redox Biol* 12:699–711
- Cascarina SM, Paul KR, Ross ED (2017) Manipulating the aggregation activity of human prion-like proteins. *Prion* 11:323–331
- Chan HM, Xiao L, Yeung KM, Ho SL, Zhao D, Chan WH, Li HW (2012) Effect of surface-functionalized nanoparticles on the elongation phase of beta-amyloid (1–40) fibrillogenesis. *Biomaterials* 33:4443–4450
- Chen SG, Stribinskis V, Rane MJ, Demuth DR, Gozal E, Roberts AM, Jagadapillai R, Liu R, Choe K, Shivakumar B et al (2016) Exposure to the functional bacterial amyloid protein curli enhances alpha-synuclein aggregation in aged Fischer 344 rats and *Caenorhabditis elegans*. *Sci Rep* 6:1–10
- Chernova TA, Wilkinson KD, Chernoff YO (2017) Prions, chaperones, and proteostasis in yeast. *Cold Spring Harb Perspect Biol* 9:a023663
- Chun H, Sharma AK, Lee J, Chan J, Jia S, Kim BE (2017) The intestinal copper exporter CUA-1 is required for systemic copper homeostasis in *Caenorhabditis elegans*. *J Biol Chem* 292:1–14
- Conchillo-Solé O, de Groot NS, Avilés FX, Vendrell J, Daura X, Ventura S (2007) AGGRESCAN: a server for the prediction and evaluation of ‘hot spots’ of aggregation in polypeptides. *BMC Bioinformatics* 8:1–17
- Connolly SM, Erwin AL, Sabb M, Hanks JL, Chang L, Torrez RM, Caso GC, Campbell AM, Mosalaganti S, Cover TL et al (2024) Structural analysis of membrane-associated forms of *Helicobacter pylori* VacA toxin. *J Mol Biol* 436:168432
- De Groot NS, Burgas MT (2015) Is membrane homeostasis the missing link between inflammation and neurodegenerative diseases? *Cell Mol Life Sci* 72:4795–4805
- De Groot NS, Gomes RA, Villar-Pique A, Babu MM, Coelho AV, Ventura S (2015) Proteome response at the edge of protein aggregation. *Open Biol* 5:140221
- Derkatch IL, Liebman SW (2013) The story of stolen chaperones. *Prion* 7:294–300
- Desler C, Durhuus JA, Rasmussen LJ (2012) Genome-wide screens for expressed hypothetical proteins. *Methods Mol Biol* 815:25–38
- Duyckaerts C, Clavaguera F, Potier MC (2019) The prion-like propagation hypothesis in Alzheimer’s and Parkinson’s disease. *Curr Opin Neurol* 32:266–271
- Dell’Angelica EC, Mullins C, Caplan S, Bonifacio JS (2000) Lysosome-related organelles. *FASEB J* 14:1265–1278
- Elliott AG, Huang JX, Neve S, Zuegg J, Edwards IA, Cain AK, Boinett CJ, Barquist L, Lundberg CV, Steen J et al (2020) An amphipathic peptide with antibiotic activity against multidrug-resistant Gram-negative bacteria. *Nat Commun* 11:3184
- Espinosa Angarica V, Ventura S, Sancho J (2013) Discovering putative prion sequences in complete proteomes using probabilistic representations of Q/N-rich domains. *BMC Genomics* 14:1–17
- Esteras-Chopo A, Serrano L, López De La Paz M (2005) The amyloid stretch hypothesis: recruiting proteins toward the dark side. *Proc Natl Acad Sci USA* 102:16672–16677
- Fan L, Xiao W (2021) Study essential gene functions by plasmid shuffling. *Methods Mol Biol* 2196:53–62
- Fang P, Kazmi SA, Jameson KG, Hsiao EY (2020) The microbiome as a modifier of neurodegenerative disease risk. *Cell Host Microbe* 28:201–222
- Fernández-Calvet A, Matilla-Cuenca L, Izco M, Navarro S, Serrano M, Ventura S, Blesa J, Herráiz M, Alkorta-Aranburu G, Galera S et al (2024) Gut microbiota produces biofilm-associated amyloids with potential for neurodegeneration. *Nat Commun* 15:4150
- Flach M, Leu C, Martinisi A, Skachokova Z, Frank S, Tolnay M, Stahlberg H, Winkler DT (2022) Trans-seeding of Alzheimer-related tau protein by a yeast prion. *Alzheimers Dement* 18:2481–2492
- Friedland RP, Chapman MR (2017) The role of microbial amyloid in neurodegeneration. *PLoS Pathog* 13:e1006654
- Friedland RP, McMillan JD, Kurlawala Z (2020) What are the molecular mechanisms by which functional bacterial amyloids influence amyloid beta deposition and neuroinflammation in neurodegenerative disorders? *Int J Mol Sci* 21:1652
- Gasset-Rosa F, Giraldo R (2015) Engineered bacterial hydrophobic oligopeptide repeats in a synthetic yeast prion, [REP-PSI (+)]. *Front Microbiol* 6:1–23
- Gil-Garcia M, Iglesias V, Pallarès I, Ventura S (2021) Prion-like proteins: from computational approaches to proteome-wide analysis. *FEBS Open Bio* 11:2400–2417
- Go MF (2002) Natural history and epidemiology of *Helicobacter pylori* infection. *Aliment Pharmacol Ther* 16:3–15
- Gonzalez-Moragas L, Berto P, Vilches C, Quidant R, Kolovou A, Santarella-Mellwig R, Schwab Y, Stürzenbaum S, Roig A, Laromaine A (2017) In vivo testing of gold nanoparticles using the *Caenorhabditis elegans* model organism. *Acta Biomater* 53:598–609
- Grant WB, Blake SM (2023) Diet’s role in modifying risk of Alzheimer’s disease: history and present understanding. *J Alzheimers Dis* 96:1353–1382
- Hajdú G, Somogyvári M, Csérmely P, Söti C (2023) Lysosome-related organelles promote stress and immune responses in *C. elegans*. *Commun Biol* 6:1–17
- Harrison PM (2019) Evolutionary behaviour of bacterial prion-like proteins. *PLoS ONE* 14:e0213030
- Hashim HM, Makpol S (2022) A review of the preclinical and clinical studies on the role of the gut microbiome in aging and neurodegenerative diseases and its modulation. *Front Cell Neurosci* 16:1007166
- He Y, Zheng MM, Ma Y, Han XJ, Ma XQ, Qu CQ, Du YF (2012) Soluble oligomers and fibrillar species of amyloid β -peptide differentially affect cognitive functions and hippocampal inflammatory response. *Biochem Biophys Res Commun* 429:125–130
- Hermann GJ, Schroeder LK, Hieb CA, Kershner AM, Rabbitts BM, Fonarev P, Grant BD, Priess JR (2005) Genetic analysis of lysosomal trafficking in *Caenorhabditis elegans*. *Mol Biol Cell* 16:3273–3288
- Holmqvist S, Chutna O, Bousset L, Aldrin-Kirk P, Li W, Björklund T, Wang ZY, Roybon L, Melki R, Li JY (2014) Direct evidence of Parkinson pathology spread from the gastrointestinal tract to the brain in rats. *Acta Neuropathol* 128:805–820
- Huttenhower C, Gevers D, Knight R, Abubucker S, Badger JH, Chinwalla AT, Creasy HH, Earl AM, Fitzgerald MG, Fulton RS et al (2012) Structure, function and diversity of the healthy human microbiome. *Nat* 486:207–214
- Iglesias V, de Groot NS, Ventura S (2015) Computational analysis of candidate prion-like proteins in bacteria and their role. *Front Microbiol* 6:1123
- Ijaq J, Chandrasekharan M, Poddar R, Bethi N, Sundararajan VS (2015) Annotation and curation of uncharacterized proteins- challenges. *Front Genet* 6:119
- Jansens KJA, Lambrecht MA, Rombouts I, Monge Morera M, Brijs K, Rousseau F, Schymkowitz J, Delcour JA (2019) Conditions governing food protein amyloid fibril formation—Part I: Egg and cereal proteins. *Compr Rev Food Sci Food Saf* 18:1256–1276
- Kauffman A, Parsons L, Stein G, Wills A, Kaletsky R, Murphy C (2011) *C. elegans* positive butanone learning, short-term, and long-term associative memory assays. *J Vis Exp* (49):e2490. <https://doi.org/10.3791/2490>
- Khaled M, Rönnbäck I, Ilag LL, Gräslund A, Strodel B, Österlund N (2023) A hairpin motif in the amyloid- β peptide is important for formation of disease-related oligomers. *J Am Chem Soc* 145:18340–18354
- Khiabani SA, Haghighat S, Khosroshahi HT, Asgharzadeh M, Kafil HS (2023) Diversity of Bacteroidaceae family in gut microbiota of patients with chronic kidney disease and end stage renal disease. *Heal Promot Perspect* 13:237

- Kim HS, Kim S, Shin SJ, Park YH, Nam Y, Kim CW, Lee KW, Kim SM, Jung ID, Yang HD et al (2021) Gram-negative bacteria and their lipopolysaccharides in Alzheimer's disease: pathologic roles and therapeutic implications. *Transl Neurodegener* 10:49
- Kim S, Kwon SH, Kam TI, Panicker N, Karuppagounder SS, Lee S, Lee JH, Kim WR, Kook M, Foss CA et al (2019a) Transneuronal propagation of pathologic α -synuclein from the gut to the brain models Parkinson's disease. *Neuron* 103:627–641.e7
- Kim SK, Guevarra RB, Kim YT, Kwon J, Kim H, Cho JH, Kim HB, Lee JH (2019b) Role of probiotics in human gut microbiome-associated diseases. *J Microbiol Biotechnol* 29:1335–1340
- Kosolapova AO, Antonets KS, Belousov MV, Nizhnikov AA (2020) Biological functions of prokaryotic amyloids in interspecies interactions: facts and assumptions. *Int J Mol Sci* 21:1–26. <https://doi.org/10.3390/ijms21197240>. [PREPRINT]
- Krishnan R, Lindquist SL (2005) Structural insights into a yeast prion illuminate nucleation and strain diversity. *Nature* 435:765–772
- Kuwajima K, Okamoto Y, Knowles T, Vendruscolo M, S nderby TV, Najarzadeh Z, Otzen DE (2022) Functional bacterial amyloids: understanding fibrillation, regulating biofilm fibril formation and organizing surface assemblies. *Mol* 27:4080
- Lambrech MA, Jansens KJA, Rombouts I, Brijs K, Rousseau F, Schymkowitz J, Delcour JA (2019) Conditions governing food protein amyloid fibril formation. Part II: Milk and legume proteins. *Compr Rev Food Sci Food Saf* 18:1277–1291
- Lancaster AK, Nutter-Upham A, Lindquist S, King OD (2014) PLAAC: a web and command-line application to identify proteins with prion-like amino acid composition. *Bioinformatics* 30:2501–2502
- Lesné SE, Sherman MA, Grant M, Kuskowski M, Schneider JA, Bennett DA, Ashe KH (2013) Brain amyloid- β oligomers in ageing and Alzheimer's disease. *Brain* 136:1383–1398
- Liao YH, Chang YJ, Yoshiike Y, Chang YC, Chen YR (2012) Negatively charged gold nanoparticles inhibit Alzheimer's amyloid- β fibrillization, induce fibril dissociation, and mitigate neurotoxicity. *Small* 8:3631–3639
- Liebman SW, Chernoff YO (2012) Prions in yeast. *Genetics* 191:1041–1072
- Liu H, Xie B, Dong X, Zhang L, Wang Y, Liu F, Sun Y (2016) Negatively charged hydrophobic nanoparticles inhibit amyloid β -protein fibrillation: The presence of an optimal charge density. *React Funct Polym* 103:108–116
- Meng L, Liu C, Li Y, Chen G, Xiong M, Yu T, Pan L, Zhang X, Zhou L, Guo T et al (2023) The yeast prion protein Sup35 initiates α -synuclein pathology in mouse models of Parkinson's disease. *Sci Adv* 9:eadj1092
- Mu  oz-Juan A, Benseny-Cases N, Guha S, Barba I, Caldwell KA, Caldwell GA, Agull   L, Yuste VJ, Laromaine A, Dalf   E (2024) Caenorhabditis elegans RAC1/ced-10 mutants as a new animal model to study very early stages of Parkinson's disease. *Prog Neurobiol* 234:102572
- Navarro-Hortal MD, Romero-M  rquez JM, L  pez-Basc  n MA, S  nchez-Gonz  lez C, Xiao J, Sumalla-Cano S, Battino M, Forbes-Hern  ndez TY, Quiles JL (2024) In vitro and in vivo insights into a broccoli byproduct as a healthy ingredient for the management of Alzheimer's disease and aging through redox biology. *J Agric Food Chem* 72:5197–5211
- Nguyen PQ, Botyanszki Z, Tay PKR, Joshi NS (2014) Programmable biofilm-based materials from engineered curli nanofibres. *Nat Commun* 5:1–10
- Nimmrich V, Grimm C, Draguhn A, Barghorn S, Lehmann A, Schoemaker H, Hillen H, Gross G, Ebert U, Bruehl C (2008) Amyloid β oligomers (A β 1–42 globulomer) suppress spontaneous synaptic activity by inhibition of P/Q-type calcium currents. *J Neurosci* 28:788
- Okonechnikov K, Golosova O, Fursov M, UGENE team (2012) Unipro UGENE: a unified bioinformatics toolkit. *Bioinformatics* 28:1166–1167
- Osherovich LZ, Cox BS, Tuite MF, Weissman JS (2004) Dissection and design of yeast prions. *PLoS Biol* 2:E86
- Pallar  s I, de Groot NS, Iglesias V, Sant'Anna R, Biosca A, Fern  ndez-Busquets X, Ventura S (2018) Discovering putative prion-like proteins in Plasmodium falciparum: a computational and experimental analysis. *Front Microbiol* 9:1737
- Pallar  s I, Iglesias V, Ventura S (2016) The Rho termination factor of Clostridium botulinum contains a prion-like domain with a highly amyloidogenic core. *Front Microbiol* 6:1516
- Panza F, Lozupone M, Solfrizzi V, Watling M, Imbimbo BP (2019) Time to test antibacterial therapy in Alzheimer's disease. *Brain* 142:2905–2929
- Parham SN, Resende CG, Tuite MF (2001) Oligopeptide repeats in the yeast protein Sup35p stabilize intermolecular prion interactions. *EMBO J* 20:2111–2119
- Park SKR, Jung T, Thuy-Boun PS, Wang AY, Yates JR, Wolan DW (2019) CompIL 2.0: an updated comprehensive metaproteomics database. *J Proteome Res* 18:616–622
- Peterson J, Garges S, Giovanni M, McInnes P, Wang L, Schloss JA, Bonazzi V, McEwen JE, Wetterstrand KA, Deal C et al (2009) The NIH human microbiome project. *Genome Res* 19:2317–2323
- Ritchie DL, Barria MA (2021) Prion diseases: a unique transmissible agent or a model for neurodegenerative diseases? *Biomolecules* 11:1–23. <https://doi.org/10.3390/biom11020207>. [PREPRINT]
- Roh HC, Collier S, Guthrie J, Robertson JD, Kornfeld K (2012) Lysosome-related organelles in intestinal cells are a zinc storage site in C. elegans. *Cell Metab* 15:88–99
- Royall JA, Ischiropoulos H (1993) Evaluation of 2',7'-dichlorofluorescein and dihydrorhodamine 123 as fluorescent probes for intracellular H₂O₂ in cultured endothelial cells. *Arch Biochem Biophys* 302:348–355
- Sabate R, Rousseau F, Schymkowitz J, Ventura S (2015) What makes a protein sequence a prion? *PLOS Comput Biol* 11:e1004013
- Sampson T (2025) Microbial amyloids in neurodegenerative amyloid diseases. *FEBS J* 292(6):1265–1281
- Sampson TR, Challis C, Jain N, Moiseyenko A, Ladinsky MS, Shastri GG, Thron T, Needham BD, Horvath I, Debelius JW et al (2020) A gut bacterial amyloid promotes α -synuclein aggregation and motor impairment in mice. *Elife* 9:e53111
- Sampson TR, Debelius JW, Thron T, Wittung-Stafshede P, Knight R, Mazmanian SK (2016) Gut microbiota regulate motor deficits and neuroinflammation in a model of Parkinson's disease. *Cell* 167:1469–1480.e12
- Seira Curto J, Fernandez MR, Cladera J, Benseny-Cases N, Sanchez de Groot N (2023) A β 40 aggregation under changeable conditions. *Int J Mol Sci* 24(9):8408
- Seira Curto J, Surroca Lopez A, Casals Sanchez M, Tic I, Fernandez Gallegos MR, Sanchez de Groot N (2022) Microbiome Impact on Amyloidogenesis. *Front Mol Biosci* 9:926702
- Sharma J, Wisniewski BT, Paulson E, Obaoye JO, Merrill SJ, Manogaran AL (2017) De novo [PSI⁺] prion formation involves multiple pathways to form infectious oligomers. *Sci Rep* 7:76
- Sivanathan V, Hochschild A (2013) A bacterial export system for generating extracellular amyloid aggregates. *Nat Protoc* 8(7):1381–1390
- Stein GM, Murphy CT (2014) C. elegans positive olfactory associative memory is a molecularly conserved behavioral paradigm. *Neurobiol Learn Mem* 115:86–94
- Tenaillon O, Skurnik D, Picard B, Denamur E (2010) The population genetics of commensal Escherichia coli. *Nat Rev Microbiol* 8:207–217
- Thapa M, Kumari A, Chin C-Y, Choby JE, Jin F, Bogati B, Chopyk DM, Koduri N, Pahnke A, Elrod EJ et al (2023) Translocation of gut commensal bacteria to the brain. Preprint at <https://doi.org/10.1101/2023.08.30.555630>
- Toombs JA, Petri M, Paul KR, Kan GY, Ben-Hur A, Rossa ED (2012) De novo design of synthetic prion domains. *Proc Natl Acad Sci USA* 109:6519–6524

- Tyedmers J, Treusch S, Dong J, McCaffery JM, Bevis B, Lindquist S (2010) Prion induction involves an ancient system for the sequestration of aggregated proteins and heritable changes in prion fragmentation. *Proc Natl Acad Sci USA* 107:8633–8638
- University of Maryland (2009) NIH human microbiome project. *Microbe Mag* 4:393–393
- Van Gerven N, Van der Verren SE, Reiter DM, Remaut H (2018) The role of functional amyloids in bacterial virulence. *J Mol Biol* 430:3657–3684
- Vidal-Veuthey B, González D, Cárdenas JP (2022) Role of microbial secreted proteins in gut microbiota-host interactions. *Front Cell Infect Microbiol* 12:964710
- Visconti A, Le Roy CI, Rosa F, Rossi N, Martin TC, Mohney RP, Li W, de Rinaldis E, Bell JT, Venter JC et al (2019) Interplay between the human gut microbiome and host metabolism. *Nat Commun* 10:1–10
- Vogt NM, Kerby RL, Dill-McFarland KA, Harding SJ, Merluzzi AP, Johnson SC, Carlsson CM, Asthana S, Zetterberg H, Blennow K et al (2017) Gut microbiome alterations in Alzheimer's disease. *Sci Rep* 7:13537
- Von Der Haar T, Jossé L, Wright P, Zenthon J, Tuite MF (2007) Development of a novel yeast cell-based system for studying the aggregation of Alzheimer's disease-associated Abeta peptides in vivo. *Neurodegener Dis* 4:136–147
- Walker A, Czyz DM (2023) Oh my gut! Is the microbial origin of neurodegenerative diseases real? *Infect Immun* 91:e0043722
- Walker AC, Bhargava R, Dove AS, Brust AS, Owji AA, Czyz DM (2022) Bacteria-derived protein aggregates contribute to the disruption of host proteostasis. *Int J Mol Sci* 23:4807
- Walker AC, Bhargava R, Vaziriyani-Sani AS, Pourciau C, Donahue ET, Dove AS, Gebhardt MJ, Ellward GL, Romeo T, Czyz DM (2021) Colonization of the *Caenorhabditis elegans* gut with human enteric bacterial pathogens leads to proteostasis disruption that is rescued by butyrate. *PLoS Pathog* 17:e1009510
- Wan W, Stubbs G (2014) Fungal prion HET-s as a model for structural complexity and self-propagation in prions. *Proc Natl Acad Sci USA* 111:5201–5206
- Wang C, Lau CY, Ma F, Zheng C (2021) Genome-wide screen identifies curli amyloid fibril as a bacterial component promoting host neurodegeneration. *Proc Natl Acad Sci USA* 118:e2106504118
- Wasmer C, Zimmer A, Sabaté R, Soragni A, Saupe SJ, Ritter C, Meier BH (2010) Structural similarity between the prion domain of HET-s and a homologue can explain amyloid cross-seeding in spite of limited sequence identity. *J Mol Biol* 402:311–325
- Wickner RB, Shewmaker FP, Bateman DA, Edskes HK, Gorkovskiy A, Dayani Y, Bezsonov EE (2015) Yeast prions: structure, biology, and prion-handling systems. *Microbiol Mol Biol Rev* 79:1–17
- Wood SJ, Maleeff B, Hart T, Wetzel R (1996) Physical, morphological and functional differences between pH 5.8 and 7.4 aggregates of the Alzheimer's amyloid peptide A β . *J Mol Biol* 256:870–877
- Yu NY, Wagner JR, Laird MR, Melli G, Rey S, Lo R, Dao P, Cenik Sahinalp S, Ester M, Foster LJ et al (2010) PSORTb 3.0: improved protein subcellular localization prediction with refined localization subcategories and predictive capabilities for all prokaryotes. *Bioinformatics* 26:1608–1615
- Zambrano R, Conchillo-Sole O, Iglesias V, Illa R, Rousseau F, Schymkowitz J, Sabate R, Daura X, Ventura S (2015) PrionW: a server to identify proteins containing glutamine/asparagine rich prion-like domains and their amyloid cores. *Nucleic Acids Res* 43:W331–W337
- project PID2020-117454RA-I00 funded by MCIN/AEI/10.13039/501100011033; the project CNS2023-144437 funded by MICIU/AEI/10.13039/501100011033 and by the European Union – NextGenerationEU/PRTR; and by L'Oréal-UNESCO For Women in Science Programme. We extend our gratitude to the following individuals: Ann Hochschild and Padraig Deighan for kindly providing the SV39 *E. coli* strain and plasmids pVS105 and pVS72. Rafael Giraldo for generously providing the 74D-694 *S. cerevisiae* strain. Antonela Lavatelli for her assistance in resolving basic experimental issues. Julian Cerón and Antonio Miranda-Vizueté for their invaluable responses to our inquiries. Anna Laromaine for sharing her *C. elegans* laboratory expertise and aiding in the construction of the initial picker. Esther Dalfo for enlightening us about the requirements of a *C. elegans* laboratory and for sharing valuable information regarding contacts and databases related to *C. elegans*. Gian G. Tartaglia for his inestimable support to start the project. Nuria Benseny for her assistance in the microFTIR experiments. Josep Cladera for his responses and discussions around the investigation. *C. elegans* N2, CL2355 and *E. coli* OP50 were provided by the CGC, which is funded by NIH Office of Research Infrastructure Programs (P40 OD010440). μ FTIR experiments were performed at MIRAS beamline at ALBA Synchrotron with the collaboration of ALBA staff. Transmission electron microscopy (TEM) images were acquired at the Servei de Microscòpia i Difracció de Raigs X (SMIDRX) of the Universitat Autònoma de Barcelona (UAB).

Author contributions

Jofre Seira Curto: Data curation; Formal analysis; Validation; Investigation; Methodology; Writing—original draft; Writing—review and editing.

Adan Dominguez Martinez: Formal analysis; Supervision; Investigation; Methodology. **Genis Perez Collell:** Data curation; Investigation; Methodology. **Estrella Barniol Simon:** Investigation. **Marina Romero Ruiz:** Investigation. **Berta Franco Bordés:** Investigation. **Paula Sotillo Sotillo:** Investigation; Methodology. **Sandra Villegas Hernandez:** Conceptualization; Writing—review and editing. **Maria Rosario Fernandez:** Conceptualization; Resources; Data curation; Formal analysis; Supervision; Validation; Investigation; Methodology; Writing—original draft; Writing—review and editing. **Natalia Sanchez de Groot:** Conceptualization; Resources; Data curation; Formal analysis; Supervision; Funding acquisition; Validation; Writing—original draft; Project administration; Writing—review and editing.

Source data underlying figure panels in this paper may have individual authorship assigned. Where available, figure panel/source data authorship is listed in the following database record: [biostudies:S-SCDT-10_1038-S44320-025-00114-4](https://biostudies.org/studies/S-SCDT-10_1038-S44320-025-00114-4).

Disclosure and competing interests statement

The authors declare no competing interests.

Open Access This article is licensed under a Creative Commons Attribution 4.0 International License, which permits use, sharing, adaptation, distribution and reproduction in any medium or format, as long as you give appropriate credit to the original author(s) and the source, provide a link to the Creative Commons licence, and indicate if changes were made. The images or other third party material in this article are included in the article's Creative Commons licence, unless indicated otherwise in a credit line to the material. If material is not included in the article's Creative Commons licence and your intended use is not permitted by statutory regulation or exceeds the permitted use, you will need to obtain permission directly from the copyright holder. To view a copy of this licence, visit <http://creativecommons.org/licenses/by/4.0/>. Creative Commons Public Domain Dedication waiver <http://creativecommons.org/>

Acknowledgements

This work was supported by: the grant FPU21/03897 funded by MICIU/AEI/10.13039/501100011033 and by FSE+; the grant RYC2019-026752-I funded by MCIN/AEI/10.13039/501100011033 and by FSE invierte en tu futuro; the

[publicdomain/zero/1.0/](https://creativecommons.org/licenses/by/4.0/) applies to the data associated with this article, unless otherwise stated in a credit line to the data, but does not extend to the graphical or creative elements of illustrations, charts, or figures. This waiver removes legal barriers to the re-use and mining of research data. According to standard

scholarly practice, it is recommended to provide appropriate citation and attribution whenever technically possible.

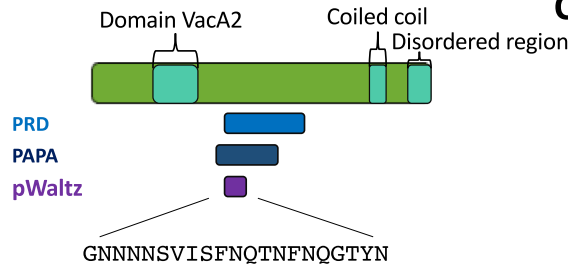
© The Author(s) 2025

Expanded View Figures

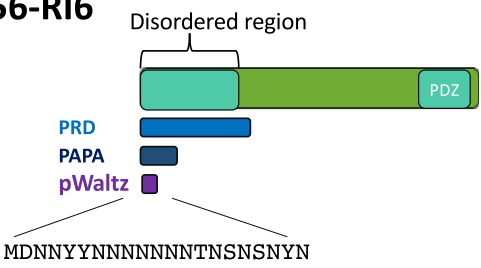
Figure EV1. Sequential information regarding the ten prion-like sequences selected from bacteria found in the gut.

Diagram showing the prion-like regions predicted for all the amyloid cores selected. In green are the main sequences. In light blue are the prion domains (PrD) predicted by PLAAC. In dark blue are the prion domains predicted by PAPA. In purple, the amyloid cores predicted by pWALTZ. Turquoise and yellow are other domains.

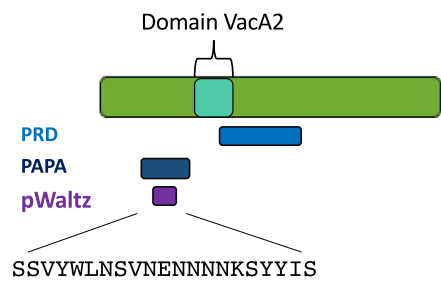
M5YJZ4-HP1



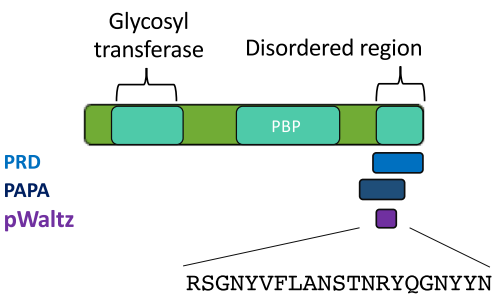
C0FU56-RI6



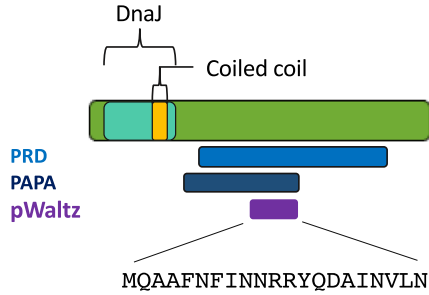
M3SJ19-HP2



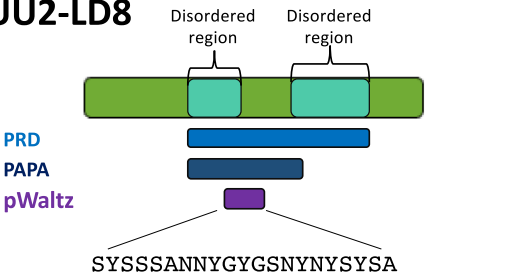
E7GXS5-SA7



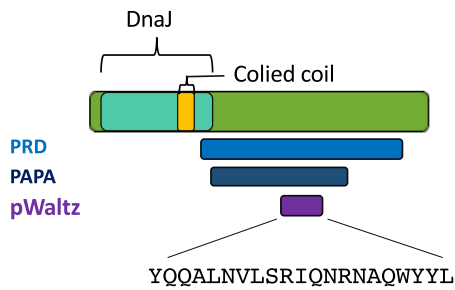
C0B555-CC3



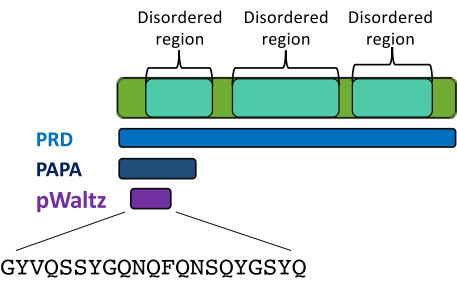
F0HUU2-LD8



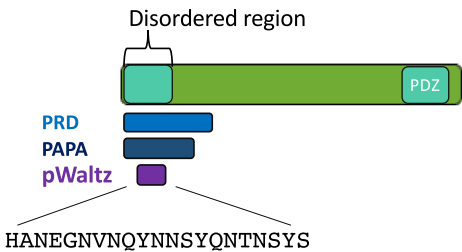
C9L6N5-BH4



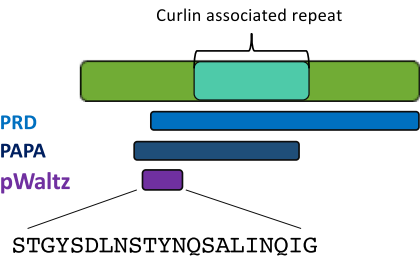
F5LFB6-P9



D4KZ46-RI5



G9Y7N7-HA10



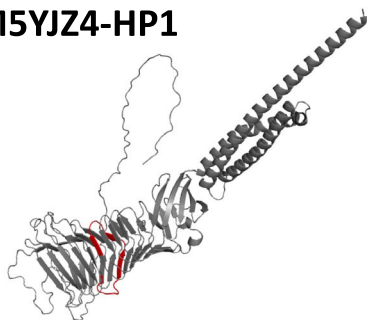
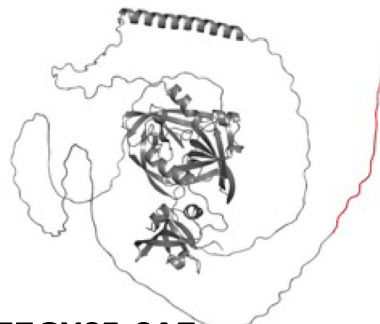
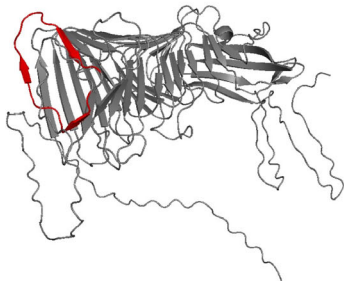
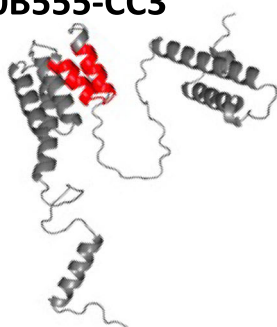
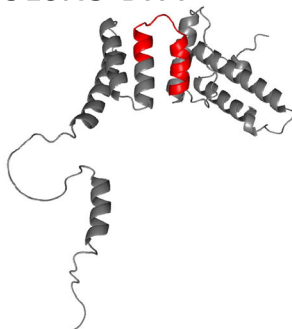
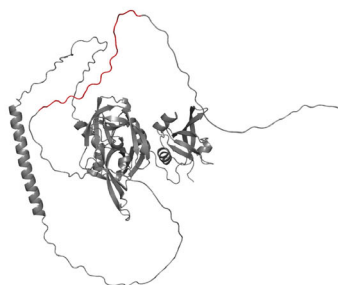
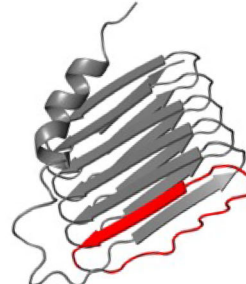
M5YJZ4-HP1**C0FU56-RI6****M3SJI9-HP2****E7GXS5-SA7****C0B555-CC3****F0HUU2-LD8****C9L6N5-BH4****F5LFB6-P9****D4KZ46-5RI****G9Y7N7-HA10**

Figure EV2. Predicted structure of the ten prion-like sequences selected from bacteria found in the gut.

The images show the Alpha-fold prediction of the whole protein structure.

Chapter III: Exogenous Amyloid Sequences: Their Role in Amyloid-Beta Heterotypic Aggregation

This chapter contains the article published in bioRxiv “Seira Curto, J., Hernandez, S. V., Fernandez, M. R., & Groot, N. S. de. (2025). Exogenous Amyloid Sequences: Their Role in Amyloid-Beta Heterotypic Aggregation. BioRxiv, 2025.01.24.634659. <https://doi.org/10.1101/2025.01.24.634659>”

The supplementary data associated with this work is available in Section “Appendix 1” of this thesis.

Exogenous Amyloid Sequences: Their Role in Amyloid-Beta Heterotypic Aggregation

Jofre Seira Curto^{1*}, Sandra Villegas Hernandez¹, Maria Rosario Fernandez¹, Natalia Sanchez de Groot^{1*}

¹Unitat de Bioquímica. Departament de Bioquímica i Biologia Molecular. Universitat Autònoma de Barcelona, Spain.

*** Correspondence:**

Corresponding Author

natalia.sanchez@uab.cat

jofre.seira@uab.cat

Keywords: Alzheimer's, aggregation, amyloid.

Abstract

Protein aggregation is a complex process influenced by environmental conditions and interactions between multiple molecules, including those of exogenous origin. Although *in vitro* simulations of aggregation are crucial for advancing research, few studies explore cross-seeding as a repeating event, despite the potential for such events when proteins circulate through the body. Here, we investigated the impact of exogenous amyloid sequences derived from the gut microbiota on the heterotypic aggregation of A β peptides. We utilized ten 21-amino acid peptides derived from bacterial genomes, previously shown to interfere with A β 40 aggregation and induce memory loss in *Caenorhabditis elegans*. Through consecutive cross-seeding assays with A β 40 and A β 42, we analyzed the effects of these peptides on aggregation kinetics and seed propagation. Our findings indicate that exogenous molecules can influence A β 's aggregation process, altering the fibrils' properties. Based on this, we introduce the "Interaction History" concept, where prior interactions shape the aggregation and propagation of A β peptides. This work supports the idea that environmental factors, such as microbial amyloids, can contribute to the heterogeneity and progression of amyloid-related diseases. Our results highlight the need for therapeutic strategies targeting diverse amyloid configurations and reinforce the importance of considering exogenous sequences as additional triggers in AD pathology.

Introduction

Protein aggregation is associated with many neurodegenerative diseases. In particular, the formation of amyloid plaques has been widely described in the brains of Alzheimer's disease (AD) patients[1–5]. These deposits are composed principally of amyloid beta peptide ($A\beta$), which exist in two major isoforms: $A\beta$ 40, the most abundant in the body, and $A\beta$ 42, the main component of amyloid plaques [4,6] (Figure 1A). These two isoforms, differ in length and aggregation propensity and can interact with each other, producing different outcomes[2,7–11]. For instance, *in vivo* studies have shown that $A\beta$ 40 overexpression inhibits $A\beta$ 42 deposition, suggesting a potential protective role for $A\beta$ 40 [9,12,13]. The balance between $A\beta$ 40 and $A\beta$ 42 is influenced by isoforms of the apolipoprotein E gene (APOE). Among these, APOE4 is particularly significant, as it promotes $A\beta$ 42 formation, exacerbating aggregation and accelerating disease progression[5,14]. At the molecular level, interlaced amyloid fibrils containing both $A\beta$ 40 and $A\beta$ 42 have been observed, supporting that these isoforms can interact during the aggregation process [9]. Similarly, compositional analyses of amyloid plaques extracted from patients' brains also revealed heterogeneous aggregation events[15,16].

Beyond the brain, $A\beta$ aggregation can also involve systemic interactions, and increasing evidence supports the idea that $A\beta$ peptides can cross-seed and propagate aggregation across different regions of the body, potentially contributing to the spread of amyloid pathology[17] (Figure 1A). $A\beta$ is present in both the central nervous system (CNS) and the peripheral circulation, maintained by a dynamic equilibrium between these two pools[18]. However, disruptions in this balance can have significant consequences for $A\beta$ homeostasis. While circulating $A\beta$ can enter the brain, elevated peripheral $A\beta$ levels may impair its clearance from the CNS, leading to increased accumulation[18,19]. This can occur when blood-brain barrier (BBB) is compromised, allowing $A\beta$ peptides to infiltrate into the brain and interact with neurons[5], potentially influencing aggregation dynamics. Additionally, circulating macrophages[20] and blood monocytes[19] may also serve as alternative transport mechanisms, facilitating the movement of $A\beta$ seeds from the periphery into the brain.

Notably, $A\beta$ aggregation is not restricted to interactions between different isoforms[8,21]; but it is also influenced by its interaction with other proteins, such as amylin[22] or alpha-synuclein[23–25], as well as non-protein molecules like RNA[26,27] and metals[28–30]. These other molecules, along with changes in local environmental conditions (e.g., pH), can produce amyloid aggregates with distinct structural and biophysical properties [31–35]. Beyond the diversity induced by external factors, amyloid fibril polymorphism can also emerge withing a single aggregation process, with multiple structures populating the different aggregational phases, and even after reaching the plateau[34,35]. Although lower fibril diversity has been observed *in vivo*, structurally distinct amyloid fibrils, also known as strains, have been linked to different clinical and pathological outcomes in AD[36,37]. In this line, it has been observed a connection between environmental factors and lifestyle with AD development[38], highlighting the potential impact of exogenous molecules in this process.

AD's research is gradually expanding to include the microbiota (Figure 1A), which plays a significant role in influencing the host's immune and regulatory processes[39]. In this context, microbiome-derived proteins can be exported and digested, for example, in the gut, resulting in molecules capable of influencing the aggregation of host proteins[39,40]. This aligns with

the reported potential of prion-like proteins for transcellular propagation[17] and interspecies transmission[25,41–44]. An increasing body of evidence suggests that microbial cells and their products can circulate through the host body, potentially reaching the brain via the vagus nerve or bloodstream[39,45], thereby able to influencing aggregation processes far away from the original site of infection (Figure 1A).

Overall, rather than a static process, amyloid aggregation is iterative, dynamic, and environment-dependent[22,23,35,24–30,34], leading to an energy landscape with multiple local minima, each corresponding to distinct fibrillar polymorphs[34,35,46]. Consequently, the introduction of an exogenous fibrillar seed can perturb this landscape by stabilizing specific polymorphs, shifting aggregation pathways, or promoting the formation of novel aggregate structures. In this context, we investigated how exogenous proteins, which may be present in the body, influence A β aggregation dynamics. To explore this, we used a collection of prion-like sequences derived from the gut microbiome[47] (Figure 1B), which have recently been shown to interfere with A β 40 aggregation *in vitro* and induce memory loss when ingested by *C. elegans*.

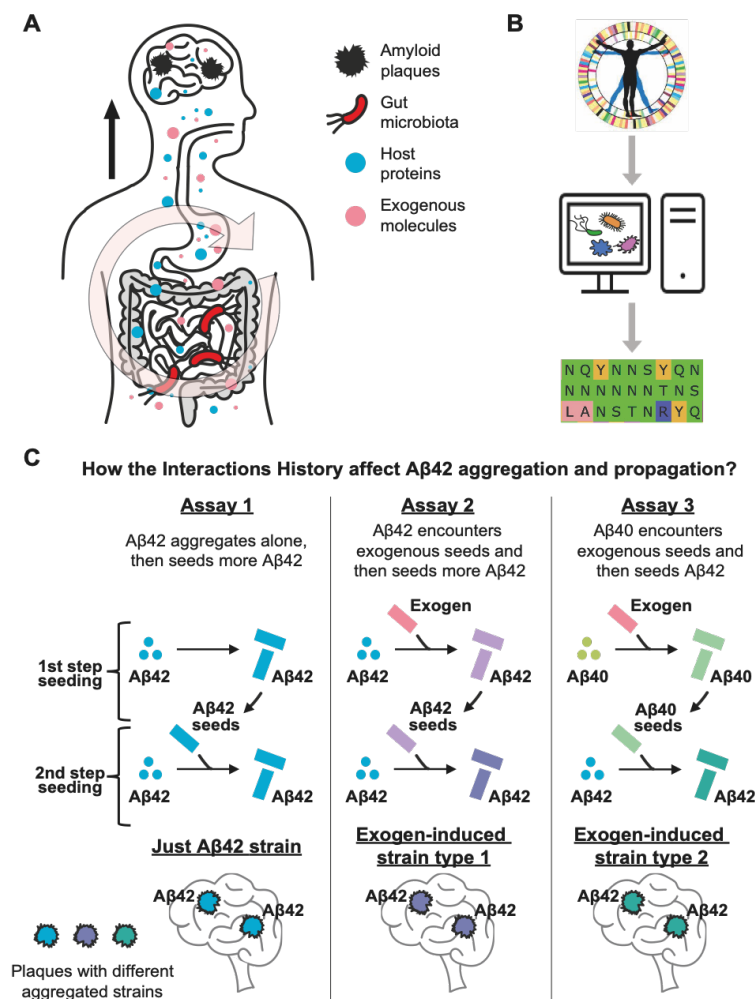


Figure 1. Exogenous prion-like sequences can affect A β aggregation and propagation. A) Microbial cells and their products can circulate through the body, encountering host proteins, reaching the brain, and influencing aggregation processes. B) Computational analysis of the

human microbiome has shown the presence of several genes coding for prion-like proteins[47]. C) Schematic representation of the experimental approach used to study the effect of Interaction History on A β 42 aggregation and propagation. We consider three hypothetical scenarios where two consecutive seeding steps influence A β 42 aggregation. Scenario 1: Only A β 42 molecules act as monomers and seeds in both seeding steps. Scenario 2: A β 42 aggregates in the presence of an exogenous molecule, and subsequently, these aggregates seed new A β 42 monomers. Scenario 3: A β 40 aggregates in the presence of an exogenous molecule, and subsequently, these A β 40 aggregates seed A β 42 monomers. Our results suggest that if these three different aggregation pathways occur in the body, they may lead to the formation of different aggregated A β 42 strains. Dots represent monomeric proteins, while bars indicate aggregated structures. Colors denote different aggregate identities: Blue for unexposed A β 42, red for exogenous amyloids, yellow for unexposed A β 40, light green for aggregate A β 40, and the other colors represent different aggregated A β 42 polymorphs.

In the present study, we aim to investigate how these bacterial sequences influence both the formation of A β 42 aggregates and, more importantly, the seeding properties of these aggregates, particularly their ability to trigger subsequent aggregation events. To this end, we focus on the cross-interactivity between A β 40 and A β 42[9] (Figure 1C). We observed that incubating A β with bacterial sequences accelerated aggregation and produced deposits with varying seeding capacities (Figures 2-4). These findings suggest that the introduction of additional molecular factors may contribute to amyloid aggregate diversity, leading to the formation of novel conformations and propagation behaviors. This highlights the potential risk associated with exogenous prion-like proteins or peptides derived from their proteolysis[48,49], as once they enter the body, they can indirectly promote the formation of additional, more toxic aggregated structures (Figure 1A). Therefore, observing no or minimal effects in a single-step aggregation assay may be misleading, as it does not consider the seeding capacity of newly formed aggregates, which can only be assessed through subsequent aggregation assays (Figure 1C). Taken together, our results support that the molecular interactions A β experiences during its journey through the body (referred to here as Interaction History, Figure 1C) may be critical factors for understanding the disease and developing effective therapeutic approaches.

Results and Discussion

Exogenous Prion-like Sequences Can Influence A β Peptides Aggregation

In our previous investigation of the gut microbiome, we build a collection of ten exogenous prion-like sequences capable of interfering with A β 40 aggregation[47] (Figure 1B). These sequences were selected based on the amyloid stretch hypothesis, which states that specific regions within a protein, known as amyloid cores, can drive amyloid nucleation[50–52]. These ten prion-like sequences are 21-residue peptides with net charges ranging from +2 to -2 and compositional similarities below 30% (Table 1)[47]. Since these sequences originate from gut microbiome bacteria, they may enter the gut lumen either through active export or after bacterial cell lysis[48,49] (Figure 1A), becoming free to interact with host proteins throughout the body. Based on this premise, in the present study, we used this collection as a model to

investigate how exogenous molecules influence the interplay between A β 40 and A β 42, with a particular focus on heterotypic interactions and cross-seeding events (Figure 1C).

Name	Uniprot ID	Species	Sequences	Net charge
HP1	M5YJZ4	<i>Helicobacter pylori</i>	GNNNNSV I S F N Q T N F N Q G T Y N	-0,1
HP2	M3SJI9	<i>Helicobacter pylori</i>	SSVYWLNSV N E N N N N K S Y Y I S	-0,1
CC3	C0B555	<i>Coprococcus comes</i>	M Q A A F N F I N N R R Y Q D A I N V L N	0,9
BH4	C9L6N5	<i>Blautia hansenii</i>	Y Q Q A L N V L S R I Q N R N A Q W Y Y L	1,9
RI5	D4KZ46	<i>Roseburia intestinalis</i>	H A N E G N V N Q Y N N S Y Q N T N S Y S	-0,9
RI6	C0FUS6	<i>Roseburia inulinivorans</i>	M D N N Y Y N N N N N N N T N S N S N Y N	-1,1
SA7	E7GX55	<i>Streptococcus anginosus</i>	R S G N Y V F L A N S T N R Y Q G N Y Y N	1,9
LD8	F0HUU2	<i>Lactobacillus delbrueckii</i>	S Y S S S A N N Y G Y G S N Y N Y S Y S A	-0,1
P9	F5LFB6	<i>Paenibacillus</i>	G Y V Q S S Y G Q N Q F Q N S Q Y G S Y Q	-0,1
HA10	G9Y7N7	<i>Hafnia alvei</i>	S T G Y S D L N S T Y N Q S A L I N Q I G	-1,1

Table 1. Set of Exogenous Prion-like Sequences. Columns (from left to right) display: sequence identifiers used in this study; UniProt accession codes; source species from which the sequences originate; amino acid sequences, with residues colored according to the Zappo color scheme, aliphatic/hydrophobic (ILVAM) - rose, aromatic (FWY) - orange, positive (KRH) - dark blue, negative (DE) - red, hydrophilic (STNQ) - light green, conformationally special (PG) - magenta, cysteine (C) - yellow. Sequences obtained from Curto, J.S. et al.[47]. Net charge measured with Protein Calculator V3.4.

To mimic the complex aggregation processes observed in living organisms, we designed an approach based on sequential heterotypic seeding assays (Figures 1A and 1C). In this study, we incorporate the interplay between A β 42 and A β 40, hypothesizing that the higher abundance of A β 40[4,6] facilitates encounters with exogenous molecules, thereby indirectly affecting A β 42 aggregation and disease progression. To explore this interplay, we monitored Thioflavin-T (Th-T) fluorescence (Figures 2-4) and collected transmission electron microscopy (TEM) images (Supplementary Figures 1 and 2) to assess how A β 42 aggregation is influenced by pre-aggregated samples assembled under different heterotypic interactions. Through these assays, we aim to shed light on the possible scenarios A β 42 might encounter as it moves through the body (Figure 1A) and elucidate how the “Interaction History” could impact its aggregation and propagation (Figure 1C).

In our previous study[47], we found that most of the bacterial prion-like sequences (8 out of 10) accelerated A β 40 aggregation, with lag time correlating with the sequences' net charge. Hence, positively charged sequences led to faster aggregation, while negatively charged ones had little effect or even slowed aggregation[53–55]. These results highlight the role of electrostatic forces in intermolecular interactions and align with earlier reports showing that negatively charged peptides inhibit A β aggregation[53,54]. In the present study, we extended our analysis to A β 42 by incubating it with these pre-aggregated bacterial peptides. Similar to the effects observed with A β 40, incubation of A β 42 with a 1:10 molar ratio of prion-like sequences predominantly enhances its aggregation (seven samples presented shorter half-time, Figure 2).

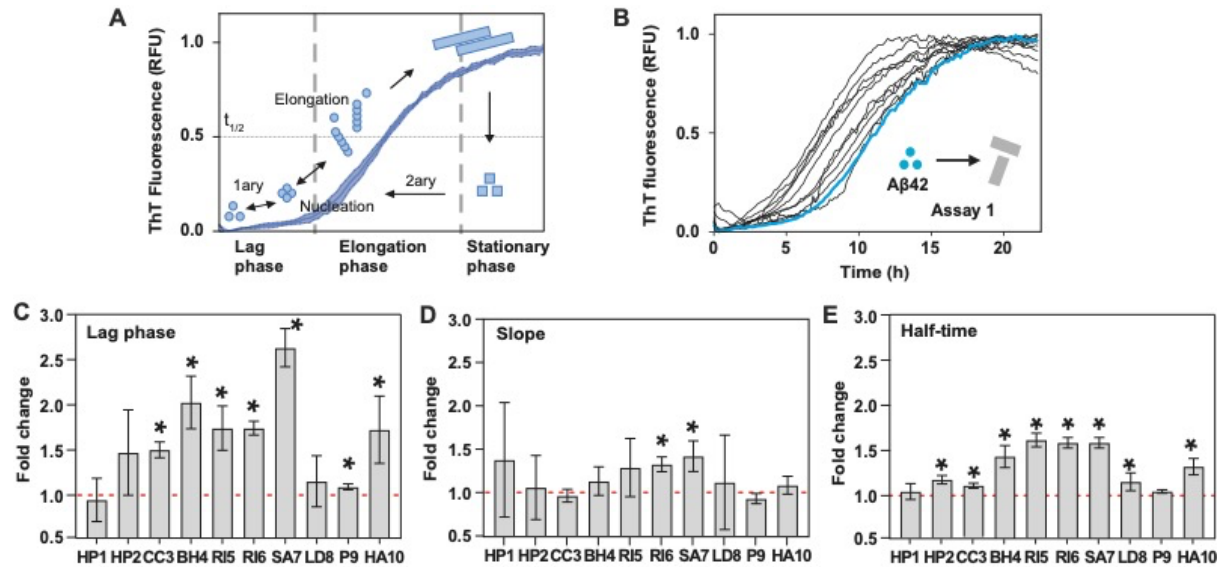


Figure 2. Exogenous Prion-like Sequences Influence A β 42 Aggregation. A) Diagram showing the different phases of a protein aggregation process, indicating the different assembly mechanisms involved. B) Aggregation kinetics of A β 42 in the presence (HP1–HA10, black lines) and absence (w/o, blue line) of seeds from exogenous prion-like sequences. See Supplementary Figure 4 for individual curves. C) Fold change in lag time (unseeded/seeded). D) Fold change in slope (seeded/unseeded). The equation fittings are shown in Figure 5. E) Fold change in half-time (unseeded/seeded). The red dashed line serves as a visual reference indicating a fold change of one relative to the aggregation assay started only with A β 42 monomers (unseeded). An asterisk (*) indicates a statistically significant difference ($p < 0.05$) compared to the condition without seeds, as determined by an unpaired t-test. Error bars indicate the standard deviation. Each condition corresponds to the results of three biological replicates, with three technical replicates per biological replicate.

Although we observed only a correlation with the absolute net charge of bacterial prion-like sequences (Supplementary Figure 3), it is noteworthy that the peptides most strongly accelerating A β 40 aggregation (SA7 and BH4)[47] also led to shorter lag times and half-times in A β 42 aggregation kinetics (Figure 2C). In general, the observed enhancement in the aggregation curves appears to be primarily attributed to a shorter lag phase, as only two samples exhibited larger slopes, while seven displayed shortened lag times (Figure 2B-D). A reduced lag time indicates a more efficient primary nucleation phase, involving oligomeric species that serve as templates, whereas a steeper slope indicates a faster aggregation rate during the growth phase, which may result from the rapid addition of monomers to existing fibrils and could also involve secondary nucleation events (Figure 2A). The half-time ($t_{1/2}$) serves as an indicator of overall aggregation efficiency, influenced by both lag phase and slope. Together, these findings suggest that these exogenous prion-like sequences primarily enhance the nucleation of A β 42 aggregation by acting as seeding points (Figure 2).

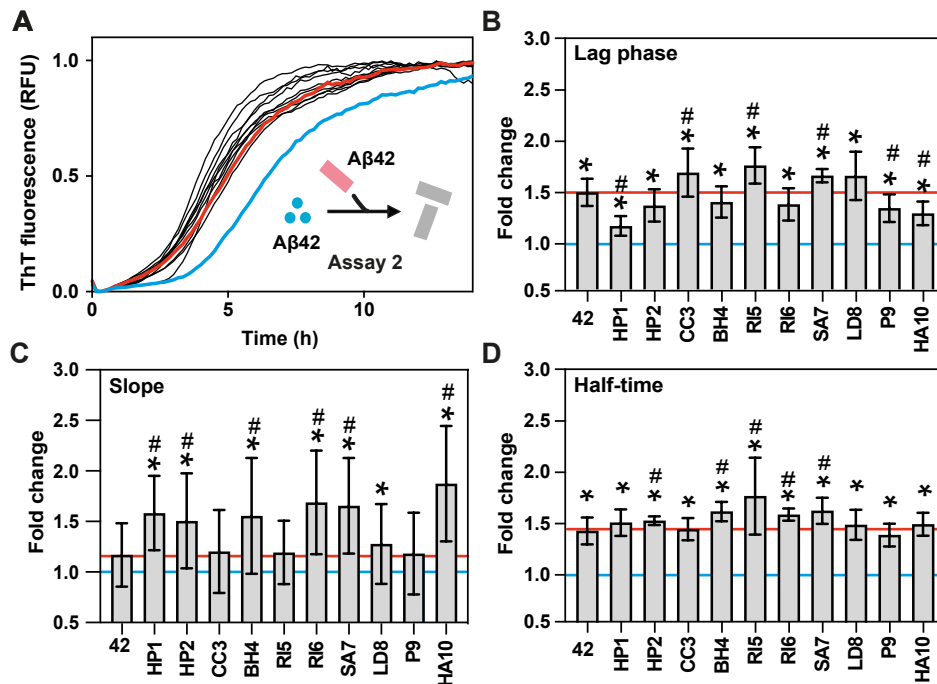


Figure 3. Exogenous Prion-like Sequences Affect A β 42 Seeds and Their Propagation. A) Aggregation kinetics of A β 42 seeded with A β 42 aggregates formed in the presence and absence (w/o) of seeds from exogenous prion-like sequences. In blue and red are highlighted the aggregation kinetics of A β 42 without seeds and with seed of pure A β 42 aggregates, respectively. See Supplementary Figure 6 for individual curves. B) Fold change in lag time (unseeded/seeded). C) Fold change in slope (seeded/unseeded). The equation fittings are shown in Supplementary Figure 7. D) Fold change in half-time (unseeded/seeded). Horizontal blue line indicates one-fold change, the value corresponding to a kinetic of A β 42 without seeds. Horizontal red line indicates the average value of the 42 column, the aggregation kinetics of A β 42 seeded with pure A β 42 aggregates. Error bars indicate the standard deviation. Each condition represents the results of three biological replicates, with three technical replicates per biological replicate. An asterisk (*) indicates a statistically significant difference ($p < 0.05$) compared to the condition without seeds, as determined by an unpaired t-test. A hash symbol (#) indicates a statistically significant difference ($p < 0.05$) compared to the condition seeded with pure A β 42 aggregates, determined by an unpaired t-test.

Effect on A β 42 Seeds and Their Propagation

After observing that bacterial prion-like sequences influence the aggregation of both A β 40[47] and A β 42, we investigated how past molecular interactions affect the propagation of A β 42 aggregates (Figure 1C). To address this, we conducted kinetic assays using pre-formed A β fibrils previously seeded with the bacterial peptides (Figure 2, Supplementary Figure 4). This second aggregation step (Figure 1C; Figure 3) involved a tenfold dilution of the exogenous peptides compared to the initial direct seeding assays. This dilution was achieved by incorporating 10% of the A β aggregates formed during the first step (Methods), keeping minimal the influence from the bacterial molecules ($\approx 1\%$) and allowing us to focus on the properties of the pre-formed aggregates.

All lag times were accelerated compared to A β 42 without seeds (Figure 3B, * symbol), with three bacterial sequences (CC3, RI5, SA7) even outperforming the kinetics seeded with pure

A β 42 aggregates, which were formed just by A β 42 molecules (Figure 3B, # symbol). Regarding the slope, seven sequences exhibited faster elongation/secondary nucleation compared to unseeded monomers, while six out of ten presented significantly larger slopes than those triggered by the pure A β 42 seeds. These findings point to an amplification effect, where the presence of bacterial peptides alter the A β 42 aggregates, generating polymorphs with enhanced seeding capabilities. This also underscores the importance of the Interaction History, demonstrating that even exogenous molecules with limited initial seeding capacity can redirect the aggregation pathway toward a new population of aggregates with enhanced propagation potential. Additionally, while the first-step assay, in which bacterial sequences acted as seeds, principally influenced the primary nucleation phase, the subsequent aggregation step, seeded with the resulting A β 42 aggregates, presented both a shorter lag time and a steeper slope, supporting the concept that sequence similarity favors the cross-seeding efficiency[56–58].

Beyond the overall aggregation acceleration, our analysis of different A β 42 seeds revealed that each bacterial prion-like sequence produces fibrillar polymorphs with distinct seeding properties (Figure 3A-D, Supplementary Figure 6). Specifically, some bacterial peptides (SA7) reduce both lag time and slope, while others selectively influence only one parameter (HP1, HP2, CC3, BH4, RI5, RI6, HA10). Some sequences have no significant effects (LD8), whereas others even delay the aggregation process (P9). These findings indicate that the fibrillar polymorphs formed in the presence of different exogenous molecules have distinct properties and can influence different phases of host protein aggregation. This, in turn, affects subsequent interactions and aggregate propagation, even during later stages when the exogenous molecule is no longer present. For instance, A β 42 seeds formed in the presence of RI5 shorten lag phase, suggesting enhanced monomer adherence during the initial nucleation phase, whereas A β 42 seeds formed in the presence of BH4 increase the slope, potentially indicating accelerated elongation driven by secondary nucleation events. This diversity in aggregation-modulating mechanisms may contribute to increase the structural heterogeneity of amyloid fibrils, further complicating the pathological landscape of AD.

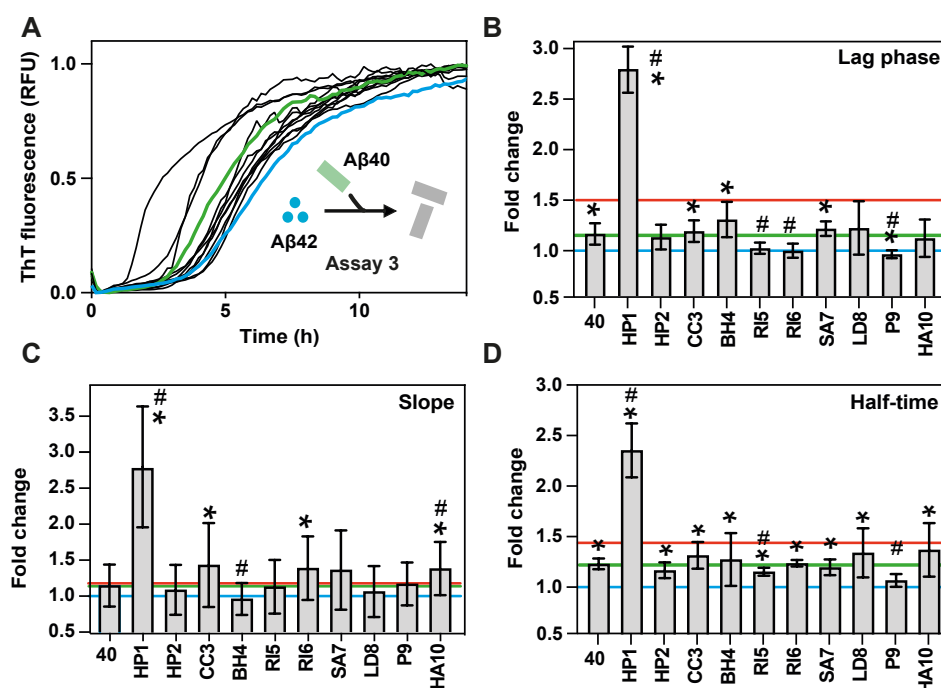


Figure 4. Exogenous Prion-like Sequences Affect A β 40 Aggregation and Its Propagation to A β 42. A) Aggregation kinetics of A β 42 seeded with A β 40 aggregates formed in the presence (HP1–HA10) and absence (w/o) of seeds from exogenous prion-like sequences. See Supplementary Figure 8 for individual curves. Green and blue lines highlight the aggregation of A β 42 seeded with pure A β 40 aggregates or without seeds, respectively. B) Fold change in lag time (unseeded/seeded). C) Fold change in slope (seeded/unseeded). The equation fittings are shown in Figure 9. D) Fold change in half-time (unseeded/seeded). The horizontal lines indicate the average value for aggregation kinetics of A β 42 seeded with pure A β 42 aggregates (red), pure A β 40 aggregates (green) or without seeds (blue). Error bars indicate the standard deviation. Each condition represents the results of three biological replicates, with three technical replicates per biological replicate. An asterisk (*) indicates a statistically significant difference ($p < 0.05$) compared to the condition without seeds, as determined by unpaired t-test. A hash symbol (#) indicates a statistically significant difference ($p < 0.05$) compared to the condition seeded with pure A β 40 aggregate, determined by an unpaired t-test. Blue Line represents the aggregation kinetics of A β 42 without any seeds.

Effect on A β 40 and Its Subsequent Seeding of A β 42

While the previous experiments focused on the self-seeding of A β 42, it is important to consider that A β 40 is the predominant isoform of amyloid-beta peptide in the human body[4,6]. Given its higher abundance, A β 40 is more likely to encounter and interact with exogenous prion-like proteins. To explore this possibility, we examined whether our collection of exogenous sequences could also influence the cross-seeding potential of A β 40 on A β 42 (Figure 4, Supplementary Figure 8).

In previous studies, we observed that most bacterial sequences, from our collection, accelerated the aggregation of monomeric A β 40[47]. In the present study, we used A β 40 aggregates formed during this initial aggregation step to seed A β 42 deposition. As a control, we tested the seeding efficiency of pure A β 40 aggregates and found that, although they reduced the lag time and half-time of A β 42 aggregation to a lesser extent than A β 42 seeds (Figure 4B and D), they induced a comparable slope increase (Figure 4C). These findings support that residues 41 and 42 play a critical role in facilitating the assembly of free monomers during the primary nucleation process, and their absence in A β 40 reduces its propagation efficiency[59].

When analyzing the effects of A β 40 aggregates formed in the presence of the bacterial peptides, we observed that only four of the ten A β 40 seeds shortened the lag phase, and among these, only one (HP1) achieved a lag time shorter than that of pure A β 40 aggregates (Figure 4B). Interestingly, three of these A β 40 seeds also enlarged the slope, validating that incubation with bacterial molecules can generate fibrillar polymorphs capable of influencing distinct aggregation phases. Overall, seven out of ten peptides redirected the aggregation pathway toward a new population of aggregates that significantly reduced the half-time of A β 42 aggregation (Figure 4D). However, only in presence of HP1, A β 40 seeds achieve a half-time reduction shorter than that of pure A β 40, and more notably, even shorter than pure A β 42 aggregates (Figure 4D, red line, p -value < 0.05 , unpaired t-test). In contrast, some bacterial peptides, such as RI5 and P9, generated A β 40 aggregates that slowed the A β 42 aggregation (Figure 4, Supplementary Figure 8).

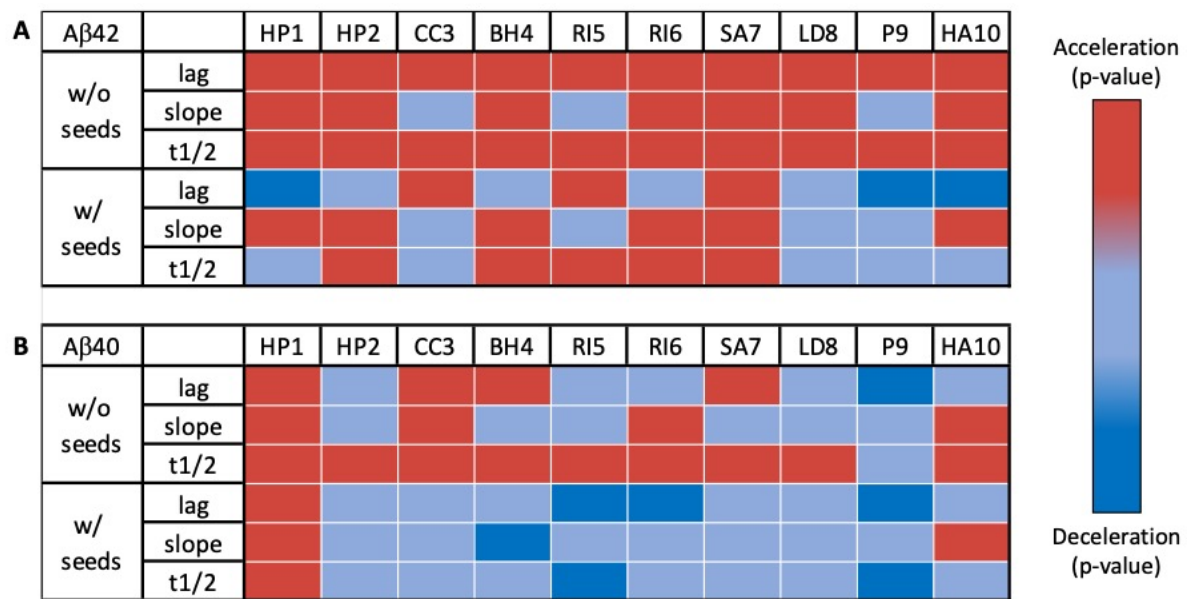


Figure 5. Differential Effects of Exogenous Prion-like Sequences on Aβ42 Aggregation. This figure provides a schematic overview of the significant data presented in Figures 3 and 4 (asterisk and hash symbols). It includes two color-coded matrices illustrating the impact of exogenous prion-like sequences on Aβ42 aggregation when occurring as a secondary or posterior seeding event. Red indicates conditions that significantly accelerate Aβ42 aggregation. Light blue represents conditions with no significant changes. Dark blue indicates conditions that significantly decelerate Aβ42 aggregation. Panel A show the results from assays using Aβ42 aggregates as seeds. Panel B show the results from assays using Aβ40 aggregates as seeds. The first row of each matrix displays the specific exogenous sequences added during seed formation. The first column indicates the statistical significance. w/o seeds refers to comparisons against the aggregation kinetics of Aβ42 without any seeds. w/ seeds refers to comparisons against Aβ42 aggregation when seeded with (A) pure Aβ42 aggregates or (B) pure Aβ40 aggregates. The second column lists the parameters analyzed, from top to bottom: Lag time, Slope and Half-time (t1/2).

The limited effect of Aβ40 aggregates, incubated with or without exogenous peptides, on Aβ42 aggregation (Figure 5) suggests that Aβ40 may have evolved to resist harmful interactions with exogenous molecules[60,61], making it less likely to propagate an aggregative conformation throughout the organism. Interestingly, HP1, the only sequence able to break this resilience, originates from a putative vacuolating cytotoxin of *Helicobacter pylori*, a bacterium associated with AD[62,63]. Consistent with this, our previous work[47] demonstrated that the HP1 sequence caused one of the most pronounced negative effects on *C. elegans* cognitive abilities.

Our findings highlight the potential of exogenous amyloid sequences to influence both direct seeding and subsequent cross-seeding events between Aβ isoforms. This effect varies among exogenous molecules, suggesting that specific molecular properties determine both the extent and direction of their influence, a feature that could inspire novel therapeutic strategies. Moreover, the structural heterogeneity of amyloid deposits, as evidenced by multiple fibril polymorphs identified in patient brain samples[10,25,44,64], suggests that

exogenous prion-like sequences may further diversify aggregate populations, adding complexity to the pathological landscape of AD.

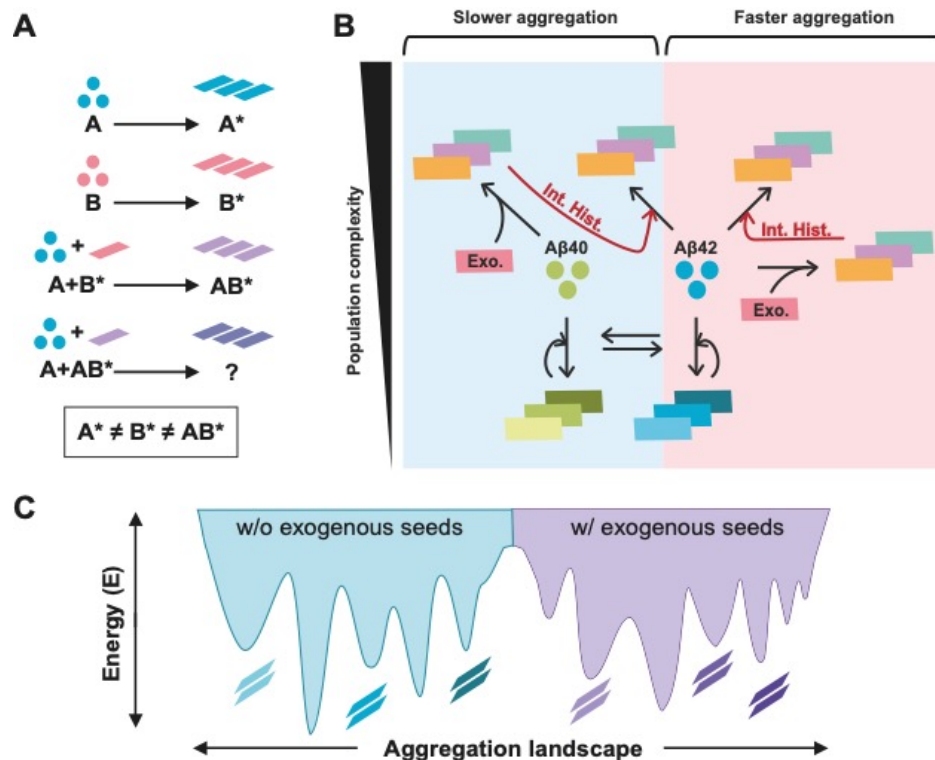


Figure 6. Influence of exogenous molecules on Aβ aggregate formation. A) This schematic illustrates how an exogenous protein (B) influences the aggregation dynamics of a host protein (A). Top row: The host protein (A) self-aggregates into fibrils (A^*). Second row: The exogenous protein (B) also undergoes self-aggregation, forming fibrils (B^*). Third row: When monomeric A aggregates in the presence of preformed B^* fibrils, a distinct aggregate (AB^*) is formed, different from A^* or B^* . Fourth row: A subsequent seeding step, where monomeric A interacts with AB^* fibrils, results in an unknown aggregation outcome, suggesting that the aggregation pathway is shaped by prior molecular interactions, leading to fibrillar polymorphism. Bottom statement: The divergence between A, B, and AB^* indicates that fibril formation is not uniform, which highlights the context-dependent nature of protein aggregation, where prior molecular interactions shape the polymorphic spectrum of aggregates. B) The aggregation of Aβ40 and Aβ42 is a dynamic process influenced by multiple interactions occurring in parallel. The presence of exogenous amyloid-like sequences (pink rectangles) introduces additional variability, modulating aggregation kinetics and the structural properties of the resulting fibrils. Since aggregates can act as seeds in consecutive cross-seeding events (curved arrows), Interaction History (red arrows) determines the evolution of amyloid species. As a result, aggregate diversity increases compared to a scenario where aggregation occurs in isolation, without exogenous influences (bottom part). This model suggests that the aggregation landscape is highly heterogeneous and sensitive to environmental factors. Circles represent monomeric proteins, while rectangles represent amyloid fibrils. C) In the absence of exogenous seeds, a protein populates a defined aggregation landscape (blue area), characterized by a specific set of aggregated structures. The presence of exogenous seeds may alter this landscape (purple area), potentially expanding the range of possible aggregation states and leading to additional polymorphs.

Conclusions

Our findings support that amyloid propagation is not merely a linear extension of existing fibrils, but a dynamic process shaped by prior molecular interactions (Interaction History). Each aggregation cycle generates structurally distinct populations[10,34,35,46] that differ in composition, morphology, and seeding capacity, even when originating from the same monomeric protein (Figure 6). While the same molecular mechanisms control both primary and secondary seeding events, aggregation conditions (e.g., pH, ionic strength, co-aggregating species) define the resulting fibrillar polymorphs[10,34,35,46]. This context dependency may contribute to the strain-like behavior of amyloid diseases[36,37], allowing distinct fibril species to emerge and selectively propagate under specific aggregation conditions.

The energy landscape of amyloid aggregation consists of multiple local minima, each corresponding to distinct fibrillar polymorphs[10,34,35,46]. The introduction of exogenous amyloid fibrils can reshape this landscape (Figure 6C), amplifying structural heterogeneity and influencing downstream aggregation events[34,35,46]. These findings highlight why single-step aggregation assays may be insufficient, since aggregates formed under different conditions generate seeds with distinct propagation capacities, influencing subsequent aggregation in unexpected ways. In our experiments, exogenous amyloid sequences led to the formation of A β 42 fibrillar polymorphs[25,44,64] with unique propagation properties. This underscores the role of environmental factors, particularly amyloids from the gut microbiota[39,40,45], in modulating A β aggregation and potentially contributing to neurodegeneration[47]. Importantly, our results indicate that heterologous assemblies may amplify aggregation, accelerating fibril formation and potentially exacerbating disease progression. Additionally, since exogenous molecules can shape subsequent interactions, aggregate propagation may occur far from the original site of exposure, even in the absence of the initiating agent.

While this study provides new insights into how exogenous amyloid sequences influence aggregation dynamics, several intriguing questions remain open for further study. A deeper structural characterization of the resulting polymorphs is needed to clarify their specific differences and determine whether exogenous molecules are incorporated into fibrils, potentially contributing to their heterogeneity. Additionally, it remains unclear whether exogenous interactions expand or limit the diversity of amyloid polymorphs. Another key aspect to explore is the potential toxicity of these aggregates, as certain polymorphs may be more pathogenic than others. Beyond the plateau phase, it is also essential to determine whether fibrillar polymorphs formed at different kinetic phases[34,35] exhibit distinct propagation properties and toxicity. This is particularly relevant in a biological system, where amyloid species from various aggregation stages may coexist, and any of them could potentially act as a trigger for acute disease onset.

Overall, this work emphasizes the need for a broader perspective on amyloid aggregation, one that considers external molecular influences, aggregation history, and fibril polymorphism. Understanding these variables could provide valuable insights into disease

mechanisms and inspire the development of therapeutic strategies to address the structural complexity of amyloid deposits in AD and related conditions.

Methods

Protein alignment and net charge

The alignments between the 10 different amyloid-forming core candidates were obtained using the KAling method within the Unipro UGENE software v43.0 [65]. Unipro UGENE software v43.0 was also used for sequence representation.

Net charge was calculated with PROTEIN CALCULATOR v3.4 at pH 7 (<https://protcalc.sourceforge.net/>).

Peptide Preparation

All samples were prepared in low protein-binding microcentrifuge tubes (ThermoFisher Scientific, Waltham, MA, USA). The bacterial amyloid sequences were obtained in lyophilized form from the Peptide Synthesis Facility, Department of Experimental and Health Sciences, Universitat Pompeu Fabra (UPF). Peptides were initially solubilized in 1,1,1,3,3,3-hexafluoroisopropanol (HFIP), then divided into aliquots and dried overnight in a fume hood at room temperature. For the amyloid aggregation, we employed the same conditions as in Curto, J.S. *et al.* 2024[47], in brief, the peptides were dissolved in DMSO to maintain monomeric states, followed by dilution in 50 mM phosphate buffer (PB), pH 7.4.

Synthetic A β 40 and A β 42 were purchased from GenScript (Rijswijk, Netherlands). Stock solutions were prepared by dissolving 1 mg of peptide in a final concentration of 250 μ M in 20 mM sodium phosphate buffer with 0.04% NH₃ and NaOH to achieve a pH of 11. The absence of aggregates was assessed using dynamic light scattering[47,66]. The peptide solution was then sonicated for 10 minutes (Fisherbrand Pittsburgh, PA, USA, FB15051) without sweep mode and stored at -80°C . For seeding experiments, the peptide was diluted at a 25 μ M concentration with 20 mM phosphate buffer (PB), pH 7.4. Then, if necessary, the specific seeds were added to a final concentration of 2 μ M and the mixture was left to aggregate at room temperature for 24 hours before their analysis.

Thioflavin-T Binding and Aggregation Kinetics

Thioflavin-T (ThT) was dissolved in Milli-Q water to a concentration of 5 mM, filtered through a 0.2- μ m filter, diluted to 0.5 mM, and stored at -20°C . ThT fluorescence for aggregation kinetics was measured every 10 minutes, measuring ThT fluorescence with a 440-nm excitation filter and a 480-nm emission filter on a plate reader (TECAN Infinite+ NANO) with bottom optics. Samples were prepared in flat-bottom, black, non-binding 96-well plates (Greiner Bio-One), with 100 μ L of sample added per well. Each condition was measured in triplicate.

For seeding experiments, A β 40 and A β 42 peptide stocks at pH 11 were diluted to a final concentration of 25 μ M in 20 mM sodium phosphate buffer with 100 mM NaCl. The corresponding pre-aggregated peptides were sonicated for 5 minutes before being added to a final concentration of 2.5 μ M. Control conditions included samples without A β 42 but with the peptide, samples without A β 42, and samples without peptides, all prepared with equivalent volumes of the corresponding buffers. All samples and controls were prepared in triplicate. The pH in each well was measured at the beginning and end of the experiment to confirm stability throughout the aggregation process and to verify consistency across

conditions. ThT was added to a final concentration of 20 μM . Aggregation reactions were conducted at 37°C without agitation, with four independent replicates. The $t_{1/2}$, defined as the time to reach 50% of the final fluorescence intensity, was measured for each condition. The lag phase was calculated as the time to reach 10% of the final fluorescence intensity. Each condition was measured with three experimental replicates, each consisting of three technical replicates. Also, the data were fitted into a sigmoidal curve using the Hill function:

$$h(x) = A \frac{x^h}{x^h + K^h} \quad (\text{Eq. 1})$$

In short, A, h and K the fitting parameters. The fittings were used to calculate the slope of the exponential phase of the aggregation kinetic as done by Rupert et al[26].

Transmission Electron Microscopy (TEM)

To prepare samples for TEM analysis, a 10 μL aliquot of the aggregated peptide solution (25 μM , incubated at 37°C for 24 hours without agitation) was applied to carbon-coated copper grids and allowed to adhere for 1 minute. Liquid excess was carefully blotted with Whatman filter paper[47]. Grids were then rinsed with distilled water and subsequently stained with 2% (w/v) uranyl acetate for 1 minute. After staining, grids were air-dried. Micrographs were obtained using a JEM-1400 transmission electron microscope (JEOL, Tokyo, Japan) set to an accelerating voltage of 80 keV.

Statistics

GraphPad PRISM 8 software was used for statistical analysis of the obtained data. In general, the data was analyzed with by unpaired t-test. Statistical significance was considered with p-values <0.05. Data is shown as the mean \pm SD.

Funding

This work was funded by grants RYC2019-026752-I, CNS2023-144437/MCIN/AEI/10.13039/501100011033, PID2020-117454RA-I00/AEI/10.13039/501100011033 from Ministerio de Ciencia e Innovación and by L'Oréal-UNESCO For Women in Science Programme.

Acknowledgments

We extend our gratitude to the following individuals:

Jacob Rupert for his comments and in-depth discussions, which provided valuable insights into our work and its implications.

Transmission electron microscopy (TEM) images were acquired at the Servei de Microscòpia i Difracció de Raigs X (SMiDRX) of the Universitat Autònoma de Barcelona (UAB).

Bibliography

- [1] L.E. Hebert, P.A. Scherr, J.L. Bienias, D.A. Bennett, D.A. Evans, Alzheimer disease in the US population: prevalence estimates using the 2000 census, *Arch. Neurol.* 60 (2003) 1119–1122. <https://doi.org/10.1001/ARCHNEUR.60.8.1119>.
- [2] F. Chiti, C.M. Dobson, Protein Misfolding, Amyloid Formation, and Human Disease: A Summary of Progress Over the Last Decade, *Annu. Rev. Biochem.* 86 (2017) 27–68.

- <https://doi.org/10.1146/ANNUREV-BIOCHEM-061516-045115>.
- [3] F. Chiti, C.M. Dobson, Protein misfolding, functional amyloid, and human disease, *Annu. Rev. Biochem.* 75 (2006) 333–366.
<https://doi.org/10.1146/ANNUREV.BIOCHEM.75.101304.123901>.
 - [4] T. Guo, D. Zhang, Y. Zeng, T.Y. Huang, H. Xu, Y. Zhao, Molecular and cellular mechanisms underlying the pathogenesis of Alzheimer’s disease, *Mol. Neurodegener.* 15 (2020). <https://doi.org/10.1186/S13024-020-00391-7>.
 - [5] H. Hampel, J. Hardy, K. Blennow, C. Chen, G. Perry, S.H. Kim, V.L. Villemagne, P. Aisen, M. Vendruscolo, T. Iwatsubo, C.L. Masters, M. Cho, L. Lannfelt, J.L. Cummings, A. Vergallo, The Amyloid- β Pathway in Alzheimer’s Disease, *Mol. Psychiatry* 26 (2021) 5481–5503. <https://doi.org/10.1038/S41380-021-01249-0>.
 - [6] G.F. Chen, T.H. Xu, Y. Yan, Y.R. Zhou, Y. Jiang, K. Melcher, H.E. Xu, Amyloid beta: structure, biology and structure-based therapeutic development, *Acta Pharmacol. Sin.* 38 (2017) 1205–1235. <https://doi.org/10.1038/APS.2017.28>.
 - [7] A.I. Sulatskaya, G.N. Rychkov, M.I. Sulatsky, E. V. Mikhailova, N.M. Melnikova, V.S. Andozhskaya, I.M. Kuznetsova, K.K. Turoverov, New Evidence on a Distinction between A β 40 and A β 42 Amyloids: Thioflavin T Binding Modes, Clustering Tendency, Degradation Resistance, and Cross-Seeding, *Int. J. Mol. Sci.* 23 (2022). <https://doi.org/10.3390/IJMS23105513>.
 - [8] J. Tran, D. Chang, F. Hsu, H. Wang, Z. Guo, Cross-seeding between A β 40 and A β 42 in Alzheimer’s disease, *FEBS Lett.* 591 (2017) 177–185. <https://doi.org/10.1002/1873-3468.12526>.
 - [9] L. Gu, Z. Guo, Alzheimer’s A β 42 and A β 40 peptides form interlaced amyloid fibrils, *J. Neurochem.* 126 (2013) 305–311. <https://doi.org/10.1111/JNC.12202>.
 - [10] Y. Yang, D. Arseni, W. Zhang, M. Huang, S. Lövestam, M. Schweighauser, A. Kotecha, A.G. Murzin, S.Y. Peak-Chew, J. MacDonald, I. Lavenir, H.J. Garringer, E. Gelpi, K.L. Newell, G.G. Kovacs, R. Vidal, B. Ghetti, B. Ryskeldi-Falco, S.H.W. Scheres, M. Goedert, Cryo-EM structures of amyloid- β 42 filaments from human brains, *Science* 375 (2022) 167–172. <https://doi.org/10.1126/SCIENCE.ABM7285>.
 - [11] G.A. Braun, A.J. Dear, K. Sanagavarapu, H. Zetterberg, S. Linse, Amyloid- β peptide 37, 38 and 40 individually and cooperatively inhibit amyloid- β 42 aggregation, *Chem. Sci.* 13 (2022) 2423–2439. <https://doi.org/10.1039/D1SC02990H>.
 - [12] C.N. Suire, S.O. Abdul-Hay, T. Sahara, D. Kang, M.K. Brizuela, P. Saftig, D.W. Dickson, T.L. Rosenberry, M.A. Leissring, Cathepsin D regulates cerebral A β 42/40 ratios via differential degradation of A β 42 and A β 40, *Alzheimers. Res. Ther.* 12 (2020). <https://doi.org/10.1186/S13195-020-00649-8>.
 - [13] S.S. Kwak, K.J. Washicosky, E. Brand, D. von Maydell, J. Aronson, S. Kim, D.E. Capen, M. Cetinbas, R. Sadreyev, S. Ning, E. Bylykbashi, W. Xia, S.L. Wagner, S.H. Choi, R.E. Tanzi, D.Y. Kim, Amyloid- β 42/40 ratio drives tau pathology in 3D human neural cell culture models of Alzheimer’s disease, *Nat. Commun.* 11 (2020). <https://doi.org/10.1038/S41467-020-15120-3>.
 - [14] C.C. Liu, N. Zhao, Y. Fu, N. Wang, C. Linares, C.W. Tsai, G. Bu, ApoE4 Accelerates Early Seeding of Amyloid Pathology, *Neuron* 96 (2017) 1024-1032.e3. <https://doi.org/10.1016/J.NEURON.2017.11.013>.
 - [15] M. Lee, W.M. Yau, J.M. Louis, R. Tycko, Structures of brain-derived 42-residue amyloid- β fibril polymorphs with unusual molecular conformations and intermolecular interactions, *Proc. Natl. Acad. Sci. U. S. A.* 120 (2023).

- <https://doi.org/10.1073/PNAS.2218831120>.
- [16] F. Xiong, W. Ge, C. Ma, Quantitative proteomics reveals distinct composition of amyloid plaques in Alzheimer's disease, *Alzheimers. Dement.* 15 (2019) 429–440. <https://doi.org/10.1016/J.JALZ.2018.10.006>.
 - [17] B.B. Holmes, M.I. Diamond, Cellular mechanisms of protein aggregate propagation, *Curr. Opin. Neurol.* 25 (2012) 721–726. <https://doi.org/10.1097/WCO.0B013E32835A3EE0>.
 - [18] M.A. Marques, J.J. Kulstad, C.E. Savard, P.S. Green, S.P. Lee, S. Craft, G.S. Watson, D.G. Cook, Peripheral amyloid-beta levels regulate amyloid-beta clearance from the central nervous system, *J. Alzheimers. Dis.* 16 (2009) 325–329. <https://doi.org/10.3233/JAD-2009-0964>.
 - [19] N. Gamez, R. Morales, The Role of Circulating A β Seeds in the Progression of Cerebral Amyloidosis, *Neurosci. Insights* 17 (2022). <https://doi.org/10.1177/26331055221123072>.
 - [20] A.F. Cintron, N. V. Dalal, J. Dooyema, R. Betarbet, L.C. Walker, Transport of cargo from periphery to brain by circulating monocytes, *Brain Res.* 1622 (2015) 328–338. <https://doi.org/10.1016/J.BRAINRES.2015.06.047>.
 - [21] M.M. Rahman, C. Lendel, Extracellular protein components of amyloid plaques and their roles in Alzheimer's disease pathology, *Mol. Neurodegener.* 16 (2021). <https://doi.org/10.1186/S13024-021-00465-0>.
 - [22] P. Bharadwaj, T. Solomon, B.R. Sahoo, K. Ignasiak, S. Gaskin, J. Rowles, G. Verdile, M.J. Howard, C.S. Bond, A. Ramamoorthy, R.N. Martins, P. Newsholme, Amylin and beta amyloid proteins interact to form amorphous heterocomplexes with enhanced toxicity in neuronal cells, *Sci. Rep.* 10 (2020). <https://doi.org/10.1038/S41598-020-66602-9>.
 - [23] K.H. Shim, M.J. Kang, Y.C. Youn, S.S.A. An, S.Y. Kim, Alpha-synuclein: a pathological factor with A β and tau and biomarker in Alzheimer's disease, *Alzheimers. Res. Ther.* 14 (2022). <https://doi.org/10.1186/S13195-022-01150-0>.
 - [24] L.K. Clinton, M. Blurton-Jones, K. Myczek, J.Q. Trojanowski, F.M. LaFerla, Synergistic Interactions between Abeta, tau, and alpha-synuclein: acceleration of neuropathology and cognitive decline, *J. Neurosci.* 30 (2010) 7281–7289. <https://doi.org/10.1523/JNEUROSCI.0490-10.2010>.
 - [25] M.I. Ivanova, Y. Lin, Y.H. Lee, J. Zheng, A. Ramamoorthy, Biophysical processes underlying cross-seeding in amyloid aggregation and implications in amyloid pathology, *Biophys. Chem.* 269 (2021). <https://doi.org/10.1016/J.BPC.2020.106507>.
 - [26] J. Rupert, M. Monti, E. Zacco, G.G. Tartaglia, RNA sequestration driven by amyloid formation: the alpha synuclein case, *Nucleic Acids Res.* 51 (2023) 11466–11478. <https://doi.org/10.1093/NAR/GKAD857>.
 - [27] T. Janas, K. Sapoń, M.H.B. Stowell, T. Janas, Selection of Membrane RNA Aptamers to Amyloid Beta Peptide: Implications for Exosome-Based Antioxidant Strategies, *Int. J. Mol. Sci.* 20 (2019). <https://doi.org/10.3390/IJMS20020299>.
 - [28] E. Álvarez-Marimon, H. Castillo-Michel, J. Reyes-Herrera, J. Seira, E. Aso, M. Carmona, I. Ferrer, J. Cladera, N. Benseny-Cases, Synchrotron X-ray Fluorescence and FTIR Signatures for Amyloid Fibrillary and Nonfibrillary Plaques, *ACS Chem. Neurosci.* 12 (2021) 1961–1971. <https://doi.org/10.1021/ACSCHEMNEURO.1C00048>.
 - [29] A. Abelein, Metal Binding of Alzheimer's Amyloid- β and Its Effect on Peptide Self-Assembly, *Acc. Chem. Res.* 56 (2023) 2653–2663.

- <https://doi.org/10.1021/ACS.ACCOUNTS.3C00370>.
- [30] A.S. Pithadia, M.H. Lim, Metal-associated amyloid- β species in Alzheimer's disease, *Curr. Opin. Chem. Biol.* 16 (2012) 67–73.
<https://doi.org/10.1016/J.CBPA.2012.01.016>.
 - [31] J. Tittelmeier, S. Druffel-Augustin, A. Alik, R. Melki, C. Nussbaum-Krammer, Dissecting aggregation and seeding dynamics of α -Syn polymorphs using the phasor approach to FLIM, *Commun. Biol.* 5 (2022). <https://doi.org/10.1038/S42003-022-04289-6>.
 - [32] J. Seira Curto, M.R. Fernandez, J. Cladera, N. Benseny-Cases, N. Sanchez de Groot, A β 40 Aggregation under Changeable Conditions, *Int. J. Mol. Sci.* 24 (2023).
<https://doi.org/10.3390/IJMS24098408>.
 - [33] R. Tycko, Amyloid polymorphism: structural basis and neurobiological relevance, *Neuron* 86 (2015) 632–645. <https://doi.org/10.1016/J.NEURON.2015.03.017>.
 - [34] L.D. Aubrey, S.E. Radford, How is the Amyloid Fold Built? Polymorphism and the Microscopic Mechanisms of Fibril Assembly, *J. Mol. Biol.* (2025) 169008.
<https://doi.org/10.1016/J.JMB.2025.169008>.
 - [35] M. Wilkinson, Y. Xu, D. Thacker, A.I.P. Taylor, D.G. Fisher, R.U. Gallardo, S.E. Radford, N.A. Ranson, Structural evolution of fibril polymorphs during amyloid assembly, *Cell* 186 (2023) 5798–5811.e26.
https://doi.org/10.1016/J.CELL.2023.11.025/ASSET/81BC20EA-6EEC-4F88-BC37-2ADA6DE0C4E3/MAIN.ASSETS/FIGS13_LRG.JPG.
 - [36] C. Duran-Aniotz, I. Moreno-Gonzalez, N. Gamez, N. Perez-Urrutia, L. Vegas-Gomez, C. Soto, R. Morales, Amyloid pathology arrangements in Alzheimer's disease brains modulate in vivo seeding capability, *Acta Neuropathol. Commun.* 9 (2021).
<https://doi.org/10.1186/S40478-021-01155-0>.
 - [37] Y. Yang, D. Arseni, W. Zhang, M. Huang, S. Lövestam, M. Schweighauser, A. Kotecha, A.G. Murzin, S.Y. Peak-Chew, J. MacDonald, I. Lavenir, H.J. Garringer, E. Gelpi, K.L. Newell, G.G. Kovacs, R. Vidal, B. Ghetti, B. Ryskeldi-Falco, S.H.W. Scheres, M. Goedert, Cryo-EM structures of amyloid-b 42 filaments from human brains, *Science* (80-.). 375 (2022) 167–172.
https://doi.org/10.1126/SCIENCE.ABM7285/SUPPL_FILE/SCIENCE.ABM7285_MДАР_REPRODUCIBILITY_CHECKLIST.PDF.
 - [38] J. Zhang, Y. Zhang, J. Wang, Y. Xia, J. Zhang, L. Chen, Recent advances in Alzheimer's disease: Mechanisms, clinical trials and new drug development strategies, *Signal Transduct. Target. Ther.* 9 (2024). <https://doi.org/10.1038/S41392-024-01911-3>.
 - [39] Y. Belkaid, T.W. Hand, Role of the microbiota in immunity and inflammation, *Cell* 157 (2014) 121–141. <https://doi.org/10.1016/J.CELL.2014.03.011>.
 - [40] J. Seira Curto, A. Surroca Lopez, M. Casals Sanchez, I. Tic, M.R. Fernandez Gallegos, N. Sanchez de Groot, Microbiome Impact on Amyloidogenesis, *Front. Mol. Biosci.* 9 (2022). <https://doi.org/10.3389/FMOLB.2022.926702>.
 - [41] B. Ren, Y. Zhang, M. Zhang, Y. Liu, D. Zhang, X. Gong, Z. Feng, J. Tang, Y. Chang, J. Zheng, Fundamentals of cross-seeding of amyloid proteins: an introduction, *J. Mater. Chem. B* 7 (2019) 7267–7282. <https://doi.org/10.1039/C9TB01871A>.
 - [42] C.J. Sigurdson, K.P.R. Nilsson, S. Hornemann, G. Manco, N. Fernández-Borges, P. Schwarz, J. Castilla, K. Wüthrich, A. Aguzzi, A molecular switch controls interspecies prion disease transmission in mice, *J. Clin. Invest.* 120 (2010) 2590–2599.
<https://doi.org/10.1172/JCI42051>.
 - [43] C. Weissmann, M. Enari, P.C. Klöhn, D. Rossi, E. Flechsig, Transmission of prions, *J.*

- Infect. Dis. 186 Suppl 2 (2002). <https://doi.org/10.1086/344575>.
- [44] P. Chaudhuri, K.P. Prajapati, B.G. Anand, K. Dubey, K. Kar, Amyloid cross-seeding raises new dimensions to understanding of amyloidogenesis mechanism, *Ageing Res. Rev.* 56 (2019). <https://doi.org/10.1016/J.ARR.2019.100937>.
 - [45] K. Oliphant, E. Allen-Vercoe, Macronutrient metabolism by the human gut microbiome: major fermentation by-products and their impact on host health, *Microbiome* 7 (2019). <https://doi.org/10.1186/S40168-019-0704-8>.
 - [46] K.W. Tipping, P. van Oosten-Hawle, E.W. Hewitt, S.E. Radford, Amyloid Fibres: Inert End-Stage Aggregates or Key Players in Disease?, *Trends Biochem. Sci.* 40 (2015) 719–727. <https://doi.org/10.1016/J.TIBS.2015.10.002>.
 - [47] J.S. Curto, A.D. Martinez, P.S. Sotillo, M.S. Garcia, M.G. del Pozo, M.R. Fernandez, N.S. de Groot, Microbiome-Derived Prion-Like Proteins and Their Potential to Trigger Cognitive Dysfunction, *BioRxiv* (2024) 2023.10.19.563052. <https://doi.org/10.1101/2023.10.19.563052>.
 - [48] S. Holmqvist, O. Chutna, L. Bousset, P. Aldrin-Kirk, W. Li, T. Björklund, Z.Y. Wang, L. Roybon, R. Melki, J.Y. Li, Direct evidence of Parkinson pathology spread from the gastrointestinal tract to the brain in rats, *Acta Neuropathol.* 128 (2014) 805–820. <https://doi.org/10.1007/S00401-014-1343-6>.
 - [49] S.K. Kim, R.B. Guevarra, Y.T. Kim, J. Kwon, H. Kim, J.H. Cho, H.B. Kim, J.H. Lee, Role of Probiotics in Human Gut Microbiome-Associated Diseases, *J. Microbiol. Biotechnol.* 29 (2019) 1335–1340. <https://doi.org/10.4014/JMB.1906.06064>.
 - [50] R. Sabate, F. Rousseau, J. Schymkowitz, S. Ventura, What makes a protein sequence a prion?, *PLoS Comput. Biol.* 11 (2015). <https://doi.org/10.1371/JOURNAL.PCBI.1004013>.
 - [51] I. Pallarès, V. Iglesias, S. Ventura, The Rho Termination Factor of *Clostridium botulinum* Contains a Prion-Like Domain with a Highly Amyloidogenic Core, *Front. Microbiol.* 6 (2016). <https://doi.org/10.3389/FMICB.2015.01516>.
 - [52] A. Esteras-Chopo, L. Serrano, M. López De La Paz, The amyloid stretch hypothesis: recruiting proteins toward the dark side, *Proc. Natl. Acad. Sci. U. S. A.* 102 (2005) 16672–16677. <https://doi.org/10.1073/PNAS.0505905102>.
 - [53] Y.H. Liao, Y.J. Chang, Y. Yoshiike, Y.C. Chang, Y.R. Chen, Negatively charged gold nanoparticles inhibit Alzheimer's amyloid- β fibrillization, induce fibril dissociation, and mitigate neurotoxicity, *Small* 8 (2012) 3631–3639. <https://doi.org/10.1002/SMLL.201201068>.
 - [54] H.M. Chan, L. Xiao, K.M. Yeung, S.L. Ho, D. Zhao, W.H. Chan, H.W. Li, Effect of surface-functionalized nanoparticles on the elongation phase of beta-amyloid (1-40) fibrillogenesis, *Biomaterials* 33 (2012) 4443–4450. <https://doi.org/10.1016/J.BIOMATERIALS.2012.03.024>.
 - [55] H. Liu, B. Xie, X. Dong, L. Zhang, Y. Wang, F. Liu, Y. Sun, Negatively charged hydrophobic nanoparticles inhibit amyloid β -protein fibrillation: The presence of an optimal charge density, *React. Funct. Polym.* 103 (2016) 108–116. <https://doi.org/10.1016/J.REACTFUNCTPOLYM.2016.04.003>.
 - [56] M.R.H. Krebs, L.A. Morozova-Roche, K. Daniel, C. V. Robinson, C.M. Dobson, Observation of sequence specificity in the seeding of protein amyloid fibrils, *Protein Sci.* 13 (2004) 1933–1938. <https://doi.org/10.1110/PS.04707004>.
 - [57] K. Konstantoulea, P. Guerreiro, M. Ramakers, N. Louros, L.D. Aubrey, B. Houben, E. Michiels, M. De Vleeschouwer, Y. Lampi, L.F. Ribeiro, J. de Wit, W. Xue, J.

- Schymkowitz, F. Rousseau, Heterotypic Amyloid β interactions facilitate amyloid assembly and modify amyloid structure, *EMBO J.* 41 (2022).
https://doi.org/10.15252/EMBJ.2021108591/SUPPL_FILE/EMBJ2021108591-SUP-0005-DATASET3.XLSX.
- [58] S. Subedi, S. Sasidharan, N. Nag, P. Saudagar, T. Tripathi, Amyloid Cross-Seeding: Mechanism, Implication, and Inhibition, *Molecules* 27 (2022).
<https://doi.org/10.3390/MOLECULES27061776>.
- [59] G. Meisl, X. Yang, E. Hellstrand, B. Frohm, J.B. Kirkegaard, S.I.A. Cohen, C.M. Dobson, S. Linse, T.P.J. Knowles, Differences in nucleation behavior underlie the contrasting aggregation kinetics of the A β 40 and A β 42 peptides, *Proc. Natl. Acad. Sci. U. S. A.* 111 (2014) 9384–9389. <https://doi.org/10.1073/PNAS.1401564111/-/DCSUPPLEMENTAL/PNAS.201401564SI.PDF>.
- [60] A. Jan, O. Adolfsson, I. Allaman, A.L. Buccarello, P.J. Magistretti, A. Pfeifer, A. Muhs, H.A. Lashuel, Abeta42 neurotoxicity is mediated by ongoing nucleated polymerization process rather than by discrete Abeta42 species, *J. Biol. Chem.* 286 (2011) 8585–8596. <https://doi.org/10.1074/JBC.M110.172411>.
- [61] C. Haass, D.J. Selkoe, Soluble protein oligomers in neurodegeneration: lessons from the Alzheimer's amyloid beta-peptide, *Nat. Rev. Mol. Cell Biol.* 8 (2007) 101–112. <https://doi.org/10.1038/NRM2101>.
- [62] N.M. Vogt, R.L. Kerby, K.A. Dill-McFarland, S.J. Harding, A.P. Merluzzi, S.C. Johnson, C.M. Carlsson, S. Asthana, H. Zetterberg, K. Blennow, B.B. Bendlin, F.E. Rey, Gut microbiome alterations in Alzheimer's disease, *Sci. Rep.* 7 (2017).
<https://doi.org/10.1038/S41598-017-13601-Y>.
- [63] F. Panza, M. Lozupone, V. Solfrizzi, M. Watling, B.P. Imbimbo, Time to test antibacterial therapy in Alzheimer's disease, *Brain* 142 (2019) 2905–2929.
<https://doi.org/10.1093/BRAIN/AWZ244>.
- [64] J. Rasmussen, J. Mahler, N. Beschoner, S.A. Kaeser, L.M. Häslar, F. Baumann, S. Nyström, E. Portelius, K. Blennow, T. Lashley, N.C. Fox, D. Sepulveda-Falla, M. Glatzel, A.L. Oblak, B. Ghetti, K.P.R. Nilsson, P. Hammarström, M. Staufenbiel, L.C. Walker, M. Jucker, Amyloid polymorphisms constitute distinct clouds of conformational variants in different etiological subtypes of Alzheimer's disease, *Proc. Natl. Acad. Sci. U. S. A.* 114 (2017) 13018–13023. <https://doi.org/10.1073/PNAS.1713215114>.
- [65] K. Okonechnikov, O. Golosova, M. Fursov, UGENE team, Unipro UGENE: a unified bioinformatics toolkit., *Bioinformatics* 28 (2012) 1166–7.
<https://doi.org/10.1093/bioinformatics/bts091>.
- [66] N. Benseny-Cases, O. Klementieva, J. Cladera, In vitro Oligomerization and Fibrillogenesis of Amyloid-beta Peptides, *Subcell. Biochem.* 65 (2012) 53–74.
https://doi.org/10.1007/978-94-007-5416-4_3.

General Discussion and Future Perspectives

1. CHAPTER I: A β 40 Aggregation under Changeable Conditions

A β aggregation has traditionally been considered an extracellular event. However, recent studies have raised concerns about the possibility of intracellular aggregation, driven by pH imbalances and impaired autophagy. For example, in astrocytes carrying the E4 allele of apolipoprotein E (ApoE4), the strongest genetic risk factor for sporadic Alzheimer's disease, lysosomes and endosomes are known to exhibit abnormal pH levels. In the present study, we hypothesized that within these acidic compartments, the aggregates formed may differ in their properties from those formed at neutral pH and may be more toxic to the organism.

We evaluated the effects of the different physiological environments that the A β 40 peptide may encounter *in vivo* by analyzing its aggregation kinetics under different conditions. Between pH 7.4 and 6.8, the aggregation kinetics were influenced by the ionic strength of the buffer. At neutral pH, A β 40 carries a net negative charge, and higher salt concentrations reduce electrostatic repulsion between peptide monomers, thereby accelerating aggregation. At acidic pH, protonation of histidine residues lowers the overall charge of the peptide, bringing it closer to neutrality. This reduction in charge decreases repulsion between monomers and eliminates the need for ionic shielding to promote aggregation, resulting in a faster and less ordered process that leads to the formation of more amorphous aggregates. Notably, these aggregates have been reported to be more toxic than ordered amyloid fibrils. Consistent with this, our experiments showed that they exhibit enhanced seeding capacity, suggesting a greater potential for propagation and transmissibility. Also, we observed that the aggregates formed at pH 7.4 barely changed their morphology at acidic pH, while those formed at pH 5.5 evolved to a more ordered form when placed at neutral pH.

Overall, this work highlights the inherent risk associated with aggregates formed under altered pH conditions, such as those present in cells with dysfunctional endosomes and lysosomes. Fibrils formed under these physiologically relevant acidic environments appear to be significantly more reactive, transmissible, and toxic than those formed at neutral pH. Moreover, their structural instability upon return to neutral pH suggests that they may act as propagating seeds once released into the cytosol.

In summary, the study supports the critical role of pH has in modulating the properties of protein aggregates. Thus, changes in pH can lead the formation of structurally distinct species, more amorphous, less stable, and more toxic. Additionally, the results also highlight the influence of ionic strength in modulating aggregation behavior. Although ionic conditions are usually stable in the body, small changes in specific areas, like near lipid membranes, may facilitate alternative aggregation pathways. Understanding the aggregates that form under these non-standard conditions is important, as they might play a role in disease and and serve as potential therapeutic targets.

2. CHAPTER II: Exogenous Prion-Like Proteins and Their Potential to Trigger Cognitive Dysfunction

The human body is constantly exposed to exogenous proteins, many of which may have the potential to interfere with A β aggregation. In this context, prion-like proteins from the gut microbiome are of particular interest, as they can persist in the body for extended periods. The prolonged presence of these microbial proteins increases the likelihood of their interaction with A β peptides and their potential influence on the development of Alzheimer's disease.

To explore this hypothesis, we searched for prion-like protein sequences within the gut microbiome. Our findings revealed the presence of such proteins in most bacterial species and their association with a wide range of biological functions. Notably, we observed a significant enrichment of prion-like proteins in *Helicobacter pylori*, a bacterium whose infection is highly prevalent among Alzheimer's patients. From this analysis, ten prion-like peptides were selected and experimentally confirmed to form amyloid aggregates *in vitro*. These aggregates were shown to interfere with A β 40 aggregation and to induce oxidative stress in neuroblastoma cells. These first findings support the idea that microbiome-derived prion-like proteins may disrupt normal A β aggregation and promote pathological processes associated with Alzheimer's disease.

Later, the prion-like properties of these peptides, including their ability to aggregate and propagate, were confirmed *in vivo* using yeast and bacterial models. The bacterial model was further exploited to produce a prion-rich diet, which was fed to *C. elegans* to assess the effects of these proteins on cognitive function. Two peptides, HP1 and HP2, both derived from *H. pylori*, were found to cause the most pronounced cognitive impairment in the worms and the highest levels of toxicity in cell culture, highlighting the potential role of this bacterium in Alzheimer's pathology. Additionally, three other peptides from different bacterial species were found to impair learning and increase oxidative stress in *C. elegans*, further supporting the idea that exogenous prion-like proteins can contribute to neurotoxicity and cognitive decline.

Importantly, not all the tested peptides were detrimental for *C. elegans*, and one was able to slow down A β 40 aggregation, suggesting that not all amyloid aggregates are harmful and that some of them may even have protective effects. This finding points out the need for further research to better understand the complex relationship between the microbiome and neurodegenerative diseases. This information could inspire the development of therapeutic strategies to reduce bacteria that produce harmful amyloids while promoting those with potentially beneficial effects.

In summary, this study demonstrates the presence of prion-like proteins in the human microbiome and shows that these proteins can interfere with A β 40 aggregation *in vitro* and exert neurotoxic effects in both human neuroblastoma cells and *C. elegans* models, particularly those derived from *Helicobacter pylori*.

3. CHAPTER III: Exogenous Amyloid Sequences: Their Role in Amyloid-Beta Heterotypic Aggregation

This work aims to provide a deeper analysis of how aggregated proteins from the gut microbiome interfere with A β peptides, with a particular focus on the formation of new polymorphs exhibiting distinct propagation properties.

To test this, we developed an approach that simulates a scenario in which A β first encounters exogenous amyloids at one site in the organism and is later transported to interact with monomeric A β species elsewhere in the body. To this end, A β 40 and A β 42 peptides were initially exposed to microbiome-derived amyloid aggregates, and the resulting protein aggregates were then used as seeds to initiate the aggregation of fresh monomeric A β 42.

This assay demonstrated that microbiome-exposed aggregates exhibited efficient seeding capability, in some cases even surpassing that of pure A β amyloid fibrils. These findings suggest that exposure to microbiome-derived amyloids leads to the formation of distinct polymorphic conformations with altered properties, capable of propagating structurally unique amyloid strains.

Among the two isoforms studied, A β 42-derived aggregates present more efficient propagation than those derived from A β 40, suggesting that A β 40, the more abundant circulating form, may be evolutionarily adapted to resist interference by exogenous amyloids. Exceptionally, HP1, a peptide from *Helicobacter pylori*, was the only microbial protein aggregate capable of significantly enhancing A β 40 seeding. This, together with its previously observed neurotoxic and cognitive effects, raises concern about its potential involvement in Alzheimer's disease.

In summary, this study shows that exposure to exogenous prion-like proteins from the gut microbiome not only accelerates A β aggregation but also alters the conformational properties of the resulting aggregates. These modified polymorphs exhibit enhanced seeding capacity and may propagate novel amyloid strains distinct from those formed under unexposed conditions.

Future studies should assess whether these structurally distinct aggregates also differ in toxicity, as this could result in the emergence of more pathogenic species. Overall, these findings reinforce the potential role of microbiome-derived amyloid proteins in modulating A β aggregation and underscore the importance of further investigating specific bacterial peptides, such as HP1, as contributors to disease progression and potential therapeutic targets.

Concluding remarks

As a general conclusion, this thesis sheds light on exogenous prion-like amyloids as potential therapeutic targets for the treatment or prevention of Alzheimer's disease and shifts the focus toward isolated molecular events that may occur under altered physiological conditions.

The observed effects of exogenous prion-like proteins on A β aggregation and seeding properties open a new avenue for exploring alternative sources of toxic amyloid species. Furthermore, the formation of structurally distinct aggregates under altered pH, conditions that may occur *in vivo*, highlights the importance of studying amyloidogenic processes not only under healthy physiological conditions but also in microenvironments that, while less common, are biologically relevant.

The interplay between A β peptides, the microbiome, and pH imbalances may contribute significantly to Alzheimer's disease progression and offer potential for novel therapeutic strategies. These could include modulating the composition of the gut microbiota to favor non-amyloidogenic species while suppressing bacteria with amyloidogenic potential. In particular, *Helicobacter pylori* raises significant concern, reinforcing the importance of both treating the infection and minimizing interactions between its amyloidogenic proteins and host proteins.

References

- Abelein, A. (2023). Metal Binding of Alzheimer's Amyloid- β and Its Effect on Peptide Self-Assembly. *Accounts of Chemical Research*, 56(19), 2653–2663. <https://doi.org/10.1021/acs.accounts.3c00370>
- Albaret, G., Sifré, E., Floch, P., Laye, S., Aubert, A., Dubus, P., Azzi-Martin, L., Giese, A., Salles, N., Mégraud, F., Varon, C., Lehours, P., Roubaud-Baudron, C., & Singhrao, S. (2020). Alzheimer's Disease and Helicobacter pylori Infection: Inflammation from Stomach to Brain? *Journal of Alzheimer's Disease*, 73(2), 801–809. <https://doi.org/10.3233/JAD-190496>
- Álvarez-Marimon, E., Castillo-Michel, H., Reyes-Herrera, J., Seira, J., Aso, E., Carmona, M., Ferrer, I., Cladera, J., & Benseny-Cases, N. (2021). Synchrotron X-ray Fluorescence and FTIR Signatures for Amyloid Fibrillary and Nonfibrillary Plaques. *ACS Chemical Neuroscience*, 12(11), 1961–1971. <https://doi.org/10.1021/acscchemneuro.1c00048>
- Alzheimer's association. (2023). 2023 Alzheimer's disease facts and figures. *Alzheimer's and Dementia*, 19(4), 1598–1695. <https://doi.org/10.1002/alz.13016>
- Alzheimer's Impact Movement. (2016). *Costs of Alzheimer's to Medicare and Medicaid. March.*
- An, L., Fitzpatrick, D., & Harrison, P. M. (2016). Emergence and evolution of yeast prion and prion-like proteins. *BMC Evolutionary Biology*, 16(1), 1–13. <https://doi.org/10.1186/s12862-016-0594-3>
- Aubrey, L. D., & Radford, S. E. (2025). How is the Amyloid Fold Built? Polymorphism and the Microscopic Mechanisms of Fibril Assembly. In *Journal of Molecular Biology* (p. 169008). Academic Press. <https://doi.org/10.1016/j.jmb.2025.169008>
- Avila, J., Lucas, J. J., Pérez, M., & Hernández, F. (2004). Role of Tau Protein in Both Physiological and Pathological Conditions. In *Physiological Reviews* (Vol. 84, Issue 2, pp. 361–384). American Physiological Society. <https://doi.org/10.1152/physrev.00024.2003>
- Balbirnie, M., Grothe, R., & Eisenberg, D. S. (2001). An amyloid-forming peptide from the yeast prion Sup35 reveals a dehydrated β -sheet structure for amyloid. *Proceedings of the National Academy of Sciences of the United States of America*, 98(5), 2375–2380. <https://doi.org/10.1073/pnas.041617698>
- Banerjee, G., Farmer, S. F., Hyare, H., Jaunmuktane, Z., Mead, S., Ryan, N. S., Schott, J. M., Werring, D. J., Rudge, P., & Collinge, J. (2024). Iatrogenic Alzheimer's disease in recipients of cadaveric pituitary-derived growth hormone. *Nature Medicine*, 30(2), 394–402. <https://doi.org/10.1038/s41591-023-02729-2>
- Barnhart, M. M., & Chapman, M. R. (2006). Curli biogenesis and function. In *Annual Review of Microbiology* (Vol. 60, pp. 131–147). <https://doi.org/10.1146/annurev.micro.60.080805.142106>
- Bennecib, M., Gong, C. X., Grundke-Iqbal, I., & Iqbal, K. (2000). Role of protein phosphatase-2A and -1 in the regulation of GSK-3, cdk5 and cdc2 and the phosphorylation of tau in rat forebrain. *FEBS Letters*, 485(1), 87–93. [https://doi.org/10.1016/S0014-5793\(00\)02203-1](https://doi.org/10.1016/S0014-5793(00)02203-1)
- Benseny-Cases, N., Cócera, M., & Cladera, J. (2007). Conversion of non-fibrillar β -sheet oligomers into amyloid fibrils in Alzheimer's disease amyloid peptide aggregation. *Biochemical and Biophysical Research Communications*, 361(4), 916–921.

- <https://doi.org/10.1016/j.bbrc.2007.07.082>
- Benseny-Cases, N., Klementieva, O., Maly, J., & Cladera, J. (2012). Granular Non-Fibrillar Aggregates and Toxicity in Alzheimer's Disease. *Current Alzheimer Research*, 9(8), 962–971. <https://doi.org/10.2174/156720512803251129>
- Bhattacharjee, S., & Lukiw, W. J. (2013). Alzheimer's disease and the microbiome. *Frontiers in Cellular Neuroscience*, 7(SEP). <https://doi.org/10.3389/fncel.2013.00153>
- Bhoite, S., van Gerven, N., Chapman, M. R., & Remaut, H. (2019). Curli Biogenesis: Bacterial Amyloid Assembly by the Type VIII Secretion Pathway. *EcoSal Plus*, 8(2), 10.1128/ecosalplus.ESP-0037–2018. <https://doi.org/10.1128/ecosalplus.esp-0037-2018>
- Binetti, G., Magni, E., Cappa, S. F., Padovani, A., Bianchetti, A., & Trabucchi, M. (1998). Visual and spatial perception in the early phase of Alzheimer's disease. *Neuropsychology*, 12(1), 29–33. <https://doi.org/10.1037/0894-4105.12.1.29>
- Blanco, L. P., Evans, M. L., Smith, D. R., Badtke, M. P., & Chapman, M. R. (2012). Diversity, biogenesis and function of microbial amyloids. In *Trends in Microbiology* (Vol. 20, Issue 2, pp. 66–73). Trends Microbiol. <https://doi.org/10.1016/j.tim.2011.11.005>
- Butler, L., & Walker, K. A. (2021). The Role of Chronic Infection in Alzheimer's Disease: Instigators, Co-conspirators, or Bystanders? In *Current Clinical Microbiology Reports* (Vol. 8, Issue 4, pp. 199–212). Springer Science and Business Media Deutschland GmbH. <https://doi.org/10.1007/s40588-021-00168-6>
- Cecchi, C., & Stefani, M. (2013). The amyloid-cell membrane system. The interplay between the biophysical features of oligomers/fibrils and cell membrane defines amyloid toxicity. *Biophysical Chemistry*, 182, 30–43. <https://doi.org/10.1016/j.bpc.2013.06.003>
- Chen, S. G., Stribinskis, V., Rane, M. J., Demuth, D. R., Gozal, E., Roberts, A. M., Jagadapillai, R., Liu, R., Choe, K., Shivakumar, B., Son, F., Jin, S., Kerber, R., Adame, A., Masliah, E., & Friedland, R. P. (2016). Exposure to the Functional Bacterial Amyloid Protein Curli Enhances Alpha-Synuclein Aggregation in Aged Fischer 344 Rats and *Caenorhabditis elegans*. *Scientific Reports*, 6. <https://doi.org/10.1038/srep34477>
- Chiti, F., & Dobson, C. M. (2006). Protein misfolding, functional amyloid, and human disease. In *Annual Review of Biochemistry* (Vol. 75, pp. 333–366). Annu Rev Biochem. <https://doi.org/10.1146/annurev.biochem.75.101304.123901>
- Chung, C. W., Stephens, A. D., Konno, T., Ward, E., Avezov, E., Kaminski, C. F., Hassanali, A. A., & Kaminski Schierle, G. S. (2022). Intracellular A β 42 Aggregation Leads to Cellular Thermogenesis. *Journal of the American Chemical Society*, 144(22), 10034–10041. <https://doi.org/10.1021/jacs.2c03599>
- Clark, C. M., & Karlawish, J. H. T. (2003). Alzheimer disease: Current concepts and emerging diagnostic and therapeutic strategies. In *Annals of Internal Medicine* (Vol. 138, Issue 5, pp. 400–410). American College of Physicians. <https://doi.org/10.7326/0003-4819-138-5-200303040-00010>
- Cohen, M., Appleby, B., & Safar, J. G. (2016). Distinct prion-like strains of amyloid beta implicated in phenotypic diversity of Alzheimer's disease. In *Prion* (Vol. 10, Issue 1, pp. 9–17). Taylor and Francis Inc. <https://doi.org/10.1080/19336896.2015.1123371>
- Conchillo-Solé, O., de Groot, N. S., Avilés, F. X., Vendrell, J., Daura, X., & Ventura, S. (2007). AGGRESCAN: A server for the prediction and evaluation of “hot spots” of aggregation in polypeptides. *BMC Bioinformatics*, 8, 65. <https://doi.org/10.1186/1471-2105-8-65>
- Coronel, R., Bernabeu-Zornoza, A., Palmer, C., Muñoz-Moreno, M., Zambrano, A., Cano, E., & Liste, I. (2018). Role of Amyloid Precursor Protein (APP) and Its Derivatives in the Biology and Cell Fate Specification of Neural Stem Cells. In *Molecular Neurobiology*

- (Vol. 55, Issue 9, pp. 7107–7117). Humana Press Inc. <https://doi.org/10.1007/s12035-018-0914-2>
- Coureuil, M., Lécuyer, H., Bourdoulous, S., & Nassif, X. (2017). A journey into the brain: Insight into how bacterial pathogens cross blood-brain barriers. In *Nature Reviews Microbiology* (Vol. 15, Issue 3, pp. 149–159). Nature Publishing Group. <https://doi.org/10.1038/nrmicro.2016.178>
- De Groot, N. S., Pallarés, I., Avilés, F. X., Vendrell, J., & Ventura, S. (2005). Prediction of “hot spots” of aggregation in disease-linked polypeptides. *BMC Structural Biology*, 5(1), 1–15. <https://doi.org/10.1186/1472-6807-5-18>
- De La Torre, J. C. (2010). The vascular hypothesis of Alzheimer’s disease: Bench to bedside and beyond. *Neurodegenerative Diseases*, 7(1–3), 116–121. <https://doi.org/10.1159/000285520>
- Decker, Y., Németh, E., Schomburg, R., Chemla, A., Fülöp, L., Menger, M. D., Liu, Y., & Fassbender, K. (2021). Decreased pH in the aging brain and Alzheimer’s disease. *Neurobiology of Aging*, 101, 40–49. <https://doi.org/10.1016/j.neurobiolaging.2020.12.007>
- Di Domizio, J., Dorta-Estremera, S., Gagea, M., Ganguly, D., Meller, S., Li, P., Zhao, B., Tan, F. K., Bi, L., Gilliet, M., & Cao, W. (2012). Nucleic acid-containing amyloid fibrils potently induce type I interferon and stimulate systemic autoimmunity. *Proceedings of the National Academy of Sciences of the United States of America*, 109(36), 14550–14555. <https://doi.org/10.1073/pnas.1206923109>
- Dill, K. A., Ozkan, S. B., Shell, M. S., & Weikl, T. R. (2008). The protein folding problem. In *Annual Review of Biophysics* (Vol. 37, pp. 289–316). <https://doi.org/10.1146/annurev.biophys.37.092707.153558>
- Dorszewska, J., Prendecki, M., Oczkowska, A., Dezor, M., & Kozubski, W. (2016). Molecular Basis of Familial and Sporadic Alzheimer’s Disease. *Current Alzheimer Research*, 13(9), 952–963. <https://doi.org/10.2174/1567205013666160314150501>
- Dua P, Z. Y. (2015). Microbial Sources of Amyloid and Relevance to Amyloidogenesis and Alzheimer’s Disease (AD). *Journal of Alzheimer’s Disease & Parkinsonism*, 05(01). <https://doi.org/10.4172/2161-0460.1000177>
- Dueholm, M. S., Petersen, S. V., Sønderkær, M., Larsen, P., Christiansen, G., Hein, K. L., Enghild, J. J., Nielsen, J. L., Nielsen, K. L., Nielsen, P. H., & Otzen, D. E. (2010). Functional amyloid in pseudomonas. *Molecular Microbiology*, 77(4), 1009–1020. <https://doi.org/10.1111/j.1365-2958.2010.07269.x>
- Duyckaerts, C., Delatour, B., & Potier, M. C. (2009). Classification and basic pathology of Alzheimer disease. In *Acta Neuropathologica* (Vol. 118, Issue 1, pp. 5–36). Acta Neuropathol. <https://doi.org/10.1007/s00401-009-0532-1>
- Emery, D. C., Shoemark, D. K., Batstone, T. E., Waterfall, C. M., Coghill, J. A., Cerajewska, T. L., Davies, M., West, N. X., & Allen, S. J. (2017). 16S rRNA next generation sequencing analysis shows bacteria in Alzheimer’s Post-Mortem Brain. *Frontiers in Aging Neuroscience*, 9(JUN), 261413. <https://doi.org/10.3389/fnagi.2017.00195>
- Espargaró, A., Busquets, M. A., Estelrich, J., & Sabate, R. (2015). Predicting the aggregation propensity of prion sequences. *Virus Research*, 207, 127–135. <https://doi.org/10.1016/j.virusres.2015.03.001>
- Esteras-Chopo, A., Serrano, L., & López De La Paz, M. (2005). The amyloid stretch hypothesis: Recruiting proteins toward the dark side. *Proceedings of the National Academy of Sciences of the United States of America*, 102(46), 16672–16677.

- <https://doi.org/10.1073/pnas.0505905102>
- Evans, M. L., Chorell, E., Taylor, J. D., Åden, J., Göthesson, A., Li, F., Koch, M., Sefer, L., Matthews, S. J., Wittung-Stafshede, P., Almquist, F., & Chapman, M. R. (2015). The bacterial curli system possesses a potent and selective inhibitor of amyloid formation. *Molecular Cell*, 57(3), 445–455. <https://doi.org/10.1016/j.molcel.2014.12.025>
- Fernández-Calvet, A., Matilla-Cuenca, L., Izco, M., Navarro, S., Serrano, M., Ventura, S., Blesa, J., Herráiz, M., Alkorta-Aranburu, G., Galera, S., Ruiz de los Mozos, I., Mansego, M. L., Toledo-Arana, A., Alvarez-Erviti, L., & Valle, J. (2024). Gut microbiota produces biofilm-associated amyloids with potential for neurodegeneration. *Nature Communications*, 15(1), 1–19. <https://doi.org/10.1038/s41467-024-48309-x>
- Fitzpatrick, A. W. P., Debelouchina, G. T., Bayro, M. J., Clare, D. K., Caporini, M. A., Bajaj, V. S., Jaroniec, C. P., Wang, L., Ladizhansky, V., Müller, S. A., MacPhee, C. E., Waudby, C. A., Mott, H. R., De Simone, A., Knowles, T. P. J., Saibil, H. R., Vendruscolo, M., Orlova, E. V., Griffin, R. G., & Dobson, C. M. (2013). Atomic structure and hierarchical assembly of a cross- β amyloid fibril. *Proceedings of the National Academy of Sciences of the United States of America*, 110(14), 5468–5473. <https://doi.org/10.1073/pnas.1219476110>
- Friedland, R. P., & Chapman, M. R. (2017). The role of microbial amyloid in neurodegeneration. In *PLoS Pathogens* (Vol. 13, Issue 12). Public Library of Science. <https://doi.org/10.1371/journal.ppat.1006654>
- Fukutani, Y., Kobayashi, K., Nakamura, I., Watanabe, K., Isaki, K., & Cairns, N. J. (1995). Neurons, intracellular and extracellular neurofibrillary tangles in subdivisions of the hippocampal cortex in normal ageing and Alzheimer's disease. *Neuroscience Letters*, 200(1), 57–60. [https://doi.org/10.1016/0304-3940\(95\)12083-G](https://doi.org/10.1016/0304-3940(95)12083-G)
- Furcila, D., Domínguez-Álvaro, M., DeFelipe, J., & Alonso-Nanclares, L. (2019). Subregional Density of Neurons, Neurofibrillary Tangles and Amyloid Plaques in the Hippocampus of Patients With Alzheimer's Disease. *Frontiers in Neuroanatomy*, 13, 477671. <https://doi.org/10.3389/fnana.2019.00099>
- Gebbink, M. F. B. G., Claessen, D., Bouma, B., Dijkhuizen, L., & Wösten, H. A. B. (2005). Amyloids - A functional coat for microorganisms. In *Nature Reviews Microbiology* (Vol. 3, Issue 4, pp. 333–341). Nat Rev Microbiol. <https://doi.org/10.1038/nrmicro1127>
- Ghag, G., Bhatt, N., Cantu, D. V., Guerrero-Munoz, M. J., Ellsworth, A., Sengupta, U., & Kaye, R. (2018). Soluble tau aggregates, not large fibrils, are the toxic species that display seeding and cross-seeding behavior. *Protein Science*, 27(11), 1901–1909. <https://doi.org/10.1002/pro.3499>
- Gilbert, M. A. G., Fatima, N., Jenkins, J., O'Sullivan, T. J., Schertel, A., Halfon, Y., Wilkinson, M., Morrema, T. H. J., Geibel, M., Read, R. J., Ranson, N. A., Radford, S. E., Hoozemans, J. J. M., & Frank, R. A. W. (2024). CryoET of β -amyloid and tau within postmortem Alzheimer's disease brain. *Nature*, 631(8022), 913–919. <https://doi.org/10.1038/s41586-024-07680-x>
- Giraldo, R. (2024). The emergence of bacterial prions. *PLoS Pathogens*, 20(6 June), e1012253. <https://doi.org/10.1371/journal.ppat.1012253>
- Grabher, B. J. (2018). Effects of Alzheimer disease on patients and their family. *Journal of Nuclear Medicine Technology*, 46(4), 335–340. <https://doi.org/10.2967/jnmt.118.218057>
- Guo, T., Noble, W., & Hanger, D. P. (2017). Roles of tau protein in health and disease. In *Acta Neuropathologica* (Vol. 133, Issue 5, pp. 665–704). Springer. <https://doi.org/10.1007/s00401-017-1707-9>

- Ha, C., Ryu, J., & Chan, B. P. (2007). Metal ions differentially influence the aggregation and deposition of Alzheimer's β -amyloid on a solid template. *Biochemistry*, 46(20), 6118–6125. <https://doi.org/10.1021/bi7000032>
- Han, Y., Wang, B., Gao, H., He, C., Hua, R., Liang, C., Zhang, S., Wang, Y., Xin, S., & Xu, J. (2022). Vagus Nerve and Underlying Impact on the Gut Microbiota-Brain Axis in Behavior and Neurodegenerative Diseases. In *Journal of Inflammation Research* (Vol. 15, pp. 6213–6230). Dove Medical Press Ltd. <https://doi.org/10.2147/JIR.S384949>
- Harach, T., Marungruang, N., Duthilleul, N., Cheatham, V., Mc Coy, K. D., Frisoni, G., Neher, J. J., Fåk, F., Jucker, M., Lasser, T., & Bolmont, T. (2017). Reduction of Abeta amyloid pathology in APPPS1 transgenic mice in the absence of gut microbiota. *Scientific Reports*, 7, 41802. <https://doi.org/10.1038/srep41802>
- Harrison, P. M. (2019). Evolutionary behaviour of bacterial prion-like proteins. *PLoS ONE*, 14(3). <https://doi.org/10.1371/journal.pone.0213030>
- Hatami, A., Monjazebe, S., Milton, S., & Glabe, C. G. (2017). Familial Alzheimer's disease mutations within the amyloid precursor protein alter the aggregation and conformation of the amyloid- β peptide. *Journal of Biological Chemistry*, 292(8), 3172–3185. <https://doi.org/10.1074/jbc.M116.755264>
- Hatters, D. M., Peters-Libeu, C. A., & Weisgraber, K. H. (2006). Apolipoprotein E structure: insights into function. In *Trends in Biochemical Sciences* (Vol. 31, Issue 8, pp. 445–454). Elsevier. <https://doi.org/10.1016/j.tibs.2006.06.008>
- Hill-Burns, E. M., Debelius, J. W., Morton, J. T., Wissemann, W. T., Lewis, M. R., Wallen, Z. D., Peddada, S. D., Factor, S. A., Molho, E., Zabetian, C. P., Knight, R., & Payami, H. (2017). Parkinson's disease and Parkinson's disease medications have distinct signatures of the gut microbiome. *Movement Disorders*, 32(5), 739–749. <https://doi.org/10.1002/mds.26942>
- Hill, J. M., Clement, C., Pogue, A. I., Bhattacharjee, S., Zhao, Y., & Lukiw, W. J. (2014). Pathogenic microbes, the microbiome, and Alzheimer's disease (AD). *Frontiers in Aging Neuroscience*, 6(JUN), 127. <https://doi.org/10.3389/fnagi.2014.00127>
- Hill, J. M., & Lukiw, W. (2015). Microbial-generated amyloids and Alzheimer's disease (AD). *Frontiers in Aging Neuroscience*, 7(JAN). <https://doi.org/10.3389/fnagi.2015.00009>
- Hoesen, G. W. V., & Hyman, B. T. (1990). Hippocampal formation: Anatomy and the patterns of pathology in Alzheimer's disease. *Progress in Brain Research*, 83(C), 445–457. [https://doi.org/10.1016/S0079-6123\(08\)61268-6](https://doi.org/10.1016/S0079-6123(08)61268-6)
- Huang, W. J., Zhang, X., & Chen, W. W. (2016). Role of oxidative stress in Alzheimer's disease (review). In *Biomedical Reports* (Vol. 4, Issue 5, pp. 519–522). Spandidos Publications. <https://doi.org/10.3892/br.2016.630>
- Iglesias, V., de Groot, N. S., & Ventura, S. (2015). Computational analysis of candidate prion-like proteins in bacteria and their role. *Frontiers in Microbiology*, 6(OCT), 1123. <https://doi.org/10.3389/fmicb.2015.01123>
- Jain, N. (2024). The molecular interplay between human and bacterial amyloids: Implications in neurodegenerative diseases. In *Biochimica et Biophysica Acta - Proteins and Proteomics* (Vol. 1872, Issue 4, p. 141018). Elsevier. <https://doi.org/10.1016/j.bbapap.2024.141018>
- Jaqua, E. E., Tran, M.-L. N., & Hanna, M. (2024). Alzheimer Disease: Treatment of Cognitive and Functional Symptoms. *American Family Physician*, 110(3), 281–293. <https://www.aafp.org/pubs/afp/issues/2024/0900/alzheimer-disease.html>
- Javed, I., Zhang, Z., Adamcik, J., Andrikopoulos, N., Li, Y., Otzen, D. E., Lin, S., Mezzenga, R.,

- Davis, T. P., Ding, F., & Ke, P. C. (2020). Accelerated Amyloid Beta Pathogenesis by Bacterial Amyloid FapC. *Advanced Science*, 7(18).
<https://doi.org/10.1002/advs.202001299>
- Kalaria, R. N. (2000). The role of cerebral ischemia in Alzheimer's disease. *Neurobiology of Aging*, 21(2), 321–330. [https://doi.org/10.1016/S0197-4580\(00\)00125-1](https://doi.org/10.1016/S0197-4580(00)00125-1)
- Karran, E., Mercken, M., & Strooper, B. De. (2011). The amyloid cascade hypothesis for Alzheimer's disease: An appraisal for the development of therapeutics. In *Nature Reviews Drug Discovery* (Vol. 10, Issue 9, pp. 698–712). Nature Publishing Group.
<https://doi.org/10.1038/nrd3505>
- Kasarello, K., Cudnoch-Jedrzejewska, A., & Czarzasta, K. (2023). Communication of gut microbiota and brain via immune and neuroendocrine signaling. In *Frontiers in Microbiology* (Vol. 14, p. 1118529). Frontiers Media S.A.
<https://doi.org/10.3389/fmicb.2023.1118529>
- Kim, K. S. (2001). Escherichia coli translocation at the blood-brain barrier. In *Infection and Immunity* (Vol. 69, Issue 9, pp. 5217–5222). American Society for Microbiology.
<https://doi.org/10.1128/IAI.69.9.5217-5222.2001>
- Kim, S., Kwon, S. H., Kam, T. I., Panicker, N., Karuppagounder, S. S., Lee, S., Lee, J. H., Kim, W. R., Kook, M., Foss, C. A., Shen, C., Lee, H., Kulkarni, S., Pasricha, P. J., Lee, G., Pomper, M. G., Dawson, V. L., Dawson, T. M., & Ko, H. S. (2019). Transneuronal Propagation of Pathologic α -Synuclein from the Gut to the Brain Models Parkinson's Disease. *Neuron*, 103(4), 627–641.e7. <https://doi.org/10.1016/j.neuron.2019.05.035>
- Knopman, D. S., Amieva, H., Petersen, R. C., Ch  telat, G., Holtzman, D. M., Hyman, B. T., Nixon, R. A., & Jones, D. T. (2021). Alzheimer disease. *Nature Reviews Disease Primers*, 7(1), 1–21. <https://doi.org/10.1038/s41572-021-00269-y>
- Kountouras, J., Tsolaki, M., Gavalas, E., Boziki, M., Zavos, C., Karatzoglou, P., Chatzopoulos, D., & Venizelos, I. (2006). Relationship between Helicobacter pylori infection and Alzheimer disease. *Neurology*, 66(6), 938–940.
<https://doi.org/10.1212/01.wnl.0000203644.68059.5f>
- Krishnan, R., & Lindquist, S. L. (2005). Structural insights into a yeast prion illuminate nucleation and strain diversity. *Nature*, 435(7043), 765–772.
<https://doi.org/10.1038/nature03679>
- Kushnirov, V. V., Kochneva-Pervukhova, N. V., Chechenova, M. B., Frolova, N. S., & Ter-Avanesyan, M. D. (2000). Prion properties of the Sup35 protein of yeast Pichia methanolica. *EMBO Journal*, 19(3), 324–331. <https://doi.org/10.1093/emboj/19.3.324>
- Kwon, D., Zhang, K., Paul, K. C., Folle, A. D., Del Rosario, I., Jacobs, J. P., Keener, A. M., Bronstein, J. M., & Ritz, B. (2024). Diet and the gut microbiome in patients with Parkinson's disease. *Npj Parkinson's Disease*, 10(1), 1–9.
<https://doi.org/10.1038/s41531-024-00681-7>
- Larsen, P., Nielsen, J. L., Dueholm, M. S., Wetzell, R., Otzen, D., & Nielsen, P. H. (2007). Amyloid adhesins are abundant in natural biofilms. *Environmental Microbiology*, 9(12), 3077–3090. <https://doi.org/10.1111/j.1462-2920.2007.01418.x>
- Larsen, P., Nielsen, J. L., Otzen, D., & Nielsen, P. H. (2008). Amyloid-like adhesins produced by floc-forming and filamentous bacteria in activated sludge. *Applied and Environmental Microbiology*, 74(5), 1517–1526. <https://doi.org/10.1128/AEM.02274-07>
- Lee, J. H., Yang, D. S., Goulbourne, C. N., Im, E., Stavrides, P., Pensalfini, A., Chan, H., Bouchet-Marquis, C., Bleiwas, C., Berg, M. J., Huo, C., Peddy, J., Pawlik, M., Levy, E.,

- Rao, M., Staufenbiel, M., & Nixon, R. A. (2022). Faulty autolysosome acidification in Alzheimer's disease mouse models induces autophagic build-up of A β in neurons, yielding senile plaques. *Nature Neuroscience*, 25(6), 688–701. <https://doi.org/10.1038/s41593-022-01084-8>
- Li, B., Chohan, M. O., Grundke-Iqbal, I., & Iqbal, K. (2007). Disruption of microtubule network by Alzheimer abnormally hyperphosphorylated tau. *Acta Neuropathologica*, 113(5), 501–511. <https://doi.org/10.1007/s00401-007-0207-8>
- Li, D., & Liu, C. (2022). Conformational strains of pathogenic amyloid proteins in neurodegenerative diseases. In *Nature Reviews Neuroscience* (Vol. 23, Issue 9, pp. 523–534). Nature Publishing Group. <https://doi.org/10.1038/s41583-022-00603-7>
- Li, X., Ospitalieri, S., Robberechts, T., Hofmann, L., Schmid, C., Rijal Upadhaya, A., Koper, M. J., Von Arnim, C. A. F., Kumar, S., Willem, M., Gnoth, K., Ramakers, M., Schymkowitz, J., Rousseau, F., Walter, J., Ronisz, A., Balakrishnan, K., & Thal, D. R. (2022). Seeding, maturation and propagation of amyloid β -peptide aggregates in Alzheimer's disease. *Brain*, 145(10), 3558–3570. <https://doi.org/10.1093/brain/awac202>
- Liu, H., Liu, H., Liu, C., Shang, M., Wei, T., & Yin, P. (2022). Gut Microbiome and the Role of Metabolites in the Study of Graves' Disease. In *Frontiers in Molecular Biosciences* (Vol. 9). Frontiers Media S.A. <https://doi.org/10.3389/fmolb.2022.841223>
- Loh, J. S., Mak, W. Q., Tan, L. K. S., Ng, C. X., Chan, H. H., Yeow, S. H., Foo, J. B., Ong, Y. S., How, C. W., & Khaw, K. Y. (2024). Microbiota–gut–brain axis and its therapeutic applications in neurodegenerative diseases. In *Signal Transduction and Targeted Therapy* (Vol. 9, Issue 1, pp. 1–53). Nature Publishing Group. <https://doi.org/10.1038/s41392-024-01743-1>
- López De La Paz, M., & Serrano, L. (2004). Sequence determinants of amyloid fibril formation. *Proceedings of the National Academy of Sciences of the United States of America*, 101(1), 87–92. <https://doi.org/10.1073/pnas.2634884100>
- Lundmark, K., Westermark, G. T., Olsén, A., & Westermark, P. (2005). Protein fibrils in nature can enhance amyloid protein A amyloidosis in mice: Cross-seeding as a disease mechanism. *Proceedings of the National Academy of Sciences of the United States of America*, 102(17), 6098–6102. <https://doi.org/10.1073/pnas.0501814102>
- Makowski, L. (2020). The Structural Basis of Amyloid Strains in Alzheimer's Disease. In *ACS Biomaterials Science and Engineering* (Vol. 6, Issue 5, pp. 2498–2505). American Chemical Society. <https://doi.org/10.1021/acsbiomaterials.9b01302>
- Manivannan, Y., Manivannan, B., Beach, T. G., & Halden, R. U. (2015). Role of Environmental Contaminants in the Etiology of Alzheimer's Disease: A Review. *Current Alzheimer Research*, 12(2), 116. <https://doi.org/10.2174/1567205012666150204121719>
- Marshall, K. E., Marchante, R., Xue, W. F., & Serpell, L. C. (2014). The relationship between amyloid structure and cytotoxicity. *Prion*, 8(2), 192–196. <https://doi.org/10.4161/pri.28860>
- Meisl, G., Kirkegaard, J. B., Arosio, P., Michaels, T. C. T., Vendruscolo, M., Dobson, C. M., Linse, S., & Knowles, T. P. J. (2016). Molecular mechanisms of protein aggregation from global fitting of kinetic models. *Nature Protocols*, 11(2), 252–272. <https://doi.org/10.1038/nprot.2016.010>
- Meisl, G., Yang, X., Dobson, C. M., Linse, S., & Knowles, T. P. J. (2017). Modulation of electrostatic interactions to reveal a reaction network unifying the aggregation behaviour of the A β 42 peptide and its variants. *Chemical Science*, 8(6), 4352–4362. <https://doi.org/10.1039/c7sc00215g>

- Meng, L., Liu, C., Li, Y., Chen, G., Xiong, M., Yu, T., Pan, L., Zhang, X., Zhou, L., Guo, T., Yuan, X., Liu, C., Zhang, Z., & Zhang, Z. (2023). The yeast prion protein Sup35 initiates α -synuclein pathology in mouse models of Parkinson's disease. *Science Advances*, 9(44). <https://doi.org/10.1126/SCIADV.ADJ1092>
- Miller, A. L., Bessho, S., Grando, K., & Tükel, Ç. (2021). Microbiome or Infections: Amyloid-Containing Biofilms as a Trigger for Complex Human Diseases. In *Frontiers in Immunology* (Vol. 12, p. 638867). Frontiers Media S.A. <https://doi.org/10.3389/fimmu.2021.638867>
- Mishan, M. A., Kanavi, M. R., Shahpasand, K., & Ahmadi, H. (2019). Pathogenic Tau Protein Species: Promising Therapeutic Targets for Ocular Neurodegenerative Diseases. *Journal of Ophthalmic & Vision Research*, 14(4), 491. <https://doi.org/10.18502/JOVR.V14I4.5459>
- Monsellier, E., Ramazzotti, M., Taddei, N., & Chiti, F. (2008). Aggregation propensity of the human proteome. *PLoS Computational Biology*, 4(10), e1000199. <https://doi.org/10.1371/journal.pcbi.1000199>
- Mrdenovic, D., Pieta, I. S., Nowakowski, R., Kutner, W., Lipkowski, J., & Pieta, P. (2022). Amyloid β interaction with model cell membranes – What are the toxicity-defining properties of amyloid β ? In *International Journal of Biological Macromolecules* (Vol. 200, pp. 520–531). Elsevier. <https://doi.org/10.1016/j.ijbiomac.2022.01.117>
- Muñoz, S. S., Garner, B., & Ooi, L. (2019). Understanding the Role of ApoE Fragments in Alzheimer's Disease. *Neurochemical Research*, 44(6), 1297–1305. <https://doi.org/10.1007/s11064-018-2629-1>
- Murphy, M. P., & Levine, H. (2010). Alzheimer's disease and the amyloid- β peptide. In *Journal of Alzheimer's Disease* (Vol. 19, Issue 1, pp. 311–323). IOS Press. <https://doi.org/10.3233/JAD-2010-1221>
- Nelson, R., Sawaya, M. R., Balbirnie, M., Madsen, A., Riekel, C., Grothe, R., & Eisenberg, D. (2005). Structure of the cross- β spine of amyloid-like fibrils. *Nature*, 435(7043), 773–778. <https://doi.org/10.1038/nature03680>
- Nichols, E., Steinmetz, J. D., Vollset, S. E., Fukutaki, K., Chalek, J., Abd-Allah, F., Abdoli, A., Abualhasan, A., Abu-Gharbieh, E., Akram, T. T., Al Hamad, H., Alahdab, F., Alanezi, F. M., Alipour, V., Almustanyir, S., Amu, H., Ansari, I., Arabloo, J., Ashraf, T., ... Vos, T. (2022). Estimation of the global prevalence of dementia in 2019 and forecasted prevalence in 2050: an analysis for the Global Burden of Disease Study 2019. *The Lancet Public Health*, 7(2), e105–e125. [https://doi.org/10.1016/S2468-2667\(21\)00249-8](https://doi.org/10.1016/S2468-2667(21)00249-8)
- NIH. (2009). NIH Human Microbiome Project. *Microbe Magazine*, 4(9), 393–393. <https://doi.org/10.1128/microbe.4.393.1>
- Noori, M., Mahboobi, R., Nabavi-Rad, A., Jamshidizadeh, S., Fakharian, F., Yadegar, A., & Zali, M. R. (2023). Helicobacter pylori infection contributes to the expression of Alzheimer's disease-associated risk factors and neuroinflammation. *Heliyon*, 9(9), e19607. <https://doi.org/10.1016/j.heliyon.2023.e19607>
- Novo, M., Freire, S., & Al-Soufi, W. (2018). Critical aggregation concentration for the formation of early Amyloid- β (1-42) oligomers. *Scientific Reports*, 8(1), 1–8. <https://doi.org/10.1038/s41598-018-19961-3>
- O'Brien, R. J., & Wong, P. C. (2011). Amyloid precursor protein processing and Alzheimer's disease. *Annual Review of Neuroscience*, 34, 185–204. <https://doi.org/10.1146/annurev-neuro-061010-113613>

- Olsson, T. T., Klementieva, O., & Gouras, G. K. (2018). Prion-like seeding and nucleation of intracellular amyloid- β . *Neurobiology of Disease*, 113, 1–10. <https://doi.org/10.1016/j.nbd.2018.01.015>
- Pérez-Grijalba, V., Romero, J., Pesini, P., Sarasa, L., Monleón, I., San-José, I., Arbizu, J., Martínez-Lage, P., Munuera, J., Ruiz, A., Tárraga, L., Boada, M., & Sarasa, M. (2019). Plasma A β 42/40 Ratio Detects Early Stages of Alzheimer's Disease and Correlates with CSF and Neuroimaging Biomarkers in the AB255 Study. *The Journal of Prevention of Alzheimer's Disease*, 6(1), 34–41. <https://doi.org/10.14283/jpad.2018.41>
- Peterson, C. T. (2020). Dysfunction of the Microbiota-Gut-Brain Axis in Neurodegenerative Disease: The Promise of Therapeutic Modulation With Prebiotics, Medicinal Herbs, Probiotics, and Synbiotics. In *Journal of Evidence-Based Integrative Medicine* (Vol. 25, p. 2515690X20957225). SAGE Publications Ltd. <https://doi.org/10.1177/2515690X20957225>
- Piaceri, I., Nacmias, B., & Sorbi, S. (2013). Genetics of familial and sporadic Alzheimer's disease. *Frontiers in Bioscience - Elite*, 5 E(1), 167–177. <https://doi.org/10.2741/e605>
- Pisa, Di., Alonso, R., Fernández-Fernández, A. M., Rábano, A., & Carrasco, L. (2017). Polymicrobial Infections in Brain Tissue from Alzheimer's Disease Patients. *Scientific Reports*, 7(1), 1–14. <https://doi.org/10.1038/s41598-017-05903-y>
- Planas-Iglesias, J., Borko, S., Swiatkowski, J., Elias, M., Havlasek, M., Salamon, O., Grakova, E., Kunka, A., Martinovic, T., Damborsky, J., Martinovic, J., & Bednar, D. (2024). AggreProt: A web server for predicting and engineering aggregation prone regions in proteins. *Nucleic Acids Research*, 52(W1), W159–W169. <https://doi.org/10.1093/nar/gkae420>
- Prasad, H., & Rao, R. (2018). Amyloid clearance defect in ApoE4 astrocytes is reversed by epigenetic correction of endosomal pH. *Proceedings of the National Academy of Sciences of the United States of America*, 115(28), E6640–E6649. <https://doi.org/10.1073/pnas.1801612115>
- Qin, J., Li, R., Raes, J., Arumugam, M., Burgdorf, K. S., Manichanh, C., Nielsen, T., Pons, N., Levenez, F., Yamada, T., Mende, D. R., Li, J., Xu, J., Li, S., Li, D., Cao, J., Wang, B., Liang, H., Zheng, H., ... Zoetendal, E. (2010). A human gut microbial gene catalogue established by metagenomic sequencing. *Nature*, 464(7285), 59–65. <https://doi.org/10.1038/nature08821>
- Rahman, M. A., Rahman, M. S., Rahman, M. H., Rasheduzzaman, M., Mamun-Or-rashid, A. N. M., Uddin, M. J., Rahman, M. R., Hwang, H., Pang, M. G., & Rhim, H. (2020). Modulatory Effects of Autophagy on APP Processing as a Potential Treatment Target for Alzheimer's Disease. *Biomedicines* 2021, Vol. 9, Page 5, 9(1), 5. <https://doi.org/10.3390/BIMEDICINES9010005>
- Raskatov, J. A., & Teplow, D. B. (2017). Using chirality to probe the conformational dynamics and assembly of intrinsically disordered amyloid proteins. *Scientific Reports* 2017 7:1, 7(1), 1–7. <https://doi.org/10.1038/s41598-017-10525-5>
- Ren, B., Zhang, Y., Zhang, M., Liu, Y., Zhang, D., Gong, X., Feng, Z., Tang, J., Chang, Y., & Zheng, J. (2019). Fundamentals of cross-seeding of amyloid proteins: An introduction. In *Journal of Materials Chemistry B* (Vol. 7, Issue 46, pp. 7267–7282). The Royal Society of Chemistry. <https://doi.org/10.1039/c9tb01871a>
- Rios, A. M., Chen, C. W., Jacotot, E. D., & Troy, C. M. (2023). Caspase-2 Inhibition for Treatment of Alzheimer's Disease. *Alzheimer's & Dementia*, 19(S21), e077194. <https://doi.org/10.1002/alz.077194>

- Rissman, R. A., Poon, W. W., Blurton-Jones, M., Oddo, S., Torp, R., Vitek, M. P., LaFerla, F. M., Rohn, T. T., & Cotman, C. W. (2004). Caspase-cleavage of tau is an early event in Alzheimer disease tangle pathology. *Journal of Clinical Investigation*, 114(1), 121–130. <https://doi.org/10.1172/jci20640>
- Rousseau, F., Schymkowitz, J., & Serrano, L. (2006). Protein aggregation and amyloidosis: Confusion of the kinds? In *Current Opinion in Structural Biology* (Vol. 16, Issue 1, pp. 118–126). Elsevier Current Trends. <https://doi.org/10.1016/j.sbi.2006.01.011>
- Sabate, R., Rousseau, F., Schymkowitz, J., Batlle, C., & Ventura, S. (2015). Amyloids or prions? That is the question. *Prion*, 9(3), 200–206. <https://doi.org/10.1080/19336896.2015.1053685>
- Sampson, T. R., Debelius, J. W., Thron, T., Janssen, S., Shastri, G. G., Ilhan, Z. E., Challis, C., Schretter, C. E., Rocha, S., Gradinaru, V., Chesselet, M. F., Keshavarzian, A., Shannon, K. M., Krajmalnik-Brown, R., Wittung-Stafshede, P., Knight, R., & Mazmanian, S. K. (2016). Gut Microbiota Regulate Motor Deficits and Neuroinflammation in a Model of Parkinson's Disease. *Cell*, 167(6), 1469–1480.e12. <https://doi.org/10.1016/j.cell.2016.11.018>
- Scheffer, S., Hermkens, D. M. A., Van Der Weerd, L., De Vries, H. E., & Daemen, M. J. A. P. (2021). Vascular Hypothesis of Alzheimer Disease: Topical Review of Mouse Models. *Arteriosclerosis, Thrombosis, and Vascular Biology*, 41(4), 1265–1283. <https://doi.org/10.1161/ATVBAHA.120.311911>
- Sebastián-Serrano, Á., Diego-García, L. De, & Díaz-Hernández, M. (2018). The neurotoxic role of extracellular tau protein. In *International Journal of Molecular Sciences* (Vol. 19, Issue 4, p. 998). MDPI AG. <https://doi.org/10.3390/ijms19040998>
- Seira Curto, J., Fernandez, M. R., Cladera, J., Benseny-Cases, N., & Sanchez de Groot, N. (2023). Aβ40 Aggregation under Changeable Conditions. *International Journal of Molecular Sciences*, 24(9). <https://doi.org/10.3390/ijms24098408>
- Seira Curto, J., Hernandez, S. V., Fernandez, M. R., & Groot, N. S. de. (2025). Exogenous Amyloid Sequences: Their Role in Amyloid-Beta Heterotypic Aggregation. *BioRxiv*, 2025.01.24.634659. <https://doi.org/10.1101/2025.01.24.634659>
- Seira Curto, J., Surroca Lopez, A., Casals Sanchez, M., Tic, I., Fernandez Gallegos, M. R., & Sanchez de Groot, N. (2022). Microbiome Impact on Amyloidogenesis. In *Frontiers in Molecular Biosciences* (Vol. 9, p. 926702). Frontiers Media S.A. <https://doi.org/10.3389/fmolb.2022.926702>
- Self, W. K., & Holtzman, D. M. (2023). Emerging diagnostics and therapeutics for Alzheimer disease. In *Nature Medicine* (Vol. 29, Issue 9, pp. 2187–2199). Nature Publishing Group. <https://doi.org/10.1038/s41591-023-02505-2>
- Selkoe, D. J., & Hardy, J. (2016). The amyloid hypothesis of Alzheimer's disease at 25 years. *EMBO Molecular Medicine*, 8(6), 595–608. <https://doi.org/10.15252/emmm.201606210>
- Sengupta, U., Nilson, A. N., & Kaye, R. (2016). The Role of Amyloid-β Oligomers in Toxicity, Propagation, and Immunotherapy. In *EBioMedicine* (Vol. 6, pp. 42–49). Elsevier B.V. <https://doi.org/10.1016/j.ebiom.2016.03.035>
- Sgourakis, N. G., Yan, Y., McCallum, S. A., Wang, C., & Garcia, A. E. (2007). The Alzheimer's Peptides Aβ40 and 42 Adopt Distinct Conformations in Water: A Combined MD / NMR Study. *Journal of Molecular Biology*, 368(5), 1448–1457. <https://doi.org/10.1016/j.jmb.2007.02.093>
- Shahnawaz, M., & Soto, C. (2012). Microcin amyloid fibrils A are reservoir of toxic oligomeric

- species. *Journal of Biological Chemistry*, 287(15), 11665–11676.
<https://doi.org/10.1074/jbc.M111.282533>
- Shea, D., & Daggett, V. (2022). Amyloid- β Oligomers: Multiple Moving Targets. In *Biophysica* (Vol. 2, Issue 2, pp. 91–110). Multidisciplinary Digital Publishing Institute.
<https://doi.org/10.3390/biophysica2020010>
- Shemesh, O. A., & Spira, M. E. (2010). Hallmark cellular pathology of Alzheimer's disease induced by mutant human tau expression in cultured Aplysia neurons. *Acta Neuropathologica*, 120(2), 209–222. <https://doi.org/10.1007/s00401-010-0689-7>
- Sondag, C. M., Dhawan, G., & Combs, C. K. (2009). Beta amyloid oligomers and fibrils stimulate differential activation of primary microglia. *Journal of Neuroinflammation*, 6, 1. <https://doi.org/10.1186/1742-2094-6-1>
- Stefani, M. (2012). Structural features and cytotoxicity of amyloid oligomers: Implications in Alzheimer's disease and other diseases with amyloid deposits. In *Progress in Neurobiology* (Vol. 99, Issue 3, pp. 226–245).
<https://doi.org/10.1016/j.pneurobio.2012.03.002>
- Sultana, R., Perluigi, M., & Butterfield, D. A. (2009). Oxidatively modified proteins in Alzheimer's disease (AD), mild cognitive impairment and animal models of AD: Role of Abeta in pathogenesis. In *Acta Neuropathologica* (Vol. 118, Issue 1, pp. 131–150).
<https://doi.org/10.1007/s00401-009-0517-0>
- Sun, F., Chen, L., Wei, P., Chai, M., Ding, X., Xu, L., & Luo, S. Z. (2017). Dimerization and Structural Stability of Amyloid Precursor Proteins Affected by the Membrane Microenvironments. *Journal of Chemical Information and Modeling*, 57(6), 1375–1387.
<https://doi.org/10.1021/acs.jcim.7b00196>
- Suzuki, T., & Nakaya, T. (2008). Regulation of amyloid β -protein precursor by phosphorylation and protein interactions. In *Journal of Biological Chemistry* (Vol. 283, Issue 44, pp. 29633–29637). Elsevier. <https://doi.org/10.1074/jbc.R800003200>
- Tartaglia, G. G., & Vendruscolo, M. (2008). The Zyggregator method for predicting protein aggregation propensities. *Chemical Society Reviews*, 37(7), 1395–1401.
<https://doi.org/10.1039/b706784b>
- Vahdat Shariatpanahi, A. (2019). *The Importance of Macrophages, Lipid Membranes and Seeding in Experimental AA Amyloidosis*. 1687. <https://doi.org/10.3384/DISS.DIVA-159658>
- Viles, J. H. (2023). Imaging Amyloid- β Membrane Interactions: Ion-Channel Pores and Lipid-Bilayer Permeability in Alzheimer's Disease. In *Angewandte Chemie - International Edition* (Vol. 62, Issue 25, p. e202215785). John Wiley & Sons, Ltd.
<https://doi.org/10.1002/anie.202215785>
- Villarejo, L. G., Bachmann, L., Marks, D., Brachthäuser, M., Geidies, A., & Müller, T. (2022). Role of Intracellular Amyloid β as Pathway Modulator, Biomarker, and Therapy Target. In *International Journal of Molecular Sciences* (Vol. 23, Issue 9, p. 4656). MDPI.
<https://doi.org/10.3390/ijms23094656>
- Wei, J., Meisl, G., Dear, A. J., Michaels, T. C. T., & Knowles, T. P. J. (2025). Kinetics of Amyloid Oligomer Formation. *Annual Review of Biophysics*, 54(Volume 54, 2025), 185–207.
<https://doi.org/10.1146/ANNUREV-BIOPHYS-080124-122953>
- Wilkinson, M., Xu, Y., Thacker, D., Taylor, A. I. P., Fisher, D. G., Gallardo, R. U., Radford, S. E., & Ranson, N. A. (2023). Structural evolution of fibril polymorphs during amyloid assembly. *Cell*, 186(26), 5798–5811.e26. <https://doi.org/10.1016/J.CELL.2023.11.025>
- Willis, L. F., Brockwell, D. J., & Radford, S. E. (2025). In the flow, how fluid dynamics shapes

- amyloid formation. In *Proceedings of the National Academy of Sciences of the United States of America* (Vol. 122, Issue 16, p. e2504573122). National Academy of Sciences. <https://doi.org/10.1073/pnas.2504573122>
- Wiseman, F. K., Al-Janabi, T., Hardy, J., Karmiloff-Smith, A., Nizetic, D., Tybulewicz, V. L. J., Fisher, E. M. C., & Strydom, A. (2015). A genetic cause of Alzheimer disease: Mechanistic insights from Down syndrome. In *Nature Reviews Neuroscience* (Vol. 16, Issue 9, pp. 564–574). Nature Publishing Group. <https://doi.org/10.1038/nrn3983>
- Wisniewski, T., & Drummond, E. (2020). APOE-amyloid interaction: Therapeutic targets. In *Neurobiology of Disease* (Vol. 138, p. 104784). Academic Press. <https://doi.org/10.1016/j.nbd.2020.104784>
- Xue, C., Lin, T. Y., Chang, D., & Guo, Z. (2017). Thioflavin T as an amyloid dye: Fibril quantification, optimal concentration and effect on aggregation. *Royal Society Open Science*, 4(1). <https://doi.org/10.1098/rsos.160696>
- Yang, Y., Arseni, D., Zhang, W., Huang, M., Lövestam, S., Schweighauser, M., Kotecha, A., Murzin, A. G., Peak-Chew, S. Y., MacDonald, J., Lavenir, I., Garringer, H. J., Gelpi, E., Newell, K. L., Kovacs, G. G., Vidal, R., Ghetti, B., Ryskeldi-Falco, B., Scheres, S. H. W., & Goedert, M. (2022). Cryo-EM structures of amyloid-b 42 filaments from human brains. *Science*, 375(6577), 167–172. <https://doi.org/10.1126/science.abm7285>
- Yuan, A. H., & Hochschild, A. (2017). A bacterial global regulator forms a prion. *Science*, 355(6321), 198. <https://doi.org/10.1126/science.aai7776>
- Zhou, Y., Smith, D., Leong, B. J., Brännström, K., Almqvist, F., & Chapman, M. R. (2012). Promiscuous cross-seeding between bacterial amyloids promotes interspecies biofilms. *Journal of Biological Chemistry*, 287(42), 35092–35103. <https://doi.org/10.1074/jbc.M112.383737>

Appendix 1- Supplementary information of chapter 1

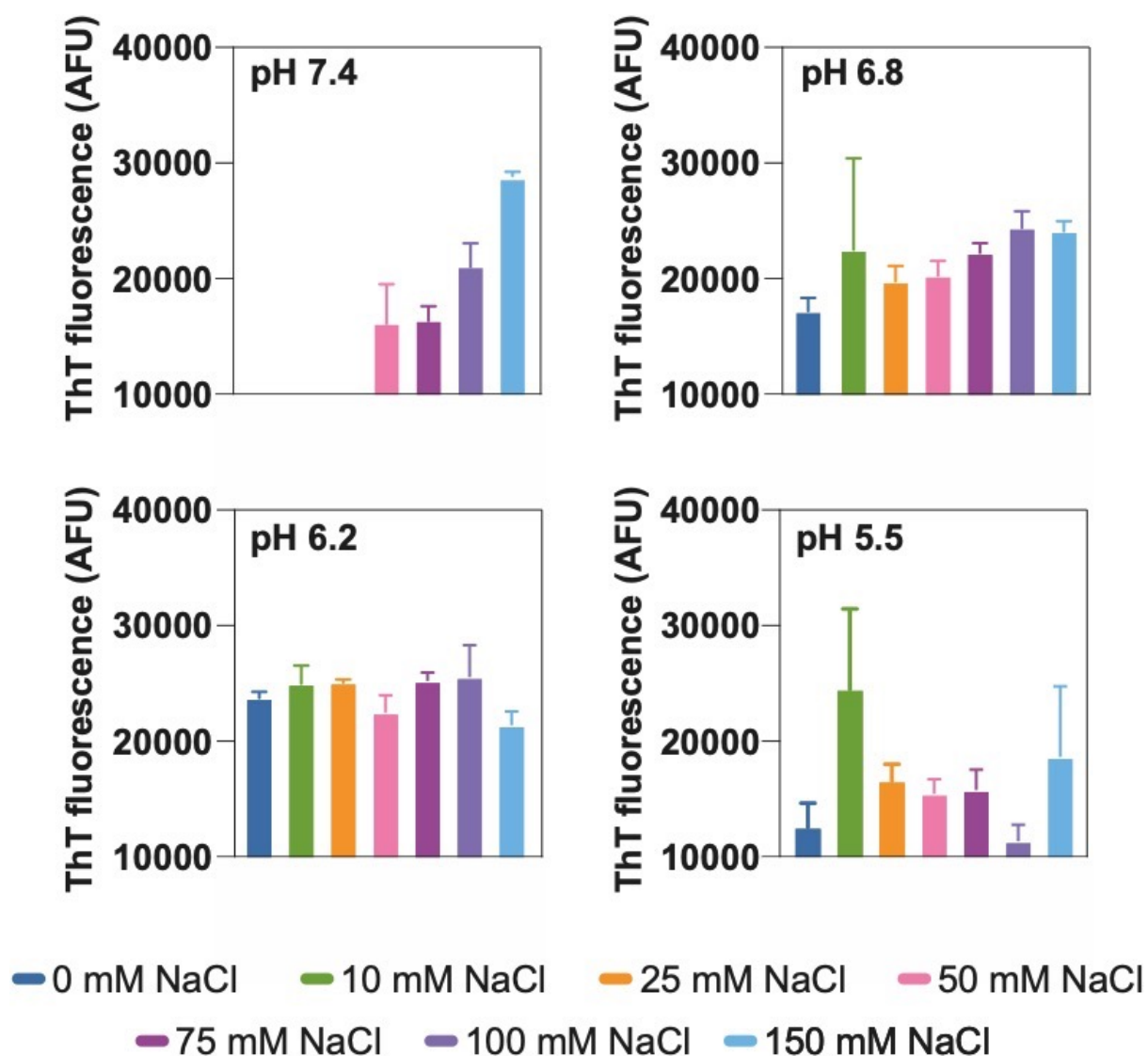


Figure S1. Plot showing the maximum Thioflavin-T signal of the kinetics presented in Figure 2 (panels A, B, C and D) against the NaCl concentration.

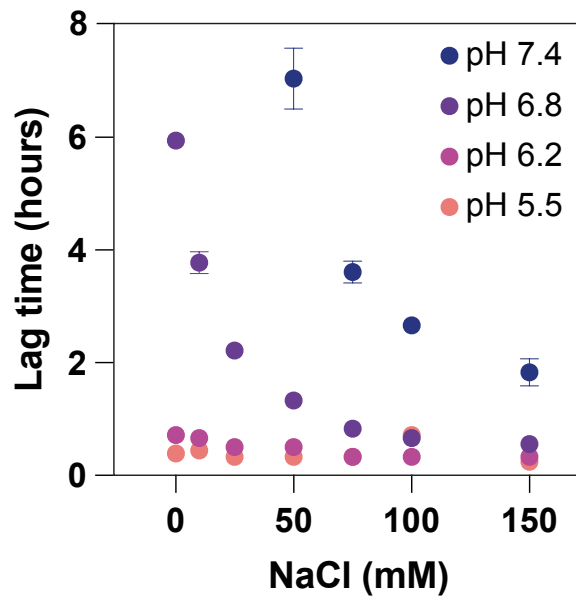


Figure S2. Plot showing the relationship between the lag-time of the kinetics presented in Figure 2 (panels A, B, C and D) against the NaCl concentration.

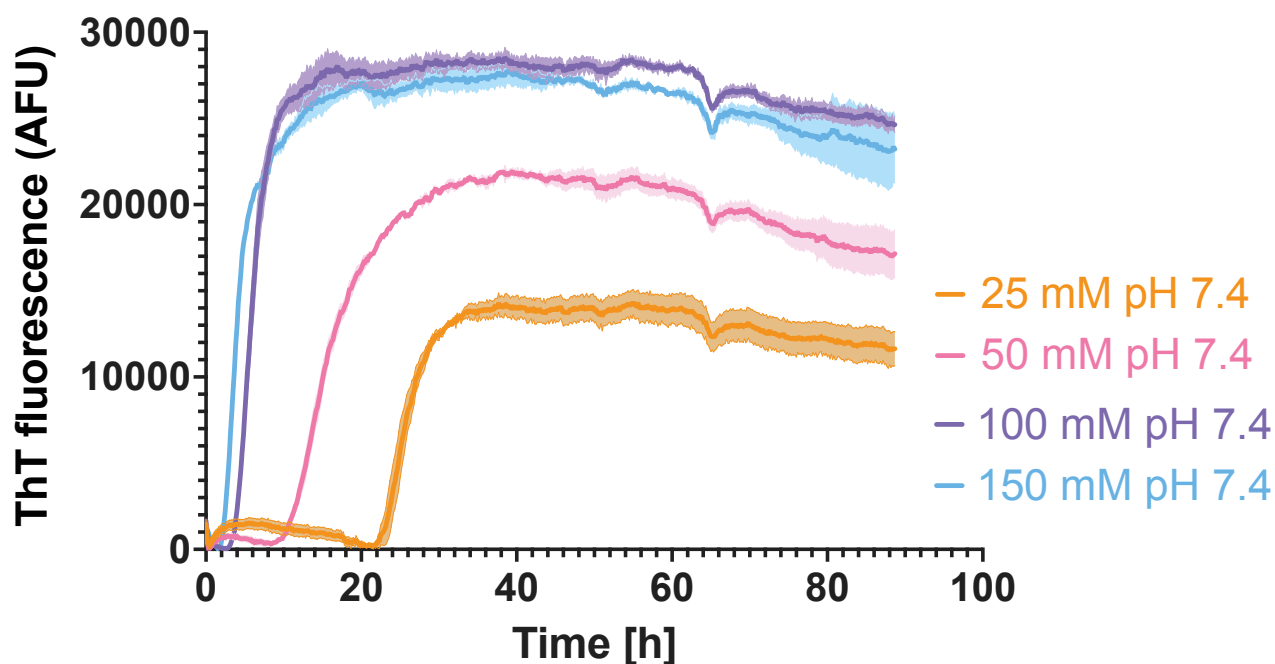


Figure S3. Plot showing reproducibility and stability of aggregation kinetics. Four examples at pH 7.4, of three replicates, showing a plateau above the 16 hours presented in Figure 1. This assay was performed on a different day and from different stock than those presented in Figure 1.

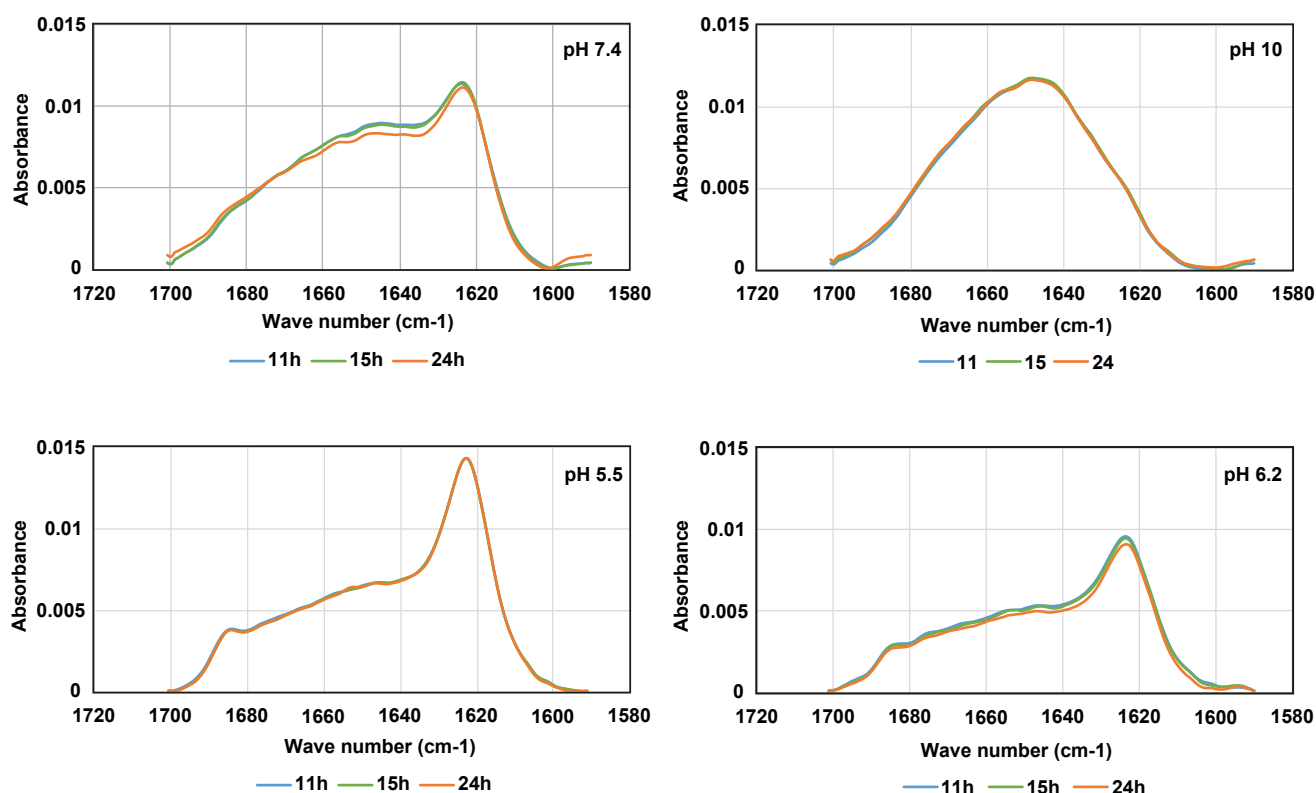
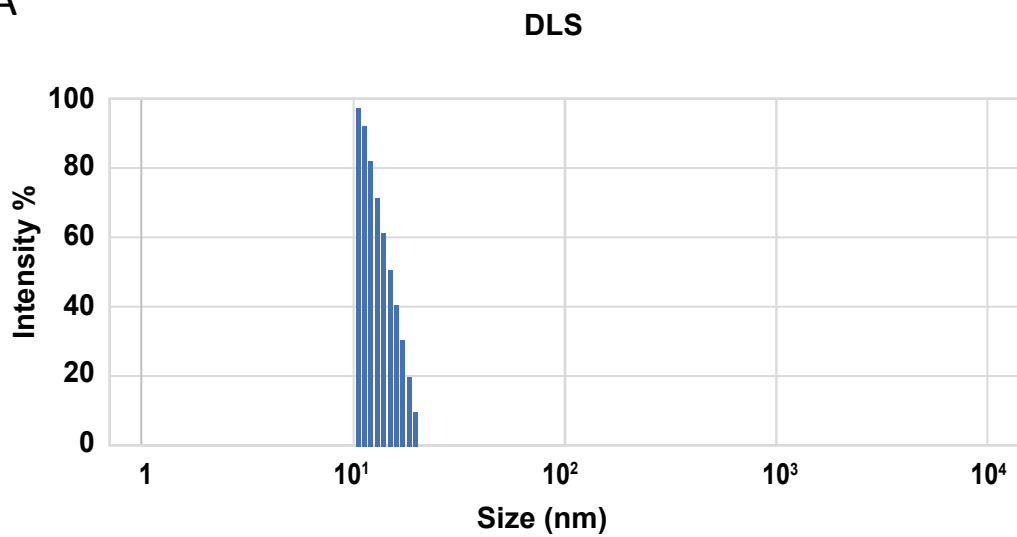


Figure S4. FTIR absorbance spectra of Aβ40 aggregates incubated at four different pHs (5.5, 6.2, 7.4 and 10) for 11, 15, and 24 hours. The absorbance remains stable from 11 to 24 hours, indicating a stable conformation during this period of time.

A



B

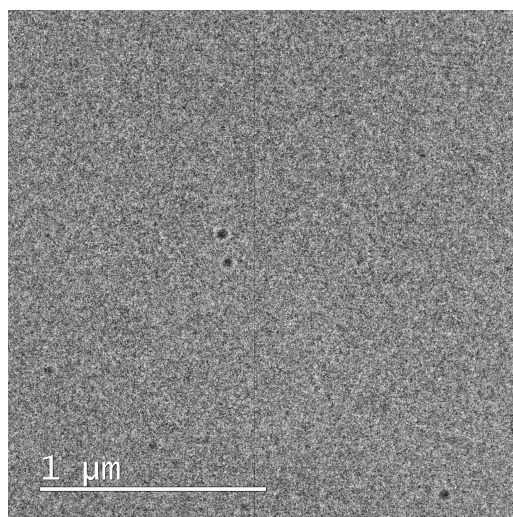


Figure S5. Absence of aggregates at the initial stock sample. A) Dynamic Light Scattering analysis of an initial stock sample (250 μ M) of A β 40 at pH 11. The signal shows just one particle size of 10 nanometers, which fits with the size of a monomeric A β peptide. B) TEM image for the initial stock sample (250 μ M) of A β 40 at pH 11.

MTT controls

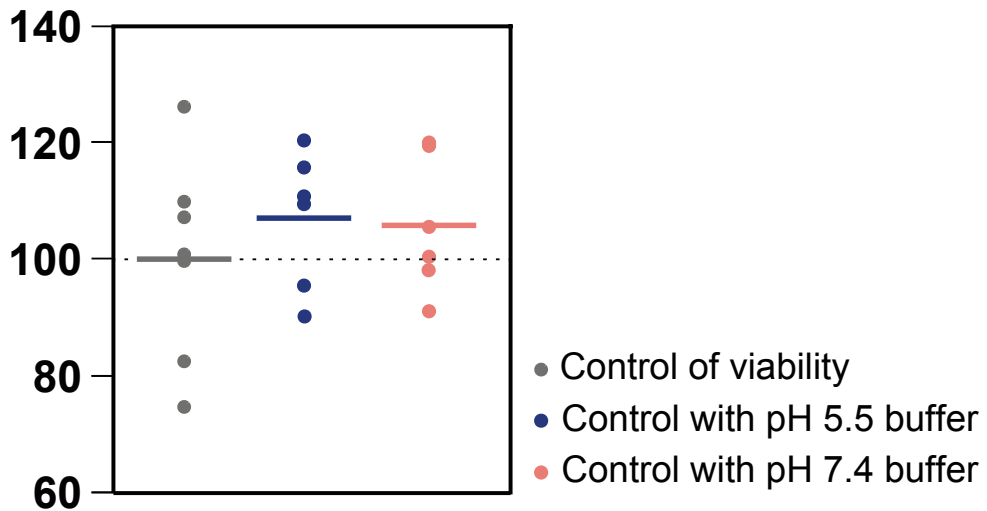


Figure S6. MTT viability assay. Percentage of cell viability, after incubating with buffers at pH 5.5 (blue) and pH 7.4 (red). The control of cells grown just in culture medium are shown in grey. The plot shows triplicates of two independent assays. The lines are the mean corresponding to each concentration of aggregates added. No significant difference was measured with Bonferroni test.

Appendix 2- Supplementary information of chapter 2

Appendix

Microbiome-Derived Prion-Like Proteins and Their Potential to Trigger Neurodegeneration

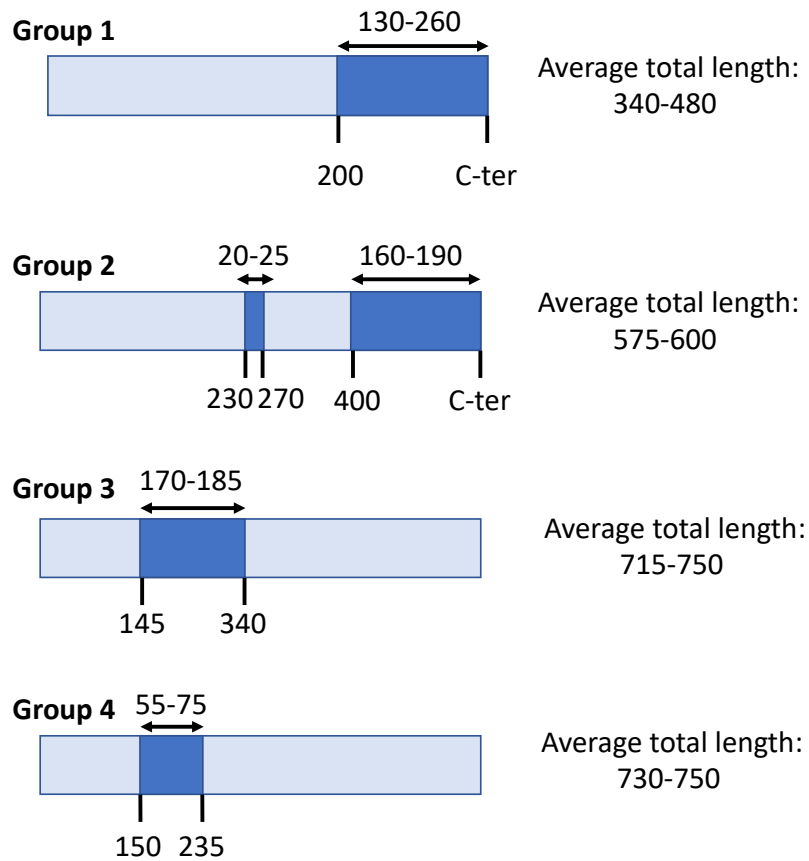
Table of Content

Supplementary Figures

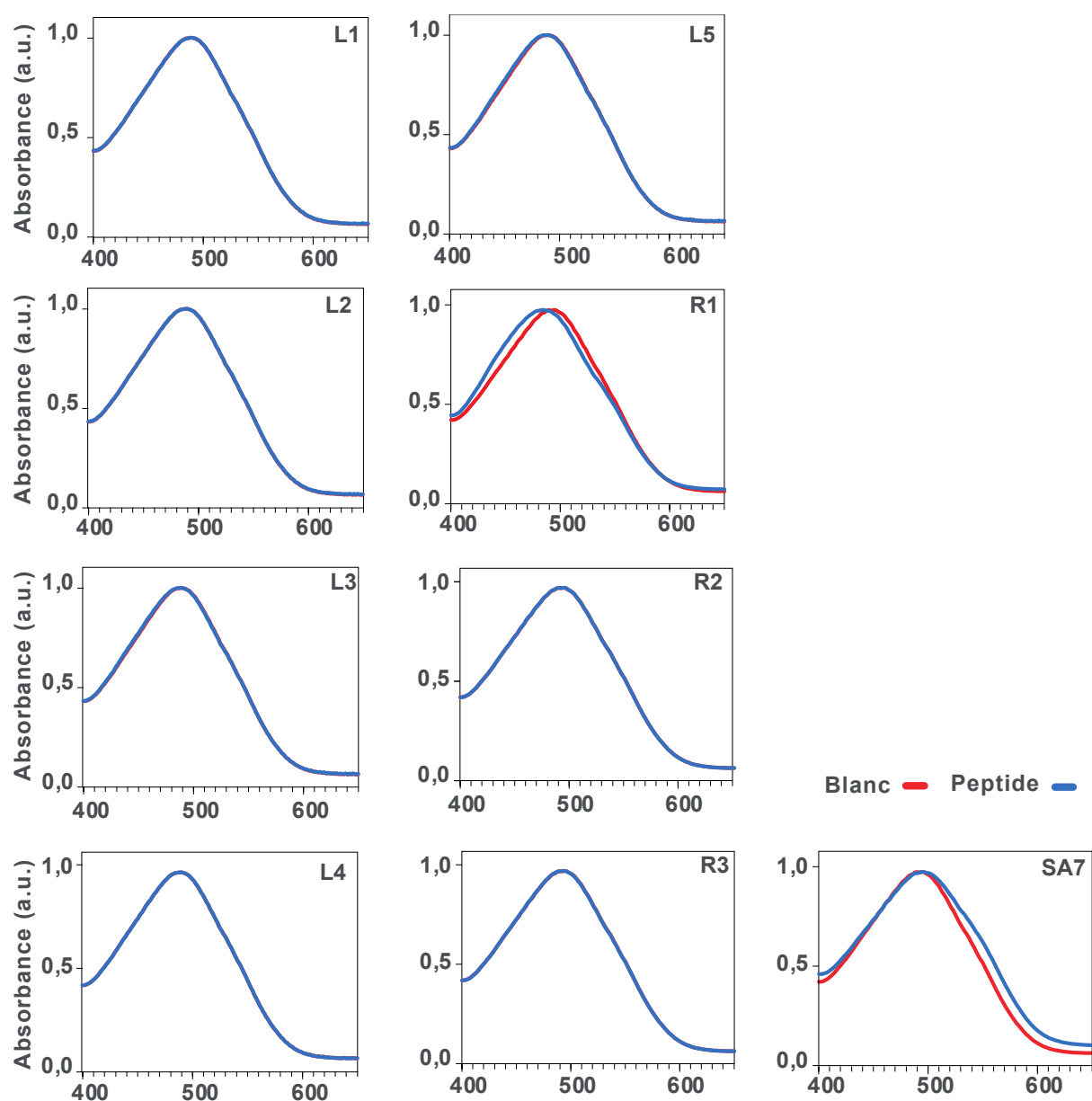
Appendix Figure S1	Page 2
Appendix Figure S2	Page 3
Appendix Figure S3	Page 4
Appendix Figure S4	Page 5
Appendix Figure S5	Page 6
Appendix Figure S6	Page 7
Appendix Figure S7	Page 8
Appendix Figure S8	Page 9
Appendix Figure S9	Page 10
Appendix Figure S10	Page 11
Appendix Figure S11	Page 12
Appendix Figure S12	Page 13
Appendix Figure S13	Page 14
Appendix Figure S14	Page 15
Appendix Figure S15	Page 16
Appendix Figure S16	Page 17
Appendix Figure S17	Page 18
Appendix Figure S18	Page 19
Appendix Figure S19	Page 20
Appendix Figure S20	Page 21
Appendix Figure S21	Page 22
Appendix Figure S22	Page 23

Appendix Supplementary Data

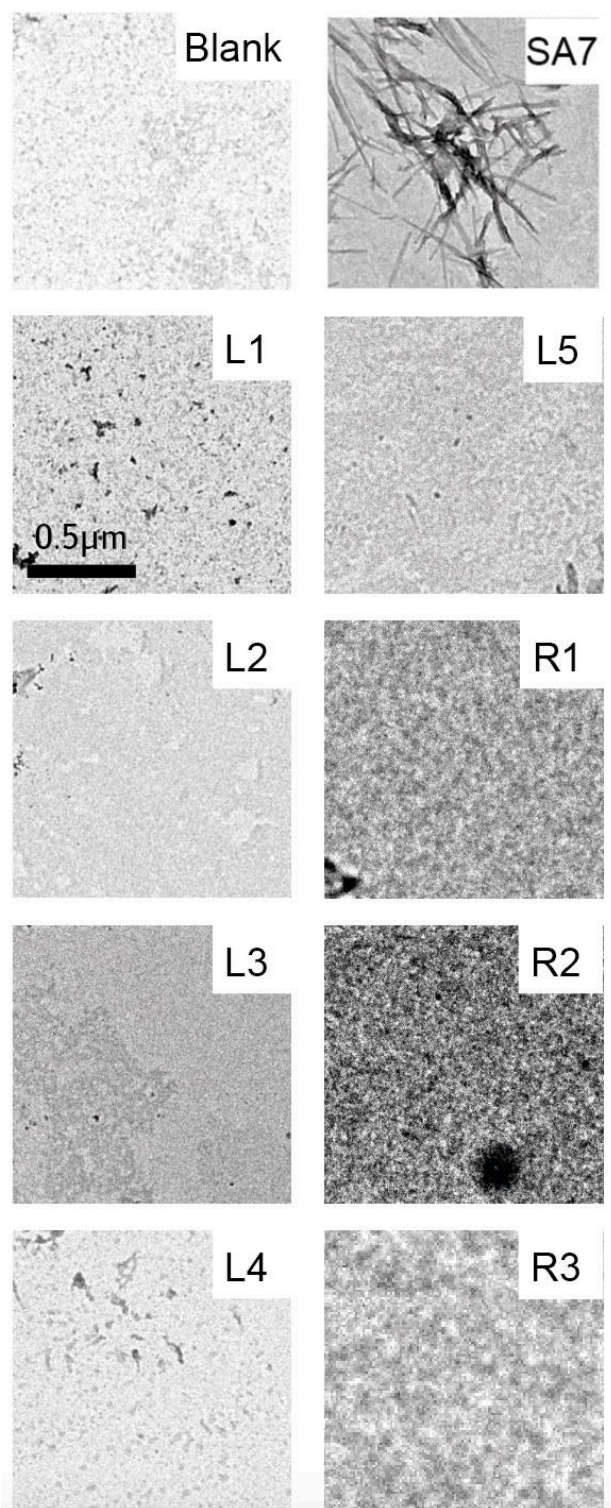
Predictions performed on the Sup35p variants	Page 24
Protein sequences expressed in <i>S. cerevisiae</i>	Page 39
Protein sequences expressed in <i>E. coli</i>	Page 40



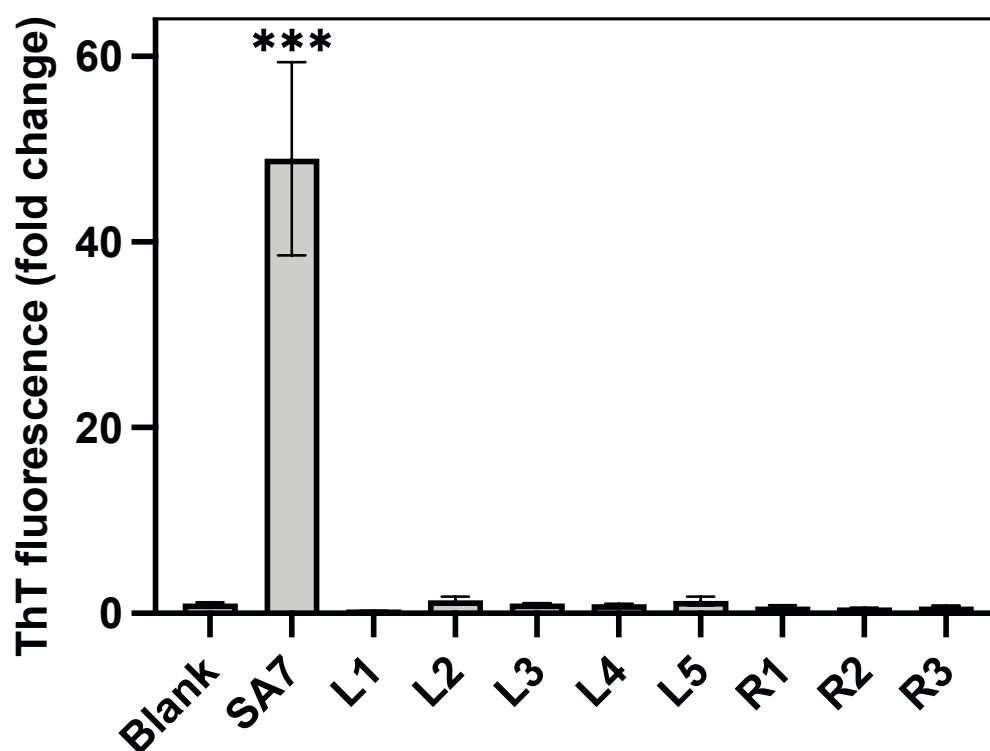
Appendix Figure S1. Common Disordered Regions Identified in Uncharacterized Proteins. The diagram displays four sequences, highlighting the consensus locations identified within the gut microbiome. This classification is based on information sourced from MobiDB Lite (Supplementary Table 1). In Supplementary Table 1, there are 370 uncharacterized sequences, constituting 40% of the dataset. Among these, 214 sequences have been determined to contain disordered regions according to MobiDB Lite. The groups shown in this figure consist of the following numbers of sequences: Group 1, 78 sequences; Group 2, 39 sequences; Group 3, 35 sequences; Group 4, 23 sequences.



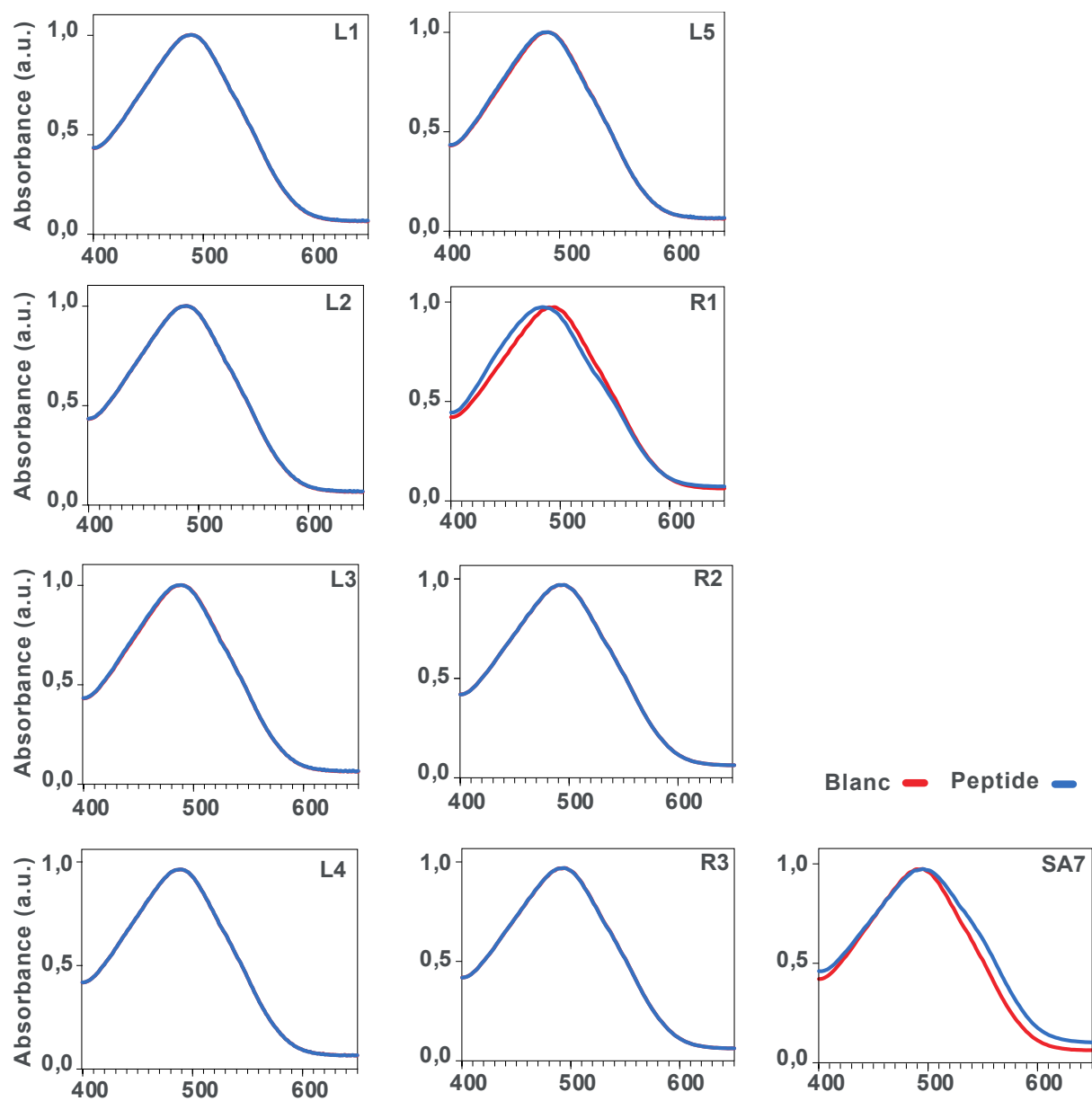
Appendix Figure S2. Congo Red binding analysis of the aggregates formed by the ten selected amyloid cores. Red indicates Congo Red absorbance without aggregates, while blue represents absorbance with aggregates.



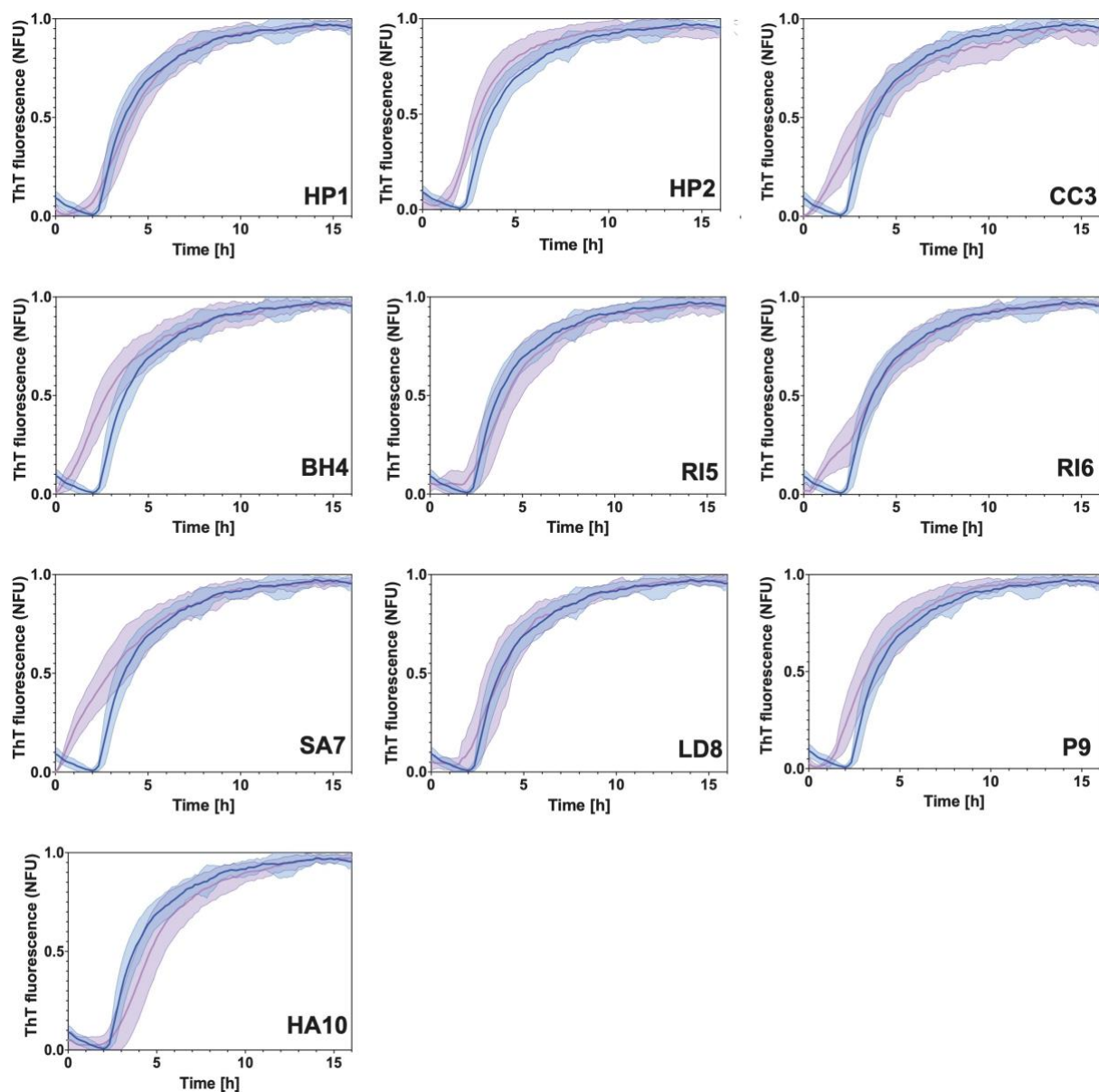
Appendix Figure S3. TEM images showing the samples of low aggregation-prone peptides.



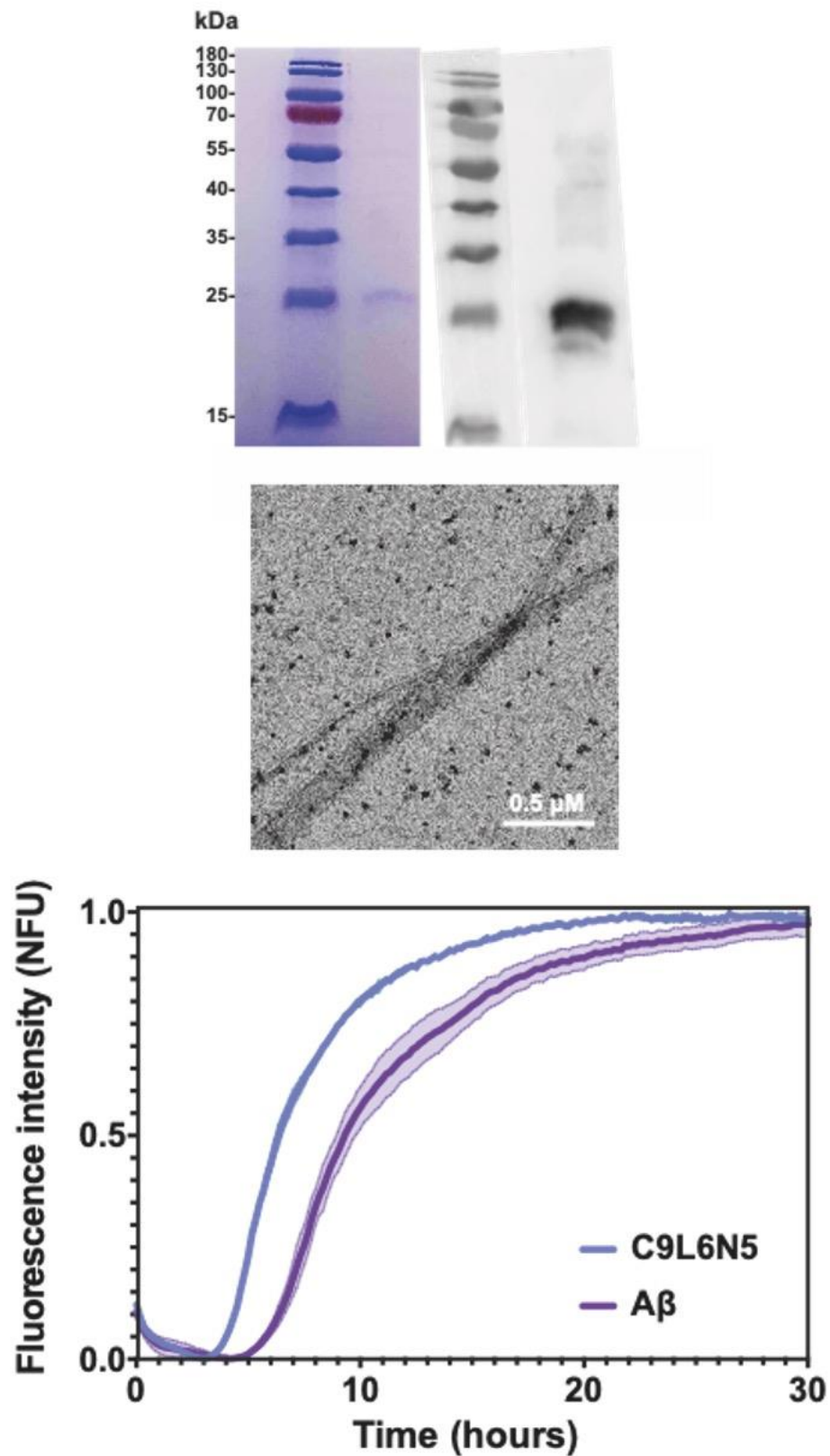
Appendix Figure S4. Thioflavin-T binding of the low aggregation-prone control peptides. Thioflavin-T fluorescence increase, fold change with respect to the blank (just buffer and ThT). The binding of the peptide SA7 was also measured as a positive control (unpaired two tail t-test, N=3).



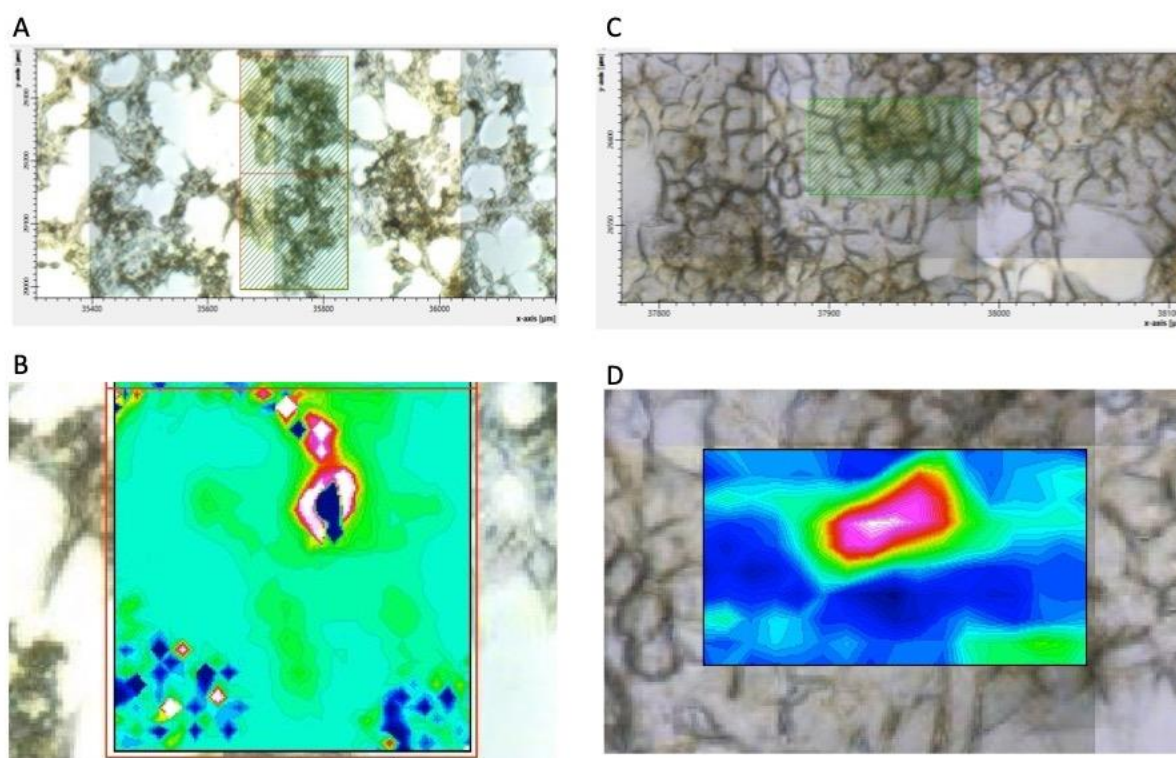
Appendix Figure S5. Congo Red binding analysis of the aggregates formed by the eighth low aggregation-prone sequences. Red indicates Congo Red absorbance without aggregates, while blue represents absorbance with the control peptides.



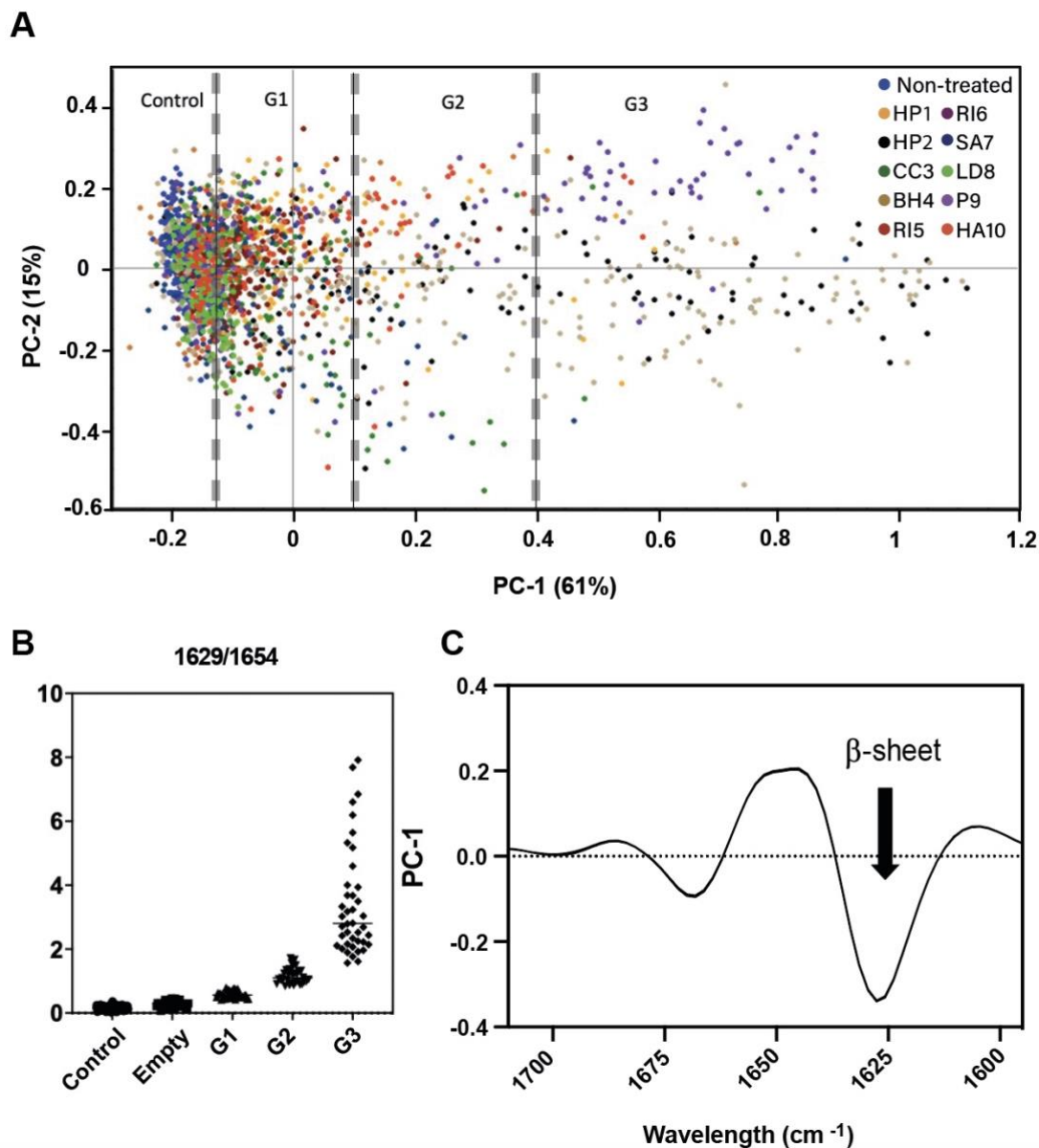
Appendix Figure S6. Aggregation kinetics plots of A β 40 seeded with ten peptides derived from the gut microbiome. The purple curve represents the aggregation kinetics of A β 40 without any seeding, whereas the blue curve represents the aggregation kinetics in the presence of pre-aggregated peptides. The shaded regions show the standard error of the mean, which has been calculated from four independent replicates, with each replicate comprising three repeated samples.



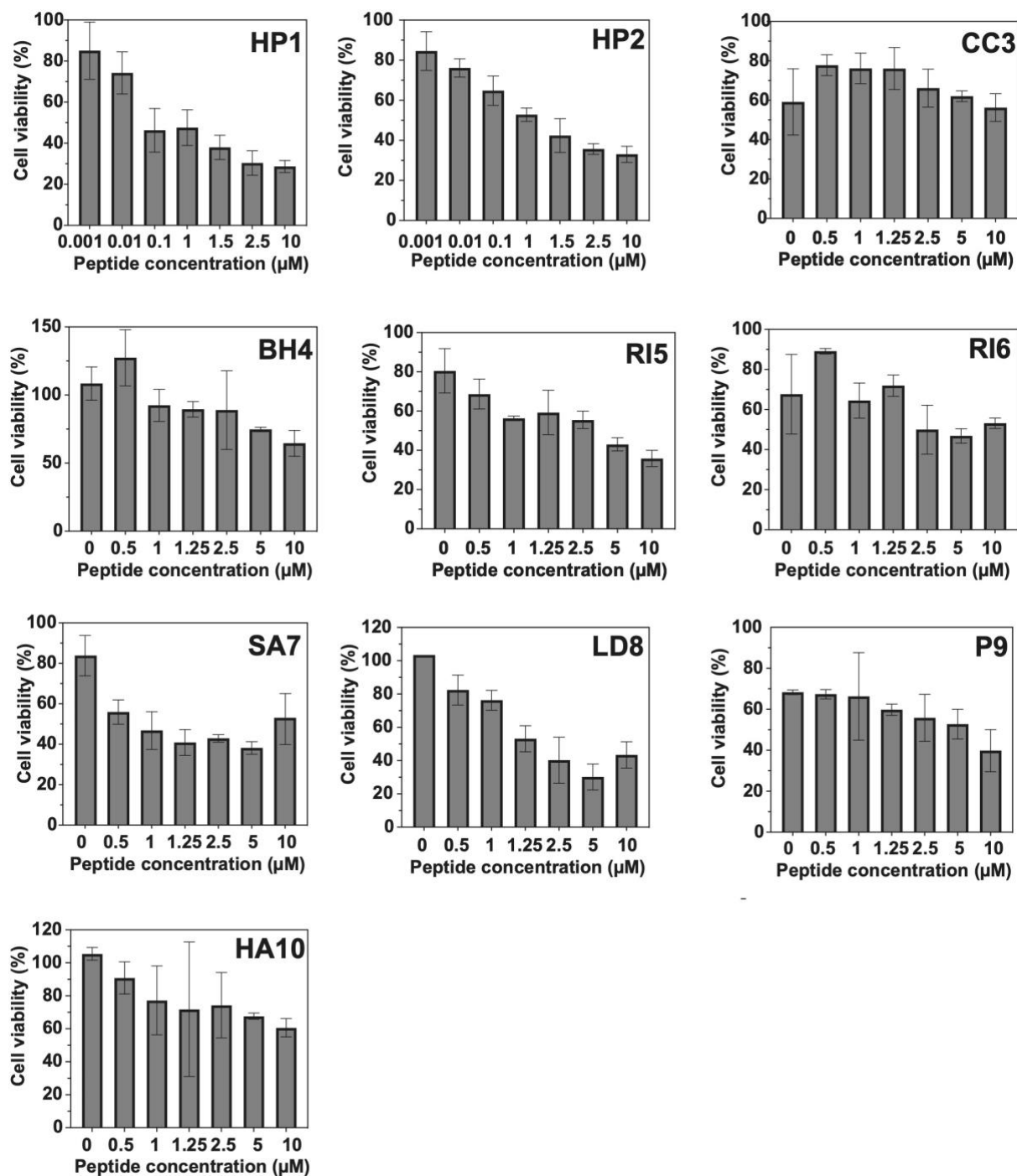
Appendix Figure S7. Purification and aggregation of C9L6N5 (containing BH4). Up, SDS-PAGE gel and western blotting (anti-His) showing one protein band after C9L6N5 purification. Middle, TEM image showing fibrillar aggregates of C9L6N5. Bottom, A β 40 aggregation kinetics not seeded (purple) and seeded (blue) with aggregates of C9L6N5.



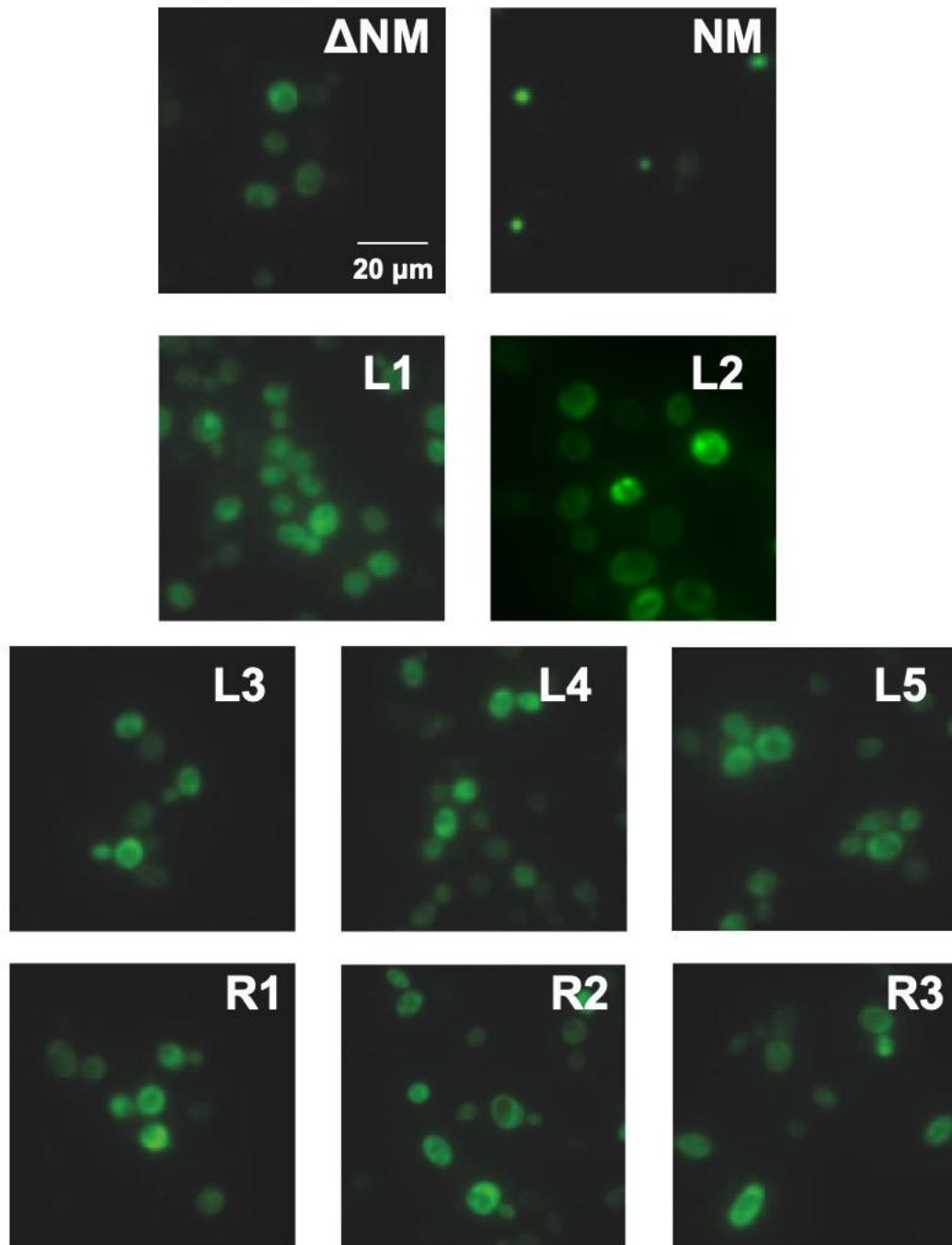
Appendix Figure S8. μ FTIR maps of cells treated with aggregated peptides derived from the microbiota. The upper panels show microscope images of cells incubated with the peptides (A) HP2 and (C) BH4. The lower panels illustrate the beta/alpha ratio ($1740/2921\text{ cm}^{-1}$), utilized for detecting the presence of amyloid fibrils formed by the peptides (B) HP2 and (D) BH4. The images indicate the distribution of preformed aggregates throughout the samples. Amyloid deposits were identified in all samples, confirming the persistence of the preaggregated peptide's under cell culture conditions.



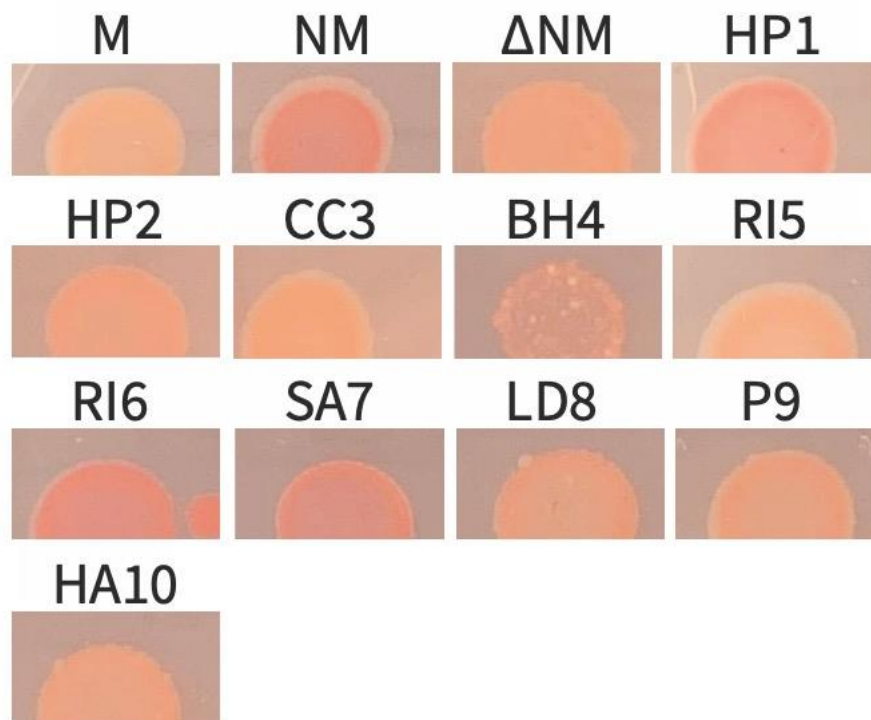
Appendix Figure S9. Results of μ FTIR analysis showing that the absorbance of β -sheet differentiates between cells incubated with and without aggregates. Neuron differentiate SH-SY5Y cells were incubated with and without the aggregates of the amyloid cores selected. Then for each sample, the presence and structure of amyloid-like aggregates were measured with μ FTIR. Two negative controls were considered: cells growth without aggregates (Control) and the zones where no aggregate was visualized under the microscope (Empty). A) Principal component analysis of the signal at the amide I region. The measurements were separated into three groups (grey dashed line) based on the PC-1, which (as seen in panel C) is principally supported by the β -sheet signal. In this line, the groups G1, G2 and G3 arrange the measurements from less to more β -sheet signal. B) Distribution of the amyloid aggregation ratio (1629/1654) for the three groups derived from PCA analysis (Control, N=1181; Empty, N=139, G1, N=465; G2, N=185; G3, N=220). This result supports that the group division, at the PCA, separates progressively increasing aggregate signals. C) Summary μ FTIR spectra of PC-1, representing 61% of the variances between the samples. The peak from 1635 cm⁻¹ to 1625 cm⁻¹ corresponds to β -sheet signal, indicating that the difference between the groups is linked to amyloid fibrils. Amyloid deposits (G1, G2, G3) were identified in all samples, confirming the persistence of aggregated peptides under cell culture conditions.



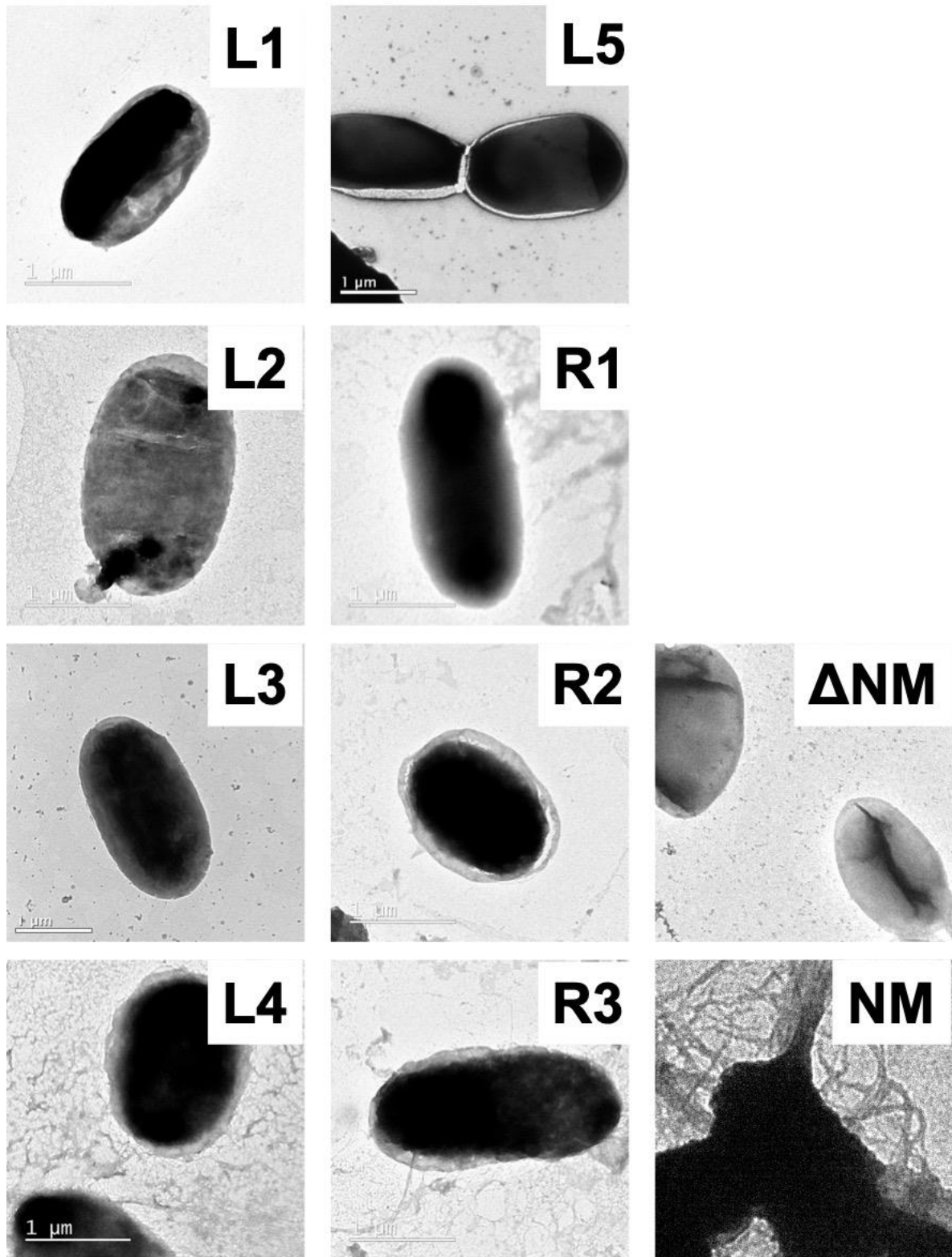
Appendix Figure S10. Cytotoxicity of amyloid-forming cores derived from the gut microbiome. Cell viability of SH-SY5Y cells after 24 hours of exposure to various peptides (N=3). Due to their high toxicity, C1 and C2 have a wider concentration range. The error bars represent the standard error of the mean (SEM).



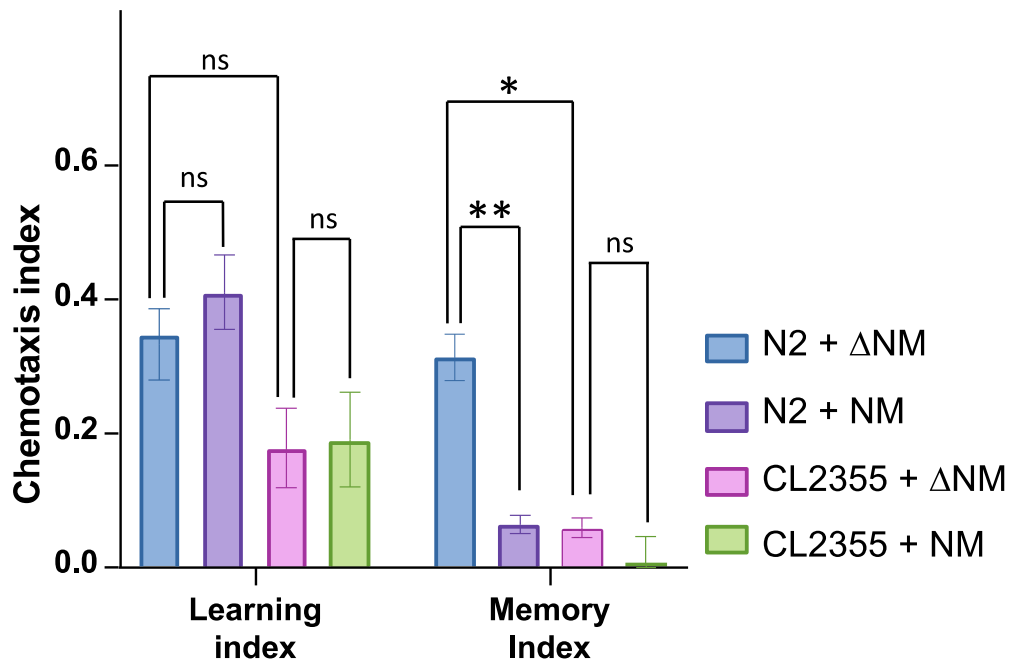
Appendix Figure S11. Yeast expressing low aggregation-prone variants of Sup35-GFP. Fluorescent images showing the location of the Sup35-GFP variants.



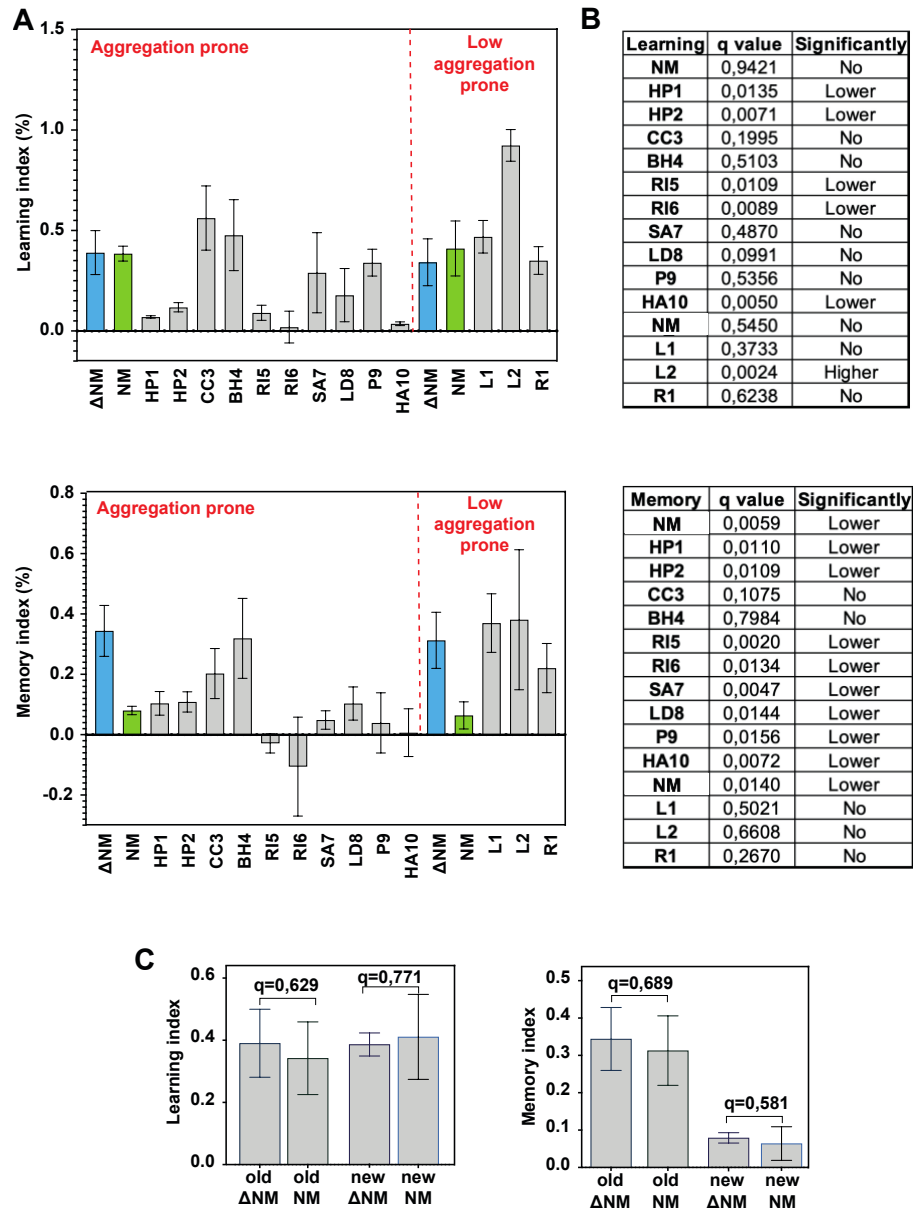
Appendix Figure S12. *E. coli* C-DAG colonies on Congo Red-containing plates. The images show the colonies of the different *E. coli* expressing the Sup35 chimeras grown on congo-red containing plates (Methods).



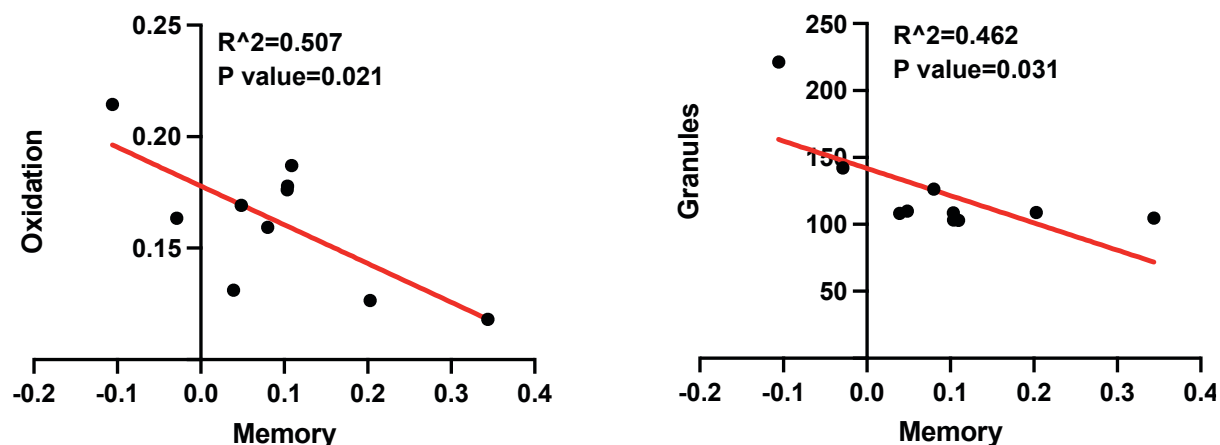
Appendix Figure S13. TEM images of the *E. coli* C-DAG system expressing low aggregation prone Sup35 variants.



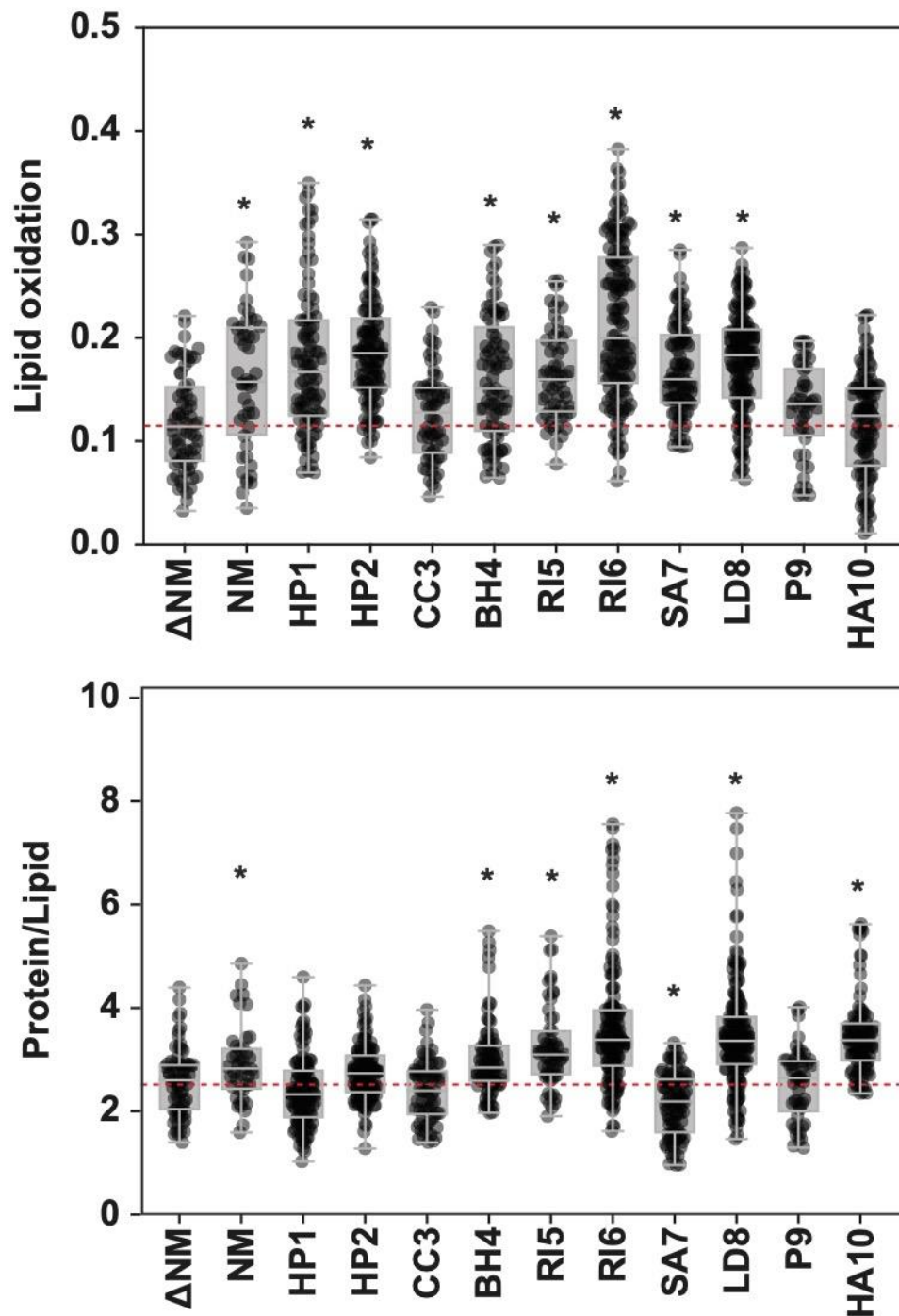
Appendix Figure S14. STAM comparison between N2 (wildtype) and CL2355 (Alzheimer's model). Chemotaxis index for learning and memory assays measured for worms fed with Δ Sup35 and Sup35NM (One-way ANOVA, N=3, *p < 0.05, **p < 0.01, ns = not significant).



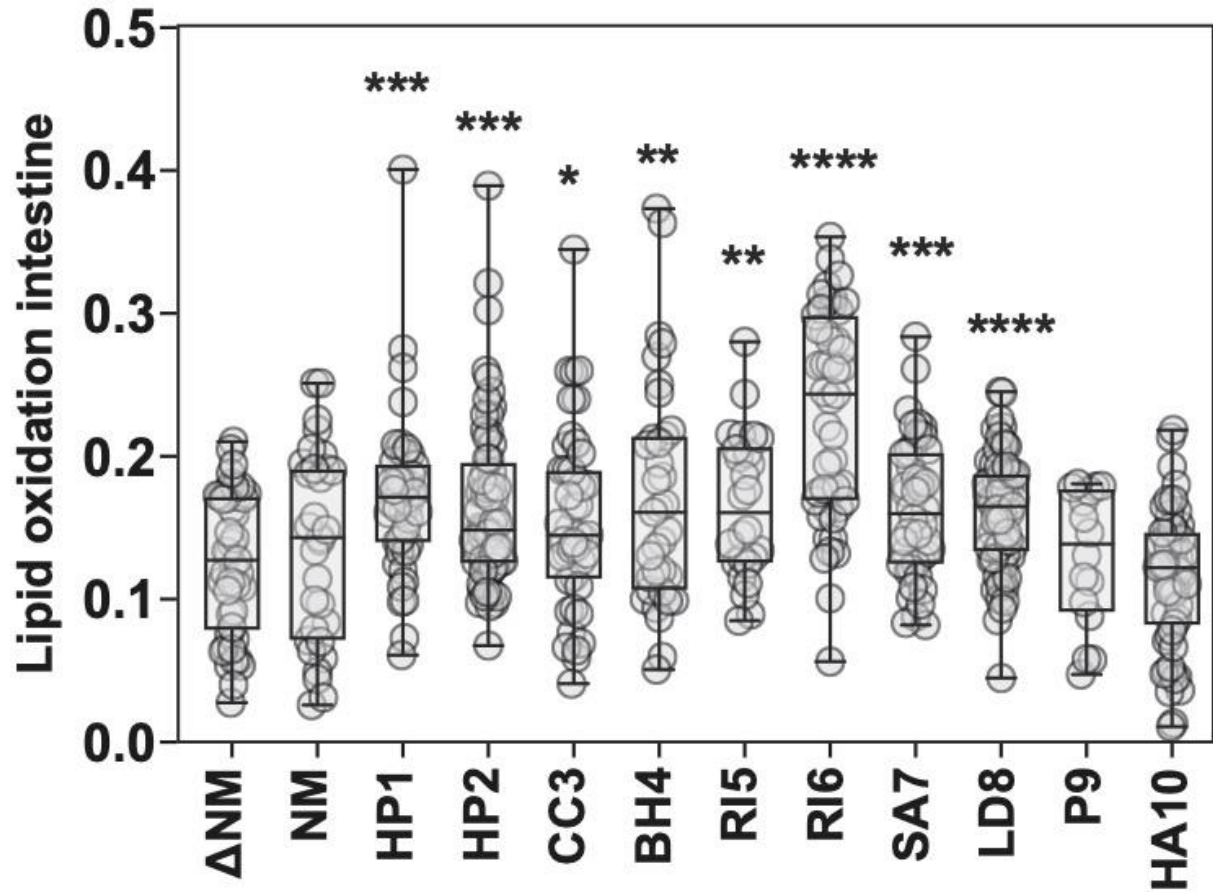
Appendix Figure S15. Low aggregation-prone STAM comparison. A) The plots show the learning (top) and memory (bottom) indices for all the samples analyzed in this study. The vertical dashed line separates two different sets of experiments: on the left, the assays performed with aggregation-prone Sup35 chimeras, and on the right, those conducted with the low-aggregation-prone variants. Samples analyzed in both experiments (internal controls) are highlighted in blue and green. B) Tables showing that the significances against their corresponding Δ NM controls, obtained when including all samples, are similar to those reported in the main article (Figure 6, which only included the aggregation-prone variants). The analysis was performed using multiple unpaired two-tailed t-tests, corrected for multiple comparisons using the Benjamini–Hochberg method ($N = 3$ biological replicates of 300–500 worms each, FDR set at 5%). C) Comparison between the same samples across the two repeated assays (Δ NM and NM). The analysis was performed using multiple unpaired two-tailed t-tests, corrected for multiple comparisons using the Benjamini–Hochberg method ($N = 3$ biological replicates of 300–500 worms each, FDR set at 5%). The learning and memory indices obtained for both samples (Δ NM and NM) in the repeated assays showed no significant differences.



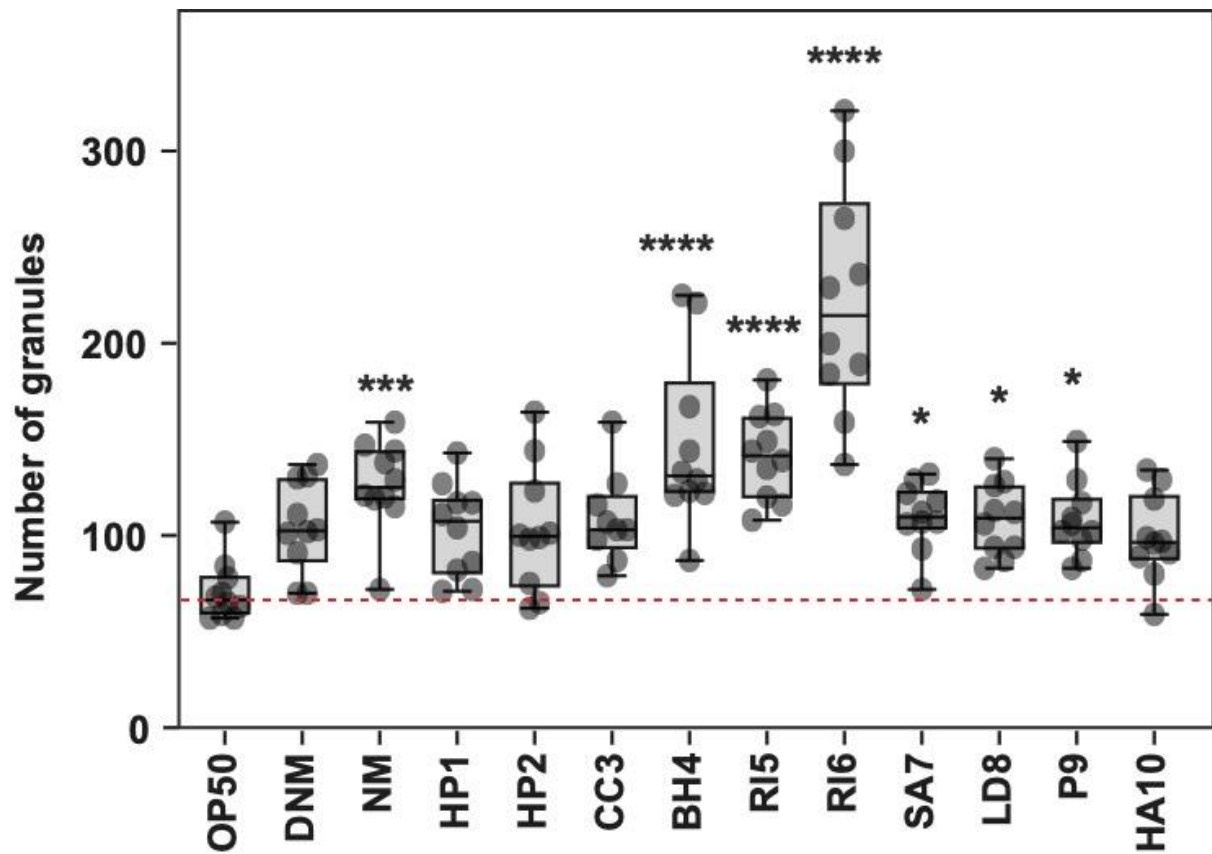
Appendix Figure S16. Scatter plots showing how lipid oxidation and number of granules correlate with the associative memory in *C. elegans*. The red line indicates the linear regression for each dataset (derived from Figures 6D and 7C). BH4 and HA10 were excluded from the analysis as they presented especially high or low values in oxidation and the number of granules, respectively. Statistical significance was assessed using Pearson correlation analysis.



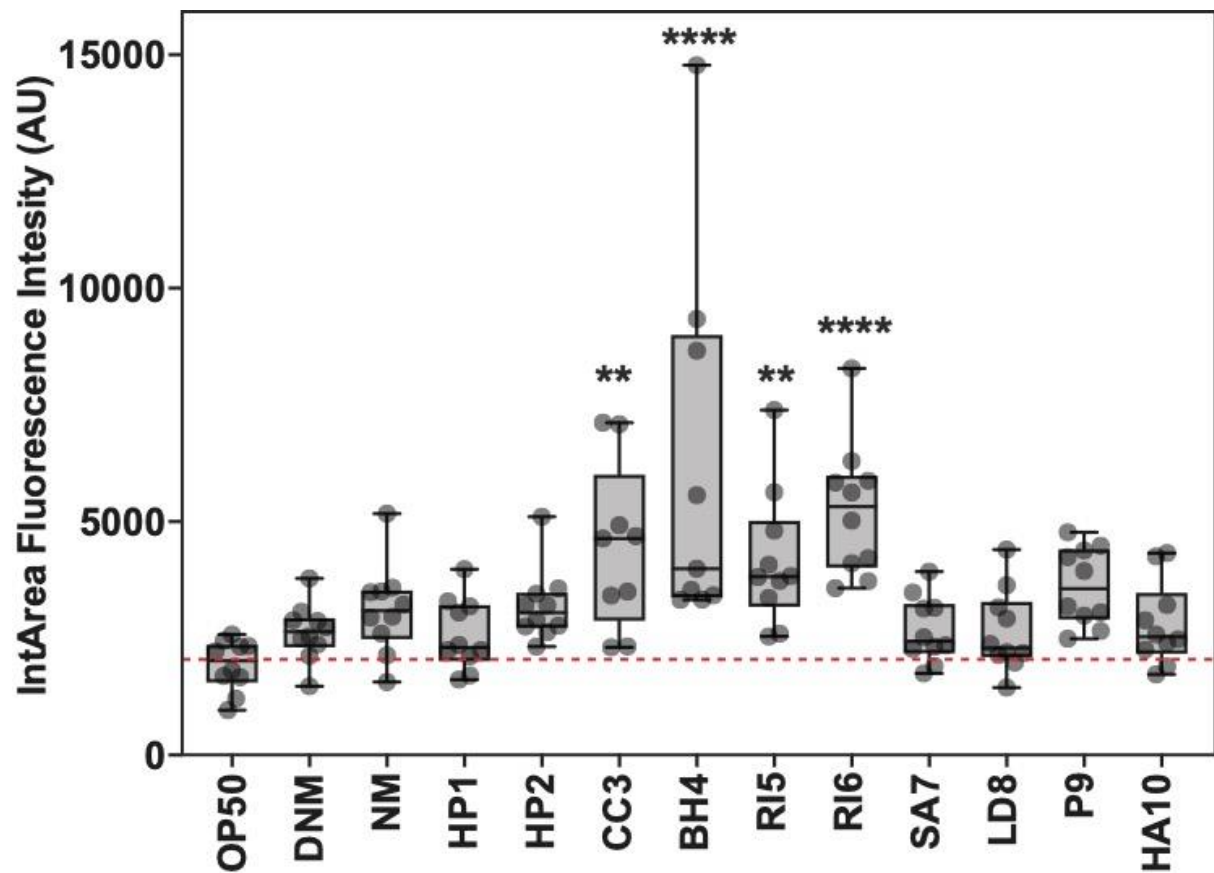
Appendix Figure S17. IR measurements of the whole body of *C. elegans* strains fed with the Sup35 chimeras. Up, distribution of the lipid peroxidation signal ($1740\text{ cm}^{-1}/(2960\text{ cm}^{-1} - 2919\text{ cm}^{-1})$). Down, proportion protein/lipid signal ($1654\text{ cm}^{-1}/(2960\text{ cm}^{-1} - 2919\text{ cm}^{-1})$). Each box represents the measurements taken within at least 10 worms. ΔNM N=67; NM N=42; C1 N=110; C2 N=120; C3 N=67; C4 N=82; C5 N=58; C6 1 N=35; C7 N=94; C8 N=159; C9 N=49; C10 N=97. The box plots bars show the minimum and maximum values, and the box lines show the median and the interquartile range. Significance was measured using an unpaired t-test (* $p < 0.05$).



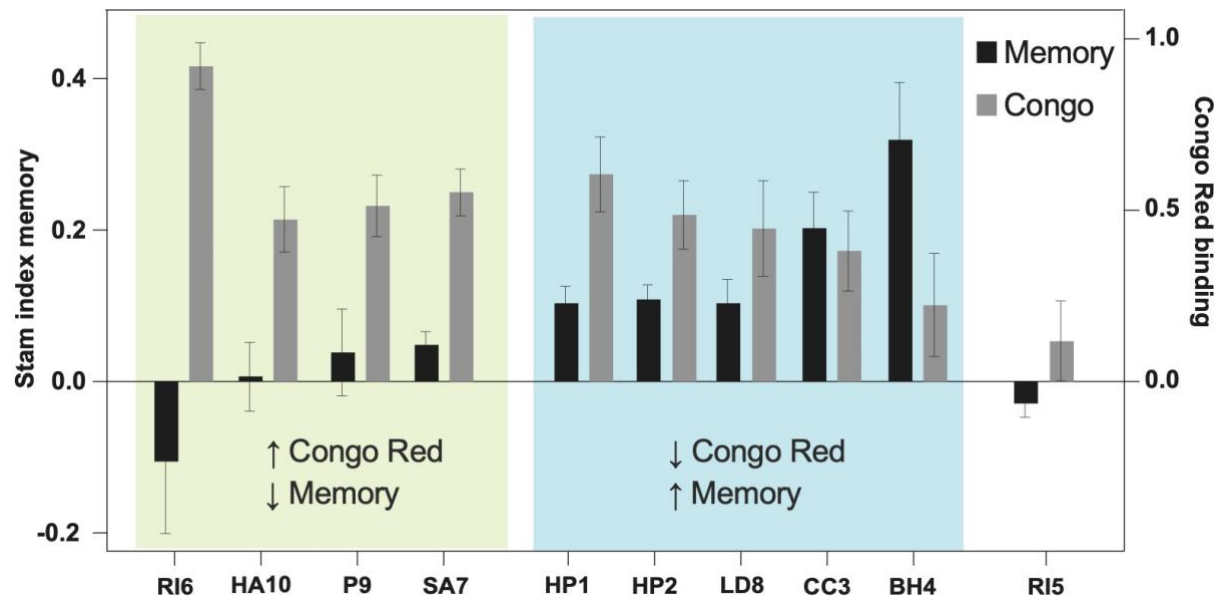
Appendix Figure S18. IR measurements focused on the intestine of *C. elegans* strains fed with the Sup35 chimeras. Distribution of the lipid peroxidation signal ($1740\text{ cm}^{-1}/(2960\text{ cm}^{-1} - 2919\text{ cm}^{-1})$). Each box represents the measurements taken within the intestine of a minimum of 10 worms per sample and a minimum of 25 points per sample. The box plots bars show the minimum and maximum values, and the box lines show the median and the interquartile range. Significance was measured using an unpaired t-test (* $p < 0.05$, ** $p < 0.01$, *** $p < 0.001$, **** $p < 0.0001$).



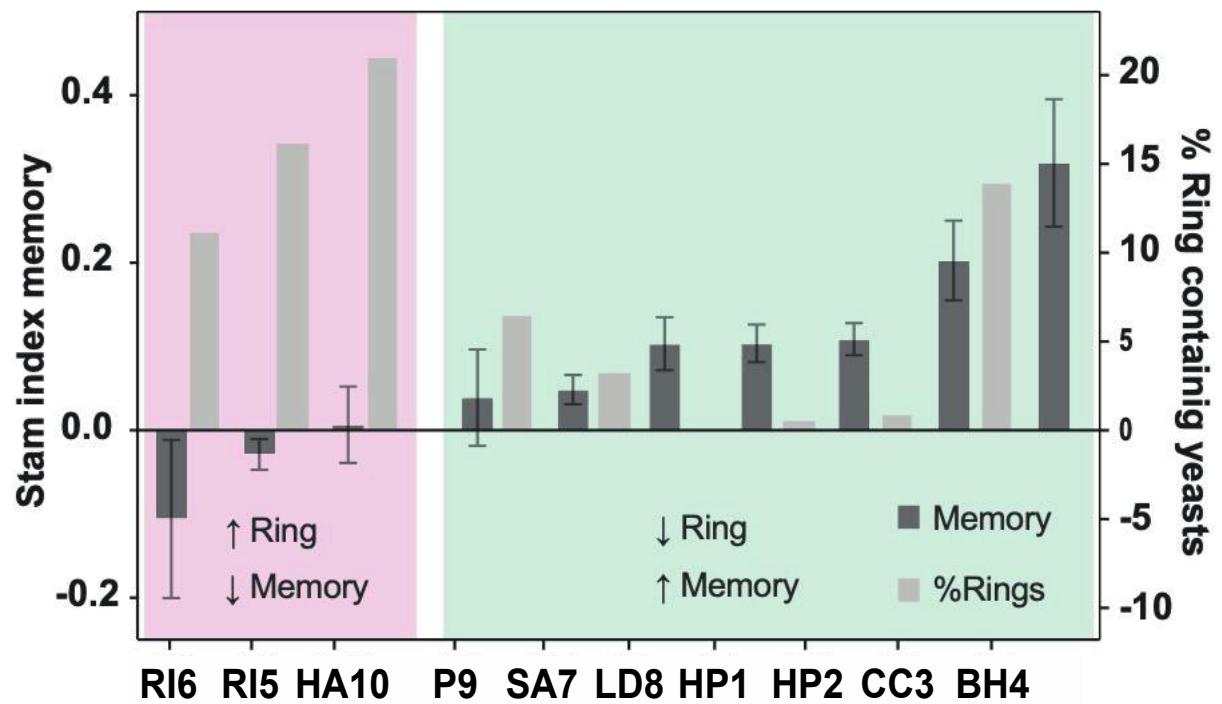
Appendix Figure S19. *C. elegans* gut granules counting. Number of gut granules in the two first intestinal rings of *C. elegans* N2 fed with *E. coli* OP50 and *E. coli* expressing various Sup35NM variants. OP50 *E. coli* strain is the standard nematode food and a biofilm-defective mutant. Error bars represent the SEM of 8-10 measurements. Each dot contains the information of one worm. Statistical significance was determined using one-way ANOVA (* $p < 0.05$, ** $p < 0.01$, *** $p < 0.001$, **** $p < 0.0001$).



Appendix Figure S20. *C. elegans* gut granules fluorescent intensity. Plot showing the distribution of the gut granules fluorescent intensity adjusted by area (IntArea, ImageJ) in the *C. elegans* fed with *E. coli* OP50 and *E. coli* expressing different variants of Sup35NM. *E. coli* strain is the standard nematode food and a biofilm-defective mutant. Error bars represent the SEM of 8-10 measurements. Statistical significance was determined using one-way ANOVA (* $p < 0.05$, ** $p < 0.01$, *** $p < 0.001$, **** $p < 0.0001$).



Appendix Figure S21. Memory index and Congo Red binding comparison. Plot comparing the memory index and the congo red binding (from Figure 5B) of *E. coli* expressing different variants of Sup35NM.



Appendix Figure S22. Memory index and presence of ring aggregates comparison. Plot comparing the memory index and the presence of ring structures in yeast (from Figure 4B) expressing different variants of Sup35NM.

Appendix Supplementary Data

Predictions performed on the Sup35p variants studied in this work.

Presented here are the sequences of the Sup35NM chimeras, with the newly detected sequences highlighted by pWALTZ (Material and Methods). Sequences in yellow indicate a precise match with the introduced amyloid-forming cores. Sequences in blue signify a partial match or mismatch with the introduced amyloid-forming cores, including the regions in Sup35NM and Sup35M highlighted in blue. The Sup35p nucleation region is denoted in bold and underlined. The introduced amyloid-forming cores are marked in bold.

List of pWALTZ detected sequences on the region detected by PAPA.

FULL	RGNYKNFNYNNNLQGYQAGFQ	73.9926	(residues from 98 to 118)
Delta	RGNYKNFNYNNNLQGYQAGFQ	73.9926	(residues from 58 to 68)
HP1	GNNNSVISFNQTNFNQGTYN	78.8660	(residues from 2 to 22)
HP2	NNNKSYYISAGGYQNYQGYS	77.6716	(residues from 14 to 34)
CC3	MQAAFNFINNRRYQDAINVLN	78.1175	(residues from 2 to 22)
BH4	RNAQWYYLAGGYQNYQGYSG	78.2290	(residues from 15 to 35)
RI5	YNNSYQNTNSYSAGGYQNYQ	80.0127	(residues from 11 to 31)
RI6	MDNNYNNNNNNNTNSNSNYN	77.1301	(residues from 2 to 22)
SA7	RSGNYVFLANSTNRYQGNYYN	75.7126	(residues from 2 to 22)
LD8	NQFQNSQYGSYQAGGYQNYQ	77.5441	(residues from 11 to 31)
P9	GYGSNYNYSYSAAGGYQNYQ	78.4679	(residues from 11 to 31)
HA10	TYNQSALINQIGAGGYQNYQ	77.2256	(residues from 11 to 31)

In **bold** the 21 peptides studied.

In **yellow** when they matches 100% with the new pWALTZ prediction.

In **blue** when they doesn't match 100% with the new pWALTZ prediction

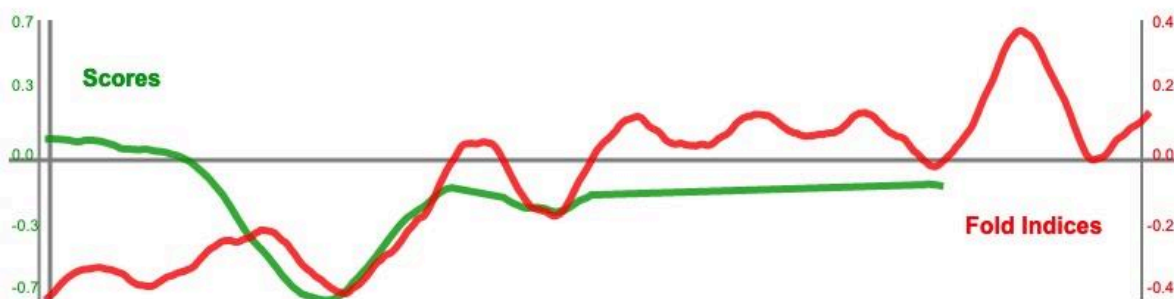
In **bold and underlined** the Sup35p nucleation region.

>Sup35NM

MSDSNQGNQQNYQQYSONGNQQQGNNRYQGYQAYNAQAQAPAGGYQQNYQGYSGYQQGGYQQ
 YNPDAGYQQQYNPQGGYQQYNPQGGYQQQFNPQGG**RGNYKNFNYNNNLQGYQAGFQ**PQSQGM
 SLNDFQKQQKQAAPKPKKTLKLVSSSGIKLANATKKVGTKPAESDKKEEEKSAETKEPTKEP
 TKVEEPVKKEEKPVQTEEKTEEKSELPKVEDLKIESTHNTNNANVT SADALIKEQEEVDD
 EVVNDMFGGKDHVSLIFMGHVDAGKSTMGGNLLYL TGSVDKRTIEKYEREAKDAGRQGWYLS
 WVM D TNKEERN DGKTIEVGKAYFETEKRRYTILDAPGHKMYVSEMIGGASQADVGV LVISAR
 KGEYETGFERGGQ TREHALLAKTQGVNKMVVVNKMD DPTVNWSKERYDQCVSNVSNFLRAI
 GYNIKTDVVFMPVSGYSGANLKD HVDPK ECPWYTGPTLLEYLDTMNHVDRHINAFMLPIAA
 KMKDLGTIVEGKIESGHIKKGQSTLLMPNKTAVEIQNIYNETENEVDMAMCGEQVKLRIGV
 EEEDISP GFVLTS PKNPIKSVTKFVAQIAIVELKSIIAAGFSCVMHVHTAIEEVHIVKLLHK
 LEKGTNRKSKKPPAF AKKG MKVIAVLETEAPVCVETYQDYPQLGRFTLRDQGT TIAIGKIVK
 IAE

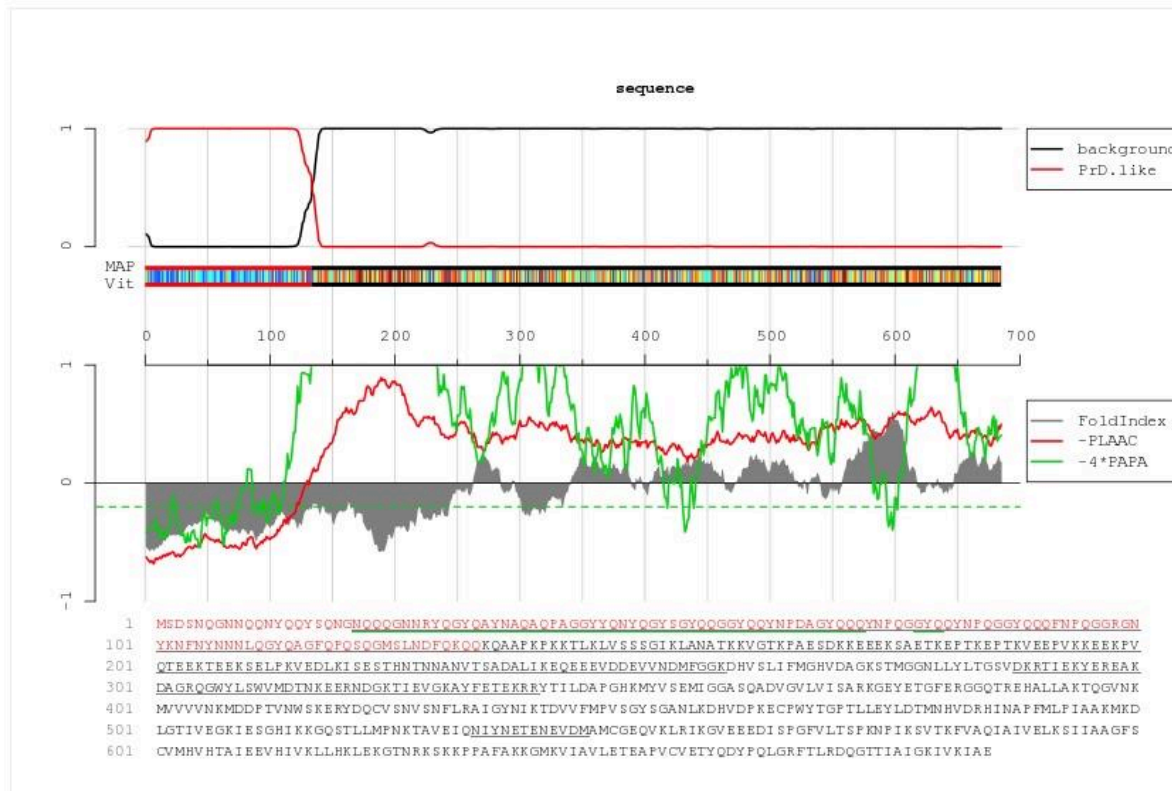
PAPA

Score = 0.10, Position = 4



PLAAC

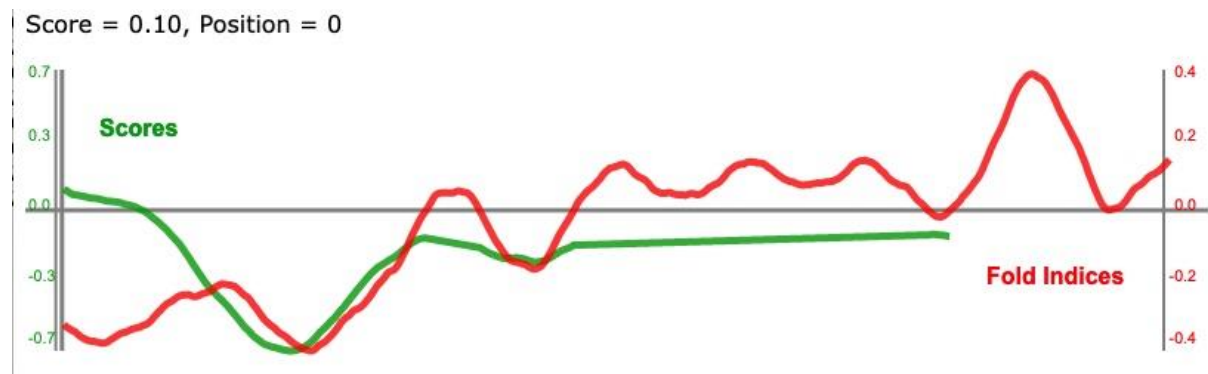
COREscore	LLR	PAPAprp	PAPAf1
23.306	23.306	0.100	-0.423



>Sup35M

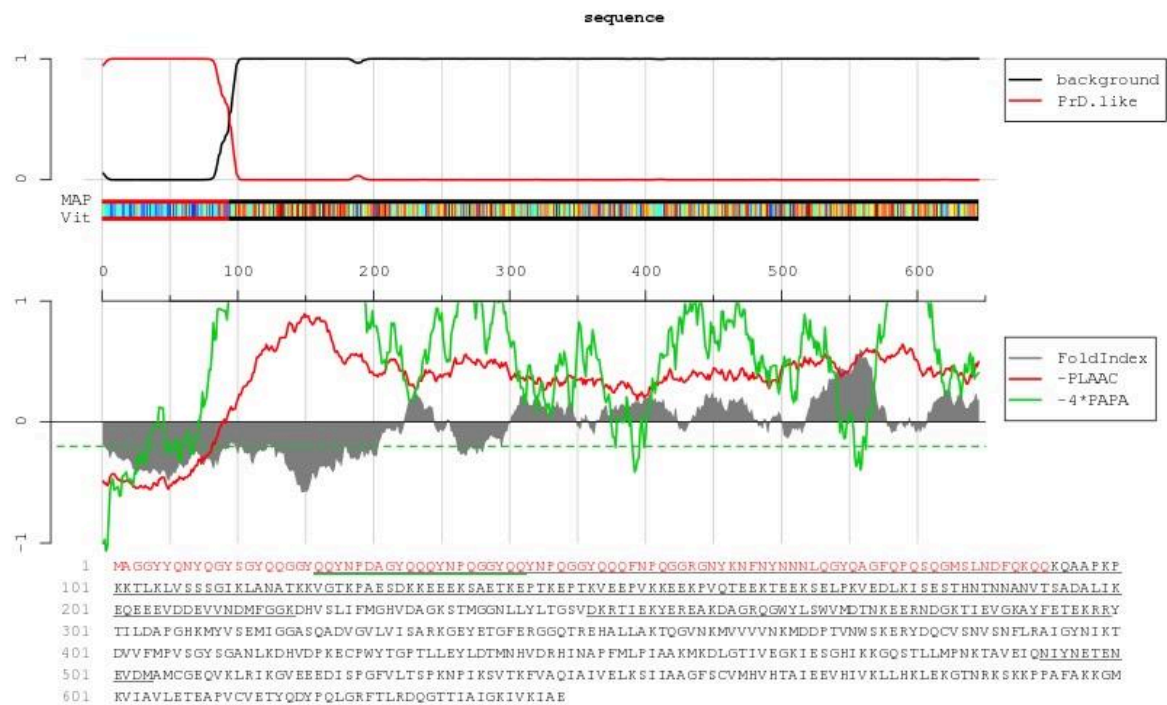
MAGGYQNYQGYSGYQQGGYQQYNPDAGYQQQYNPQGGYQQYNPQGGYQQQFNPQGGRGNYK
NFNYNNNLQGYQAGFQ PQSQGMSLND FQKQQKQAAPKPKKTLKLVSSSGIKLANATKKVGTK
PAESDKKEEEKSAETKEPTKEPTKVVEEPVKKEEKPVQTEEKTEEKSELPKVEDLKISESTHN
TNNANVTSADALIKEQEEEVDDEVVNDMFGGKDHVSLIFMGHVDAGKSTMGGNLLYLTGSVD
KRTIEKYEREAKDAGRQGWYLSWVMDTNKEERNNDGKTIEVGKAYFETEKRRYTILDAPGHKM
YVSEMIGGASQADVGLVISARKGEYETGFERGGQTREHALLAKTQGVNKMVVVNKMDDPT
VNWSKERYDQCVSNVSNFLRAIGYNIKT DVVFMVPSGYSGANLKDHVDPKECPWYTGPTLLE
YLDTMNHVDRHINAPFMLPIAAKMKDLGTIVEGKIESGHIKKGQSTLLMPNKTAVEIQNIYN
ETENEVDMAMCGEQVKLRIGVEEEDISPFGVLTSPKNPIKSVTKFVAQIAIVELKSIIAAG
FSCVMHVHTAIEEVHIVKLLHKLEKGTNRKSKKPPAFAKKGMKVIADVLETEAPVCVETYQDY
PQLGRFTLRDQGT TIAIGKIVKIAE

PAPA



PLAAC

COREscore	LLR	PAPAprp	PAPAf1
19.025	19.025	0.099	-0.342



>HP1

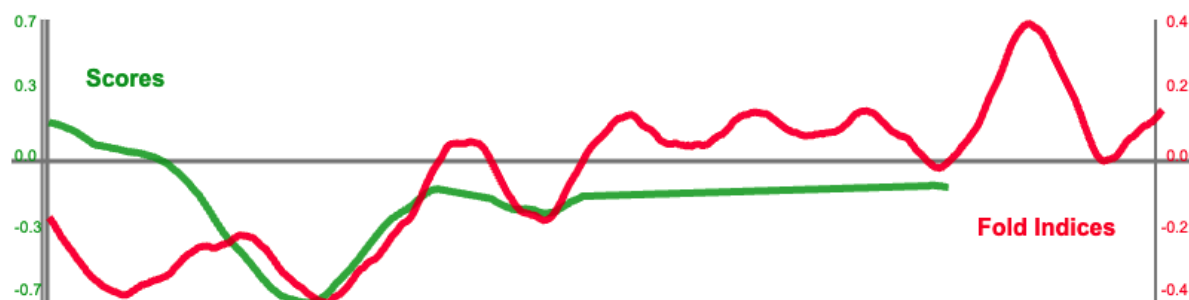
MGNNSVISFNQTNFNQGTYNAGGYQNYQGYSGYQGGYQQYNPDAGYQQQYNPQGGYQQ
YNPQGGYQQQFNPQGGRGNYKNFNYNNNNLQGYQAGFQPQSQGMSLNDFOKQKQQAAPKPKKT
LKLVSSSSGIKLANATKKVGTKPAESDKKEEEKSAETKEPTKEPTKVEEPVKKEEKPVQTEEK
TEEKSELPKVEDLKI SESTHNTNNANVTSADALIKEQEEVDDEVVNDMFGGKDHVSLIFMG
HVDAGKSTMGGNLLYLTGSVDKRTIEKYEREAKDAGRQGWYLSWVMDTNKEERNDGKTIEVG
KAYFETEKRRYTILDAPGHKMYVSEMI GGASQADVGV LVI SARKGEYETGFERGGQTREHAL
LAKTQGVNKMVVVNKMDDPTVNW SKERYDQCVSNVSNFLRAIGYNIKTDDVVFMFVSGYSGA
NLKDHDVPKECPWYTGPTLLEYLDTMNHVDRHINAFMLPIAAKMKDLGTIVEGKIESGHIK
KGQSTLLMPNKTAVEIQNIYNETENEVDMA MCGEQVKLR IKGVEEEDISPFGVLTSPKNPIK
SVTKFVAQIAIVELKSI IAGFSCVMHVHTAIEEVHIVKLLHKLEKGTNRKSKKPPAFAKKM
MKVIAVLETEAPVCVETYQDYPQLGRFTLRDQGTITIAIGKIVKIAE

PAPA

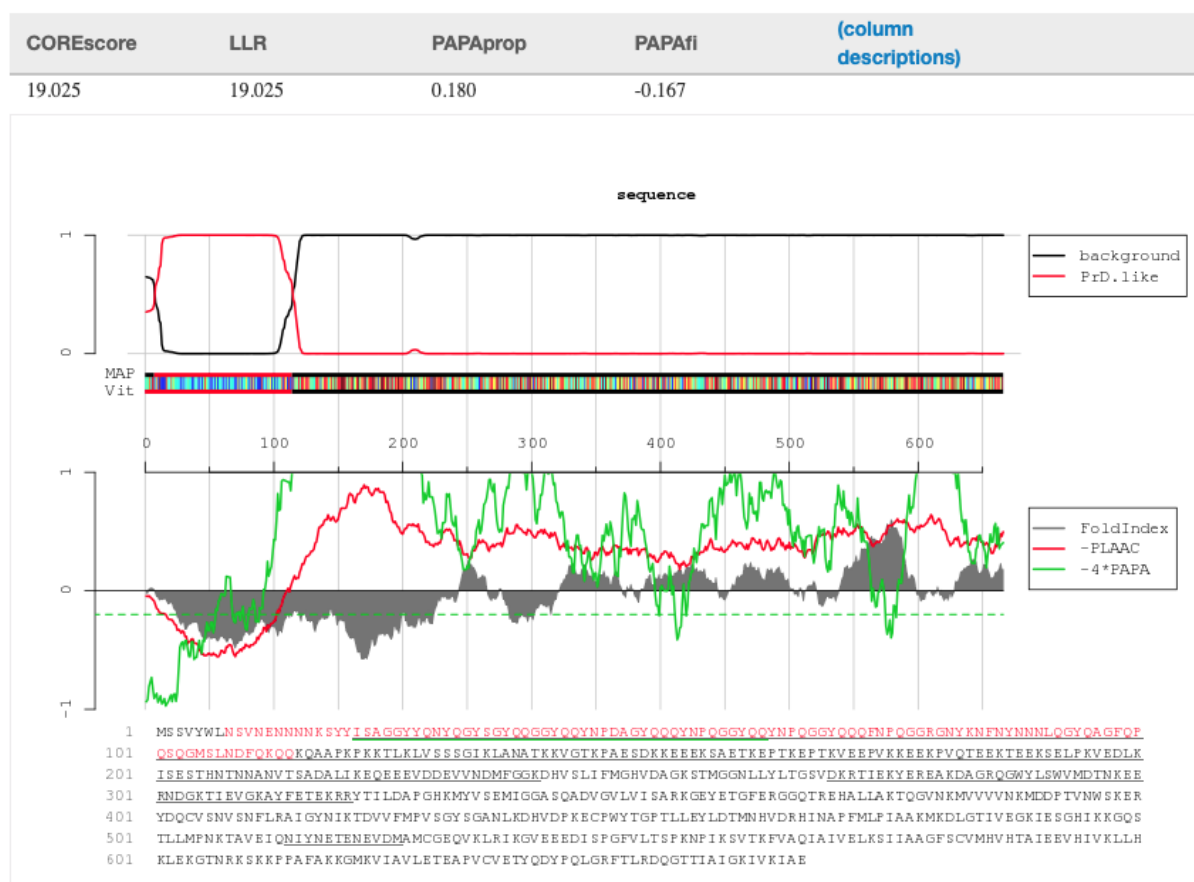
MSVVYWLNSVNNENN**NNNKSYYIS****AGGGYYQNYQGGYS**GYQQGGYQQYNPDAGYQQQYQYNPQGGYQQ
 YNPQGGYQQQFNPQGGGRGNKYKNFNYNNNNLQGYQAGFQPPQSQGMSLNDFFQKQQKQAAPKPKKT
 LKLVSSSGIKLANATKKVGTKPAESDKKEEEKSAETKEPTKEPTKVEEPVKKEEKPVQTEEK
 TEEKSELPKVEDLKI SESTHNTNNANVTSADALIKEQEEEVDDDEVVNDMFGGKDHVSLIFMG
 HVDAGKSTMGGNLLYL TGSVDKRTIEKYEREAKDAGRQGWYLSWVMDTNKEERNNDGKTIEVG
 KAYFETEKRRYTIL DAPGHKMYVSEMI GGASQADVGLVVISARKGEYETGFERGGQTREHAL
 LAKTQGVNKMVVVVNKMDDPTVNWSKERYDQCVSNVSNFLRAIGYNIKTDVVFMPVSGYSGA
 NLKDHVDPKECPWYTGPTLLEYLDTMNHVDRHINAPFMLPIAAKMKDLGTIVEGKIESGHIK
 KGQSTLLMPNKTAVEIQNIYNETENEVDMMAMCGEQVKLRIGVEEEDISPGFVLTSPKNPIK
 SVTKFVAQIAIVELKSI I AAGFSCVMHVHTAIEEVHIVKLLHKLEKGTNRKSKKPPAFAKKG
 MKVIAVLETEAPVCVETYODYPOLGRFTLRDOGT TIAIGKIVKIAE

PAPA

Score = 0.18, Position = 0



PLAAC

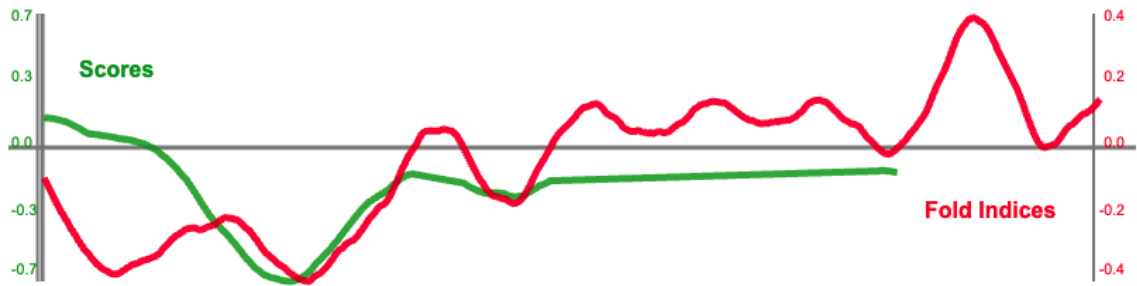


>CC3

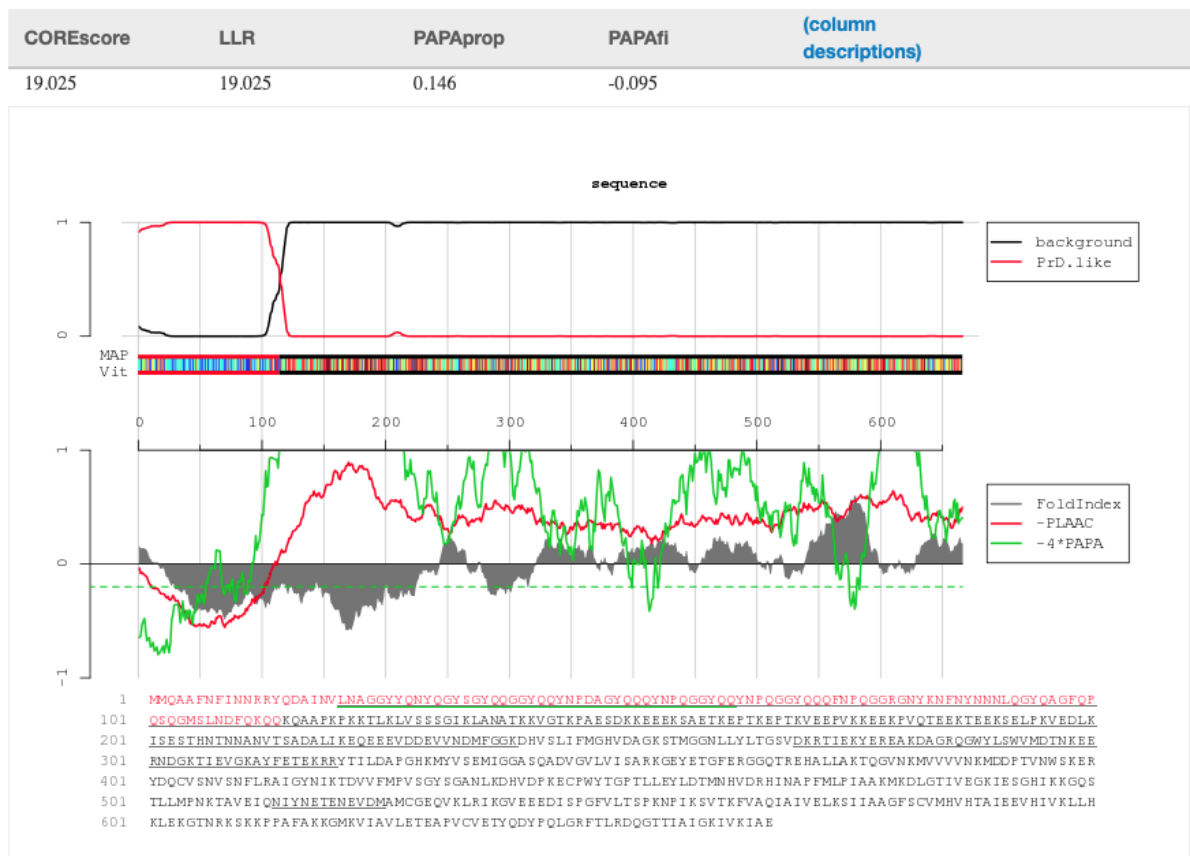
MMQAAFNFINNRRYQDAINVLNAGGYQNYQGYSGYQQGGYQQYNPDAGYQQQYNPQGGYQQYQGGYQNYKNFNNNNLQGYQAGFQPQSQGMSLNDFOKQQAAPKPKTKLVSSSGIKLANATKKVGTGKPAESDKKEEEKSAETKEPTKEPTKVEEPVKKEEKFPVQTEETEEKSELFPKVEDLKISESTHNTNNANVTADALIKEQEEVDDEVNDMFGGKDHVSLIFMGHVDAGKSTMGGNLLYLTGSVDKRTIEKYEREAKDAGRQGWYLSWVMDTNKEERNNDGKTIEVGKAYFETEKRRYTILDAPGHKMYVSEMIGGASQADVGLVLSARKGEYETGFERGGQTRHALAKTQGVNKMVVVNKMDPTVNWSKERYDQCVSNVSNFLRAIGYNIKTDDVFMFVSGYSGANLKDHDVDPKECPWYTGP TLLEYLDTMNHVDRHINAFFMLPIAAKMKDLGTIVEGKIESGHIKKGQSTLLMPNKTAVEIQNIYNETENEVDMA MCGEQVKLRIGVEEEDISPFGVLTSPKNPIK

SVTKFVAQIAIVELKSIIAAGFSCVMHVHTAIEEVHIVKLLHKLEKGTNRKSKKPPAFKKG
MKVIAVLETEAPVVCVETYQDYPQLGRFTLRDQGTtiaigkivkiaE

PAPA
Score = 0.15, Position = 0



PLAAC

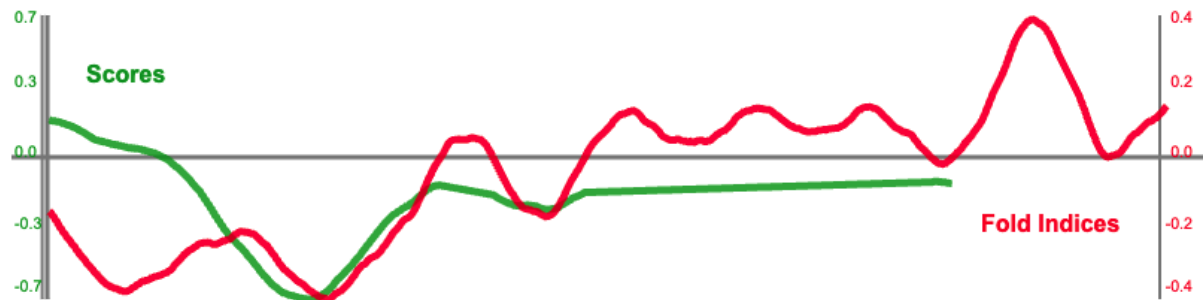


>BH4
MYQQALNVLRSRIQNRNAQWYYLAGGYQNYQGYSGYQQGGYQQYNPDAGYQQQYNPQGGYQQ
YNPQGGYQQQFNPQGGRGNYKNFNYNNNLQGYQAGFQPQSQGMSLNDFOKQQAAPKPKKT
LKLVS SSGIKLANATKKVGTKPAESDKKEEEKSAETKEPTKEPTKVEEPVKKEEKFPVQTEET
TEEKSELPKVEDLKISESTHNTNNANVTSADALIKEQEEVDDEVVNDMFGGKDHVSLIFMG
HVDAGKSTMGGNLLYLTGSVDKRTIEKYEREAKDAGRQGWYLSWVMDTNKEERNDGKTIEVG
KAYFETEKRRYTILDAPGHKMYVSEMIGGASQADVGVGLVISARKGEYETGFERGGQTRHAL

LAKTQGVNKMVVVNKMDDPTVNWSKERYDQCVSNVSNFLRAIGYNIKTDVVFMPVSGYSGA
 NLKDHVDPKECPWYTGPTLLEYLDTMNHVDRHINAPFMLPIAAKMKDLGTIVEGKIESGHIK
 KGQSTLLMPNKTAVEIQNIYNETENEVDAMCGEQVKLRIKGVVEEDISPGFVLTSPKNPIK
 SVTKFVAQIAIVELKSIIAAGFSCVMHVHTAIEEVHIVKLLHKLEKGTNRKSKKPPAFAKKG
 MKVIAVLETEAPVCVETYQDYPQLGRFTLRDQGTITIAIGKIVKIAE

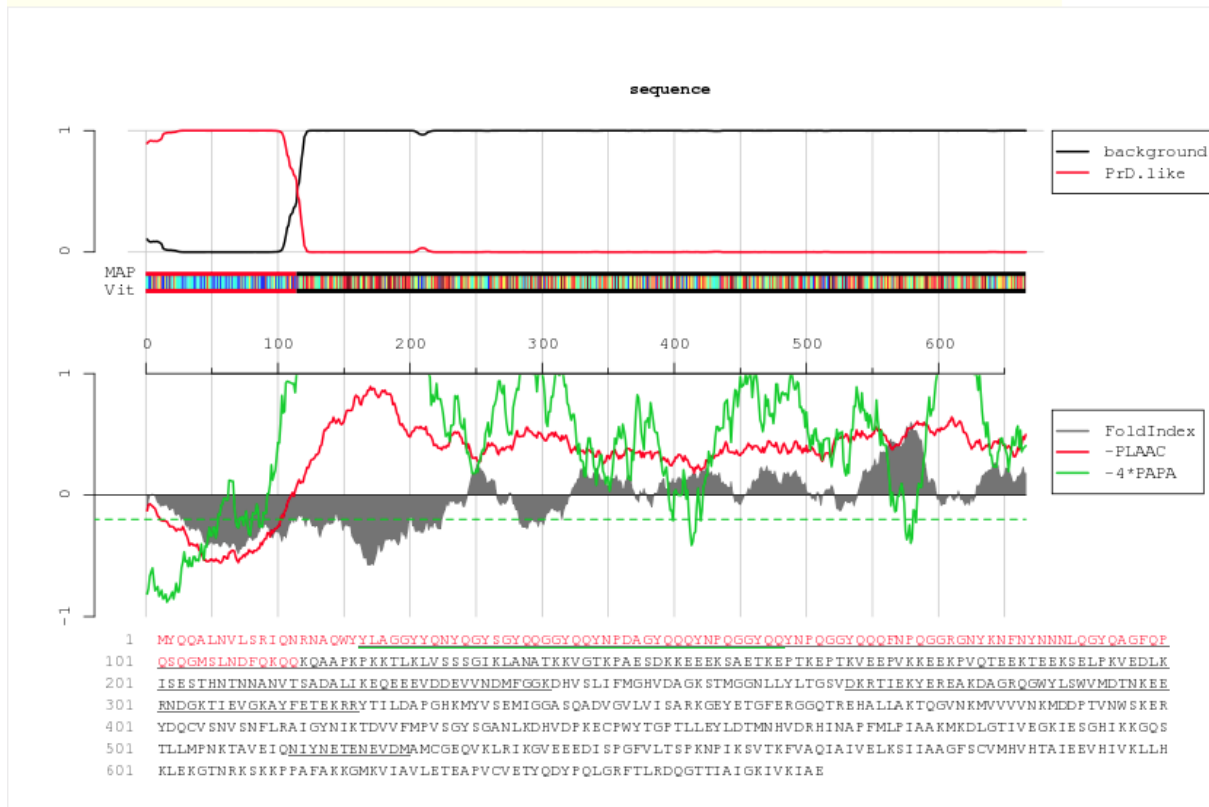
PAPA

Score = 0.17, Position = 0



PLAAC

COREscore	LLR	PAPAprp	PAPAFi	(column descriptions)
19.025	19.025	0.171	-0.161	

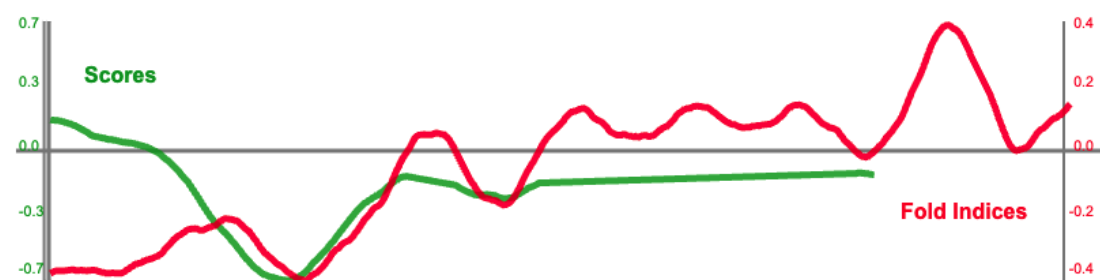


>RI5

MHANEGNVNQYNNSYQNTNSYSAGGGYYQNYQGYSGYQQGGYQQYNPDAGYQQOYNFQGGYQQ
 YNPQGGYQQQFNPQGGRGNYKNFNYNNNLQGYQAGFQPQSQGMSLNDFFQKQKQAAPFKPKKT
 LKLVSSSGIKLANATKKVGTKPAESDKKEEEKSAETKEPTKEPTKVEEPVKKEEKFPVQTEEK

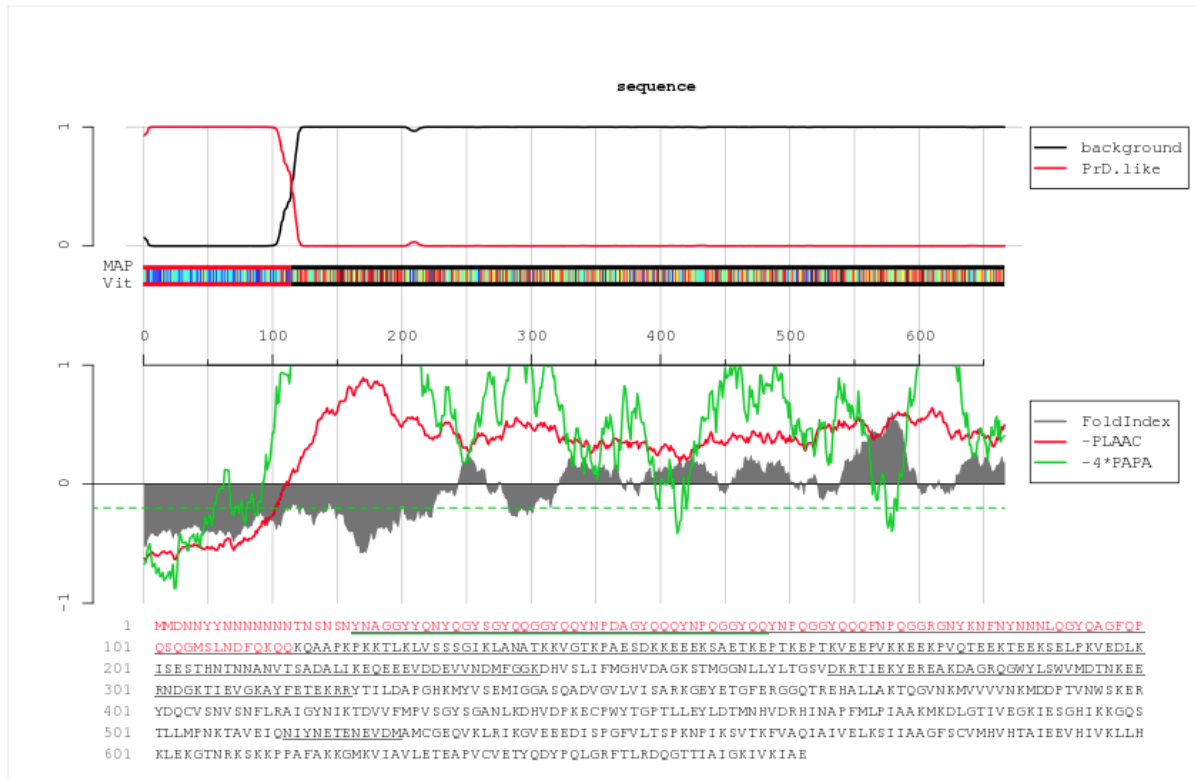
MDNNYYNNNNNNNTNSNSNYNAGGYYQNYQGYSGYQQGGYQQYNPDAGYQQQYNPQGGYQQ
 YNPQGGYQQQFNPQGGRGNYKNFNYNNNLQGYQAGFQPQSQGMSLNDFOKQQKQAAPKPKKT
 LKLVSSSGIKLANATKKVGTGTPAESDKKEEEKSAETKEPTKEPTKVEEPVKKEEKPVQTEEK
 TEEKSELPKVEDLKI SESTHNTNNANVT SADALIKEQEEVDDEVVNDMFGGKDHVSLIFMG
 HVDAGKSTMGGNLLYL TGSVDKRTIEKYEREAKDAGRQGWYLSWMDTNKEERN DGKTIEVG
 KAYFETEKRRYTILDAPGHKMYVSEMIGGASQADVGLV I SARKGEYETGFERGGQTREHAL
 LAKTQGVNKMVVVNKMDDPTVNWSKERYDQCVSNVSNFLRAIGYNIKTDVVFMPVSGYSGA
 NLKDHVDPKECPWYTGPTLLEYLDTMNHVDRHINAPFMLPIAAKMKDLGTIVEGKIESGHIK
 KGQSTLLMPNKTAVEIQNIYNETENEVDMA MCGEQVKLR IKGVEEEDISP GFVLTSPKNPIK
 SVTKFVAQIAIVELKSI IAGFSCVMHVHTAIEEVHIVKLLHKLEKGTNRKSKKPPAFKKG
 MKVIAVLETEAPVCVETYQDYPQLGRFTLRDQGT TIAIGKIVKIAE

PAPA
 Score = 0.16, Position = 0



PLAAC
 sequence

COREscore	LLR	PAPAprior	PAPAFI	(column descriptions)
20.492	20.492	0.157	-0.398	

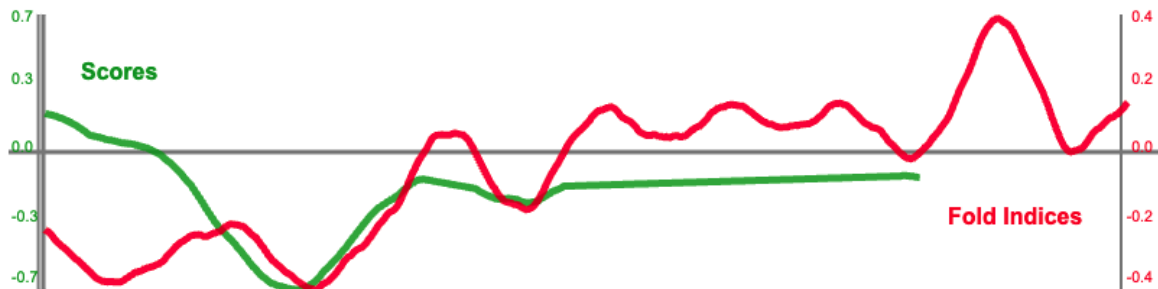


>SA7

M**R****S****G****N****V****F****L****A****N****S****T****N****R****Y****Q****G****N****Y****N**AGGYYQNYQGYSGYQQGGYQQYNPDAGYQQQYNPQGGYQQ
YNPQGGYQQQFNPQGGRGNYKNFNYNNNNLQGYQAGFQPQSQGMSLNDFFQKQQKQAAPKPKKT
LKLVSSSGIKLANATKKVGTKPAESDKKEEEKSAETKEPTKEPTKVEEPVKKEEKPVQTEEK
TEEKSELPKVEDLKI SESTHNTNNANVT SADALIKEQEEVDDEVVNDMFGGKDHVSLIFMG
HVDAGKSTMGGNLLYL TGSVDKRTIEKYEREAKDAGRQGWYLSWMDTNKEERNNDGKTIEVG
KAYFETEKRRYTILDAPGHKMYVSEMIGGASQADVGVLVISARKGEYETGFERGGQTREHAL
LAKTQGVNKMVVVVNKMDDPTVNWSKERYDQCVSNVSNFLRAIGYNIKTDVVFMPVSGYSGA
NLKDHVDPKECPWYTGPTLLEYLDTMNHVDRHINAPFMLPIAAKMKDLGTIVEGKIESGHIK
KGQSTLLMPNKTAVEIQNIYNETENEVDAMCGEQVKLRIGVEEEDISPGFVLTS PKNPIK
SVTKFVAQIAIVELKSIIAAGFSCVMHVHTAIEEVHIVKLLHKLEKGTNRKSKKPPAFAKKG
MKVIAVLETEAPVCVETYQDYPQLGRFTLRDQGT TIAIGKIVKIAE

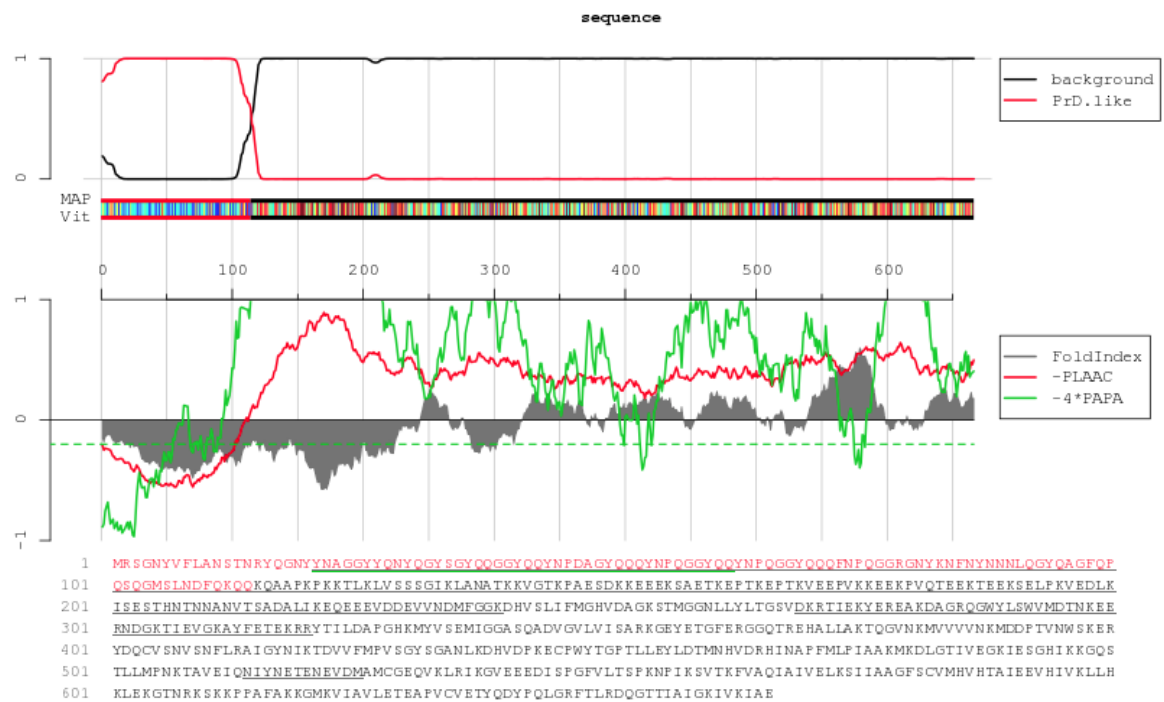
PAPA

Score = 0.18, Position = 0



PLAAC

COREscore	LLR	PAPAprp	PAPAffi	(column descriptions)
19.025	19.025	0.183	-0.237	

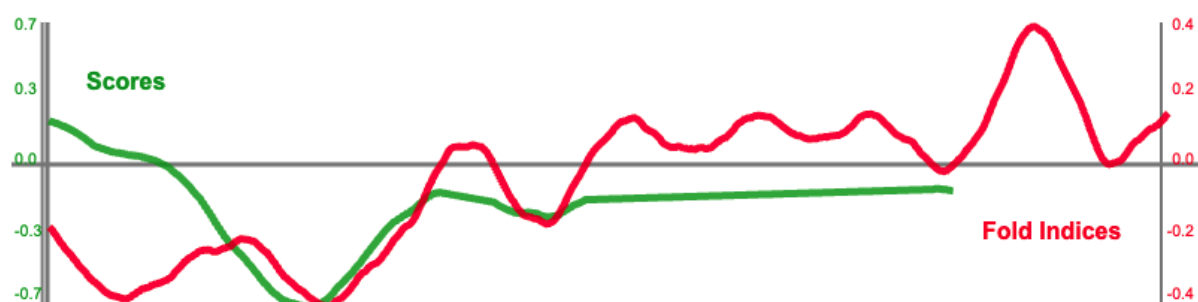


>LD8

MSYSSSANNYGYGSNNYSYSAAGGYQNYQGYSGYQQGGYQQYNPDAGYQQQYNPQGGYQQ
YNPQGGYQQQFNPQGGRGNYKNFNYNNNLQGYQAGFQFPQSQGMSLNDFOKQKQAAPKPKKT
LKLVS SSGIKLANATKKVGTKPAESDKKEEEKSAETKEPTKEPTKVEEPVKKEEKFPVQTEET
TEEKSELPKVEDLKISESTHNTNNANVTADALIKEQEEVDDDEVVNDMFGGKDHVSLIFMG
HVDAGKSTMGGNLLYLTGSVDKRTIEKYEREAKDAGRQGWYLSWMDTNKEERNDGKTIEVG
KAYFETEKRRYTILDAPGHKMYVSEMIGGASQADVGLVISARKGEYETGFERGGQTREHAL
LAKTQGVNKMVVVNKMDDPTVNWSKERYDQCVSNVSNFLRAIGYNIKTDDVFMFVSGYSGA
NLKDHVDPKECPWYTGPTLLEYLDTMNHVDRHINAFMLPIAAKMKDLGTIVEGKIESGHIK
KGQSTLLMPNKTAVEIQNIYNETENEVDMA MCGEQVKLRIGVEEEDI SPGFVLTS PKNPIK
SVTKFVAQIAIVELKSI IAGFSCVMHVHTAIEEVHIVKLLH KLEKGTNRKSKKPPAFKKG
MKVIAVLETEAPVCVETYQDYPQLGRFTLRDQGT TIAIGKIVKIAE

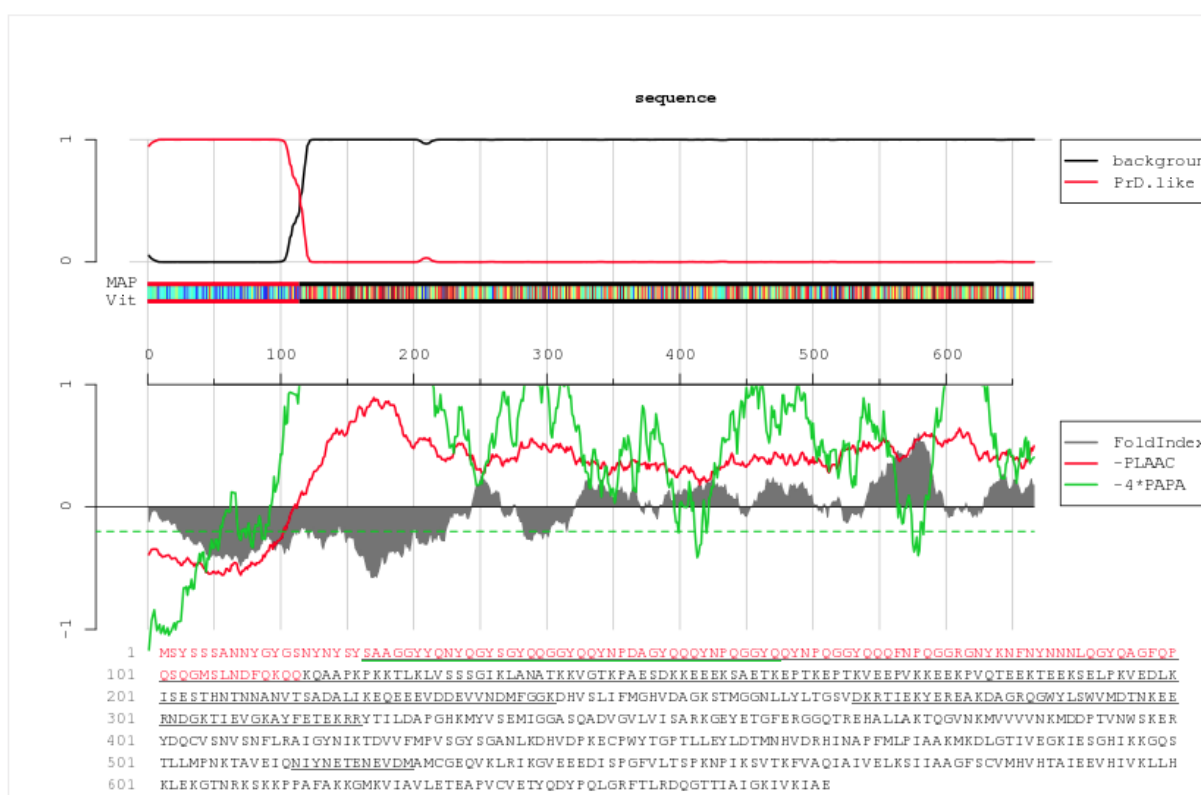
PAPA

Score = 0.20, Position = 0



PLAAC

COREscore	LLR	PAPAprior	PAPAFI	(column descriptions)
19.025	19.025	0.201	-0.186	



>P9

MGYVQSSYGQ**NQFQNSQYGSYQAGGYQNYQ**GYSGYQQGGYQQYNPDAGYQQQYNPQGGYQQ
 YNPQGGYQQQFNPQGGRGNYKNFNYNNNLQGYQAGFQPQSQGMSLNDFFQKQQAAPKPKKT
 LKLVSSSGIKLANATKKVGTKEPAESDKKEEEKSAETKEPTKEPTKVEEPVKKEEKFPVQTEEK
 TEEKSELKVEDLKISESTHNTNNANVTADALIKEQEEVDDEVNDMFGGKDHVSLIFMG
 HVDAGKSTMGGNLLYLTSVDRKRTIEKYEREAKDAGRQGWYLSWMDTNKEERNDGKTIEVG
 KAYFETEKRRYTILDAPGHKMYVSEMIGGASQADVGLVVISARKGEYETGFERGGQTRHAL
 LAKTQGVNKMVVVNKMDDPTVNWSKERYDQCVSNVSNFLRAIGYNIKTVDVFMFVSGYSGA
 NLKDHVDKKECPWYTGTLLLEYLDTMNHVDRHINAPFMLPIAAKMKDLGTIVEGKIESGHIK
 KGQSTLLMPNKTAVEIQNIYNETENEVDAMCGEQVKLRIGVEEEDISPGEVLTSPKNPIK

